

UNIVERSITY OF PADOVA

DOCTORAL THESIS

---

**Design, characterization and validation  
of an innovative biosensor for illegal  
hypertrophy treatments detection in  
cattle breeding**

---

*Author:*  
Dr. Giulio Rosati

*Supervisor:*  
Prof. Carlo Reggiani  
*Co-supervisor:*  
Prof. Alessandro Paccagnella

*A thesis submitted in fulfillment of the requirements  
for the degree of Doctor of Philosophy in Biotechnologies*

*in the*

Department of Biomedical Sciences

September 2015

# Declaration of Authorship

I, Giulio Rosati, declare that this thesis titled, 'Design, characterization and validation of an innovative biosensor for illegal hypertrophy treatments detection in cattle breeding' and the work presented in it are my own. I confirm that:

- This work was done wholly or mainly while in candidature for a research degree at this University.
- Where any part of this thesis has previously been submitted for a degree or any other qualification at this University or any other institution, this has been clearly stated.
- Where I have consulted the published work of others, this is always clearly attributed.
- Where I have quoted from the work of others, the source is always given. With the exception of such quotations, this thesis is entirely my own work.
- I have acknowledged all main sources of help.
- Where the thesis is based on work done by myself jointly with others, I have made clear exactly what was done by others and what I have contributed myself.

Signed: Giulio Rosati

---

Date: 31st of July 2015

---

The research activities described in this thesis have been partially supported by the project:

*"Sistema microelettronico per l'individuazione tempestiva di trattamenti illeciti sugli animali da allevamento".*

Founded by the Veneto Region: Programma di sviluppo rurale, Misura 124 - Cooperazione per lo sviluppo di nuovi prodotti, processi e tecnologie nel settore agricolo, alimentare e forestale.

*"Non chi comincia ma quel che persevera."*

Nave scuola della Marina Militare Italiana "Amerigo Vespucci"

UNIVERSITY OF PADOVA

# *Abstract*

Department of Biomedical Sciences

Doctor of Philosophy

## **Design, characterization and validation of an innovative biosensor for illegal hypertrophy treatments detection in cattle breeding**

by Giulio ROSATI

### *English version*

The work done during this PhD program, and presented in this thesis had the goal to design, develop and characterize a system for the detection of illegal anabolic treatments in cattle breeding, independently from the particular anabolic substance used. The system is aimed to allow for faster and cheaper controls with respect to standard techniques such as mass spectrometry, gas chromatography, and histological exams. Moreover, the system allows for on-the-field controls, drastically reducing the costs related to sample transportation, analysis, and trained personnel.

The main strength of this system is the independence of the anabolic treatments detection, from the particular substance employed, which makes this system optimal as screening method. Then, once identified the animals which has been treated, further analysis can be performed by standard techniques for the anabolic substance identification and quantification.

The independence from the anabolic substance is achieved by adopting a novel paradigm for anabolic treatments detection, based on the identification of a common hypertrophic effect induced by the anabolic substance on an in-vitro culture of mouse myogenic cells. The cells provided with the anabolic substances receptors, are engineered to react to the hypertrophic stimulus with the over-production of lactate, which is then released in the cell medium. Then, the lactate concentration in the medium is detected by an electrochemical enzyme-based biosensor, which allows for a rapid and precise quantification by a cheap and miniaturizable device. The quantification of lactate produced by the engineered cells allows the detection of on-going hypertrophic effect and thus of the presence of anabolic substances in the biological sample collected from the cattle.

UNIVERSITY OF PADOVA

## *Sommario*

Department of Biomedical Sciences

Doctor of Philosophy

### **Design, characterization and validation of an innovative biosensor for illegal hypertrophy treatments detection in cattle breeding**

by Giulio ROSATI

#### *Italian version*

Il lavoro svolto durante questo dottorato di ricerca e riassunto in questa tesi ha avuto l'obiettivo di progettare, realizzare e caratterizzare un sistema unificato per la rilevazione di trattamenti anabolizzanti sui capi di bestiame bovini da carne, indipendentemente dalla sostanza utilizzata per i trattamenti. La tecnologia ideata consente di effettuare gli esami in modo molto più rapido che con i sistemi tradizionali e direttamente sul campo, su campioni d'urina dell'animale. Il suo principale punto di forza è l'indipendenza dal tipo di sostanza utilizzata che la rende ottimale per essere utilizzata come tecnica di screening. Una volta individuati gli animali trattati mediante il sistema, sarà possibile andare ad identificare e quantificare la sostanza anabolizzante mediante le tecniche standard di analisi. Tale indipendenza è ottenuta cambiando il paradigma di rilevazione delle sostanze e basandolo sull'effetto ipertrofico che queste hanno in vitro su una coltura di cellule miogeniche. L'effetto ipertrofico attiva nella linea cellulare miogenica, dotata dei recettori per le sostanze anabolizzanti e geneticamente modificata allo scopo, la sovrapproduzione di acido lattico, che viene rilasciato dalla cellula nel mezzo. Qui l'acido lattico viene quindi quantificato da un biosensore elettrochimico enzimatico, grazie al quale è possibile ottenerne una veloce e precisa quantificazione con un'apparato di misura economico e miniaturizzabile. La quantificazione della concentrazione di acido lattico prodotto dalle cellule consente, a ritroso, di individuare la presenza di sostanze anabolizzanti nel campione d'urina dell'animale.

## *Acknowledgements*

I acknowledge the spin-offs of the University of Padova ARC - Centro di Ricerche Applicate s.r.l. and Next Step Engineering s.r.l. for the devices and the competences brought during this PhD program. I thank a lot Alessandro De Toni, Matteo Scaramuzza, Elisabetta Pasqualotto, Mauro Perino and Professor Alessandro Paccagnella for the mentoring and the help given both in the nice and unpleasant moments of my PhD. A special thank goes to Professor Carlo Reggiani.

# Contents

<b>Declaration of Authorship</b>	<b>i</b>
<b>Abstract</b>	<b>iv</b>
<b>Sommario</b>	<b>iv</b>
<b>Acknowledgements</b>	<b>vi</b>
<b>Contents</b>	<b>vii</b>
<b>List of Figures</b>	<b>x</b>
<b>List of Tables</b>	<b>xvii</b>
<b>Abbreviations</b>	<b>xviii</b>
<b>1 Introduction</b>	<b>1</b>
1.1 Meat market in Europe . . . . .	1
1.2 Illegal anabolic treatments in cattle breeding . . . . .	4
1.3 Engineered cells and organisms . . . . .	5
1.4 Electrochemical biosensors . . . . .	6
1.5 The Myo-Screen project . . . . .	6
1.6 Work Packages . . . . .	8
<b>2 Illegal anabolic treatments to cattle breeding</b>	<b>9</b>
2.1 History . . . . .	9
2.2 National Residues Plan . . . . .	9
2.3 Anabolic compound detection . . . . .	13
2.3.1 Analytical techniques for cat. A samples analysis . . . . .	13
2.3.1.1 Mass spectrometry (MS) . . . . .	13
2.3.1.2 Gas chromatography (GC) . . . . .	16
2.3.2 Histological tests . . . . .	18
2.3.3 Issues with the present detection techniques . . . . .	19
2.4 The Myo-Screen project: problems and solutions . . . . .	20



---

<b>3</b>	<b>Myogenic cells for hypertrophy transduction</b>	<b>22</b>
3.1	The skeletal muscle . . . . .	22
3.2	Cell signaling and receptors . . . . .	25
3.2.1	Ionotropic cell surface receptors . . . . .	26
3.2.2	Metabotropic cell surface receptors . . . . .	26
3.2.3	Intracellular cell surface receptors . . . . .	27
3.2.4	The MAPK pathway . . . . .	28
3.2.5	The IGF1 signal system . . . . .	33
3.2.6	The $\beta$ -adrenergic signal system . . . . .	34
3.2.7	The steroids signalling system . . . . .	34
3.3	Cell cultures . . . . .	35
3.3.1	Cell types and culture characteristics . . . . .	37
3.3.2	Phases of cell growth . . . . .	38
3.3.3	Cell quantification . . . . .	41
3.3.3.1	Counting chamber . . . . .	41
3.3.3.2	CFU counting . . . . .	42
3.3.3.3	Spectrophotometry . . . . .	42
3.3.3.4	Electrical resistance . . . . .	43
3.3.3.5	Flow cytometry . . . . .	43
3.3.3.6	Image counting . . . . .	43
3.3.4	Culture environment . . . . .	44
3.3.4.1	Constituents of media . . . . .	44
3.3.4.2	Serum and serum-free cultures . . . . .	46
3.4	Genetic engineering techniques . . . . .	49
3.4.1	Gene isolation . . . . .	50
3.4.2	Gene complementing . . . . .	51
3.4.3	Genes insertion in the host cell . . . . .	51
3.4.3.1	Transformation . . . . .	51
3.4.3.2	Transduction . . . . .	54
3.4.3.3	Transfection . . . . .	56
3.4.4	Selection . . . . .	58
3.4.5	Confirmation . . . . .	59
3.5	The Myo-Screen engineered cells . . . . .	60
3.5.1	Illegal substances and cell receptors . . . . .	61
3.5.2	Cell line selection . . . . .	62
3.5.2.1	FBS deprivation tests . . . . .	63
3.5.2.2	Medium/buffers tests . . . . .	64
3.5.3	Anabolic substances effect on cells . . . . .	65
3.5.3.1	Signaling pathway . . . . .	65
3.5.3.2	Genomic effect . . . . .	67
3.5.4	Cells genetic engineering . . . . .	72
3.5.4.1	Verification of the IGF1 promoter triggering effect . . . . .	76
3.5.4.2	Transfection for continuous lactate production . . . . .	77
3.5.4.3	Transfection for stimulated lactate production . . . . .	79
<b>4</b>	<b>Electrochemical biosensor for lactate detection</b>	<b>82</b>
4.1	Biosensors fundamentals . . . . .	82

---

4.1.1	Biosensors performance parameters . . . . .	83
4.1.2	Affinity vs catalytic biosensors . . . . .	84
4.1.3	Measurement techniques . . . . .	86
4.1.3.1	Electrochemical Impedance Spectroscopy (EIS) . . . . .	87
4.1.3.2	Cyclic Voltammetry (CV) . . . . .	87
4.1.3.3	Amperometric i-t curves . . . . .	88
4.1.3.4	Surface Plasmon resonance (SPR) . . . . .	89
4.1.4	Devices design and fabrication . . . . .	90
4.1.4.1	Finite Element Modeling and simulations . . . . .	90
4.1.4.2	Electrochemical devices fabrication methods . . . . .	90
4.1.4.3	Devices validation . . . . .	93
4.2	Lactate enzyme-based biosensors . . . . .	94
4.2.1	Strategies and enzymes for lactate detection . . . . .	94
4.2.2	Enzymes immobilization . . . . .	95
4.3	The Myo-Screen Lactate biosensor . . . . .	97
4.3.1	Devices characterization . . . . .	98
4.3.1.1	EIS measurements . . . . .	98
4.3.1.2	CV measurements . . . . .	104
4.3.2	NADH detection . . . . .	108
4.3.2.1	UV-Vis spectrophotometry of NADH in different medi- um/buffers . . . . .	110
4.3.2.2	CV measurements of NADH in different medium/buffers	112
4.3.2.3	NADH calibration curves . . . . .	119
4.3.3	LDH-mediated catalysis optimization . . . . .	122
4.3.4	Lactate detection . . . . .	128
4.3.4.1	Protocol selection . . . . .	128
4.3.4.2	Lactate calibration curve . . . . .	131
<b>5</b>	<b>Real samples interference study and biosensor calibration</b>	<b>135</b>
5.1	Urine samples interference . . . . .	136
5.1.1	Spectrophotometrical and CV characterizations . . . . .	136
5.1.2	Natural LA concentrations . . . . .	138
5.2	Biosensor calibration in urine samples . . . . .	139
5.2.1	Calibration in 100% veal urine . . . . .	140
5.2.2	Comparison with diluted urine samples calibrations . . . . .	143
5.3	Myogenic cells interference . . . . .	148
5.3.1	Tests protocol . . . . .	149
5.3.2	Basal LA cells production . . . . .	150
5.4	Engineered cells for continuous lactate over-production . . . . .	153
<b>6</b>	<b>Conclusions</b>	<b>160</b>

# List of Figures

1.1	Meat production in europe in 2013 . . . . .	2
1.2	Production of beef and veal, by type of bovine animals in 2013 (Eurostat 2013) . . . . .	3
1.3	Bovine livestock and its production cycle in Europe (Eurostat 2013) . . . . .	3
1.4	The main meaning of food quality for Italian consumers (%) . . . . .	4
1.5	Myo-Screen project working principle. . . . .	7
2.1	Percentage distribution of the analyzed samples in actuation of the PNR 2014 divided by substance group category (see table 2.1) . . . . .	12
2.2	Trends of the number of analyzed samples (on the left) and of the number of not complying samples (on the right) in recent years. . . . .	13
2.3	Scheme of a mass spectrometry system. . . . .	15
2.4	Shematics of a gas chromatography system . . . . .	16
2.5	Example of a positive hystologic sample of a seven month bovine. The anabolic treatments caused a huge increase in the adipose tissue (the white cells) in the thymus [9]. . . . .	19
3.1	Structure of the skeletal muscle and its substructures organization. . . . .	23
3.2	Scheme of the metabolic pathways for the generation of ATP in the aerobic and anaerobic cases. . . . .	25
3.3	Noradrenaline activates $G_q$ and hence phospholipase $C_\beta$ in many cells including smooth muscle. . . . .	27
3.4	MAPK signaling pathway scheme, from the cell membrane receptors to the DNA expression regulation. . . . .	30
3.5	Examples of cell morphology: (a) HeLa epithelial cells, (b) BAE-1 endothelial cells, (c) MRC-5 fibroblasts cells, (d) SH-SY5Y neuronal cells. . . . .	38
3.6	Representation of the cells growth phases over time. . . . .	40
3.7	White light and fluorescence pictures of C2C7 myo-genic cells. . . . .	64
3.8	Signaling pathway from the anabolic substances binding with their receptors to the transcription factors in the nucleous through the MAPKs . . . . .	66
3.9	Phosphorylated/not phosphorylated ERK bands obtained by the Western blot tests and their intensity ratio for C2C7 cells treated with four different anabolic compounds for 5 minutes. Cells treated with 20% FBS were used as positive control, untreated cells as negative one. . . . .	67
3.10	Target genes expression dependence upon the Clenbuterol concentration. The n.t. cells have not been treated with any anabolic substance. . . . .	68
3.11	Target genes expression dependence upon the Testosterone concentration. The n.t. cells have not been treated with any anabolic substance. . . . .	69

3.12	Target genes expression dependence upon the Estradiol concentration. The n.t. cells have not been treated with any anabolic substance. . . . .	69
3.13	Time course of the IGF1 gene expression for cells treated with Clenbuterol, Testosterone and Estradiol. . . . .	70
3.14	Time course of the IGF1R gene expression for cells treated with Clenbuterol, Testosterone and Estradiol. . . . .	71
3.15	Time course of the Pgc1- $\alpha$ gene expression for cells treated with Clenbuterol, Testosterone and Estradiol. . . . .	71
3.16	Time course of the EGR2 gene expression for cells treated with Clenbuterol, Testosterone and Estradiol. . . . .	72
3.17	Mouse IGF1 promoter DNA sequence of the ATG exon 1 (GenBank: Y18062.1, 2070 bp) . . . . .	73
3.18	The Lipofection is a four step process that involves attachment to the cell, endocytosis into the cell, endosomal escape and nuclear entry for transcription to mRNA. The mRNA is then exported from the nucleus to the cytoplasm and translated into the protein of interest. . . . .	74
3.19	Life Technologies Lipofectamine3000 <sup>®</sup> protocol used for the C2C7 cells transfection in 24 wells plates. . . . .	75
3.20	Cycle sequencing schematic. Consecutive annealing, extension and denaturation steps are cyclically repeated in order to increase the sequencing yield. . . . .	75
3.21	The figure on the left depicts the concept of the Luciferase test. The figure on the right represents the pGL4 vector prepared for the test, where the upstream element is the IGF1 promoter. . . . .	77
3.22	Schematic drawing of the pcDNA3-LDH vector used for the C2C7 transfection for the continuous or constitutive lactate production (left) and Western Blot of the expressed LDH and of Actine as control . . . . .	78
3.23	Western blot and densitometry for the LDH levels analysis in two preparations of C2C7, C2C7 pcDNA3 and C2C7 pcDNA3-LDH cells. The tubulin expression was used for normalization. . . . .	78
3.24	Western blot and densitometry for the LDH levels analysis in COS-1 cells (A), HeLa cells (B), NIH-3T3 cells (C), and HEK293T cells (D), respectively for the wild type cells, the pcDNA3, and the pcDNA3-LDH transfected ones. Tubulin expression was used for the levels normalization. . . . .	80
3.25	Western blot and densitometry for the LDH levels analysis in two preparations of C2C7, C2C7 pcDNA3 and C2C7 pcDNA3-LDH cells. The tubulin expression was used for normalization. . . . .	81
4.1	Main blocks of a general biosensor and comparison with the olfactory system for the detection of a specific analyte. . . . .	82
4.2	Example of a glucose amperometric biosensor calibration curve. The glucose concentration is measured as an electrical current which varies linearly with it, in the biosensor quantification range. The sensitivity of this biosensor is $1.1\mu A/mM$ . . . . .	83
4.3	Representations of the same signal with four SNR values: for the top left plot the SNR is 0.5, for the bottom left one the SNR is 0.3, while for the top right plot the SNR is 5, and for the right bottom one the SNR is 20. . . . .	84
4.4	Schematic representation of the limits of detection, quantification, and linearity in a general biosensor's calibration plot. . . . .	84

4.5	Schematic representation of the sequence of operations for the target protein detection in an ELISA assay using the Horseradish Peroxidase (HRP) enzyme and TMB as label for the colorimetric test. . . . .	85
4.6	Compact scheme representing the detection pathways used by amperometric enzyme-based biosensors over years. The central cube faces represent the electrode surface where the electron transfer allows the amperometric detection. . . . .	86
4.7	Schematic representation of a generic three-electrode electrochemical cell. . . . .	87
4.8	Typical cyclic voltammogram of a reversible redox system. The arrows along the curve give a representation of the measured current values over time during the linear variation of the potential from $E_{initial}$ to $E_{final}$ and back to $E_{initial}$ . The cathodic peak is related to the reduction of the oxidated molecules in the solution while the anodic one is related to the oxidation of the reduced ones. . . . .	88
4.9	Schematic representation of a possible implementation of SPR biosensor based on a gold film functionalized by probe molecules exposed to the analyte in a flow cell and by a polarized light source, a prism, and an optical detection unit. . . . .	89
4.10	Schematic representation of a sputtering process (the collisions cascade between the Argon ions collision to the target and the target atom emission is not represented). . . . .	92
4.11	DropSens Carbon device (DS-110) . . . . .	98
4.12	Bode diagrams of the EIS measurements in PBS 1x on DropSens Au devices. The average impedance data measured over three devices were plotted for respectively the first and the fiftieth sweeps. . . . .	99
4.13	Bode diagrams of the EIS measurements in PBS 1x on DropSens C devices. The average impedance data measured over three devices were plotted for respectively the first and the fiftyth sweeps. . . . .	100
4.14	Percentage variations of the mean impedance magnitude measured on DropSens Au devices in function of both the frequency and the sweep number. . . . .	100
4.15	Percentage variations of the mean impedance phase measured on DropSens Au devices in function of both the frequency and the sweep number. . . . .	101
4.16	Percentage variations of the mean impedance magnitude measured on DropSens C devices in function of both the frequency and the sweep number. . . . .	101
4.17	Percentage variations of the mean impedance phase measured on DropSens C devices in function of both the frequency and the sweep number. . . . .	102
4.18	Equivalent circuit elements fitted values from the EIS sweep in PBS on DropSens Au devices. . . . .	103
4.19	Equivalent circuit elements fitted values from the EIS sweep in PBS on DropSens C devices. . . . .	103
4.20	Cyclic voltammograms measured in ferro/ferricyanide 1 mM in PBS over DSAu devices with different Scan rate values . . . . .	105
4.21	Cyclic voltammograms measured in ferro/ferricyanide 1 mM in PBS over DSC devices with different Scan rate values . . . . .	105
4.22	Cathodic and anodic mean peak currents modules in function of the square root of the CV scan rate over DSAu devices. . . . .	106

4.23	Cathodic and anodic mean peak currents modules in function of the square root of the CV scan rate over DSC devices. . . . .	106
4.24	Peaks potential mean differences in function of the square root of the CV scan rate over DSAu devices. . . . .	107
4.25	Peaks potential mean differences in function of the square root of the CV scan rate over DSC devices. . . . .	107
4.26	Average CV measurements performed in 1 mM ferro/ferricyanide at a scan rate of 100 mV/s on three DSAu and three DSC devices. . . . .	108
4.27	Schemes of the $NAD^+$ and of the $NADH$ molecules and representation of the UV-Visible spectra of the two molecules. . . . .	109
4.28	Cuvette transmittance tests performed on two glass and two quartz empty cuvettes, with respect to a blank measurement in air. . . . .	110
4.29	Optical center height tests performed by progressively filling a 4 ml quartz cuvette with 250 $\mu$ l of ferricyanide per each measurement. . . . .	111
4.30	UV-Vis spectra obtained by measuring ten NADH concentrations in four buffers, with respect to four blank measurements in each pure buffer. The continuous curve is related to HBRS spectra, the dashed one to PBS, the dash-dotted curve to the DMEM, and finally the dotted one to Tris-HCl. . . . .	112
4.31	Comparison between the theoretical NADH concentrations of the prepared solutions and the experimental concentrations obtained from the 339 nm absorbance peak. . . . .	113
4.32	NADH consecutive CV measurements on DSCs (left column) and DSAus (right column) in the buffers: DMEM, HBRS, PBS, 50 mM Tris-HCl (respectively from the top). . . . .	114
4.33	Peak current averages obtained from the CV measurements on three DSAu devices per each buffer. The bars represent the standard deviations obtained averaging the peak currents of the three devices. . . . .	115
4.34	Peak current averages obtained from the CV measurements on three DSC devices per each buffer. The bars represent the standard deviations obtained averaging the peak currents of the three devices. . . . .	116
4.35	Peak current averages obtained from the CV measurements on three DSC devices per each buffer and subtracting the peak currents obtained from the blank measurements. The bars represent the standard deviations obtained averaging the peak currents of the three devices. . . . .	117
4.36	Peak current averages obtained from the CV one-shot measurements on three DSC devices per each NADH concentration and per each media/buffer. The bars represent the standard deviations obtained averaging the peak currents of the three devices. . . . .	118
4.37	75 CV cycles measured in DMEM on a DSC device with a scan rate of 100 mV/s. The first cycles are plotted in red while the last ones are represented in purple. . . . .	118
4.38	Current values at 0.8 V in function of the cycle number, recorded by the CV measurements on DSC devices in DMEM. The blue curve shows the current values obtained by 75 consecutive CV cycles on a DMEM drop, while the red curve represent the values recorded by 5 CV measurements each of 15 cycles, changing each time the DMEM drop on the DSC electrodes. . . . .	119
4.39	UV-Vis spectra of NADH dissolved in Tris-HCl 50 mM and in HBRS with respect to blank measurements in Tris-HCl and HBRS, respectively. . . . .	120

4.40	Comparison between the experimental and theoretical NADH concentrations obtained from the 339 nm peaks of the measurements in Tris-HCl and HBRS. . . . .	120
4.41	Average one-shot CV measurements performed on DSCs on the NADH solutions previously tested by the UV-Vis measurements. The plot on the top shows the measurements in Tris-HCl while that one on the bottom shows those in HBRS. . . . .	121
4.42	Calibration curves obtained by the NADH measurements in Tris-HCl and HBRS. The lines represents the dots linear fits, while the dashed lines shows the blank currents measured in Tris-HCl and HBRS, respectively. . . . .	121
4.43	Structure of the rabbit muscle LDH isoenzyme. The four M subunits are coloured in green, brown, blue, and purple. . . . .	123
4.44	Consecutive absorbance spectra measured in the catalysis solution (with 1 U/ml LDH) with respect to a 1.8 ml of Tris-HCl 50 mM and 0.2 ml of PBS blanking solution. . . . .	125
4.45	LA catalysis kinetics obtained by consecutive UV-Vis spectra measurements over time (dots representing the 339 nm absorbance), and by kinetic measurements at 339 nm with a resolution of 1 s. The baseline of the measurements was 1.8 ml of Tris-HCl 50 mM and 0.2 ml of PBS. . . . .	126
4.46	LA catalysis UV-Vis calibration curves obtained measuring the kinetics at 339 nm in solutions with ten LA concentrations from $1\mu M$ to $1000\mu M$ and three LDH dilutions, from 1 to 100 U/ml. . . . .	127
4.47	Michaelis-Menten kinetic curves calculated from the data represented in the previous figure, with three LDH dilutions. . . . .	127
4.48	Comparison of the NADH concentrations obtained from the 339 nm UV-Vis kinetics of the catalysis of 10 mM LA and PA in HBRS, in presence of $625\mu M$ NAD or NADH in HBRS respectively, and of LDH 100 U/ml in PBS 1x. . . . .	128
4.49	Comparison of the kinetics of 1 mM LA catalysis by the same concentration of $NAD^+$ and of LDH in HBRS and in HBRS+0.5 M Hydrazine. . . . .	129
4.50	Scheme of the strategies tested for the LA in HBRS detection. . . . .	130
4.51	Calibration curve obtained by the UV-Vis and the CV tests with the protocols in HBRS and in Tris-HCl on DSC devices. . . . .	130
4.52	UV-Visible 339 nm kinetics of the LA catalysis in the cuvette with $625\mu M NAD^+$ in 50 mM Tris-HCl and 100 U/ml LDH in PBS 1x. . . . .	132
4.53	CV measurements on DSCs of the LA/LDH/NAD solutions at the end of the UV-Vis kinetics. . . . .	132
4.54	LA calibration curve. The inset reports the same current values in function of the experimental NADH concentrations calculated from the UV-Vis data at the end of the kinetics measurements. . . . .	133
4.55	Correlation plot of the UV-Vis spectrophotometric and of the Cyclic Voltammetry measurements for the LA detection. . . . .	134
5.1	UV-Visible spectra of beef and veal urine dilutions in HBRS. . . . .	136
5.2	339 nm absorbance values of beef and veal urine dilutions in HBRS. . . . .	137
5.3	CV measurements of beef and veal urine dilutions in HBRS. . . . .	137
5.4	456 mV oxidation current values of beef and veal urine dilutions in HBRS. . . . .	138
5.5	339 nm kinetics of veal urine dilutions in HBRS. . . . .	139

5.6	CV measurements of veal urine dilutions in HBRS, after the end of the UV-Vis kinetics measurements. . . . .	140
5.7	UV-Vis kinetic measurements at 339 nm of the catalysis of LA dissolved in urine. . . . .	141
5.8	UV-Vis calibration plot of the NADH steady state concentrations obtained from the catalysis of LA dissolved in veal urine. The lines represents the NADH concentrations obtained by the tests in pure veal urine. . . . .	141
5.9	Average CVs obtained from the measurements of the LA in urine solution after the catalysis. The measurements are plotted in three graphics in order to distinguish them clearly. The first measurement in urine without added LA is plotted in all the graphics as reference (red curve). . . . .	142
5.10	Average currents and related standard deviations, recorded at 456 mV, of the CV measurements on the LA in urine solutions after the catalysis. . . . .	143
5.11	Correlation plot of the steady state NADH concentration obtained from the UV-Vis measurements, and of the currents recorded at 456 mV during the CV measurements on the same solutions. The star and the asterisk represent the NADH and $I_p$ values for the measurements in veal urine without the LA addition. . . . .	144
5.12	NADH concentrations obtained at the end of the LA catalysis kinetics in different urine dilutions in HBRS. The inset shows the 339 nm kinetics recorded for the LA concentrations (HBRS continuous line, urine 1% dashed line, urine 10% dashed-dotted line, urine 100% dotted line). . . . .	144
5.13	UV-Vis calibration curves reporting the NADH concentrations at the end of the LA catalysis kinetics in different urine dilutions in HBRS. . . . .	145
5.14	Cyclic voltammeteries measured in different LA concentrations in the urine dilutions, after the LA catalysis by the LDH enzyme (HBRS red curves, urine 1% blue curves, urine 10% magenta curves, urine 100% black curves). . . . .	146
5.15	Biosensor calibration curves of LA in urine dilutions in HBRS. The dashed lines represent the 456 mV current values recorded for each calibration curve in the UV-Vis blanking solution. . . . .	147
5.16	Correlation plot of the NADH concentrations obtained from the 339 nm absorbance values at the end of the kinetics, and the 456 mV currents measured by CV on the same solutions. . . . .	148
5.17	UV-Vis spectrophotometric kinetics of the NADH formation at 340 nm in the quartz cuvette containing the LDH enzyme and the $NAD^+$ cofactor and the cells samples. . . . .	150
5.18	Average currents and related standard deviations obtained by cyclic Voltammeteries on three devices per each cells sample and sampling time of the first cell cultures set. The black curves represent the blank measurements, performed adding HBRS instead of the cell sample in the quartz cuvette. . . . .	151
5.19	Average currents and related standard deviations obtained by cyclic Voltammeteries on six devices per each cells sample and sampling time, three for the first cell cultures set and three for the second one. The black curves represent the blank measurements, performed adding HBRS instead of the cell sample in the quartz cuvette. . . . .	152
5.20	Calibration plot of the UV-Vis spectrophotometric measurements (control technique) and of the electrochemical cyclic voltammetric NADH (lactate) detection techniques for the data of the two cell samples sets. . . . .	153



---

5.21	UV-Vis spectrophotometric kinetics of the NADH formation at 340 nm in the quartz cuvette containing the LDH enzyme and the $NAD^+$ cofactor and the cells samples. . . . .	154
5.22	Steady-state NADH concentrations obtained from the NADH formation kinetics measured by UV-Vis spectrophotometry at 300 seconds. . . . .	155
5.23	Average currents and related standard deviations obtained by cyclic Voltammeteries on three devices per each cells sample and sampling time of the first cell cultures set. The black curves represent the blank measurements, performed adding HBRS instead of the cell sample in the quartz cuvette. . . . .	156
5.24	Average oxidation currents recorded at 456 mV during the cyclic voltammeteries on the first set cell samples. . . . .	156
5.25	Average currents and related standard deviations obtained by cyclic Voltammeteries on six devices per each cells sample and sampling time, three for the first cell cultures set and three for the second one. The black curves represent the blank measurements, performed adding HBRS instead of the cell sample in the quartz cuvette. . . . .	157
5.26	Average oxidation currents recorded at 456 mV during the cyclic voltammeteries on the cell samples of the first and second sets. . . . .	158
5.27	Calibration plot of the UV-Vis spectrophotometric measurements (control technique) and of the electrochemical cyclic voltammetric NADH (lactate) detection techniques for the data of the two cell samples sets. . . . .	158

# List of Tables

2.1	Main illegal anabolic substances tested in bovines, their categories, and their control concentrations in the respective sample materials. . . . .	11
2.2	Results of the PNR 2014 divided by substance category. . . . .	12
2.3	Main illegal anabolic substances tested in bovines, their categories, and their control concentrations in the respective sample materials. . . . .	14
3.1	Common cell types, their origin, and cells morphology . . . . .	39
3.2	Example of cell growth/maintenance media and common buffers compositions (given in mg/l). Tris-HCl composition refers to a pH 8.8 solution. . . . .	47
3.3	Main illicit anabolic substances, their categories, and the cell receptors which detect them. . . . .	62
3.4	Main illicit anabolic substances, their categories, and the cell receptors which detect them. . . . .	63
3.5	Number of cells before and after the six day experiment in DMEM without FBS for the selected cell lines. . . . .	64
3.6	Luciferase test results for the C2C7 cells transfected by the IGF1 modified pGL4 vector with respect to the basic vector. . . . .	77
4.1	NADH calibration curves linear fits parameters for the detection in 50 mM Tris-HCl and in HBRS. . . . .	122
4.2	Michaelis-Menten kinetics parameters obtained by the catalysis velocity curves fits, with three LDH dilutions. . . . .	126
5.1	Coefficients of the linear fits of the correlation plot data for the urine dilutions. . . . .	147
5.2	456 mV average currents and related standard deviations obtained for the DSC devices, and the cells experiments reproducibility tests. . . . .	152

# Abbreviations

<b>CV</b>	<b>Cyclic Voltammetry</b>
<b>DMEM</b>	<b>Dulbecco's Modified Eagle's Medium</b>
<b>EIS</b>	<b>Electromchemical Impedance Spectroscopy</b>
<b>ERK</b>	<b>Extracellular Regulated Kinase</b>
<b>HBRS</b>	<b>HEPES Buffered Ringer's Solution</b>
<b>IGF-I (or Igf1)</b>	<b>Insulin growth Factor 1</b>
<b>LA</b>	<b>Lactic Acid</b>
<b>LDH</b>	<b>Lactate DeHydrogenase</b>
<b>LOx</b>	<b>Lactate Oxidase</b>
<b>MAPK</b>	<b>Mitogen Activated Protein Kinase</b>
<b>MCH</b>	<b>MerCapto-1-Hexanol</b>
<b>NAD</b>	<b>Nicotinamide Adenine Dinucleotide (oxidized)</b>
<b>NADH</b>	<b>Nicotinamide Adenine Dinucleotide (reduced)</b>
<b>PA</b>	<b>Pyruvic Acid</b>
<b>PBS</b>	<b>Phosphate Buffered Saline</b>
<b>PEDOT</b>	<b>Poly(3,4-EthyleneDioxyThiophene)</b>
<b>SAM</b>	<b>Self-Assembling Monolayer</b>

*To my parents and to Catalina Li Puma, as a small reward for  
their sustain and encouragement*

# Chapter 1

## Introduction

### 1.1 Meat market in Europe

In terms of value, in Europe bovine animals represent 8.1% of total agricultural output and 33% of animal output, without taking account of animal products (e.g., milk).

The major part of the meat bovine herd is located in four European Member States: France (34.5%), Spain (14.9%), the United Kingdom (13.0%) and Ireland (9.1%). Together, they represent more than 70% of the European meat herd. This type of herd is susceptible to changes in the sector's limited profitability and is thus sensitive to the level of subsidies from the common agricultural policy. Between 2009 and 2013, production of meat from heifers and bulls fell in both EU-28 (-10%) and EU-15 (-13%). However, there has been an increase for veal, i.e. meat from calves (aged under 8 months) and young cattle (aged between 8 and 12 months), and for which production increased by around 27% in the EU-28 and 30% for EU-15 during this period. Meanwhile, the average carcass weight has increased by 2% for adult cattle (aged one year and over) and by 7% for calves and young cattle.

Italy is the fourth European country in the production of beef and veal, after France and Germany as can be seen in figure 1.1 and in the table of figure 1.2. However, Italy imports more than the 25% of the bovine meat which consumes (ERSAF - Market evolution service 2011).

Compared with pigmeat production, beef production has a longer production cycle (figure 1.3), its feed efficiency is lower and the value of individual animals is higher. In addition, the diversity of animals produced for slaughter (feeding mode, age, dairy or meat breeds) makes the production systems more complex. All these factors have led to tight margins and low profitability. The purchasing power of consumers is also a key

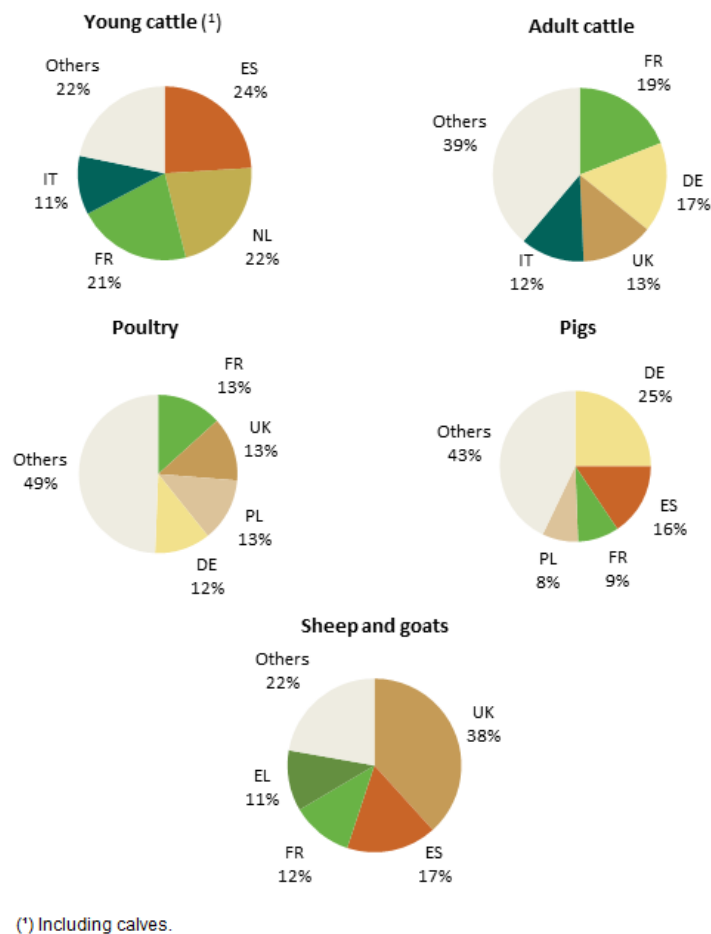


FIGURE 1.1: Meat production in Europe in 2013

determinant of the level of meat consumption. This is noticeable especially in the beef and veal sector where prices are significantly higher than for pig (or poultry) meat. This explains why pigs and poultry are raised and consumed much more in Europe.

In the recent years, the Italian consumer has shown an increased lack of confidence toward the consumption of meat products and particularly towards the meat of ruminant animals. The main reasons of this negative trend are:

- The new food habits of the young generations;
- The negative impact of the food scandals involving meat products;
- The progressive decline of the organoleptic traits of the meat.

As in many other North European Countries, Italy is showing a continuous increase in the number of vegetarians particularly among the young generations. Support to this trend comes by the progressive concern of the people about the animal rights and the

	Total	Calves and young cattle	Heifers	Cows	Bullocks	Bulls
<b>EU-28</b>	<b>7 271.7</b>	<b>1 008.5</b>	<b>1 033.2</b>	<b>2 140.1</b>	<b>623.9</b>	<b>2 465.9</b>
Belgium	249.9	54.4	2.5	115.9	0.0	77.2
Bulgaria	5.7	0.8	0.7	3.1	:	:
Czech Republic	64.8	0.7	5.3	26.6	0.1	32.2
Denmark	125.2	27.8	11.6	59.5	2.3	24.4
Germany	1 106.0	56.0	139.0	363.0	8.0	541.0
Estonia	7.6	0.1	0.7	4.7	0.1	2.0
Ireland	517.6	0.9	137.9	112.3	186.3	80.3
Greece	50.1	7.8	5.0	7.2	0.9	29.2
Spain	580.8	242.2	68.1	90.1	1.9	178.7
France	1 407.9	214.1	142.2	582.5	69.0	400.2
Croatia	47.3	5.8	5.1	8.1	0.0	28.7
Italy	855.3	110.2	158.7	141.7	3.5	441.2
Cyprus	5.2	0.9	0.5	1.3	0.0	1.8
Latvia	15.7	1.1	2.3	8.5	0.0	3.8
Lithuania	36.8	0.5	4.8	18.1	0.0	13.5
Luxembourg	8.0	0.2	1.4	2.0	0.3	4.1
Hungary	22.6	0.6	1.9	15.5	0.0	4.7
Malta	1.1	0.0	0.1	0.4	0.0	0.7
Netherlands	379.1	222.4	2.8	130.5	0.0	23.3
Austria	227.2	7.1	31.7	64.5	10.4	113.6
Poland	339.0	6.1	41.7	100.2	0.0	191.0
Portugal	84.1	21.5	9.8	17.3	0.6	34.9
Romania	29.3	7.1	1.7	14.6	1.3	4.6
Slovenia	32.1	1.8	3.1	5.6	0.2	21.4
Slovakia	9.5	0.1	0.6	4.8	0.0	4.0
Finland	80.4	0.3	9.6	23.7	0.0	46.8
Sweden	135.7	14.1	16.2	41.9	9.5	54.1
United Kingdom	847.7	4.1	228.2	176.9	329.6	108.8
Iceland	3.8	0.0	0.5	1.4	0.0	1.4
Serbia	35.5	3.2	3.4	4.9	0.0	23.9

FIGURE 1.2: Production of beef and veal, by type of bovine animals in 2013 (Eurostat 2013)

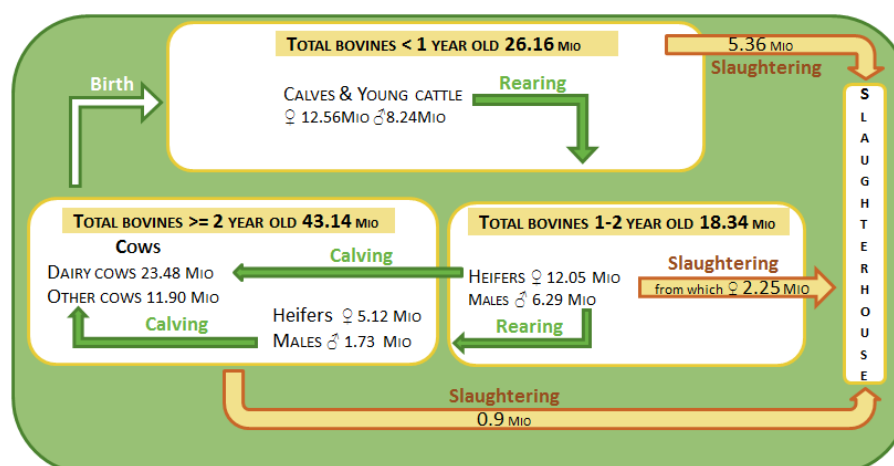


FIGURE 1.3: Bovine livestock and its production cycle in Europe (Eurostat 2013)

rearing conditions of the farm animals which has led to the issue of several EU regulations in the matter of animal welfare (EU, 2003). Food scandals like the BSE or the dioxin-contaminated poultry in Belgium or those ones related to anabolic treatments, have created a negative shadow on the safety and genuineness of meat products. In April 2000, the Italian Institute of Food Research and Nutrition (INRAN, 2000) carried out an opinion poll on what Italian consumers thought about the food safety at that time. Virtually, every Italian had heard about the BSE problem. People were also very much aware of the cases of food-born botulism and salmonella that occurred in Italy shortly before the poll as well as the discovery of dioxin-contaminated poultry and eggs in Belgium. Therefore, it was not surprising that they rated meat and eggs to be unsafe foods.

A recent poll carried out to understand the consumer perception of food quality by the Italian consumer has rated in the top positions factors such as genuineness and safety leaving flavor and cost behind (figure 1.4).

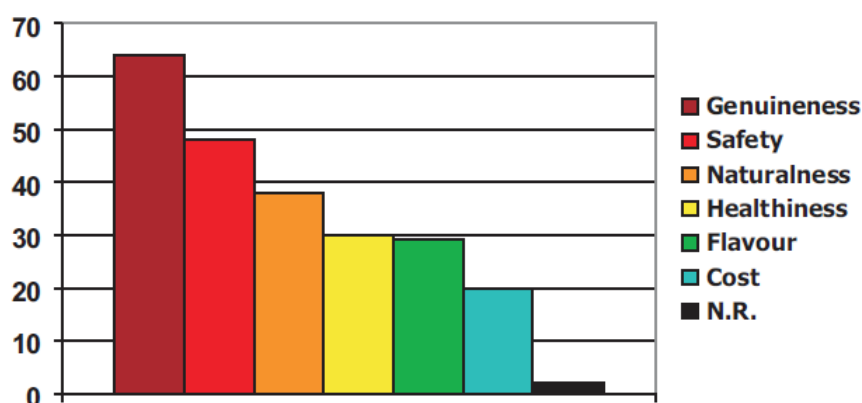


FIGURE 1.4: The main meaning of food quality for Italian consumers (%)

The general decline observed in the organoleptic traits of the meat has arisen from several reasons. In the case of red meat the loss of taste and flavour can be mainly related to the reduced marbling since the lipid fraction plays a key role in the determination of these traits [1]. Moreover, the reduced intramuscular fat deposition has a negative effect on meat tenderness which in cattle has also been worsened by the progressive reduction in the time of muscle tissue maturation after slaughtering [2] and this could be related also to the anabolic treatments.

## 1.2 Illegal anabolic treatments in cattle breeding

In this big market, there is the need to check, both the imported meat and the internally produced one, for the presence of substances and compounds which can be dangerous



for the consumer health. Between all these compounds, a particular class is that one of the anabolic substances, which are used by the breeders to increase the muscle growth of the animal and thus to increase their profits. For this reason, Europe has introduced a plan for the control of meat and each member state has to carry on control policies which have to satisfy this plan's points. In Italy, these controls are performed within the National Residues Plan, which is described in Chapter 2.

At the present time these controls are hampered by the enormous number of anabolic substances which can be employed and by the use of always new substances. This forces the control authorities in a continuous race for the insertion of these new substances on the "black list", as the creation of a new antibiotic in medicine is accompanied by the apparition of new resistant bacteria. Therefore, in the present the need is for control systems which are not sensitive to the presence of a substance but to its effects on the animal. For this reason histological tests on animal's organs have been introduced as screening method for anabolic treatments control, but this method and the standard substances identification and quantification techniques still have a lot of problems (as discussed in Chapter 2). Two main problems, which limit the applicability of the anabolic treatments controls are the impossibility of on-the-field measurements, the time consumption of the tests, and their costs.

### 1.3 Engineered cells and organisms

In recent years our ability and knowledge about the manipulation of the genetic material of cells and organisms has led to smart solutions in several sectors as agriculture, healthcare, and energy harvesting. Genetic engineering consists in the modification of the genetic material of an organism or a cell in order to alter the expression of particular proteins by the organism.

In agriculture, the genetically modified organisms (GMO) are plants which express proteins able to protect them from the action of parasites or from severe climate conditions, and to increase the productivity. In the healthcare sector, the recombinant DNA technology is used to produce widely used drugs such as insulin and human growth hormone, decreasing their costs, or to fight genetic diseases.

Nowadays, modified organisms for biomass treatments are becoming a promising improvement in the energy harvesting sector, allowing to generate fuel gasses like hydrogen or methane from biomass.

Cells, engineered or not are currently used also in the biosensors field. Monitoring systems for the cells adhesion over substrates or for cells electroporation have been realized

by micro-electrodes arrays and electrochemical impedance measurements. Cells receptors have been used as biological components for the detection of toxins or particular proteins, monitoring the cells detachment from conductive surfaces.

## 1.4 Electrochemical biosensors

Biosensors are systems formed by a bio-component, such as enzymes, antibodies, DNA, cells or tissues and by a transducer, which can be electrochemical, optical, acoustic etc. The bio-component is sensitive to a particular substance, the analyte, which has to be detected by the biosensor. The interaction between the bio-component and the analyte is sensed by transducer which converts this event to a signal that can be elaborated.

There are two types of interaction between the bio-component and the analyte: the affinity interaction, where the analyte specifically binds to the bio-component, and the catalytic interaction, in which the enzymatic bio-component reacts with the analyte producing substances detectable by the transducer.

Nowadays, biosensors are a widespread technology in our society. It's sufficient to think to the pregnancy tests, based on colorimetric or electrochemical hormones detection by specific antibodies (affinity interaction), or to the glucose measurement systems, used by people affected by diabetes and based on the electrochemical detection of the enzyme-based glucose catalysis products (catalytic interaction).

Electrochemical enzyme-based biosensors constitutes one of the most classical biosensors category that has been studied since 1960, and is normally characterized by the electrochemical detection of the products of a catalytic reaction. Usually, the reaction takes place on electrodes covered by the enzyme. A potential is applied to these electrodes and the resulting current, proportional to the catalysis products and thus to the analyte concentration, is read through the same electrodes. There exist several techniques for this kind of measurements, applying different potential signals as sinusoidal waves or ramps. Two of the most common are Electrochemical Impedance Spectroscopy (EIS) and Cyclic Voltammetry (CV).

## 1.5 The Myo-Screen project

The Myo-Screen project has the goal to design, develop and validate a biosensor to detect the presence of anabolic compounds in living breeding animals by a rapid, non-invasive, and on-the-field screening of a small urine sample. The main innovation brought by this project is the detection of the anabolic substances presence in the sample, not by their formulation or structure, but by their common hypertrophic effect on a culture of

mouse myogenic cells. Therefore, the biosensor will be able to detect the presence of any anabolic compound, even of the unknown ones, by their effect.

The hypertrophic effect on the myogenic cells, induced by the anabolic substances in the urine sample, will be monitored by an electrochemical biosensor. This will be possible engineering the myogenic cells to over-produce lactate in presence of the anabolic substances, and detecting the lactate production by the biosensor.

Figure 1.5 illustrates the working principle of the Myo-Screen system: the animal urine sample (1.5a) is poured into the myogenic mouse cell culture (1.5b) and incubated for a fixed time. During this time the cells' receptors bind the anabolic substances present in the urine sample and start a signaling cascade inside the cells (1.5c), which causes the lactate overproduction in the cells medium (1.5d). The cell medium is then removed and added by the Lactate Dehydrogenase enzyme (LDH) which catalyzes the lactate conversion in pyruvate producing also the same concentration of a compound called NADH (1.5e). Finally, the NADH produced is oxidized on a carbon screen-printed sensor, obtaining an electrical current proportional to its concentration (1.5f), and thus allowing to verify the presence of anabolic substances in the animal urine sample.

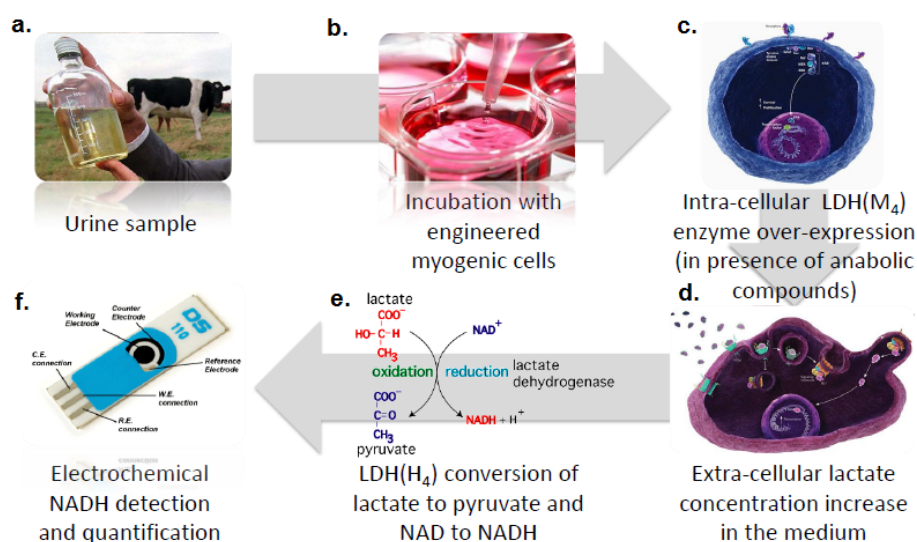


FIGURE 1.5: Myo-Screen project working principle.

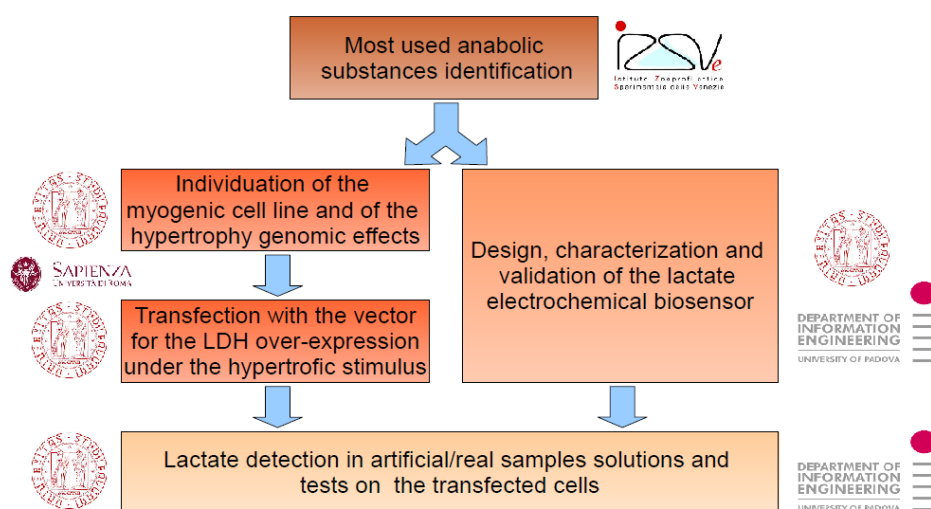
This project has been carried on by four partners:

- University of Padova - Departments of Biomedical Sciences and of Information Engineering
- The Association of the Veneto region meat producers (UNICARVE)
- The Experimental Zoo-prophylactic Institute of Venice (IZSvE)
- University "La Sapienza", Rome



## 1.6 Work Packages

The work has been divided into five parts: the first part dealt with the individuation and classification of the most used anabolic compounds in animal breeding, and with the determination of the specific cell receptors for these substances. These tasks have been carried out by the IZSve. The second part consisted in the individuation of a myogenic cell line with the anabolic compounds receptors, and in the determination of the genomic effects of induced hypertrophy on these cells. In the third part of the work, the promoters of the over-expressed genes by the hypertrophic stimuli have been used for the transfection of the gene codifying for the L-Lactate Dehydrogenase enzyme (LDH). This causes an increment of the intracellular and extracellular lactate concentration in presence of anabolic compounds. Both the second and third parts involved the Biomedical Sciences Department of the University of Padova, with the advice of the University of Rome, "La Sapienza". The fourth part of the work had the goal to design and develop a reliable lactate electrochemical biosensor, able to detect the lactate over-production of the cells in presence of anabolic compounds. This work package has been carried on in parallel with the second and the third ones. Finally, the last part of the work deals with the integration of the cellular and the sensor parts, and with the validation of the whole biosensor on real samples, reducing the possible interferences due to the wide variety of substances which will be present in the final solution, in contact with the biosensor. The last two work packages have been performed with the collaboration of the Information Engineering Department of the University of Padova.



## Chapter 2

# Illegal anabolic treatments to cattle breeding

### 2.1 History

The illegal use of anabolic substances on breeding animals took place in Italy since 1960. This procedure allows to improve the nutrients assimilation from the animals, obtaining an increase of the muscle growth rate, and consequently softer and less fat meats [3]. The problem of the effects of the anabolic substances treatments on health are under discussion since 1981, when the WHO regional office for Europe took stock of the situation of these substances use in Europe and defined limits and detection methods for each substance [4]. Today, it's known that the exposure to growth factors is harmful for the animal and for the consumer, causing damages to the endocrine glands and to the immune system. Moreover, these substances are also potentially at the origin of genotoxic and carcinogenic effects [5].

The current legislation in Italy prohibits the dispensation of these substances, if not for defined therapeutic or zoo-technical treatments [6].

### 2.2 National Residues Plan

In Italy, the activities related to the residual controls in food are planned and reported in the annual National Residues Plan (PNR). The actuation of this plan has the goal to detect pharmacological active substances, contaminants and residues within the animal breeding process and during the first transformation of the animal origin products.

These compounds presence is checked in the living animals, in their feces, in the biological

liquids and tissues, in animal origin products, and in animal feeding and water.

The PNR is actuated in order to find out the cases of:

- Administration of illegal substances;
- Abusive administration of authorized substances in not authorized conditions;
- Non conformity of the vet medicines residues with the maximal limits (UE n.37/2010);
- Non conformity of the pesticides and environmental contaminants quantities.

This plan identifies the competent authorities for planning, coordinating, verifying and executing the official controls, and also to actuate the non conformity actions. These authorities are the following:

- The Health Ministry (central authority): for the annual arrangement of the plan, and to coordinate the regional services for the residues surveillance, and of all the control services for the use of illegal substances or products in breeding. Moreover, the central authority is responsible for the information collection, for the evaluation of the actions, and of the obtained results. Finally, the central authority has the duty to transmit the collected information to the European Commission.
- Regional Departments of Health and Agriculture (regional authority): are responsible for the repartition of the Regional Residues Plan actions and to coordinate the activities of the territorial vet services (Local Health Agencies - ASL). The regional authority has also the responsibility to verify the correct plan execution and to establish the Regional Operational Supervision Units (NORV).
- Local Health Agencies - ASL (local authority): have the duty to perform the official controls and to execute the following non-conformity actions.

The residues and substances to be quantified in the collected samples, defined by the legislative ordinance 158 of the 16th of March 2006 are reported in the following table.

The PNR control tests sampling is performed unexpectedly and in not fixed moments or days of the week, with variable intervals during the year. The activities related to the PNR are mainly three:

- Planned activities: which are organized by the ministry, depending on the volumes of the national productions and following the European regulations;

Category	Subtype	A - Anabolic substances and illegal substances
Group A	A1	Stilbens and derived salts and esters
	A2	Antithyroid agents
	A3	Steroids
	A4	Resorcilic acid lactones
	A5	$\beta$ -agonists
	A6	Substances included in the CEE rule n. 2377/90
Category	Subtype	B - Veterinary medicines and contaminant agents
Group B	B1	Antibacterial substances
	B2a	Antielmintics
	B2b	Coccidiostatics
	B2c	Carbamamats and piretroids
	B2d	Tranquillants
	B2e	NSAIDs
	B2f	Other substances with pharmacological actions
	B3a	Organochlorurated compounds
	B3b	Organophosphate compounds
	B3c	Chemical elements
	B3d	Mycotoxins
	B3e	Colorants
	B3f	Other

TABLE 2.1: Main illegal anabolic substances tested in bovines, their categories, and their control concentrations in the respective sample materials.

- Extra-plan activities: extra sampling disposed by the Ministry or the Regions toward specific targets if the planned activities proved the non conformity of the related samples;
- Suspect: extra sampling disposed in case of suspects after histo-anatomical-pathologic tests.

The samples are analyzed by the accredited laboratories of the Zoo-prophylactic Experimental Institutes (ISZ) network, with techniques and criteria approved by the 2002/657/CE decision.

All the ISZs monthly upload the results obtained in the informative system NSIS/PNR for the samples of their competence. The regional departments verify the information in the system and validate them for the transmission to the Ministry and to the European Commission.

In 2014, the planned activities of the PNR allowed to test 40806 samples, 16276 for the presence of residues of category A (39.9 % of the total), and 24530 for category B (60.1% of the total).

The highest number of samples have been collected for bovines (191625), overcoming the minimum number of samples recommended by the Community standards. In particular,

in the Veneto region, the bovine samples have been the 131.5% of the planned number. The analysis of the samples have been mainly directed to substances of the categories B1 and B2, as represented in figure 2.1, while the 41% of the analysis have been directed to category A substances (anabolic substances).

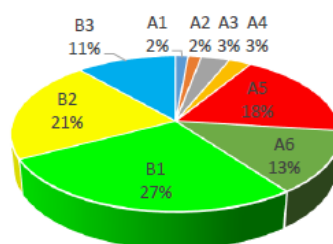


FIGURE 2.1: Percentage distribution of the analyzed samples in actuation of the PNR 2014 divided by substance group category (see table 2.1)

In 2014, the samples which resulted in the excess of residues from the analysis have been 44 (the 0.11% of the total of the analyzed samples). In the 34.1% of the positive samples it has been detected the presence of substances of category A, while the 65.9% was characterized by the presence of substances of category B, as schematized in the following table.

Category	Sample analyzed	Not complying samples
<b>A</b>	<b>16276</b>	<b>15</b>
A1	587	0
A2	616	0
A3	1325	0
A4	1052	13
A5	7422	0
A6	5274	2
<b>B</b>	<b>24530</b>	<b>29</b>
<b>B1</b>	<b>11185</b>	<b>15</b>
<b>B2</b>	<b>8679</b>	<b>6</b>
<b>B3</b>	<b>4666</b>	<b>8</b>
<b>Total</b>	<b>40806</b>	<b>44</b>

TABLE 2.2: Results of the PNR 2014 divided by substance category.

The results obtained in 2014 are in line with the trend recorded during the last years, both in terms of analyzed samples and of not complying ones. Moreover, the not complying samples percentage is in line with the results obtained by the other EU states in 2014 (0.11%)

The PNR plan procedures state that the freezed samples must be delivered to the analysis lab within 4 days from the sampling. Anyway, only 9 regions over 21 respected this delivery time for more than the 95% of the samples. Veneto respected the delivery time



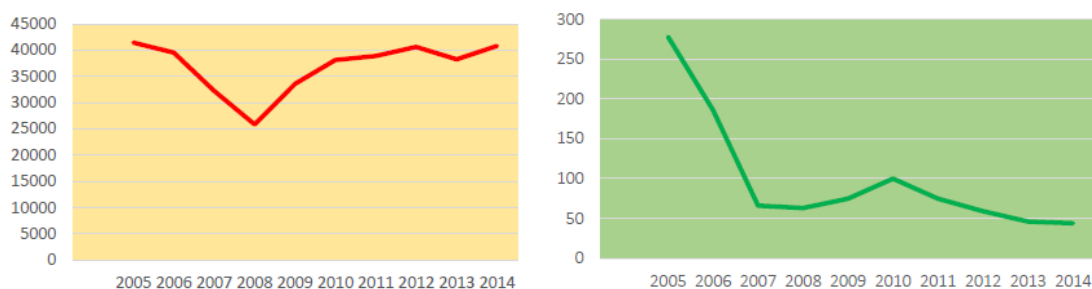


FIGURE 2.2: Trends of the number of analyzed samples (on the left) and of the number of not complying samples (on the right) in recent years.

for the 83.7% of the samples and the average percentage has been 92.6%.

When the samples are delivered to the laboratories, the maximum time allowed for the emission of the analytic report is of 14 days for the detection of category A substances and of 42 days for the detection of category B compounds. Only one Region over 21 respected both these times for more than the 90% of the samples. The Veneto Region respected the cat. A substances analysis time and the cat. B one, for respectively the 91.8% and the 78.6% of the samples.

## 2.3 Anabolic compound detection

The main families of anabolic substances used in cattle breeding, with their control levels and the respective fluids or locus of investigation are reported in table 2.3.

To analyze the animal samples several techniques are available but all of them need advanced laboratory procedures and a variable amount of time which is usually longer than a week.

### 2.3.1 Analytical techniques for cat. A samples analysis

The most used techniques for the detection of anabolic substances (cat. A) in bovine samples are mass spectrometry (MS) and gas chromatography (GC) which can also be used in tandem configuration [7], [8].

#### 2.3.1.1 Mass spectrometry (MS)

The main technique used for the analytical tests on the samples is mass spectrometry. This technique is based on the ionization of a molecule and on its consecutive fragmentation in ions with different mass/charge ratio ( $M/z$ ). The mass spectrometry experiment consists in the ionization of gas phase molecules, in the separation of the produced ions

Substance	Category	Sample	Control level
Diethylstilbestrol	Stilbens	Urine	1.0 $\mu\text{g}/\text{kg}$
Dienestrol	Stilbens	Urine	1.0 $\mu\text{g}/\text{kg}$
Esestrol	Stilbens	Urine	1.0 $\mu\text{g}/\text{kg}$
Thiouracile	Thyroid antagonists	Urine, Thyroid	10.0 $\mu\text{g}/\text{kg}$
Methylthiouracile	Thyroid antagonists	Urine, Thyroid	10.0 $\mu\text{g}/\text{kg}$
Propylthiouracile	Thyroid antagonists	Urine, Thyroid	10.0 $\mu\text{g}/\text{kg}$
Fenylthiouracile	Thyroid antagonists	Urine, Thyroid	10.0 $\mu\text{g}/\text{kg}$
Tapazole	Thyroid antagonists	Urine, Thyroid	10.0 $\mu\text{g}/\text{kg}$
Mercaptobenzoimidazole	Thyroid antagonists	Urine, Thyroid	10.0 $\mu\text{g}/\text{kg}$
Ethynilestradiol	Synthetic estrogens	Muscle	2.0 $\mu\text{g}/\text{kg}$
Estradiol	Estrogens (natural)	Plasma, Urine	0.04 $\mu\text{g}/\text{kg}$
Testosterone	Androgens (natural)	Plasma, Urine	10.0 $\mu\text{g}/\text{kg}$
Progesterone	Progestinics (natural)	Plasma, Urine	1.0 $\mu\text{g}/\text{kg}$
Methyltestosterone	Androgens (synthetic)	Urine	1.0 $\mu\text{g}/\text{kg}$
Nortestosterone	Androgens, (synthetic)	Urine	2.0 $\mu\text{g}/\text{kg}$
Trenbolone	Androgens, (synthetic)	Urine	2.0 $\mu\text{g}/\text{kg}$
Boldenone	Androgens, (synthetic)	Urine	1.0 $\mu\text{g}/\text{kg}$
Zeranol	Resorcilic acid lactones	Urine	2.0 $\mu\text{g}/\text{kg}$
Clenbuterol	Clenbut.-like $\beta$ -agonists	Urine, liver	1.0 $\mu\text{g}/\text{kg}$
Bhromebuterol	Clenbut.-like $\beta$ -agonists	Urine, liver	1.0 $\mu\text{g}/\text{kg}$
Clenpenterol	Clenbut.-like $\beta$ -agonists	Urine, liver	1.0 $\mu\text{g}/\text{kg}$
Mabuterol	Clenbut.-like $\beta$ -agonists	Urine, liver	1.0 $\mu\text{g}/\text{kg}$
Mapenterol	Clenbut.-like $\beta$ -agonists	Urine, liver	1.0 $\mu\text{g}/\text{kg}$
Cimaterol	Clenbut.-like $\beta$ -agonists	Urine, liver	1.0 $\mu\text{g}/\text{kg}$
Cimbuterol	Clenbut.-like $\beta$ -agonists	Urine, liver	1.0 $\mu\text{g}/\text{kg}$
Salbutamol	Salbut.-like $\beta$ -agonists	Urine, liver	3.0 $\mu\text{g}/\text{kg}$
Terbutaline	Salbut.-like $\beta$ -agonists	Urine, liver	3.0 $\mu\text{g}/\text{kg}$
Isoxuprine	Salbut.-like $\beta$ -agonists	Urine, liver	3.0 $\mu\text{g}/\text{kg}$
Ractopamine	Salbut.-like $\beta$ -agonists	Urine, liver	3.0 $\mu\text{g}/\text{kg}$
Zilpaterol	Salbut.-like $\beta$ -agonists	Urine, liver	3.0 $\mu\text{g}/\text{kg}$

TABLE 2.3: Main illegal anabolic substances tested in bovines, their categories, and their control concentrations in the respective sample materials.

and in their detection. The experiment result is the mass spectrum which represents the abundance of the ions with respect to their  $M/z$  ratio. The fragmentation profiles obtained by mass spectrometry are peculiar of each compound and constitutes its fingerprint. This allows for the individuation of the structure formula even of small quantities of unknown compounds.

The sample introduction in the ionization chamber can be done both for solid samples (using a probe), and for liquid/gas samples, by a valves system which allows to get the access to the chamber without any contamination from the external. The sample quantity needed is in the micrograms/nanograms orders of magnitude. It's possible to use the output of a GC or HPLC system as input for the mass spectrometer. These techniques called GC-MS and HPLC-MS are very useful in the analysis of products mix.

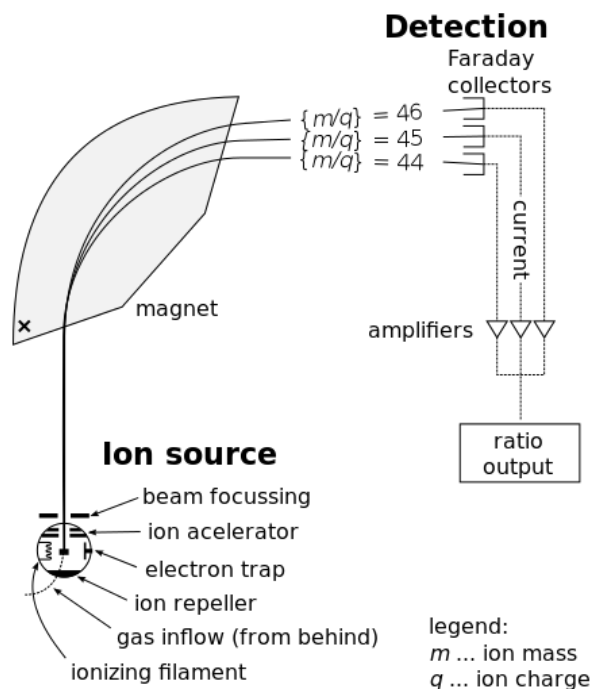


FIGURE 2.3: Scheme of a mass spectrometry system.

The sample is ionized in the ionization chamber where an ionic source produces an electronic beam which hits and ionizes the sample molecules. The electrons which didn't hit the molecules are collected by an electron trap and the not ionized molecules are removed by the high vacuum pump. The ionized molecules are accelerated and carried to the analyzer.

Depending on the power of the ionization the MS techniques can be distinguished in hard techniques, which cause a high fragmentation, and soft techniques. The analyzer can be of different types:

- Magnetic analyzer - is the most used as it allows for the highest resolution. It's based on the deflection by a magnetic field through a curved pipe, selecting the ions with a particular  $M/z$  ratio;
- Double focus analyzer - it adds an electrostatic filter after the magnetic selector in order to further focus the ions beam;
- Quadrupole analyzer - it's constituted by four cylinders kept at an oscillating potential which cause the ions to have a particular trajectory, which becomes sinusoidal if they have a particular  $M/z$  ratio;
- Ionic trap analyzer - it's a variant of the quadrupole analyzer which uses three electrodes to create an ion trap, in order to increase the sensitivity.

Finally, the detecting unit usually is an electronic multiplier composed by a cascade of electrodes.

### 2.3.1.2 Gas chromatography (GC)

It's a common type of chromatography used to separate and analyze compounds that can be vaporized without decomposition. This technique is often used to separate the different components of a mixture in order to prepare the samples for other identification techniques, e.g. mass spectrometry.

In gas chromatography, the so called mobile phase is a carrier gas, usually helium (inert) or nitrogen (unreactive), while the stationary phase is a microscopic layer of liquid or polymer on an inert solid support inside a glass or metal tubing called column. The gaseous compounds being analyzed interact with the walls of the column, which is coated with the stationary phase. This causes each compound to elute at a different time, known as the retention time of each compound. The differences between the retention times allow to separate the compounds in the mixture.

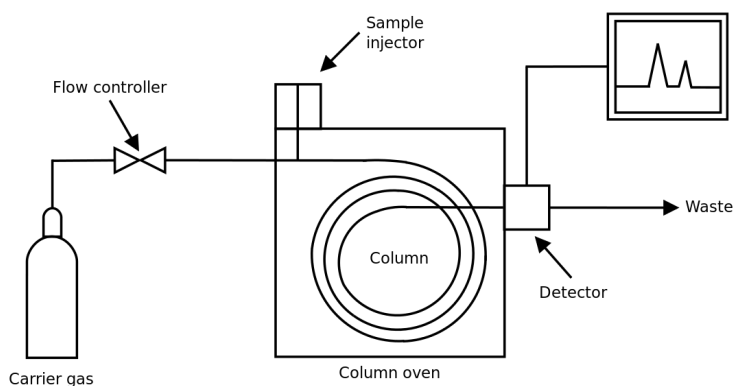


FIGURE 2.4: Schematics of a gas chromatography system

A detector is used to monitor the outlet stream from the column, thus the time at which each component reaches the outlet and the amount of that component can be determined. Generally, substances are qualitatively identified by the order in which they emerge from the column and by the retention time of the analyte in the column.

The most commonly used detectors are the flame ionization detector (FID) and the thermal conductivity detector (TCD). Both are sensitive to a wide range of components, and both work over a wide range of concentrations. While TCDs are essentially universal and can be used to detect any component other than the carrier gas (as long as their thermal conductivities are different from that of the carrier gas, at detector temperature), FIDs are sensitive primarily to hydrocarbons, and are more sensitive to them than TCD. However, a FID cannot detect water. Both detectors are also quite robust. Since

TCD is non-destructive, it can be operated in-series before a FID (destructive), thus providing complementary detection of the same analytes.

The type of detector determines also which gas to use as the carrier gas. Typical carrier gases include helium, nitrogen, argon, hydrogen and air. When analyzing gas samples, however, the carrier selection is sometimes based on the sample's matrix, for example, when analyzing a mixture in argon, an argon carrier is preferred, because the argon in the sample does not show up on the chromatogram. Safety and availability can also influence carrier selection, for example, hydrogen is flammable, and high-purity helium can be difficult to obtain in some areas of the world. As a result of helium becoming more scarce, hydrogen is often being substituted for helium as a carrier gas in several applications.

The purity of the carrier gas is also frequently determined by the detector, though the level of sensitivity needed can also play a significant role. Typically, purities of 99.995% or higher are used. The most common purity grades required by modern instruments for the majority of sensitivities are 5.0 grades, or 99.999% pure meaning that there is a total of 10 ppm of impurities in the carrier gas that could affect the results. The highest purity grades in common use are 6.0 grades, but the need for detection at very low levels in some forensic and environmental applications has driven the need for carrier gases at 7.0 grade purity and these are now commercially available. Trade names for typical purities include "Zero Grade," "Ultra-High Purity (UHP) Grade," "4.5 Grade" and "5.0 Grade."

The column in a GC are contained in an oven, the temperature of which is precisely controlled electronically. The rate at which a sample passes through the column is directly proportional to the temperature of the column. The higher the column temperature, the faster the sample moves through the column. However, the faster a sample moves through the column, the less it interacts with the stationary phase, and the less the analytes are separated. In general, the column temperature is selected to compromise between the length of the analysis and the level of separation.

The carrier gas linear velocity affects the analysis in the same way that temperature does (see above). The higher the linear velocity the faster the analysis, but the lower the separation between analytes. Selecting the linear velocity is therefore the same compromise between the level of separation and length of analysis as selecting the column temperature. The linear velocity will be implemented by means of the carrier gas flow rate, with regards to the inner diameter of the column.

Regarding the stationary phase, the polarity of the solute is crucial for its choice, which in an optimal case would have a similar polarity as the solute. Common stationary phases in open tubular columns are cyanopropylphenyl dimethyl polysiloxane, carbowax polyethyleneglycol, biscyanopropyl cyanopropylphenyl polysiloxane and diphenyl dimethyl polysiloxane. For packed columns more options are available.

The real chromatographic analysis starts with the introduction of the sample onto the column. The development of capillary gas chromatography resulted in many practical problems with the injection technique. The technique of on-column injection, often used with packed columns, is usually not possible with capillary columns. The injection system in the capillary gas chromatograph should fulfill the following two requirements:

1. The amount injected should not overload the column;
2. The width of the injected plug should be small compared to the spreading due to the chromatographic process. Failure to comply with this requirement will reduce the separation capability of the column. As a general rule, the volume injected and the volume of the detector cell should be about 1/10 of the volume occupied by the portion of sample containing the molecules of interest (analytes) when they exit the column.

The choice of column depends on the sample and the active measured. The main chemical attribute regarded when choosing a column is the polarity of the mixture, but functional groups can play a large part in column selection. The polarity of the sample must closely match the polarity of the column stationary phase to increase resolution and separation while reducing run time. The separation and run time also depends on the film thickness (of the stationary phase), the column diameter and the column length.

### **2.3.2 Histological tests**

In 2013, EFSA published the "Scientific opinion on the public health hazards to be covered by inspection of meat (bovine animals)" [5]. This article reports the use of samples like feces, eyes, hairs, etc. for the analysis because of the higher persistence of residues in them. Moreover, the use of indirect techniques such as genomic, proteomic and metabolomic tests is encouraged for the identification of treated animals.

In Italy, the Health Ministry recently associated the histology tests to the chemical analysis of the samples, in order to look for Histo-anato-pathological damages in organs collected in the slaughter houses. This techniques, in the case of positive results, authorizes the traditional investigation in the company of origin of the suspected animal. The histological test individuates the microscopic alterations induced by growth promoting substances (natural or synthetic anabolic substances) on target organs i.e. thymus, thyroid and sexual glands. This kind of control allows for the detection of the secondary biological effect of molecules like steroids, thyreostatics and cortisonics, which effect remains longer than in the official samples for the chemical analysis (serum, liver,

urine, hairs, eyes, muscle, thyroid, adipose tissue). However, this type of analysis gives only the probability that an animal has been treated with anabolic substances.

The 2014 PNR histological tests has been conducted by the CIBA (National Reference Center for the Anabolic Substances Investigations) which detected an increment in the cortisone treatments and a similar number of suspected anabolic treatments, with respect to the previous years. However, some Regions didn't participate to the tests, i.e., Veneto and Basilicata.

With this kind of tests the estimations indicate that almost the 15% of the bovine animals could be subject to illegal anabolic treatments in our country [9].

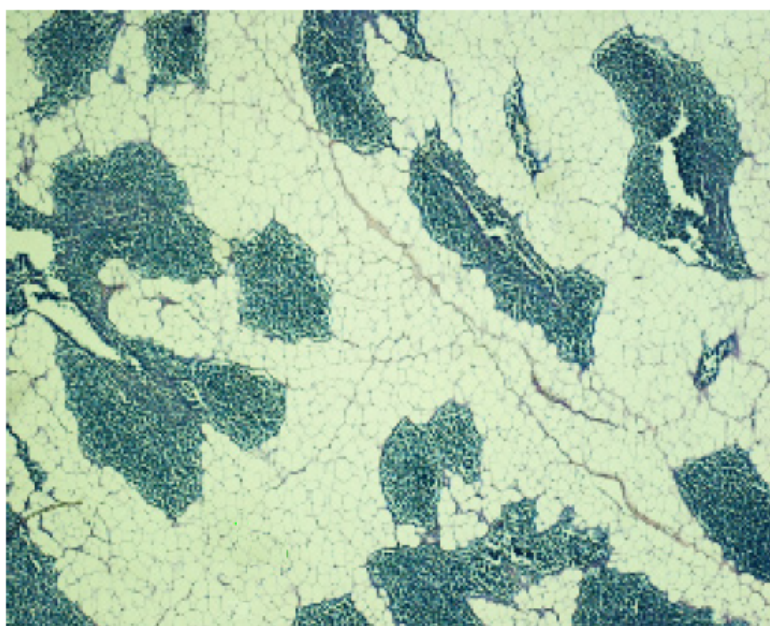


FIGURE 2.5: Example of a positive hystologic sample of a seven month bovine. The anabolic treatments caused a huge increase in the adipose tissue (the white cells) in the thymus [9].

There is a huge difference between this conclusion and the 0.11% of treatments individuated by the standard techniques. This difference highlights the possible inappropriateness of the standard techniques as weapons to stem the anabolic treatments diffusion.

### 2.3.3 Issues with the present detection techniques

There are several issues within the detection techniques nowadays used to monitor the use of anabolic substances in cattle breeding. The recent introduction of histological tests as control procedure in the official PNR protocol is a step forward. However, this technique is based on a probabilistic approach, thus it can only rise the suspect of illegal

treatments which will need further investigations.

Moreover, the histological test is performed on the animal organs, therefore it's possible only when the animal is processed at the slaughterhouse. This means that the eventual suspects verifications will take place on other animals of the same breeder.

Another relevant drawback of all the techniques presented above is the fact that they have to be performed in a laboratory, with consistent efforts for the sample delivering, the possibility of damages and the needing of trained personnel and time, with the related high costs.

Conversely, a detection technique "on-the-field" would allow to perform rapid controls by a minimally trained person, and to increase their frequency, and consequently increasing the "surprise effect" on the breeder.

Anyway, the most problematic issue of all these techniques, and more generally of this anabolic substances control approach, is that everything depend from the official list of banned substances.

This list states what is permitted and what is forbidden but, even though it's continually updated, it can't contain all the illegal substances which are used. The illegal pharmaceutical commerce behind the animal anabolic treatments carries always new substances to the market and even the old ones, not controlled anymore, sometimes reappear.

## **2.4 The Myo-Screen project: problems and solutions**

The issues and problems related to the present anabolic substances detection techniques, described in the previous paragraph, are the innovation boost through the development of innovative detection methods. Nowadays, the focus of the new techniques is not on the substance detection but on its effects revelation, as with the histological tests on the animal's organs.

With this method, the identification of the substance type is not important because the goal, at least in a first screening step, is just the verification of the presence of the hypertrophic effects in the animal organism. However, since the histological tests are based on different animal organs, there is always the possibility that the variations observed could be due to something not related to the illegal anabolic substances, such as pathologies or peculiarities of the animal.

Therefore, these results need a confirmation by the standard substance detection techniques.

The key idea behind the Myo-Screen project is to follow this new direction toward the identification of the anabolic substances effects, but on a mouse myogenic cell culture prepared in the laboratory, and put in contact with a urine sample of the animal suspected to be treated by illegal substances. These type of cells, deeply described in



the following chapter, undergoes severe modifications if exposed to anabolic substances, which cause an hypertrophic effect and the expression of several proteins. Therefore, the cell culture state monitoring will allow for the detection of the illegal substances presence (over certain concentrations) in the animal urine.

In order to simplify the observation of the anabolic substances effect on the myogenic cell culture, the cells have been modified to express the Lactate Dehydrogenase (LDH) enzyme in presence of these substances. This causes the increase of the intra- and extra-cellular lactate concentrations, which can be detected by a portable electrochemical lactate sensor, testing the cell's solution after the cells exposition to the animal urine sample.

For the prototype of the Myo-Screen project system, a single anabolic substance has been selected for the tests on real urine samples by the Experimental Zoo-prophylactic Institute of Legnaro (IZSVe). This substance is Clenbuterol and has been found to be widely used for the illegal cattle anabolic treatments. Other important substances, used in the preliminary tests on the cells are Testosterone and 17- $\beta$  Estradiol, as presented in the next chapter.

## Chapter 3

# Myogenic cells for hypertrophy transduction

### 3.1 The skeletal muscle

The skeletal muscle is a complex biological machine which converts chemical energy into mechanical and thermal energy. Each muscle is composed by thousands of large elongated cells, called muscle fibers placed in parallel to each other and connected at both ends to tendons. Each muscle is covered by three layers of connective tissue: epimysium, perimysium and endomysium. The first one contains the entire muscle and is formed by a dense layer of collagen fibers which separate the muscle from the nearby tissues and organs. The perimysium is made by interstitial connective tissue and divides the muscle in compartments. Each compartment contains a set of muscular fibers called fascicle. Perimysium also contains nerves and blood vessels. Inside a fascicle, each muscle fiber is surrounded by a basal membrane and by reticular connective fibers called endomysium, that links the muscle fiber to the other ones. This layer of reticular fibers contains a network of blood vessels and nerves contacting directly the single muscle fibers. Between the muscle fiber and the connective envelope there are some stem cells for the reparation of the damaged muscle tissue called satellite cells. These cells can proliferate, merge and form new fibers. At each end of the muscle, the collagen fibers of epimysium, perimysium and endomysium converge into a unique dense connective tissue called tendon, by which muscles are attached to the bones.

Each mature muscle fiber has a characteristic cylindrical shape, its diameter varies between 100 and 500  $\mu m$ , and can reach a length of some centimeters. The fiber contains several nuclei beneath the plasmatic membrane (called sarcolemma). Inside the fiber there are long cylindrical elements called myofibrils, with a diameter of about 1-3  $\mu m$ ,

which fill virtually the entire fiber volume.

In the remaining space inside the fibers there are a small Golgi apparatus, many mitochondria, the endoplasmic/sarcoplasmic reticulum, glycogen, and myoglobin, a chromoprotein which binds oxygen and gives to the fibers the characteristic red color. Importantly, the fibers contain a particular form of endoplasmic reticulum, called sarcoplasmic reticulum which acts as calcium storage. Muscle fibers appear striated as their internal myofibrils structure is highly organized. The myofibrils unit are responsible for the muscle contraction and are composed by a regular distribution of cytoskeletal elements, i.e., myosin and actin filaments.

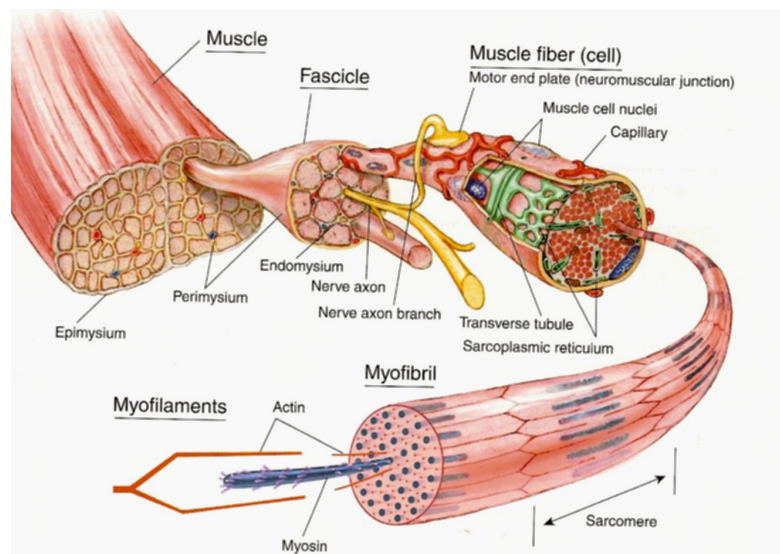


FIGURE 3.1: Structure of the skeletal muscle and its substructures organization.

The muscle contraction function has the goal to generate force, both to keep the body balance, and to produce movements. The muscle contraction process involves several phases, i.e., the excitation, excitation-contraction, and contraction phases. The skeletal muscle communicates with the nervous system thanks to neuromuscular junctions. Actually, the skeletal muscle fibers are innervated by the motoneuron- $\alpha$  axons terminals, which determine the contraction of the muscle fiber.

The muscle contraction needs high amounts of energy. This energy derives from the ATP, which is consumed at a rate 100 folds higher in maximal contraction compared to rest state. ATP is available for the muscle through different biochemical processes:

1. Phosphocreatine - When muscle fiber is in rest condition, it produces more ATP than what is needed. The excess ATP can be accumulated as phosphocreatine, a high energy compound. During the contraction, myosin consumes ATP, producing ADP and inorganic phosphate. The energy stored in phosphocreatine is used to

regenerate ATP from ADP in a reaction catalyzed by the enzyme creatinephosphokinase (CPK). A muscle fiber in rest state contains a creatinephosphate concentration six times greater than ATP concentration. When the fiber is contracting for a prolonged period of time, this amount allows to maintain the ATP available for no more than 15 seconds.

2. ATP production - Glycolysis is an anaerobic process used by the cells to produce two molecules of ATP from each molecule of glucose. During this process also pyruvic acid is produced and when it enters in the Krebs cycle it allows to obtain 17 ATP molecules per each pyruvic acid molecule employed, in a process called oxidative phosphorylation. This process is possible only in presence of oxygen which is supplied by blood. Therefore, when the energy request is low and oxygen is available, large amount of ATP is produced by oxidative phosphorilayion, while ATP is produced by glycolysis when the muscle is engaged in a heavy and short exercise condition since the oxygen available is not enough. When the ATP is produced by the anaerobic glicolysis, the process produces more pyruvic acid than what is needed, thus its concentration increases. To reduce the NADH oxidized during glycolysis it is converted to lactic acid. Lactic acid is then released from the fibers and transported to the liver where it can be converted back in glucose. High amount of piruvic and lactic acid can cause a decrease of pH in muscle cells and in the whole body. When the ATP is produced by the anaerobic glicolysis, the process produces more pyruvic acid than what is needed, thus its concentration increase in the sarcolemma and it's reduced to lactic acid. Lactic acid is then transported to the liver where it's converted back in glucose but it also decrease the pH in the muscle cells, causing pain during intense exercise.

Depending on metabolism, the skeletal muscle fibers can be classified in four types [10]:

- Type I: slowly contracting oxidative fibers which are characterized by a dark color due to myoglobine presence, a small diameter and contain abundant oxidative enzymes. These fibers are fatigue resistant;
- Type IIB: fast contracting glycolytic fibers, not resistant to fatigue. These fibers have a large sarcoplasmatic reticulum for the rapid release of calcium ions and are characterized by an anaerobic metabolism;
- Type IIA: fast contracting oxidative-glycolitic fatigue resistant fibers;
- Type IIX: which have characteristic intermediate between type IIA and IIB.

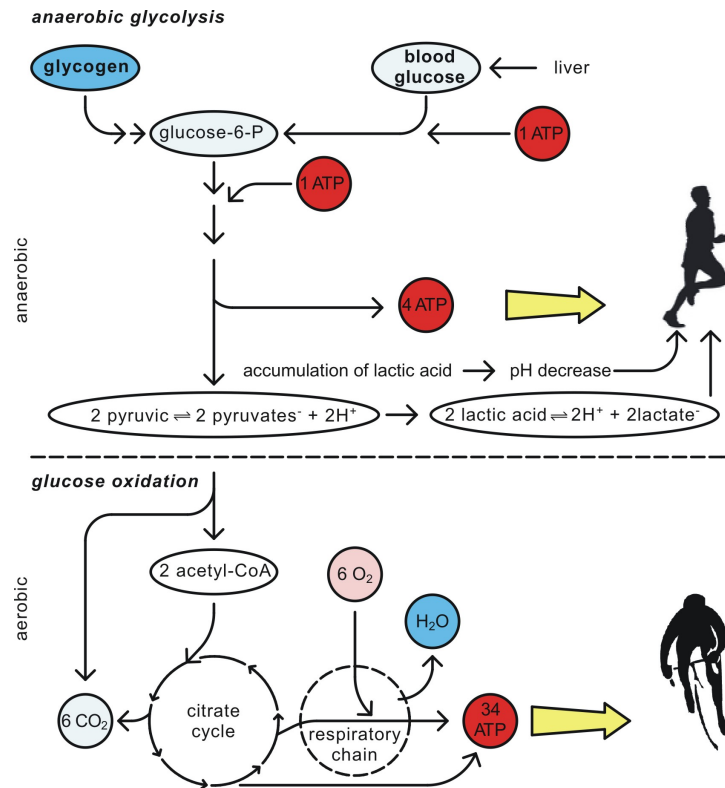


FIGURE 3.2: Scheme of the metabolic pathways for the generation of ATP in the aerobic and anaerobic cases.

Different types of fibers have different types of myosin molecules. In fact, both the myosin heavy and light chains are present with different isoforms [10] with different and distinct distributions. Most skeletal muscles have both fast and slow fibers in a specific proportion and the improvement related to the training type are partly based on change of this proportion.

### 3.2 Cell signaling and receptors

The millions of cells that make up a multicellular organism can work together only because they continually exchange chemical messages called transmitters. Transmitter mechanisms can be classified in two ways. The first depends on their lifetime in the extracellular fluid. A transmitter that is rapidly broken down or taken up into cells acts only near its release site. One that is broken down slowly can diffuse a long way and may act on cells a long way away. The shortest lived transmitters of all are those released at synapses, where the distance from release site to receptor is only 100 nm. At the other extreme are transmitters that last many minutes or, sometimes, even longer. Hormones are long-lived transmitters that are released into the blood and travel around the body before being broken down. Most are released by specialized groups of secretory

cells that form a structure called an endocrine gland. Paracrine transmitters may also last many minutes before being broken down, but they are released into specific tissues rather than into the blood, and only diffuse within the tissue before they are destroyed. The second way of classifying transmitter mechanisms depends on the location and action of the receptor on the target cell. There are three types of receptors: ionotropic cell surface receptors, metabotropic cell surface receptors, and intracellular receptors.

### 3.2.1 Ionotropic cell surface receptors

Ionotropic cell surface receptors are channels that open when a specific chemical binds to the extracellular face of the channel protein. The nicotinic acetylcholine receptor, so named because the drug nicotine binds to it, is one example. In the absence of a transmitter called acetylcholine, the channel is closed. When acetylcholine binds, the channel opens and allows ions to pass through. The electrochemical gradient driving sodium ions into the cell is much greater than that driving potassium ions out of the cell, so when the channel opens, sodium ions enter the cell carrying positive charge and depolarizing the plasma membrane. A similar mechanism holds for the inositol trisphosphate-gated calcium channel. There is, however, a major difference: the IP3 channels are opened by cytosolic solutes, while ionotropic cell surface receptors are opened by extracellular solutes, such as acetylcholine.

### 3.2.2 Metabotropic cell surface receptors

Metabotropic cell surface receptors are linked to enzymes. When the ADP receptor binds extracellular ADP, it activates  $G_q$  and hence phospholipase  $C_\beta$ . The  $\beta$ -adrenergic receptor are linked to  $G_s$  and hence adenylate cyclase and this enzyme increases cytosolic cAMP. Tyrosine kinase receptors are themselves protein kinases which are activated when their ligand binds. The  $\alpha$ -adrenergic receptor is another receptor that causes cytosolic calcium concentration to increase, mainly acting through phospholipase C activation. The  $\alpha$ - and  $\beta$ -adrenergic receptors are distinct membrane proteins that bind the same transmitters, adrenaline and noradrenaline. To simplify the issue somewhat, we can say that noradrenaline acts mainly on  $\alpha$  receptors and adrenaline acts mainly on  $\beta$  receptors. Because the  $\alpha$  and  $\beta$  receptors are distinct proteins, it is possible to design drugs ( $\alpha$  and  $\beta$  blockers) that interfere separately with one or the other.

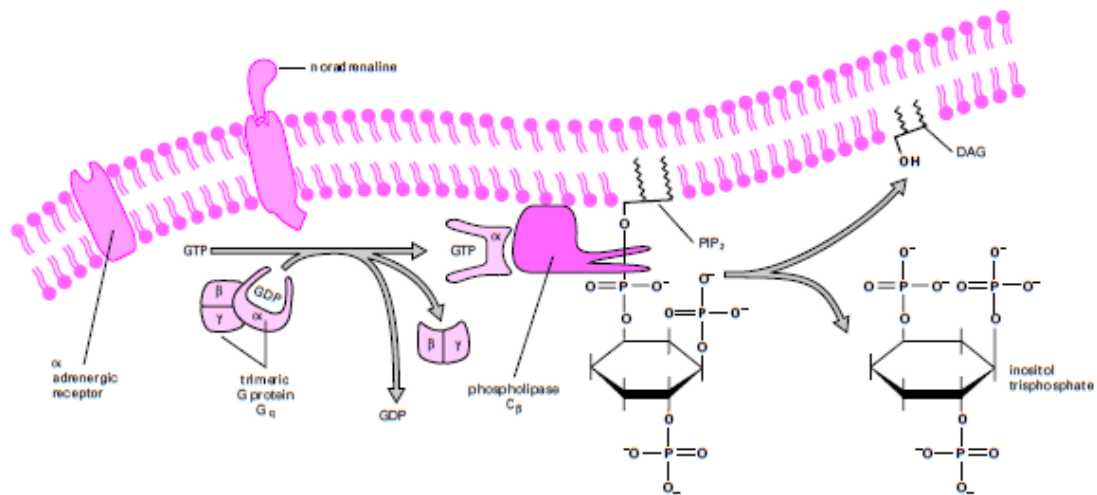


FIGURE 3.3: Noradrenaline activates  $G_q$  and hence phospholipase  $C_\beta$  in many cells including smooth muscle.

### 3.2.3 Intracellular cell surface receptors

Intracellular receptors are localized within the cell (mainly in the cytosol) and bind transmitters that diffuse through the plasma membrane. The receptors for nitric oxide and steroid hormones are two examples.

Nitric oxide, or NO, is a transmitter in many tissues. It is not stored ready to be released but is made from arginine at the time it is needed. NO diffuses easily through the plasma membrane and binds to various cytosolic proteins that are NO receptors. One particularly important NO receptor is the enzyme guanylate cyclase, which in the presence of NO converts the nucleotide GTP to the intracellular messenger cyclic guanosine monophosphate, or cGMP.

Steroid hormones have intracellular receptors such as the glucocorticoid receptor. In the absence of hormone this receptor remains in the cytosol and is inactive because it is bound to an inhibitor protein. However, when the glucocorticoid hormone binds to its receptor, the inhibitor protein is displaced. The complex of the glucocorticoid receptor with its attached hormone now moves into the nucleus. Here two molecules of the complex bind to a 15-bp sequence known as the hormone response element (HRE), which lies upstream of the TATA box. The HRE is a transcriptional enhancer sequence. The binding of the glucocorticoid hormone receptor to the HRE stimulates transcription.

### 3.2.4 The MAPK pathway

The MAPK (Mitogen-Activated Protein Kinase) pathway is one of the primordial signaling systems that nature has used in several permutations to accomplish an amazing variety of tasks. It exists in all eukaryotes, and controls such fundamental cellular processes as Proliferation, Differentiation, Survival and Apoptosis. Mammalian MAPK can be divided into four groups based on their structure and function: ERKs (Extracellular signal-Regulated Kinases), p38MAPKs, JNKs (c-Jun NH<sub>2</sub>-terminal Kinases) and ERK5 (Extracellular signal-Regulated Kinase-5) or BMK. Activation of these MAPKs occurs through a cascade of upstream kinases; a MAPKKK (MAPK Kinase Kinase) first phosphorylates a dual-specificity protein kinase MAPKK (MAPK Kinase), which in turn phosphorylates the MAPK. This set-up provides not only for signal amplification, but, maybe even more importantly, for additional regulatory interfaces that allow the kinetics, duration and amplitude of the activity to be precisely tuned. ERK, a member of the MAPK family, have been established as major participants in the regulation of cell growth and differentiation, but when improperly activated contribute to malignant transformation. ERK1 and 2 form a central component in the MAPK cascade. The MAPK/ERK signaling cascade is activated by a wide variety of receptors involved in growth and differentiation including GPCRs (G-Protein Coupled Receptors), RTKs (Receptor Tyrosine Kinases), Integrins, and Ion channels. The specific components of the cascade vary greatly among different stimuli, but the architecture of the pathway usually includes a set of adaptors like SHC, GRB2 (Growth Factor Receptor Bound protein-2), Crk, etc. linking the receptor to a GEF (Guanine nucleotide Exchange Factor) like SOS (Son of Sevenless), C3G, etc. transducing the signal to small GTP binding proteins (Ras, Rap1), which in turn activate the core unit of the cascade composed of a MAPKKK (Raf), a MAPKK (MEK1/2 (MAPK/ERK Kinase-1/2)) and MAPK (ERK). An activated ERK dimer can regulate targets in the cytosol and also translocate to the nucleus where it phosphorylates a variety of transcription factors regulating gene expression [11], [12]. GPCRs constitute a superfamily of Plasma membrane receptors. Members of this family include receptors for many Hormones, Neurotransmitters, Chemokines and Calcium ion, as well as sensory receptors for various odors, and bitter and sweet tastes. GPCR play an important role in activation of ERKs. Stimulation of the GN-AlphaI (Guanine Nucleotide Binding Protein-Alpha Inhibiting Activity Polypeptide)-coupled Neuropeptide Y1 and GN-AlphaQ (Guanine Nucleotide-Binding Protein-Alpha-Q) -coupled Muscarinic M1 Acetylcholine Receptors lead to the activation of ERK. When the GPCR becomes activated, it leads to the exchange of GDP for GTP on the GN-Alpha subunit. Upon activation, GN-AlphaI or GN-AlphaQ subunits are separated from GN-Beta (Guanine Nucleotide-Binding Protein-Beta) and GN-Gamma (Guanine Nucleotide-Binding Protein-Gamma) subunits and are converted to their GTP



bound states that exhibit distinctive regulatory features on the nine tmACs (Transmembrane Adenylate Cyclases) in order to regulate intracellular cAMP (Cyclic Adenosine 3',5'-monophosphate) levels. cAMP activate Rap1A (Ras-Related Protein-1A) and Rap1B (Ras-Related Protein Rap1B) through EPAC (Exchange Protein Activated by cAMP)-dependent pathway. cAMP activates cAMP-GEFI (cAMP-Regulated Guanine Nucleotide Exchange Factor-I)/EPAC1 and cAMP-GEFII (cAMP-Regulated Guanine Nucleotide Exchange Factor-II)/EPAC2 that in turn activate Rap1A and Rap1B, respectively. Rap1A and Rap1B then forms an active complex with BRaf (v-Raf Murine Sarcoma Viral Oncogene Homolog-B1) for MEK1/2 activation finally resulting in ERK1/2 activation. cAMP may also activate PKA (Protein Kinase-A), which may further activate Rap and thus BRaf. On the other hand, PKA also inactivates C-Raf. GN-Alpha also directly activate PI3K (Phosphatidylinositide-3 Kinase) and c-Src and modulate their activity through stimulation of Ras under the influence of many extracellular factors. Rac is also a key downstream target/effector of PI3K. A new mechanism have been identified that regulates MEK1-ERK interactions and is dependent on Rac and PAK (p21-Activated Kinase). Besides GN-Alpha subunit, GN-Beta Gamma complex can also lead to activation of ERK. GN-Beta and GN-Gamma subunits when activated separate from GN-alpha subunit and it further activates PKC (Protein Kinase-C) via PLC-Beta (Phospholipase-C-Beta). PLC-Beta converts PIP2 (Phosphatidylinositol 4,5-bisphosphate) to DAG (Diacylglycerol), which activates PKC. PKC once formed can activate ERKs via Ras, Raf and MEKs. PKC also activates Src-PYK2 (Proline-Rich Tyrosine Kinase-2) complex which activates GRB2, which is also involved in ERK activation [13], [14].

The canonical ERK MAPK cascade is also stimulated upon the binding of extracellular Growth factors to their respective transmembrane RTKs (Receptor Tyrosine Kinases). The subsequent auto-phosphorylation of the cytoplasmic tails of the receptor on tyrosine leads to the tyrosine phosphorylation of the adapter protein SHC. SHC can then recruit the GRB2-SOS complex to the membrane via the SH2 domain of GRB2 binding to the phosphotyrosine on SHC. SOS, a GEF for Ras, can then exchange the GDP bound to Ras to GTP. Once Ras binds GTP, it can then recruit the serine/threonine kinase Raf to the membrane. When Raf translocate to the membrane, it becomes activated and then phosphorylates the dual specificity kinase MEK. MEK binds and restricts inactive ERK to the cytosol. The MEK and ERK complex dissociates when MEK is activated and phosphorylates ERK. The ERK may then dimerize and this dimerization is apparently required for ERK to translocate into the nucleus by an active functions. Growth Factors may also activate ERK through PLC-Gamma and PKC. Integrins also play an important role in regulating the efficiency of the RTK/Ras/ERK pathway. Integrin regulation occurs at three (or more) different loci within the ERK pathway. First, in

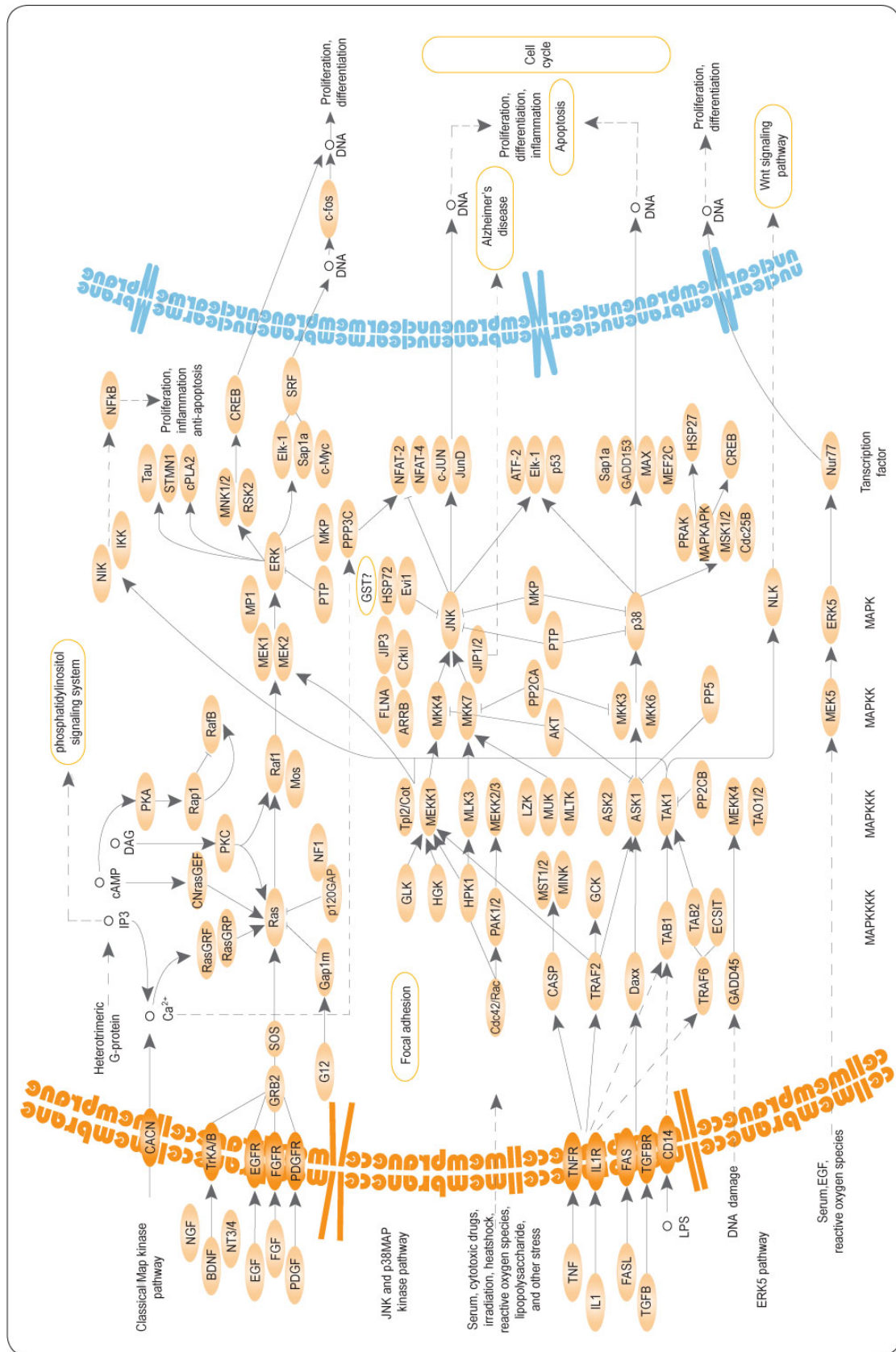


FIGURE 3.4: MAPK signaling pathway scheme, from the cell membrane receptors to the DNA expression regulation.

some cell systems, Integrin engagement with ligands enhances the activation and autophosphorylation of the RTKs. Secondly, Integrin engagement enhances the efficiency of the cytoplasmic cascade comprising Raf1, MEK and ERK. Finally, Integrin engagement is necessary for trafficking of activated ERK from the cytoplasm to the nucleus. FAK (Focal Adhesion Kinase) is a major nonreceptor tyrosine kinase activated after Integrin-mediated adhesion to ECM (Extracellular Matrix) proteins such as FN (Fibronectin). Interaction between FAK and the cytoplasmic tail of Beta1 Integrins results in autophosphorylation of FAK tyrosine 397 (FAK pY397) that can lead to stimulation of a cell-signaling cascade that ultimately activates the Ras/MAPK/ERK pathway. In addition to FAK, members of the Src family of nonreceptor protein-tyrosine kinases also associate with focal adhesions and are involved in Integrin signaling. Interestingly, Src and FAK appear to function in association with each other as a result of the binding of the Src SH2 domain to an autophosphorylation site of FAK. Src then phosphorylates additional sites on FAK. Tyrosine phosphorylation of FAK creates binding sites for the SH2 domains of other downstream signaling molecules, including PI3K and Rac. A key target of Rac is the protein-serine/threonine kinase PAK. Rac and CDC42 (Cell Division Cycle-42) can synergize with Raf to promote activation of the ERKs through mechanisms involving PAK1 phosphorylation of the MEK1 proline-rich sequence and PAK3 phosphorylation of Raf1. PAK3 can phosphorylate Raf1, enhancing Raf1 activation. Raf1 finally activates ERK1/2 via MEK1/2. The non-receptor tyrosine kinase PYK2 appears to function at a point of convergence of Integrins and certain GPCR signaling cascades. PYK2 acts with Src to link GN-AlphaI- and GN-AlphaQ-coupled receptors with GRB2 and SOS to activate the ERK signalling pathway [15], [16].

TCR (T-Cell Receptor)-CD3 complex also plays an important role in regulating ERK pathways in T-Cells. VHR is particularly interesting from a TCR signalling point of view because it accumulates at the T-Cell/APC (Antigen-Presenting-Cell) contact site, where it is phosphorylated at Tyr-138 by ZAP70 (Zeta-Chain-Associated Protein Kinase). This phosphorylation is required for VHR to inhibit the ERK MAPKs, giving ZAP70 an unanticipated control over MAPK dephosphorylation, in addition to its role as upstream activator of the Ras/Raf/MEK pathway. Other negative regulators of ERK pathway include PP2A (Protein Phosphatase-2A) and MKPs (MAPK Phosphatase). PP2A inhibits ERK pathway by dephosphorylating MEKs and is involved in the control of many cellular functions including metabolism, transcription, translation, RNA splicing, DNA replication, cell cycle progression, transformation, and apoptosis. The mammalian MAPK signaling system employ scaffold proteins, in part, to organize the MAPK signaling components into functional MAPK modules, thereby enabling the efficient activation of specific MAPK pathways. The ERK scaffold protein KSR (kinase suppressor of Ras) binds ERK, its direct activator MEK and Raf. In unstimulated

cells KSR is mainly cytoplasmic but translocates to the Plasma membrane after growth factor stimulation, thus targeting MEK and ERK to the plasma membrane. A second targeting protein, p14, targets ERK2 to an endosomal location through its interaction with MP1 (MAPKK1-Interacting Protein-1), an adaptor protein that binds MEK and ERK. In addition, MEKK1 (MAP/ERK Kinase Kinase-1) can serve both as a scaffold and as MAPKKK, interacting specifically with MAPKK and MAPK [15], [17], [18].

ERK once activated can either translocate to the nucleus to phosphorylate and activate transcription factors, while other pools of activated ERK phosphorylate a number of cytoplasmic targets. Cytosolic substrates for ERK include several pathway components involved in ERK negative feedback regulation. Multiple residues on SOS are phosphorylated by ERK following growth factor stimulation. SOS phosphorylation destabilizes the SOS-GRB2 complex, eliminating SOS recruitment to the plasma membrane and interfering with Ras activation of the ERK pathway. Negative feedback by ERK also occurs through direct phosphorylation of the EGF (Epidermal Growth Factor) receptor at Thr669. Finally, ERKs have also been demonstrated to negatively regulate themselves by phosphorylating MKPs (MAP Kinase Phosphatases), which reduces the degradation of these phosphatases through the Ubiquitin-directed Proteasome complex. ERK also activate MNKs (MAPK-Interacting Kinases) by phosphorylation at Thr197 and Thr202. MNKs upregulate eIF4E (eukaryotic initiation factor-4E) through phosphorylation at Ser209 and play an important role in translation or they may also phosphorylate PLA2 (Phospholipase-A2). ERK1 and ERK2 regulate transcription indirectly by phosphorylating the RSKs (90 kDa Ribosomal protein S6 Kinases). Active RSKs appear to play a major role in transcriptional regulation, translocating to the nucleus and phosphorylating such factors as the product of proto-oncogene c-Fos at Ser362, SRF (Serum Response Factor) at Ser103, and CREB (Cyclic AMP Response Element-Binding protein) at Ser133. p90RSK also play an important role in cell survival by phosphorylating BAD (Bcl2-Antagonist of Cell Death). Another important cytoplasmic target of ERK is IKK-Alpha (I-KappaB Kinase-Alpha). IKK-Alpha phosphorylates I-KappaB-Alpha, which leads to ubiquitination and then leads to the degradation of I-KappaB-Alpha by the Proteasome, resulting in the translocation of NF-KappaB to the nucleus. In the nucleus it binds to its consensus sequence (5'-GGGACTTTC-3') and positively regulates the transcription of genes involved in immune and inflammatory responses, cell growth control, and apoptosis [19], [20].

Upon phosphorylation, nuclear translocation of ERK1 and ERK2 is critical for both gene expression and DNA replication induced by growth factors. In the nucleus, ERK phosphorylates an array of targets, including transcription factors and a family of RSK-related kinases, the MSKs (Mitogen- and Stress-activated protein Kinases). MSKs phosphorylate and activate the AP1 component ATF1 (Activating Transcription Factor-1)

at Ser63, and may be more important in vivo than RSKs in CREB phosphorylation at the activating Ser133. MSKs were also found to phosphorylate Histone H3 at Ser10 and Ser28, and the HMG14 (High-Mobility-Group protein-14) at Ser6, facilitating the rapid induction of immediate early genes following mitogenic stimulation. Probably the best-characterized transcription factor substrates of ERKs are TCFs (Ternary Complex Factors), including Elk1, which is directly phosphorylated by ERK1 and ERK2 at multiple sites, including the activating Ser383. Upon complex formation with SRF, phosphorylated TCFs transcriptionally activate the numerous Mitogen-inducible genes regulated by SREs (Serum Response Elements). TCFs Sap1 and Sap2 are also phosphorylated by ERK, as are other Ets family members. Another direct target of ERK is the product of proto-oncogene c-Myc, a short-lived transcription factor involved in multiple aspects of growth control. Following phosphorylation at Thr58 and Ser62 within its transactivation domain, Myc activates transcription as a heterodimeric partner with Max. ERK can also phosphorylate CREB directly as well as AP1 components c-Jun and c-Fos. ERK1/2 also phosphorylates MLCK (Myosin Light Polypeptide Kinase), Capn (Calpain), Pax6 (Paxillin-6) and FAK that play important role in Cytoskeletal rearrangement. Other ERK targets include STAT1/3 (Signal Transducer and Activator of Transcription-1/3) and ESR (Estrogen Receptor). Finally, it can be concluded that ERKs are involved in the regulation of important neuronal functions, including neuronal plasticity in normal and pathological conditions. The kinetics and localization of ERK are intrinsically linked, in that the duration of ERK activation dictates its subcellular compartmentalization and/or trafficking. The latter, in turn, dictates whether ERK-expressing cells would enter a program of cell death, survival or differentiation. With aberrations in the ERK cascade implicated in a high proportion of human cancers, many emerging therapies target proteins in the pathway. As these candidate therapies against ERK signaling components undergo development and enter trials, reagents that monitor their targets' inhibition are critical for future success [21], [22], [23].

### 3.2.5 The IGF1 signal system

The IGF-I (Insulin Growth Factor-I) represent an important muscle growth mediator [24]. There are different IGFI isoforms, those expressed in the skeletal muscle acting locally in an autocrine/paracrine way to stimulate muscle growth [25]. Several biological effects of IGF-I are mediated by the IGFI type I receptor, which has a hetero-tetrameric structure with an extracellular binding domain, a trans- membrane region, and an intracellular domain with tyrosine kinasic activity. IGF-I binds to the receptor which mediates the phosphorylation of tyrosine inside the cell. These tyrosine may belong to substrates like IRS-1 (Insulin receptor substrate-1) which activates the regulatory

subunit of the PI3K enzyme (Phosphatidylinositol 3-kinase). This, in turn, activates the Akt protein which phosphorylates a series of substrates mediating protein synthesis, gene transcription, and cell proliferation [26]. The most relevant target proteins in the hypertrophy induction are m-TOR (mammalian target of rapamycin), and GSK-3 $\beta$  (Glycogen synthase kinase-3) [27], [28].

Moreover IGF-I can induce hypertrophy through the activation of the transduction pathway of the calcineurin dependent signal, which involves the induction of the transcription factor NFAT [29].

### 3.2.6 The $\beta$ -adrenergic signal system

The chronic administration of  $\beta$ -adrenergic agonists, i.e., Clenbuterol, Formeterol and Albuterol, significantly stimulates the skeletal muscle hypertrophy [30], [31].

It has been observed that the adrenergic induced-hypertrophy is the result of an increase of the proteins synthesis and of the decrease of their degradation. In in vivo experiments, it has been observed a muscle mass increase, an increment of the RNA levels, of the proteins, and of the RNA/DNA and protein/DNA ratios. Even the protein synthesis rate has been increased by these substances [30].

Similar studies on mice skeletal muscle cells showed that the  $\beta$ -adrenergic agonists mediate the hypertrophic effect through the binding to the  $\beta$ 2-adrenergic receptor [32]. This receptor is a member of the super-family of the receptor connected to a G protein, and the binding with the ligand cause the G $\alpha$  subunit to activate. This induces the activation of the adenylate cyclase which, in turn, is responsible for the cAMP production (cyclic adenosine monophosphate). The increase of the cAMP levels causes the activation of protein kinase A (PKA), which promotes the transcription of several genes through the CREB phosphorylation (cAMP response element binding protein) activating the protein synthesis. Moreover, the adrenergic stimulation can also modulate the AKT-mTOR pathway, described in the previous paragraph [33], [34].

### 3.2.7 The steroids signalling system

The steroid hormones are chemical messengers synthesized from cholesterol. They are produced and released from several organs as gonads and adrenal glands. These hormones are not stored but, after a specific stimulus they are readily synthesized and released in the plasma where they have to bind to transport proteins since they are almost not soluble in water.

The steroid hormones can diffuse through the lipidic component of the plasma membrane and bind to specific intracellular receptors. Their action is defined as "genomic

effect” since the hormone-receptor complex moves to the nucleus, where it binds to specific DNA sequences called ”hormones-responsive elements”. The binding activates the transcription of specific genes thus stimulating the protein synthesis.

However, for some steroid hormones as testosterone, estrogens and aldosterone, it has been reported the mediation by specific membrane receptors able to trigger cellular responses much more rapid with a ”non genomic effect” [35]. The main androgenic hormone is testosterone, which is produced by the interstitial Leydig cells in the gonads. Its function is to promote the reproductive process and to determine the appearing of the secondary sexual characteristics.

Since the 40s, testosterone is known for its effects on muscle tissue growth. Supraphysiological doses markedly increase the muscle mass and strength [36], [37]. Recent *in vitro* studies point out that androgens can influence the myogenic process also through a local IGF-I concentration increase [38].

### 3.3 Cell cultures

The cell is the basic unit of life. Microorganisms such as bacteria, yeast, and amoebae exist as single cells. By contrast, the adult human is made up of about 30 trillion cells which are mostly organized into collectives called tissues. Cells are, with a few notable exceptions, small with lengths measured in micrometers and their discovery stemmed from the pioneeristic work of a small group of seventeenth-century microscope makers who observed that a new and undiscovered world lay beyond the limits of the human eye. These pioneers set in motion a science and an industry that continues to the present day.

During the last 20 years we have witnessed the extraordinary impact of biotechnology in the academic research laboratory and in industry. This development not only has provided a stimulus for the creation of a large number of companies in the new biotechnology industry, but it has also been a catalyst for new approaches in existing industries. The result has been the development of many, important, new methods of diagnosis and therapy in human healthcare and, increasingly, new approaches to solving problems in agriculture. These applications represent the tangible and often remarkable end products of biotechnology, and it is clear that their development would not have been possible without the development of an equally remarkable array of new manufacturing technologies and laboratory tools. Within the biotechnologist’s toolkit, animal cell culture has come to play a particularly prominent role. In the pharmaceutical industry, cell culture is used to produce a significant proportion of biopharmaceuticals as well as monoclonal

anti- bodies for diagnostic use. In addition, the use of animal and human cells is expanding in a wide range of other applications: drug screening, tissue engineering, gene therapy, toxicology and traditional applications such as virology. Clearly, the practical application of animal and human cell culture has to be underpinned by well-developed laboratory protocols. There are a significant number of cell culture procedures that are used across the broad range of cell culture applications in both academic and industrial laboratories and frequently there are several methods that can be used to solve a given problem.

Large numbers of cell lines look identical. Cell lines with very different origins and biological characteristics typically cannot be separated on grounds of morphology or culture characteristics. Infection or contamination of a cell line with an adventitious virus or mycoplasma may significantly change the characteristics of the cells but again such contamination may not be apparent. Cell lines will also change with time in culture, and to add to all these natural hazards it is all too easy to incorrectly label or cross-contaminate different cell lines in a busy cell culture laboratory.

The opportunities for inadvertently introducing error into a cell line are limitless and ever present. It is in the nature of the science that once introduced, an error will be propagated, compounded, consolidated and disseminated.

The integrity and biological characteristics of a cell line have to be actively maintained by a well organized management system based on systematic cell banking supported by testing regimens in a structured quality assured environment. Such a controlled environment will only prevail in a dedicated professionally organized cell culture laboratory or cell bank. A small research laboratory with a high throughput of short-term research students, a minimum of permanent laboratory staff and no formal quality management program will find it difficult to maintain its cell lines unchanged over many years.

For all these reasons it is strongly recommended that new cell lines should only be acquired from a specialist, reputable culture collection such as ECACC. Moreover, if a laboratory believes it already has a certain cell line in its liquid nitrogen store, the identity and purity of such a cell line should be questioned in the absence of a well recorded culture history and recent test data. If there is a doubt, it is straightforward and cost effective to replace such cell stocks with authenticated material from a Culture Collection. When a Culture Collection acquires a new cell line it will characterize the cell line using techniques such as isoenzyme analysis and DNA profiling so that the identity of the cell line subsequently can be verified. The Collection will then establish a hierarchy of Master and Working cell banks, cryo-preserved in liquid nitrogen, that are demonstrated free from microbial contamination including mycoplasma. Customers are supplied from the authenticated Working Cell Banks (WCB). Replacement WCBs are manufactured from the original Master Cell Bank (MCB) and the new WCB will again



be fully tested.

ECACC supplies its cell lines with advice on how to maintain the line. The technical support team can subsequently assist with difficulties and provide additional technical information about the cell line. Culture Collections exist to ensure that animal cell research is conducted using standardized, authenticated material that ensures the work can be reproduced. An authenticated cell line of known provenance is the very bedrock of any cell based project.

### 3.3.1 Cell types and culture characteristics

- **Primary Cultures:** primary cultures are derived directly from excised, normal animal tissue either as an explant culture or following dissociation into a single cell suspension by enzyme digestion. Such cultures are initially heterogeneous but later become dominated by fibroblasts. The preparation of primary cultures is labour intensive and they can be maintained *in vitro* only for a limited period of time. During their relatively limited lifespan primary cells usually retain many of the differentiated characteristics of the cell *in vivo*. Important Note: Primary cultures by definition have not been passaged, as soon as they are passaged they become a cell line and are no longer primary. ‘Primary’ cells sourced from most suppliers are in fact low-passage cell lines.
- **Continuous Cultures:** continuous cultures are comprised of a single cell type that can be serially propagated in culture either for a limited number of cell divisions (approximately thirty) or otherwise indefinitely. Cell lines of a finite life are usually diploid and maintain some degree of differentiation. The fact that such cell lines senesce after approximately thirty cycles of division means it is essential to establish a system of Master and Working banks in order to maintain such lines for long periods. Continuous cell lines that can be propagated indefinitely generally have this ability because they have been transformed into tumor cells. Tumor cell lines are often derived from actual clinical tumors, but transformation may also be induced using viral oncogenes or by chemical treatments. Transformed cell lines present the advantage of almost limitless availability, but the disadvantage of having retained very little of the original *in vivo* characteristics.
- **Culture Morphology:** in terms of growth mode cell cultures take one of two forms, growing either in suspension (as single cells or small free floating clumps) or as a monolayer that is attached to the tissue culture flask. The form taken by a cell line reflects the tissue from which it was derived e.g. cell lines derived from blood (leukaemia, lymphoma) tend to grow in suspension whereas cells derived from solid tissue (lungs, kidney) tend to grow as monolayers.

Attached cell lines can be classified as endothelial such as BAE-1, epithelial such as HeLa, neuronal such as SH-SY5Y, or fibroblasts such as MRC-5 and their morphology reflects the area within the tissue of origin.

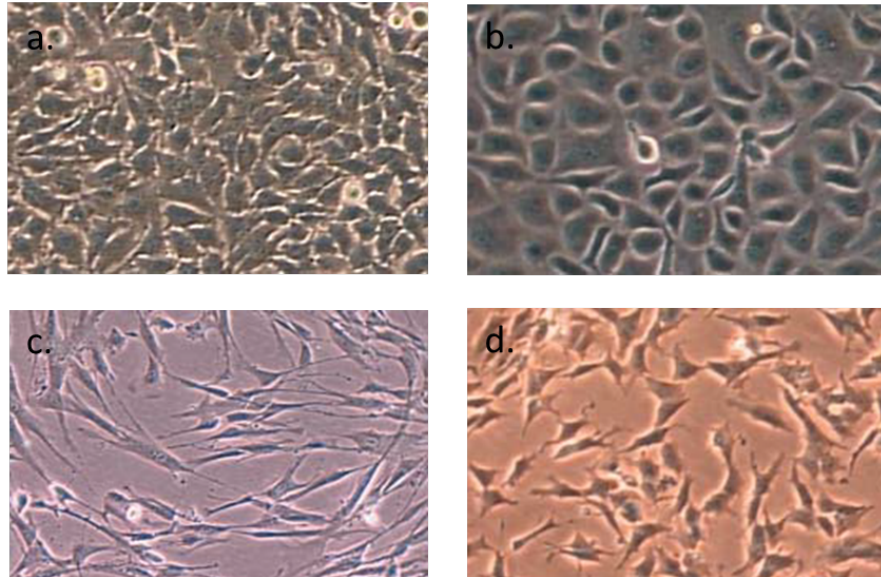


FIGURE 3.5: Examples of cell morphology: (a) HeLa epithelial cells, (b) BAE-1 endothelial cells, (c) MRC-5 fibroblasts cells, (d) SH-SY5Y neuronal cells.

### 3.3.2 Phases of cell growth

It is important to know and record the growth characteristics of the cell line of use before starting any experiments. An alteration in cellular growth can indicate a significant problem within the cell line and if undetected can have detrimental effects on experimental results. A typical growth curve for cultured cells displays a sigmoid pattern of proliferation. The growth phases associated with normal cells are defined as:

1. Lag Phase – at this stage the cells do not divide. During this period the cells adapt to the culture conditions and the length of this phase will depend upon the growth phase of the cell line at the time of subculture and also the seeding density.
2. Logarithmic (Log) Growth Phase – cells actively proliferate and an exponential increase in cell density arises. The cell population is considered to be the most viable at this phase, therefore it is recommended to assess cellular function at this stage. Each cell line will show different cell proliferation kinetics during the log phase and it is therefore the optimal phase for determining the population doubling time.

Cell line	Species	Cell type
NIH3T3	mouse	embryonal fibroblasts
C3H10T1/2	mouse	embryonal mesenchimal
C2C12	mouse	myoblasts
mRAW 264.7	mouse	macrophages
3T3-F442A	mouse	preadipocytes
MC3T3-E1	mouse	osteoblasts
H9C2	rat	embryonal ventricular myoblasts
C6	rat	glioma
L6	rat	skeletal muscle
RGM1	rat	epithelial cells of the normal gastric mucose
INS-1 $\beta$ -cells	rat	insulinoma
A549	human	alveolar adenocarcinoma epithelial cells
hTERT	human	miometral telomerase reverse transcriptase cells
H292	human	respiratory epithelial cells
SaOS-2	human	osteoblasts like
TE-85	human	osteoblast like
MG-63	human	osteoblast like
MCF7	human	breast cancer
T-47D	human	breast cancer
ZR-75-1	human	breast cancer
HCC1954	human	breast cancer
SK-BR-3	human	breast cancer
PC-3	human	prostate cancer
DU-145	human	prostate cancer
LNCaP	human	prostate cancer
CWR22R	human	prostate cancer

TABLE 3.1: Common cell types, their origin, and cells morphology

3. Plateau (or Stationary) Phase – cellular proliferation slows down due to the cell population becoming confluent. It is at this stage the number of cells in the active cell cycle drops to 0-10% and the cells are most susceptible to injury.
4. Decline Phase – cell death predominates in this phase and there is a reduction in the number of viable cells. Cell death is not due to the reduction in nutrient supplements but the natural path of the cellular cycle.

Two terms are predominantly used to define the age of a cell culture: (i) passage number - indicates the number of times the cell line has been sub-cultured and (ii) the population doubling (pd) number - indicates the number of cell generations the cell line has undergone i.e. the number of times the cell population has doubled. The in vitro age of a cell culture is particularly useful to know for cell lines with a finite lifespan or unstable characteristics that change over time in continuous culture.

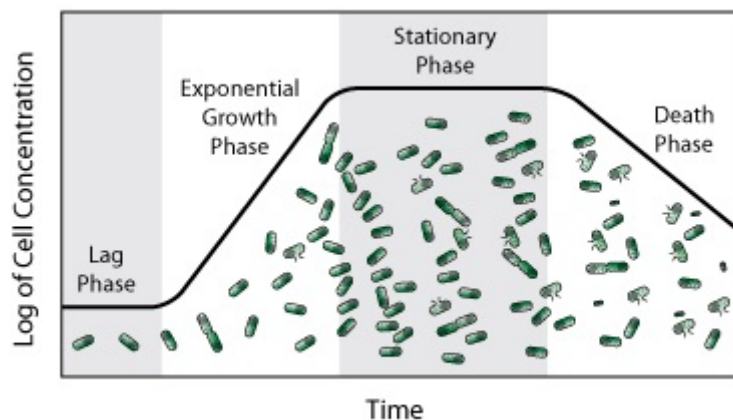


FIGURE 3.6: Representation of the cells growth phases over time.

It is bad practice to maintain a cell line in continuous or extended culture for the following reasons:

- Risk of microbial contamination
- Loss of characteristics of interest (e.g. surface antigen or monoclonal antibody expression)
- Genetic drift particularly in cells known to have an unstable karyotype (e.g. CHO, BHK 21)
- Loss of cell line due to exceeding finite life-span e.g. human diploid cells such as MRC-5
- Risk of cross contamination with other cell lines
- Increased consumables and staff costs

All of these potential risk factors may be minimized by the implementation of a cell banking system as described below. This type of system is known as a tiered banking system or Master Cell Banking system. On initial arrival into the laboratory a new cell culture should be regarded as a potential source of contamination e.g. harbouring bacteria, fungi and mycoplasma and should be handled under quarantine conditions until proven negative for such microbial contaminants. Following initial expansion 3-5 ampoules should be frozen as a Token Stock before a Master Cell Bank is prepared. One of the Token Stock ampoules should then be thawed and expanded to produce a Master Cell Bank of 10-20 ampoules depending upon the anticipated level of use. Ampoules of this Master Cell Bank (2-3) should be allocated for quality control comprising confirmation that the cell count and viability of the bank is acceptable and that the

bank is free of bacteria, fungi and mycoplasma. Additional tests (such as viral screening and authenticity testing) may also be required. Once these tests have been completed satisfactorily an ampoule from the Master Cell Bank should be thawed and cultured to produce a Working Cell Bank. The size of this bank will again depend on the envisaged level of demand. Quality control tests (cell count and also important at this stage to confirm that the Master and Working Cell Banks are genetically identical by DNA profiling techniques).

Implementation of this banking system ensures:

- Material is of a consistent quality
- Experiments are performed using cultures in the same range of passage numbers
- Cells are only in culture when required
- The original cell line characteristics are retained

### **3.3.3 Cell quantification**

The cell counting is an important subset of cytometry, the measurement of the characteristics of cells i.e. cell size, cell count, cell morphology, cell cycle phase, DNA content and existence of specific proteins on the cell surface or in the cytoplasm. Cell counts within liquid media (such as blood, plasma, lymph, or laboratory rinsate) are usually expressed as a number of cells per unit of volume, thus expressing a concentration.

There are several methods for cell counting. Some are primitive and do not require special equipment, thus can be done in any biological laboratory, whereas others rely on sophisticated electronic appliances.

#### **3.3.3.1 Counting chamber**

A counting chamber, also known as hemocytometer, is a microscope slide that is especially designed to enable cell counting. The slide has a sink in its middle; the area of the sink is marked with a grid. A drop of a cell culture is placed in the sink. Looking at the sample under the microscope, the researcher uses the grid to manually count the number of cells in a certain area. The depth of the sink is predefined, thus the volume of the counted culture can be calculated and the concentration of the cells with it.

Counting chambers are often used in clinical blood counts. Their advantage is being cheap and fast; this makes them the preferred counting method in fast biological experiments in which it needs to be merely determined whether a cell culture has grown as

expected. Usually the culture examined needs to be diluted, otherwise the high density of cells would make counting impossible. The need for dilution is a disadvantage, as every dilution adds inaccuracy to the measurement.

### 3.3.3.2 CFU counting

To quantify the number of cells in a culture, the cells can be simply plated on a Petri dish with growth medium. If the cells are efficiently distributed on the plate, it can be generally assumed that each cell will give rise to a single colony or Colony Forming Unit (CFU). The colonies can then be counted, and based on the known volume of culture that was spread on the plate, the cell concentration can be calculated. As is with counting chambers, cultures usually need to be heavily diluted prior to plating; otherwise, instead of obtaining single colonies that can be counted, a so-called "lawn" will form: thousands of colonies lying over each other. Additionally, plating is the slowest method of all: most microorganisms need at least 12 hours to form visible colonies.

Although this method can be time consuming, it gives an accurate estimate of the number of viable cells (because only they will be able to grow and form visible colonies). It is therefore extensively used in experiments aiming to quantify the number of cells resisting drugs or other external conditions (for instance the Luria–Delbrück experiment or the gentamicin protection assay). In addition, the enumeration of colonies on agar plates can be greatly facilitated by using colony counters.

### 3.3.3.3 Spectrophotometry

Cell suspensions are turbid: they absorb or scatter some of the light letting the rest of it pass through. The higher the cell concentration is, the higher the turbidity. Spectrophotometers are electrical appliances that can measure intensity of light very accurately. The culture is placed in a transparent cuvette, the cuvette is placed in the machine, and the optical density can be measured immediately. Optical density (OD) is proportional to the biomass in the cell suspension. Using spectrophotometry for measuring the turbidity of cultures is known as turbidometry. Of all the electrical appliances used for measuring biomass, a spectrophotometer is the cheapest and its operation the fastest and most straightforward. This has made spectrophotometry the methods of choice for quick measurements of bacterial growth and related applications. A drawback of spectrophotometry is its limited accuracy; it is the only method in which the cells are not counted directly—the machine measures light, not cells. This, combined with the stochastic nature of liquid cultures, enables only an estimation of cell numbers.

#### **3.3.3.4 Electrical resistance**

A Coulter counter is an appliance that can count cells as well as measure their volume. It is based on the fact that cells show great electrical resistance. In a Coulter counter the cells, swimming in a solution that conducts electricity, are sucked one by one into a tiny gap. Flanking the gap are two electrodes that conduct electricity. When no cell is in the gap, electricity flows unabated, but when a cell is sucked into the gap the current is resisted. The Coulter counter counts the number of such events and also measures the current (and hence the resistance), which directly correlates to the volume of the cell trapped.

Coulter counters are much cheaper than flow cytometers, and for applications that require cell numbers and sizes, such as cell-cycle research, they are the method of choice. Its advantage over the methods above is the large number of cells that can be processed in a short time, namely: thousands of cells per second. This offers great accuracy and statistical significance.

#### **3.3.3.5 Flow cytometry**

Flow cytometry is by far the most sophisticated and expensive method for cell counting. In a flow cytometer the cells flow in a narrow stream in front of a laser beam. The beam hits them one by one, and a light detector picks up the light that is reflected from the cells.

Flow cytometers have many other abilities, such as analyzing the shape of cells and their internal and external structures, as well as measuring the amount of specific proteins and other biochemical markers of the cells. Therefore, flow cytometers are rarely purchased for the sole purpose of counting cells.

#### **3.3.3.6 Image counting**

Recent approaches consider the use of high-quality microscopy images over which a statistical classification algorithm is used to perform automated cell detection and counting as an image analysis task. Generally performs with a constant error rate as an off-line (batch) type process. A range of image classification techniques can be employed for this purpose.

### 3.3.4 Culture environment

In general terms cultured cells require a sterile environment and a supply of nutrients for growth. In addition, the culture environment should be stable in terms of pH and temperature. Over the last 30 years various defined basal media types have been developed and are now available commercially.

Originally, balanced salt solutions were used to maintain contractility of mammalian heart tissue and the Tyrode salt solution was designed for use in work with primary mammalian cells. These have since been modified and enriched with amino acids, vitamins, fatty acids and lipids. Consequently media suitable for supporting the growth of a wide range of cell types are now available. The precise media formulations have often been derived by optimising the concentrations of every constituent.

#### 3.3.4.1 Constituents of media

Media are composed by a wide variety of constituents. Each type of constituent performs a specific function as outlined below:

- Inorganic salts: the inclusion of inorganic salts in media performs several functions. Primarily they help to retain the osmotic balance of the cells and help regulate membrane potential by provision of sodium, potassium and calcium ions. Many of these are required in the cell matrix for cell attachment and as enzyme cofactors.
- Buffering systems: most cells require pH conditions in the range 7.2-7.4 and close control of pH is essential for optimum culture conditions. There are major variations to this optimum. Fibroblasts prefer a higher pH (7.4-7.7) whereas, continuous transformed cell lines require more acid conditions pH (7.0-7.4).

Regulation of pH is particularly important immediately following cell seeding when a new culture is going to be established and is usually achieved by one of two buffering systems; (i) a “natural” buffering system where gaseous CO<sub>2</sub> balances with the H<sub>2</sub>CO<sub>3</sub>/HCO<sub>3</sub><sup>-</sup> concentration ratio of the culture medium and (ii) chemical buffering using a zwitterion called HEPES. Cultures using natural bicarbonate/CO<sub>2</sub> buffering systems need to be maintained in an atmosphere of 5-10% CO<sub>2</sub> in air usually supplied in a CO<sub>2</sub> incubator. Bi-carbonate/CO<sub>2</sub> is low cost, non-toxic and also provides other chemical benefits to the cells. HEPES has superior buffering capacity in the pH range 7.2-7.4 but is relatively expensive and can be toxic to some cell types at higher concentrations. HEPES buffered cultures do not require a controlled gaseous atmosphere. Most commercial culture media include phenol red as a pH indicator so that the pH status of the medium is constantly indicated



by the colour. Usually the culture medium should be changed/replenished if the colour turns yellow (acid) or purple (alkali).

- **Carbohydrates:** the main source of energy is derived from carbohydrates generally in the form of sugars. The major sugars used are glucose and galactose, however, some media contain maltose or fructose. The concentration of sugar varies from basal media containing 1g/L to 4.5g/L in some more complex media. Media containing the higher concentration of sugars are able to support the growth of a wider range of cell types.
- **Amino acids:** amino acids are the building blocks of proteins. ‘Essential’ amino acids must be added to culture media as cells are not able to synthesize these themselves. The concentration of amino acids in the culture medium will determine the maximum cell density that can be achieved as once depleted the cells will no longer be able to proliferate.  
In relation to cell culture, glutamine, an essential amino acid, is particularly significant. In liquid media or stock solutions glutamine degrades relatively rapidly. Optimal cell performance usually requires supplementation of the media with glutamine prior to use. Adding supplements of non-essential amino acids to media both stimulates growth and prolongs the viability of the cells in culture.
- **Vitamins:** serum is an important source of vitamins in cell culture. However, many media are also enriched with vitamins making them consistently more suitable for a wider range of cell lines. Vitamins are precursors for numerous co-factors. Many vitamins, especially B group vitamins, are necessary for cell growth and proliferation and for some lines the presence of B12 is essential. Some media also have increased levels of vitamins A and E. The vitamins commonly used in media include riboflavin, thiamine and biotin.
- **Proteins and peptides:** these are particularly important in serum free media. The most common proteins and peptides include albumin, transferrin, fibronectin and fetuin and are used to replace those normally present through the addition of serum to the medium.
- **Fatty acids and lipids:** like proteins and peptides these are important in serum free media since they are normally present in serum e.g. cholesterol and steroids essential for specialized cells.
- **Trace elements:** these include trace elements such as zinc, copper, selenium and tricarboxylic acid intermediates. Selenium is a detoxifier and helps remove oxygen free radicals.

- Preparation of media: Whilst all media may be made from the basic ingredients this is time consuming and may predispose to contamination. For convenience most media are available as ready mixed powders or as 10x and 1x liquid media. If powder or 10x media are purchased it is essential that the water used to reconstitute the powder or dilute the concentrated liquid is free from mineral, organic and microbial contaminants. It must also be pyrogen free and of tissue culture grade. In most cases water prepared by reverse osmosis and resin cartridge purification with a final resistance of 16-18 M $\Omega$  is suitable. Once prepared, the media should be filter sterilized before use.

### 3.3.4.2 Serum and serum-free cultures

Serum is a complex mix of albumins, growth factors and growth inhibitors and is probably one of the most important components of cell culture medium. The most commonly used serum is fetal bovine serum (FBS). Other types of serum are available including newborn calf serum and horse serum. The quality, type and concentration of serum can all affect the growth of cells and it is therefore important to screen batches of serum for their ability to support the growth of cells. In addition, there are other tests that may be used to aid the selection of a batch of serum including cloning efficiency, plating efficiency and the preservation of cell characteristics. Serum is also able to increase the buffering capacity of cultures that can be important for slow growing cells or where the seeding density is low (e.g. cell cloning experiments). It also helps to protect against mechanical damage which may occur in stirred cultures or whilst using a cell scraper. A further advantage of serum is the wide range of cell types with which it can be used despite the varying requirements of different cultures in terms of growth factors. In addition, serum is able to bind and neutralize toxins. However, serum is subject to batch-to-batch variation that makes standardization of production protocols difficult. There is also a risk of contamination associated with the use of serum. These risks can be minimized by obtaining serum from a reputable source since suppliers of large quantities of serum perform a battery of quality control tests and supply a certificate of analysis with the serum. In particular, serum is screened for the presence of bovine viral diarrhoea virus (BVDV) and mycoplasma. Heat inactivation of serum (incubation at 56°C for 30 minutes) can help to reduce the risk of contamination since some viruses are inactivated by this process. However, the routine use of heat inactivated serum is not an absolute requirement for cell culture. The use of serum also has a cost implication not only in terms of medium formulation but also in downstream processing. A 10% FBS supplement contributes 4.8 mg of protein per ml of culture fluid which complicates downstream processing procedures such as protein purification.

Component type	Components	DMEM	HBR5	PBS	Tris
Aminoacids	Glycine	30	0	0	0
	L-Alanine	84	0	0	0
	L-Cystine 2HCl	63	0	0	0
	L-glutamine	580	0	0	0
	L-Histidine HCl	42	0	0	0
	L-Isoleucine	105	0	0	0
	L-Leucine	105	0	0	0
	L-Lysine HCl	146	0	0	0
	L-Methionine	30	0	0	0
	L-Phenylalanine	66	0	0	0
	L-Serine	42	0	0	0
	L-Threonine	95	0	0	0
	L-Tryptophan	16	0	0	0
	L-Tyrosine disodium salt	72	0	0	0
L-Valine	94	0	0	0	
Vitamins	Choline chloride	4	0	0	0
	Folic acid	4	0	0	0
	D-calcium pantothenate	4	0	0	0
	Niacinamide	4	0	0	0
	Pyridoxine HCl	4	0	0	0
	Riboflavin	0.4	4	4	0
	Thiamine HCl	4	0	0	0
	i-Inositol	7.2	0	0	0
Inorganic salts	Calcium chloride anhyd.	264	294	100	0
	Cupric sulfate	0.1	0	0	0
	Magnesium chloride	0	204	0	0
	Magnesium sulfate	200	0	47	0
	Potassium chloride	400	370	200	0
	Sodium bicarbonate	3700	0	0	0
	Sodium chloride	6400	9058	8000	0
	Sodium phosphate m.	141	276	1150	0
	Potassium phosphate m.	0	0	200	0
Others	D-glucose	4500	1800	0	0
	Phenol red	15	0	0	0
	HEPES	0	2384	0	0
	Trizma Base <sup>®</sup>	0	0	0	1230
	Trizma HCl <sup>®</sup>	0	0	0	5130

TABLE 3.2: Example of cell growth/maintenance media and common buffers compositions (given in mg/l). Tris-HCl composition refers to a pH 8.8 solution.

Fetal bovine serum (FBS) has been used to prepare a number of biological media and has an excellent record of safety. The recognition of Bovine Spongiform Encephalopathy (BSE) in 1986 and its subsequent spread into continental Europe along side the announcement of the probable link between BSE and a new variant of Creutzfeldt Jacob disease in Humans stimulated an increased concern about safe sourcing of all bovine materials. In 1993, the Food and Drug Administration (FDA) "recommended against the use of bovine derived materials from cattle which have resided in, or originated from countries where BSE has been diagnosed".

The current European Union (EU) guidelines on viral safety focus on sourcing, testing and paying particular attention to the potential risk of cross contamination during slaughtering or collection of the starting tissue.

As far as BSE is concerned, the EU guidance on minimizing the risk of BSE transmission via medicinal products, EMEA/410/01 Rev. 2, recommends the main measures to be implemented in order to establish the safety of bovine material. Similarly the focus is on geographical origin, the age of the animals, the breeding and slaughtering conditions, the tissue to be used and the conditions of its processing.

The use of FBS in production processes of medicinal products is acceptable provided good documentation on sourcing, age of the animals and testing for the absence of adventitious agents is submitted. All responsible suppliers of FBS for bio-pharmaceutical applications will provide such documentation.

Regulatory requirements in Europe stress the importance of justifying the use of material of bovine, caprine or ovine origin in the production of pharmaceutical products. Thus, although FBS has been used for many years in the production process of many medicinal products such as viral vaccines and recombinant DNA products, at present there is a justified trend to remove all material of animal origin from manufacturing processes. Sigma-Aldrich has recognised this growing trend and works closely with customers to optimise animal free media formulations to meet each customer's cell culture requirements. Serum-free cell lines that have been adapted to media that do not contain serum are available from ECACC. The United States Department of Agriculture (USDA) regulates all products that contain a primary component of animal origin. With specific reference to serum the USDA has declared that for materials which fall under their jurisdiction, only biological products manufactured using serum from approved countries of origin will be allowed in to USA.

Standard tests performed on serum commonly include tests to determine the presence and/or level of the following:

- Sterility
- Virus Contamination

- Mycoplasma Contamination
- Endotoxin
- Haemoglobin
- Total Protein
- Immunoglobulin
- Hormone Testing
- pH (at room temperature)
- Osmolality

### 3.4 Genetic engineering techniques

Genetic engineering is the direct manipulation of an organism genome using biotechnology. New DNA may be inserted in the host genome by first isolating and copying the genetic material of interest using molecular cloning methods to generate a DNA sequence, or by synthesizing the DNA, and then inserting this construct into the host organism. Genes may be removed, or "knocked out", using a nuclease. Gene targeting is a different technique that uses homologous recombination to change an endogenous gene, and can be used to delete a gene, remove exons, add a gene, or introduce point mutations.

An organism that is generated through genetic engineering is considered to be a genetically modified organism (GMO). The first GMOs were bacteria generated in 1973 and GM mice were generated in 1974. Insulin-producing bacteria were commercialized in 1982 and genetically modified food has been commercially available since 1994.

Genetic engineering techniques have been applied in numerous fields including research, agriculture, industrial biotechnology, and medicine. Enzymes used in laundry detergent and medicines such as insulin and human growth hormone are now manufactured in GM cells, experimental GM cell lines and GM animals such as mice or zebrafish are being used for research purposes, and genetically modified crops have been commercialized.

Genetic engineering alters the genetic make-up of an organism using techniques that remove heritable material or that introduce DNA prepared outside the organism either directly into the host or into a cell that is then fused or hybridized with the host. This involves using recombinant nucleic acid (DNA or RNA) techniques to form new combinations of heritable genetic material followed by the incorporation of that material either indirectly through a vector system or directly through micro-injection, macro-injection

and micro-encapsulation techniques. If genetic material from another species is added to the host, the resulting organism is called transgenic. If genetic material from the same species or a species that can naturally breed with the host is used the resulting organism is called cisgenic. Genetic engineering can also be used to remove genetic material from the target organism, creating a gene knockout organism.

The process of genetic engineering involves different consecutive steps. The first one is gene isolation, which has the objective to isolate and obtain the gene from the source organism. Then, the gene has to be complemented by a promoter and a terminator in order to be expressed by the host cell. Now, the complemented gene has to be inserted into the host cell, procedure which is called transformation, transfection or transduction depending on the type of host cell and vector. In fact, in case of a bacterial host we talk about transformation or transduction if the vector is a virus, conversely it's transfection in the case of eukaryotic animal cells. Whichever the host type, there are several techniques that allow the completed gene insertion in the cell. In every case, not all the host cells will be transformed with the new genetic material, therefore it's necessary to select and differentiate the transformed from the untransformed cells. The last step that has to be accomplished in the process is the confirmation of the gene integration in the host cell. An alternative method to obtain the gene when its sequence is known is artificial gene synthesis. Currently based on solid-phase DNA synthesis, it differs from molecular cloning and polymerase chain reaction (PCR) in that the user does not have to begin with preexisting DNA sequences. Therefore, it is possible to make a completely synthetic double-stranded DNA molecule with no apparent limits on either nucleotide sequence or size.

### 3.4.1 Gene isolation

To isolate a gene which sequence is not known from the source cell, the DNA is first digested with a random digestion method, commonly by cutting the DNA with restriction enzymes. A partial restriction digest cuts only some of the restriction sites, resulting in overlapping DNA fragment lengths. The DNA fragments are put into individual plasmid vectors and grown inside bacteria. Once in the bacteria the plasmid is copied as the bacteria divides. To determine if a useful gene is present on a particular fragment the bacterial library is screened for the desired phenotype. Thus, if the phenotype is detected then it is possible that the bacteria contains the target gene. Conversely, if the gene does not have a detectable phenotype or a DNA library does not contain the correct gene, other methods can be used to isolate it. In fact in the case the position of the gene can be determined using molecular markers then chromosome walking is one way to isolate the correct DNA fragment, while if the gene expresses close homology to a

known gene in another species, it could be isolated by searching for genes in the library that closely match the known gene.

When the DNA sequence of the gene and the organism is known, restriction enzymes can cut the DNA on either side of the gene and gel electrophoresis can sort the fragments according to length. The DNA band at the correct size should contain the gene, where it can be excised from the gel. Then, polymerase chain reaction (PCR) can be used to amplify the gene, which can then be isolated through gel electrophoresis.

### 3.4.2 Gene complementing

The gene to be inserted into the genetically modified organism must be combined with other genetic elements in order for it to work properly. As well as the gene to be inserted most constructs contain a promoter and terminator region as well as a selectable marker gene. The promoter region initiates transcription of the gene and can be used to control the location and level of gene expression, while the terminator region ends transcription. The selectable marker, which in most cases confers antibiotic resistance to the organism it is expressed in, is needed to determine which cells are transformed with the new gene in the selection stage. The constructs are made using recombinant DNA techniques, such as restriction digests, ligations and molecular cloning.

### 3.4.3 Genes insertion in the host cell

#### 3.4.3.1 Transformation

The transformation is the genetic modification of a bacteria cell by the direct uptake or incorporation of exogenous genetic material. This process naturally occurs in several species of bacteria, but it can also be performed by artificial means in other cells.

Transformation was first demonstrated in 1928 by British bacteriologist Frederick Griffith. Griffith discovered that a strain of *Streptococcus pneumoniae* could be made virulent after being exposed to heat-killed virulent strains. Griffith hypothesized that some "transforming principle" from the heat-killed strain was responsible for making the harmless strain virulent. In 1944 this "transforming principle" was identified as being genetic material by Oswald Avery, Colin MacLeod, and Maclyn McCarty. They isolated DNA from a virulent strain of *S. pneumoniae* and using just this DNA were able to make a harmless strain virulent. They called this uptake and incorporation of DNA by bacteria "transformation". The results of Avery's experiments were at first skeptically received by the scientific community and it was not until the development of genetic markers and the discovery of other methods of genetic transfer (conjugation

in 1947 and transduction in 1953) by Joshua Lederberg that Avery's experiments were accepted.

In general, transformation is a complex, energy requiring developmental process. In order for a bacterium to bind, take up and recombine exogenous DNA into its chromosome it must become competent, that is, enter a special physiological state. Competence development in *Bacillus subtilis* requires expression of about 40 genes. The DNA integrated into the host chromosome is usually (but with rare exceptions) derived from another bacterium of the same species, and is thus homologous to the resident chromosome. The capacity for natural transformation appears to occur in a number of prokaryotes, and thus far 67 prokaryotic species (in seven different phyla) are known to undergo this process. Competence for transformation is typically induced by high cell density and/or nutritional limitation, conditions associated with the stationary phase of bacterial growth. Transformation in *Haemophilus influenzae* occurs most efficiently at the end of exponential growth as bacterial growth approaches stationary phase. Transformation in *Streptococcus mutans*, as well as in many other streptococci, occurs at high cell density and is associated with biofilm formation. Competence in *B. subtilis* is induced toward the end of logarithmic growth, especially under conditions of amino acid limitation. Competence is specifically induced by DNA damaging conditions. For instance, transformation is induced in *Streptococcus pneumoniae* by the DNA damaging agents mitomycin C (a DNA crosslinking agent) and fluoroquinolone (a topoisomerase inhibitor that causes double-strand breaks). In *B. subtilis*, transformation is increased by UV light, a DNA damaging agent. In *Helicobacter pylori*, ciprofloxacin, which interacts with DNA gyrase and introduces double-strand breaks, induces expression of competence genes, thus enhancing the frequency of transformation. About 1% of bacterial species are capable of naturally taking up DNA under laboratory conditions; more may be able to take it up in their natural environments. DNA material can be transferred between different strains of bacteria, in a process that is called horizontal gene transfer. Some species upon cell death release their DNA to be taken up by other cells, however transformation works best with DNA from closely related species. These naturally competent bacteria carry sets of genes that provide the protein machinery to bring DNA across the cell membranes.

Artificial competence can be induced in laboratory procedures that involve making the cell passively permeable to DNA by exposing it to conditions that do not normally occur in nature. Typically, the cells are incubated in a solution containing divalent cations (often calcium chloride) under cold conditions, before being exposed to a heat pulse (heat shock).

It has been found that growth of Gram negative bacteria in 20 mM Mg reduces the



number of protein to lipopolysaccharide bonds by increasing the ratio of ionic to covalent bonds, which increases membrane fluidity, facilitating transformation. The role of lipopolysaccharides here are verified from the observation that shorter O-side chains are more effectively transformed — perhaps because of improved DNA accessibility. The surface of bacteria such as *E. coli* is negatively charged due to phospholipids and lipopolysaccharides on its cell surface, and the DNA is also negatively charged. One function of the divalent cation therefore would be to shield the charges by coordinating the phosphate groups and other negative charges, thereby allowing a DNA molecule to adhere to the cell surface.

DNA entry into *E. coli* cells is through channels known as zones of adhesion or Bayer's junction, a typical cell carries as many as 400 such zones. Their role was established when cobalamine (which also uses these channels) was found to competitively inhibit DNA uptake. It is suggested that exposing the cells to divalent cations in cold condition may also change or weaken the cell surface structure of the cells making it more permeable to DNA. The heat-pulse is thought to create a thermal imbalance on either side of the cell membrane, which forces the DNA to enter the cells through either cell pores or the damaged cell wall.

Electroporation is another method of promoting competence. In this method the cells are briefly shocked with an electric field of 10-20 kV/cm which is thought to create holes in the cell membrane through which the plasmid DNA may enter. After the electric shock the holes are rapidly closed by the cell's membrane-repair mechanisms.

The discovery of artificially induced competence in bacteria allow bacteria such as *Escherichia coli* to be used as a convenient host for the manipulation of DNA as well as expressing proteins. Typically plasmids are used for transformation in *E. coli*. In order to be stably maintained in the cell, a plasmid DNA molecule must contain an origin of replication, which allows it to be replicated in the cell independently of the replication of the cell's own chromosome.

The efficiency with which a competent culture can take up exogenous DNA and express its genes is known as transformation efficiency and is measured in colony forming unit (CFU) per  $\mu\text{g}$  DNA used. A transformation efficiency of  $1 \times 10^8$  CFU/ $\mu\text{g}$  for a small plasmid like pUC19 is roughly equivalent to 1 in 2000 molecules of the plasmid used being transformed.

In calcium chloride transformation, the cells are prepared by chilling cells in the presence of  $\text{Ca}^{2+}$  (in  $\text{CaCl}_2$  solution) making the cell become permeable to plasmid DNA. The cells are incubated on ice with the DNA, and then briefly heat-shocked (e.g., at  $42^\circ\text{C}$  for 30–120 seconds). This method works very well for circular plasmid DNA. Non-commercial preparations should normally give  $10^6$  to  $10^7$  transformants per  $\mu\text{g}$  of plasmid; a poor preparation will be about  $10^4$  per  $\mu\text{g}$  or less, but a good preparation of competent cells can give up to  $10^8$  colonies per  $\mu\text{g}$  of plasmid. Protocols however

exist for making supercompetent cells that may yield a transformation efficiency of over 10<sup>9</sup>. The chemical method, however, usually does not work well for linear DNA, such as fragments of chromosomal DNA, probably because the cell's native exonuclease enzymes rapidly degrade linear DNA. In contrast, cells that are naturally competent are usually transformed more efficiently with linear DNA than with plasmid DNA.

The transformation efficiency using the *CaCl*<sub>2</sub> method decreases with plasmid size, and electroporation therefore may be a more effective method for the uptake of large plasmid DNA. Cells used in electroporation should be prepared first by washing in cold double-distilled water to remove charged particles that may create sparks during the electroporation process.

### 3.4.3.2 Transduction

Transduction is the process by which DNA is transferred from one bacterium to another by a virus. It also refers to the process whereby foreign DNA is introduced into another cell via a viral vector. Transduction does not require physical contact between the cell donating the DNA and the cell receiving the DNA (which occurs in conjugation), and it is DNase resistant (transformation is susceptible to DNase).

Transduction is a common tool used by molecular biologists to stably introduce a foreign gene into a host cell's genome.

When bacteriophages (viruses that infect bacteria) infect a bacterial cell, their normal mode of reproduction is to exploit the replication, transcription, and translation machinery of the host bacterial cell to make numerous virions, or complete viral particles, including the viral DNA or RNA and the protein coat.

Transduction happens through either the lytic cycle or the lysogenic cycle. If the lysogenic cycle is adopted, the phage chromosome is integrated (by covalent bonds) into the bacterial chromosome, where it can remain dormant for thousands of generations. If the lysogenic cycle is induced (by UV light for example), the phage genome is excised from the bacterial chromosome and initiates the lytic cycle, which culminates in lysis of the cell and the release of phage particles. The lytic cycle leads to the production of new phage particles which are released by lysis of the host.

The packaging of bacteriophage DNA has low fidelity and small pieces of bacterial DNA, together with the bacteriophage genome, may become packaged into the bacteriophage genome. At the same time, some phage genes are left behind in the bacterial chromosome. There are generally three types of recombination events that can lead to this incorporation of bacterial DNA into the viral DNA, leading to two modes of recombination.

Generalized transduction is the process by which any bacterial gene may be transferred

to another bacterium via a bacteriophage, and typically carries only bacterial DNA and no viral DNA. In essence, this is the packaging of bacterial DNA into a viral envelope. This may occur in two main ways, recombination and headful packaging. If bacteriophages undertake the lytic cycle of infection upon entering a bacterium, the virus will take control of the cell's machinery for use in replicating its own viral DNA. If by chance bacterial chromosomal DNA is inserted into the viral capsid which is usually used to encapsulate the viral DNA, the mistake will lead to generalized transduction. If the virus replicates using 'headful packaging', it attempts to fill the nucleocapsid with genetic material. If the viral genome results in spare capacity, viral packaging mechanisms may incorporate bacterial genetic material into the new virion.

The new virus capsule now loaded with part bacterial DNA continues to infect another bacterial cell. This bacterial material may become recombined into another bacterium upon infection.

When the new DNA is inserted into this recipient cell it can fall to one of three fates:

1. The DNA will be absorbed by the cell and be recycled for spare parts.
2. If the DNA was originally a plasmid, it will re-circularize inside the new cell and become a plasmid again.
3. If the new DNA matches with a homologous region of the recipient cell's chromosome, it will exchange DNA material similar to the actions in bacterial recombination.

Specialized transduction is the process by which a restricted set of bacterial genes is transferred to another bacterium. The genes that get transferred (donor genes) depend on where the phage genome is located on the chromosome. Specialized transduction occurs when the prophage excises imprecisely from the chromosome so that bacterial genes lying adjacent to the prophage are included in the excised DNA. The excised DNA is then packaged into a new virus particle, which then delivers the DNA to a new bacterium, where the donor genes can be inserted into the recipient chromosome or remain in the cytoplasm, depending on the nature of the bacteriophage. When the partially encapsulated phage material infects another cell and becomes a "prophage" (is covalently bonded into the infected cell's chromosome), the partially coded prophage DNA is called a "heterogenote". Example of specialized transduction is  $\lambda$  phages in *Escherichia coli* discovered by Esther Lederberg.

### 3.4.3.3 Transfection

Transfection is the process of introducing nucleic acids with non-viral methods in eukaryotic cells. The word transfection is a blend of trans- and infection. Genetic material (such as supercoiled plasmid DNA or siRNA constructs) may be transfected. Transfection of eukaryotic cells typically involves opening transient pores or "holes" in the cell membrane to allow the uptake of material. This can be accomplished by using chemical or physical protocols:

- Calcium phosphate;
- Dendrimers;
- Liposomes;
- Cationic polymers;
- Electroporation;
- Sonoporation;
- Optical transfection;
- Protoplast fusion;
- Impalefection;
- Magnetofection;
- Particle bombardment;
- Nucleofection.

One of the cheapest methods uses calcium phosphate, originally discovered by F. L. Graham and A. J. van der Eb in 1973. HEPES-buffered saline solution (HeBS) containing phosphate ions is combined with a calcium chloride solution containing the DNA to be transfected. When the two are combined, a fine precipitate of the positively charged calcium and the negatively charged phosphate will form, binding the DNA to be transfected on its surface. The suspension of the precipitate is then added to the cells to be transfected (usually a cell culture grown in a monolayer). By a process not entirely understood, the cells take up some of the precipitate, and with it, the DNA. This process has been a preferred method of identifying many oncogenes.

Other methods use highly branched organic compounds, so-called dendrimers, to bind the DNA and get it into the cell.

A very efficient method is the inclusion of the DNA to be transfected in liposomes, i.e. small, membrane-bounded bodies that are in some ways similar to the structure of a cell and can actually fuse with the cell membrane, releasing the DNA into the cell. For eukaryotic cells, transfection is better achieved using cationic liposomes (or mixtures), because the cells are more sensitive.

Another method is the use of cationic polymers such as DEAE-dextran or polyethylenimine. The negatively charged DNA binds to the polycation and the complex is taken up by the cell via endocytosis.

Electroporation (Gene electrotransfer) is a popular method, where transient increase in the permeability of cell membrane is achieved when the cells are exposed to short pulses of an intense electric field.

Cell squeezing is a method invented in 2012 by Armon Sharei, Robert Langer and Klavs Jensen at MIT. It enables delivery of molecules into cells by a gentle squeezing of the cell membrane. It is a high throughput vector-free microfluidic platform for intracellular delivery. It eliminates the possibility of toxicity or off-target effects as it does not rely on exogenous materials or electrical fields.

Sonoporation uses high-intensity ultrasound to induce pore formation in cell membranes. This pore formation is attributed mainly to the cavitation of gas bubbles interacting with nearby cell membranes since is enhanced by the addition of ultrasound contrast agent, a source of cavitation nuclei.

Optical transfection is a method where a tiny (less than 1  $\mu m$  diameter) hole is transiently generated in the plasma membrane of a cell using a highly focused laser. This technique was first described in 1984 by Tsukakoshi et al., who used a frequency tripled *Nd : YAG* to generate stable and transient transfection of normal rat kidney cells. In this technique, one cell at a time is treated, making it particularly useful for single cell analysis.

Protoplast fusion is a technique in which transformed bacterial cells are treated with lysozyme in order to remove the cell wall. Following this, fusogenic agents (e.g., Sendai virus, PEG, or electroporation) are used in order to fuse the protoplast carrying the gene of interest with the target recipient cell. A major disadvantage of this method is that bacterial components are non-specifically introduced into the target cell as well.

Impalefection is a method of introducing DNA bound to a surface of a nanofiber that is inserted into a cell. This approach can also be implemented with arrays of nanofibers that are introduced into large numbers of cells and intact tissue.

Hydrodynamic delivery: in mice and rats, but to a lesser extent in larger animals, DNA most often in plasmids, including transposons, can be delivered to the liver using hydrodynamic injection that involves infusion of a relatively large volume in the blood in less than 10 seconds; nearly all of the DNA is expressed in the liver by this procedure. A

direct approach to transfection is the gene gun, where the DNA is coupled to a nanoparticle of an inert solid (commonly gold) which is then "shot" directly into the target cell's nucleus.

Magnetofection, or Magnet assisted transfection is a transfection method, which uses magnetic force to deliver DNA into target cells. Nucleic acids are first associated with magnetic nanoparticles. Then, application of magnetic force drives the nucleic acid particle complexes towards and into the target cells, where the cargo is released.

Another particle-based method of transfection is known as particle bombardment. The nucleic acid is delivered through membrane penetration at a high velocity, usually connected to microprojectiles.

DNA can also be introduced into cells using viruses as a carrier. In such cases, the technique is called viral transduction, and the cells are said to be transduced.

Other methods of transfection include nucleofection, which has proved very efficient in transfection of the THP-1 cell line, creating a viable cell line that was able to be differentiated into mature macrophages, heat shock.

For some applications of transfection, it is sufficient if the transfected genetic material is only transiently expressed. Since the DNA introduced in the transfection process is usually not integrated into the nuclear genome, the foreign DNA will be diluted through mitosis or degraded. Cell lines expressing the Epstein–Barr virus (EBV) nuclear antigen 1 (EBNA1) or the SV40 large-T antigen, allow episomal amplification of plasmids containing the viral EBV (293E) or SV40 (293T) origins of replication, greatly reducing the rate of dilution. If it is desired that the transfected gene actually remain in the genome of the cell and its daughter cells, a stable transfection must occur. RNA can also be transfected into cells to transiently express its coded protein, or to study RNA decay kinetics. The latter application is referred as siRNA transfection or RNA silencing, and has become a major application in research (to replace the "knock-down" experiments, to study the expression of proteins) with potential applications in gene-therapy.

#### **3.4.4 Selection**

In a cloning experiment, a gene may be inserted into a plasmid used for transformation. However, in such experiment, not all the plasmids may contain a successfully inserted gene. Additional techniques may therefore be employed further to screen for transformed cells that contain plasmid with the insert.

Antibiotic resistance is the most commonly used marker for prokaryotes. The transforming plasmid contains a gene that confers resistance to an antibiotic that the bacteria are otherwise sensitive to. The mixture of treated cells is cultured on media that contain the antibiotic so that only transformed cells are able to grow. A common agent for

selecting stable transfection is Geneticin, also known as G418, which is a toxin that can be neutralized by the product of the neomycin resistance gene.

Reporter gene can be used as markers, such as the *lacZ* gene which codes for  $\beta$ -galactosidase used in blue-white screening. This method of screening relies on the principle of  $\alpha$ -complementation, where a fragment of the *lacZ* gene (*lacZ $\alpha$* ) in the plasmid can complement another mutant *lacZ* gene (*lacZ $\Delta$  M15*) in the cell. Both genes by themselves produce non-functional peptides, however, when expressed together, as when a plasmid containing *lacZ- $\alpha$*  is transformed into a *lacZ $\Delta$  M15* cells, they form a functional  $\beta$ -galactosidase. The presence of an active  $\beta$ -galactosidase may be detected when cells are grown in plates containing *X - gal*, forming characteristic blue colonies. However, the multiple cloning site, where a gene of interest may be ligated into the plasmid vector, is located within the *lacZ $\alpha$*  gene. Successful ligation therefore disrupts the *lacZ $\alpha$*  gene, and no functional  $\beta$ -galactosidase can form, resulting in white colonies. Cells containing successfully ligated insert can then be easily identified by its white coloration from the unsuccessful blue ones.

Another method of selection is the use of certain auxotrophic markers that can compensate for an inability to metabolize certain amino acids, nucleotides, or sugars. This method requires the use of suitably mutated strains that are deficient in the synthesis or utility of a particular biomolecule, and the transformed cells are cultured in a medium that allows only cells containing the plasmid to grow.

Other commonly used reporter genes are green fluorescent protein (GFP), which produces cells that glow green under blue light, and the enzyme luciferase, which catalyzes a reaction with luciferin to emit light. The recombinant DNA may also be detected using other methods such as nucleic acid hybridization with radioactive RNA probe, while cells that expressed the desired protein from the plasmid may also be detected using immunological methods.

To accomplish this, a marker gene is co-transfected, which gives the cell some selectable advantage, such as resistance towards a certain toxin. Some (very few) of the transfected cells will, by chance, have integrated the foreign genetic material into their genome. If the toxin is then added to the cell culture, only those few cells with the marker gene integrated into their genomes will be able to proliferate, while other cells will die. After applying this selective stress (selection pressure) for some time, only the cells with a stable transfection remain and can be cultivated further.

### 3.4.5 Confirmation

The finding that a recombinant organism contains the inserted genes is not usually sufficient to ensure that they will be appropriately expressed in the intended tissues. To

confirm the presence of the gene, PCR, Southern hybridization and DNA sequencing are employed to determine the chromosomal location and number of gene copies.

To assess gene expression, transcription, RNA processing patterns and expression and localization of protein products must usually be assessed, using methods including northern hybridization, quantitative RT-PCR, Western blot, immunofluorescence and phenotypic analysis. When appropriate, the organism's offspring are studied to confirm that the trans-gene and associated phenotype are stably inherited. In some cases further generations must be produced and confirmed, to ensure the absence of undesirable traits in the modified organism.

### 3.5 The Myo-Screen engineered cells

In the Myo-Screen project, the myo-genic engineered cells are the key element for the transduction of the illegal anabolic substances presence in the bovine urine sample.

Normal myogenic cells react to hypertrophic stimuli by activating a series of intracellular signaling pathways which connect the substance-receptor binding event to a variation in the expression of several genes or to an imbalance between protein synthesis and degradation.

Therefore, the phases of this process are the following:

1. Binding of the anabolic compound molecules to the correspondent cell receptors (Outside or inside the cell membrane);
2. Activation of the correspondent signaling pathway which cause a cascade of events pointing to activate/deactivate the transcription factors in the nucleus;
3. Increment/decrement in the expression of the proteins related to the genes under the transcription factors control;
4. Effects of the expression variation inside/outside the cell.

The key-idea behind the project is to discover which genes are specifically expressed in presence of the anabolic substances and to use their promoters, together with the DNA sequence codifying for the Lactate Dehydrogenase (LDH) enzyme, in order to obtain a LDH over-expression in presence of any anabolic compound. The LDH over-expression will cause an increase in the intracellular LDH concentration. Then, the cells will expel the lactate surplus, increasing its extracellular concentration.

Therefore, the cells will release the lactate surplus, increasing its extracellular concentration. Therefore, the engineered myogenic cells will be able to react in the same way



(overproducing lactate) to the presence of any anabolic compound, known or not. In order to obtain these engineered cells, the following steps have been performed:

1. Identification of the main illicit anabolic substances used within the bovine breeding, and of the types of receptors which binds them on the membrane of the myogenic cells;
2. Identification of a stable cell line expressing all the above identified receptors;
3. Test of the cell responsivity to a set of receptors agonists (anabolic substances); This step has been divided into the verification of the signaling cascade activation, and into study of the genomic effect to determine which genes are involved with the hypertrophic stimulus;
4. Preparation of plasmids with the LDH coding gene and a constitutively active promoter;
5. Stable transfection of the cells with the plasmids for the continuous or constitutive lactate over-expression;
6. Cloning of the over-expressed gene promoters and preparation of plasmids for the hypertrophy-stimulated LDH over-expression;
7. Stable transfection of the cells with the plasmids for the hypertrophy-stimulated LDH over-expression;

Steps number four and five have been introduced in order to test the efficiency of the system of lactate production (by the engineered cells) and detection ,i.e., the electrochemical lactate sensor in ideal conditions. The success of these test is a fundamental prerequisite for the project.

### **3.5.1 Illegal substances and cell receptors**

The main illicit substances used for bovine treatments in breeding are reported in table 2.3, together with their category and control levels. Conversely, table 3.3 shows the cell receptor which binds to the same illicit substances.

The receptors involved in the detection of these substances by the cell are four, i.e., receptors for Estrogens (ER), Androgens (AR), Progesterone (PR), and  $\beta$ 2-adrenergic ( $\beta$ 2-Ar) compounds. Therefore, a basic requirement is that the myogenic cells to be engineered for the substances detection must have all these receptors.

Substance	Category	Receptors
Diethylstilbestrol	Stilbens	Estrogens
Dienestrol	Stilbens	Estrogens
Esestrol	Stilbens	Estrogens
Thiouracile	Thyroid antagonists	
Methylthiouracile	Thyroid antagonists	
Propylthiouracile	Thyroid antagonists	
Fenylthiouracile	Thyroid antagonists	
Tapazole	Thyroid antagonists	
Mercaptobenzoimidazole	Thyroid antagonists	
Ethinylestradiol	Synthetic estrogens	Estrogens
Estradiol	Estrogens (natural)	Estrogens
Testosterone	Androgens (natural)	Androgens
Progesterone	Progestinics (natural)	Progesterone
Methyltestosterone	Androgens (synthetic)	Androgens
Nortestosterone	Androgens, (synthetic)	Androgens
Trenbolone	Androgens, (synthetic)	Androgens
Boldenone	Androgens, (synthetic)	Androgens
Zeranol	Resorcilic acid lactones	Estrogens
Clenbuterol	Clenbut.-like $\beta$ -agonists	$\beta$ 2-adrenergic
Bhromebuterol	Clenbut.-like $\beta$ -agonists	$\beta$ 2-adrenergic
Clenpenterol	Clenbut.-like $\beta$ -agonists	$\beta$ 2-adrenergic
Mabuterol	Clenbut.-like $\beta$ -agonists	$\beta$ 2-adrenergic
Mapenterol	Clenbut.-like $\beta$ -agonists	$\beta$ 2-adrenergic
Cimaterol	Clenbut.-like $\beta$ -agonists	$\beta$ 2-adrenergic
Cimbuterol	Clenbut.-like $\beta$ -agonists	$\beta$ 2-adrenergic
Salbutamol	Salbut.-like $\beta$ -agonists	$\beta$ 2-adrenergic
Terbutaline	Salbut.-like $\beta$ -agonists	$\beta$ 2-adrenergic
Isoxuprine	Salbut.-like $\beta$ -agonists	$\beta$ 2-adrenergic
Ractopamine	Salbut.-like $\beta$ -agonists	$\beta$ 2-adrenergic
Zilpaterol	Salbut.-like $\beta$ -agonists	$\beta$ 2-adrenergic

TABLE 3.3: Main illicit anabolic substances, their categories, and the cell receptors which detect them.

### 3.5.2 Cell line selection

A wide variety of cell lines were considered for the process of genetic engineering in the project. Unfortunately, no cells expressing the Progesteron receptor were found. However, several cell lines expressing the other receptor were identified (Table 3.4).

Between these cases, particular attention was directed to NIH3T3, C3H10T1/2, C2C7 and H9C2 cell lines. A literature search was performed to consolidate the theoretical basis for the usage of one of these cell lines for the project purpose. The NIH3T3 cell line have been used to highlight the importance of adrenoceptors in the cardiovascular system [39], the role of androgen receptors in the cell migration [40], and that one of estrogens in breast tumor [41].

Cell line	Type	Specie	$\beta 2$ -Ar	AR	ER	PR
NIH3T3	Embryo fibroblasts	mouse	X	X	X	
C3H10T 1/2	Embryo Mesenchimals	mouse	X	X	X	
C2C7	myoblasts	mouse	X	X	X	
mRAW 264.7	Macrophages	mouse	X			
3T3-F442A	preadipocytes	mouse	X			
MC3T3-E1	osteoblasts	mouse	X			
H9C2	Ventr. embryo myoblasts	rat	X	X	X (Er $\beta$ )	
C6	Glioma	rat	X			
L6	Skeletal muscle	rat	X		X (Er $\alpha$ )	
RGM1	gastric muc. epith.	rat	X			
INS-1 $\beta$ -cells	Insulinome	rat	X			
A549	Adenocarcinome epith.	human	X			
hTERT	miometr. rev. transcript.	human	X			
H292	Respiratory epithelials	human	X			
SaOS-2	osteoblasts-like	human	X			
TE-85	osteoblasts-like	human	X			
MG-63	osteoblasts-like	human	X			
MCF7	breast cancer	human			X (ER $\alpha$ )	
T47-D	breast cancer	human			X (ER $\alpha,\beta$ )	
ZR-75-1	breast cancer	human			X (ER $\alpha$ )	
HCC1954	breast cancer	human			X (ER $\alpha,\beta$ )	
SK-BR-3	breast cancer	human			X (ER $\alpha,\beta$ )	
PC-3	prostate cancer	human		X		
DU-145	prostate cancer	human		X		
LN-CaP	prostate cancer	human		X		
CWR22R	prostate cancer	human		X		

TABLE 3.4: Main illicit anabolic substances, their categories, and the cell receptors which detect them.

The C3H10T1/2 cell line androgen and  $\beta 2$ -adrenergic receptors have been studied by Jasuja et al. [42] and Takahata et al. [43], respectively.

Conversely, the C2C7 cell line have been sub-cloned from the C2C12 in CH3 mice, which have been recently characterized by Baek et al. in 2011, Wannenes et al [44], Yong et al. in 2010, and Vasconsuelo et al. [45].

Finally, H9C2 cell line androgen and Estradiol receptors have been studied by Ikeada et al in 2010, Urata et al [46], and Yano et al. in 2007.

### 3.5.2.1 FBS deprivation tests

An important characteristic of the cell line to be selected for this project is its survival into a medium as poor as possible of substances which could interfere with the lactate biosensor electrochemical measurements. A first fundamental point in the medium choice is that its composition has to be completely known. Therefore, the Fetal Bovine Serum

(FBS) has to be avoided. In order to check if the cells can survive without FBS, the four cell lines selected for the project were grown in Dulbecco's Modified Eagle Medium (DMEM) and 20% FBS, then rinsed and kept in pure DMEM for six days. The cells were counted, by image counting, at the beginning and at the end of the experiment. As reported in table 3.5, the cells of all the cell lines survived but only the C2C7 cells kept their final number almost identical to the initial one, while the other cell lines increased their number.

Counting set	NIH3T3	C3H10T1/2	C2C7	H9C2
Initial	225672	299172	292343	301679
Final	402527	374863	296951	394564
Variation	176855	75691	4608	92885

TABLE 3.5: Number of cells before and after the six day experiment in DMEM without FBS for the selected cell lines.

The stability of the cells number during the experiments will allow to easily normalize the lactate production in contact with the urine animal sample to the cell number. Therefore, the C2C7 cell line was selected for the next experiment in the project. Figure 3.7 shows both white light and fluorescence microscope pictures of the C2C7 cells.

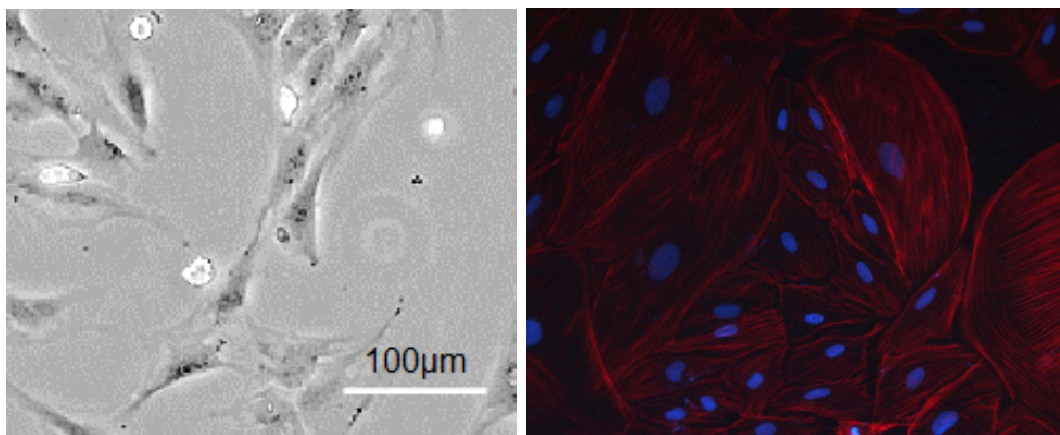


FIGURE 3.7: White light and fluorescence pictures of C2C7 myogenic cells.

### 3.5.2.2 Medium/buffers tests

Once selected the cell line, another series of tests regarding the cell medium were performed. In fact, the exclusion of FBS allows to know the complete composition of the cell medium but this doesn't exclude the presence in the medium of substances which could interfere with the electrochemical measurements.

Therefore, the survival of the C2C7 cells in different buffer solutions/medium was tested with an incremental approach. Four medium/buffers were selected, starting from a minimal one, i.e. Tris-HCl, and going on with more rich medium/buffers, i.e. Phosphate

Buffered Saline (PBS), often used within a large set electrochemical measurements, and HEPES-Buffered Ringer's Solution (HBRS). The last and richest medium considered was DMEM. The compositions of these medium/buffers is reported in table 3.2 of this chapter.

The cells were kept in DMEM without FBS for 48 hours, then the medium was substituted with the medium/buffer. For each buffer, four cultures with a density of  $12.5 \text{ cells/cm}^2$  were prepared. Two cultures were kept inside the incubator and the other two were kept outside, at room temperature. Their status was checked at the microscope at 2, 4, 6, 8, 24 hours. As expected, after 24 hours the cells in DMEM were still adherent to the flask surface, while the cell in PBS and Tris-HCl showed signs of deterioration just 1 and 2 hours after the beginning of the experiment, respectively. The cultures status at 4, 6, 8 hours shows an increment of the cells in suspension. At 24 hours all the cells of all the cultures were detached from the flask surface.

The cells in HBRS in the incubator start detaching from the flask after 4 hours and died entirely after 24 hours. Conversely, the 70-80% of the cells outside the incubator survived after 48 hours.

### 3.5.3 Anabolic substances effect on cells

The classes of anabolic substances analyzed cause different effect on the cells. Their detection by the correspondent receptors causes a cascade of events which arrive to the nucleus, affecting the gene expression, thus modifying the proteome of the cells. Therefore, this cascade of events can be divided into a signaling pathway, which is triggered by the substance detection by the receptor and is concluded by the activation of specific transcription factors, and a genomic effect, that is related to specific genes over-expression and the over-production of the relative proteins.

#### 3.5.3.1 Signaling pathway

Regarding the signaling pathway, in literature there are several studies which investigate the non-genomic fast effect of  $\beta$ 2-adrenergic, androgen, estrogen and progesteron receptors effects. Most of these studies prove that these substances have a direct effect on the MAPK signaling pathway, previously described in this chapter. For example, in 2012 Kaya et al. stated that  $\beta$ 2-adrenergic receptor mediates ERK phosphorylation [47], while Dubois proved found that Androgens may exert fast non-genomic effects through interactions between the AR receptor and the tyrosine kinase c-Src, inducing the MAPK signaling cascade [48]. In 2008, Boland stated that, among the rapid actions

of the Estradiol receptor, the activation of PI3K/Akt and MAPKs have been demonstrated [49] and even Progesterone induces a rapid increase in ERK phosphorylation in cells doted by the correspondent receptor [50]. The scheme of figure 3.8 summarizes the effect of the anabolic substance classes considered in this project. All these substances cause a variation in the ERK phosphorylation. Therefore, a preliminary test to observe their short term non-genomic effect was directed to the quantification of the phosphorylated ERK.

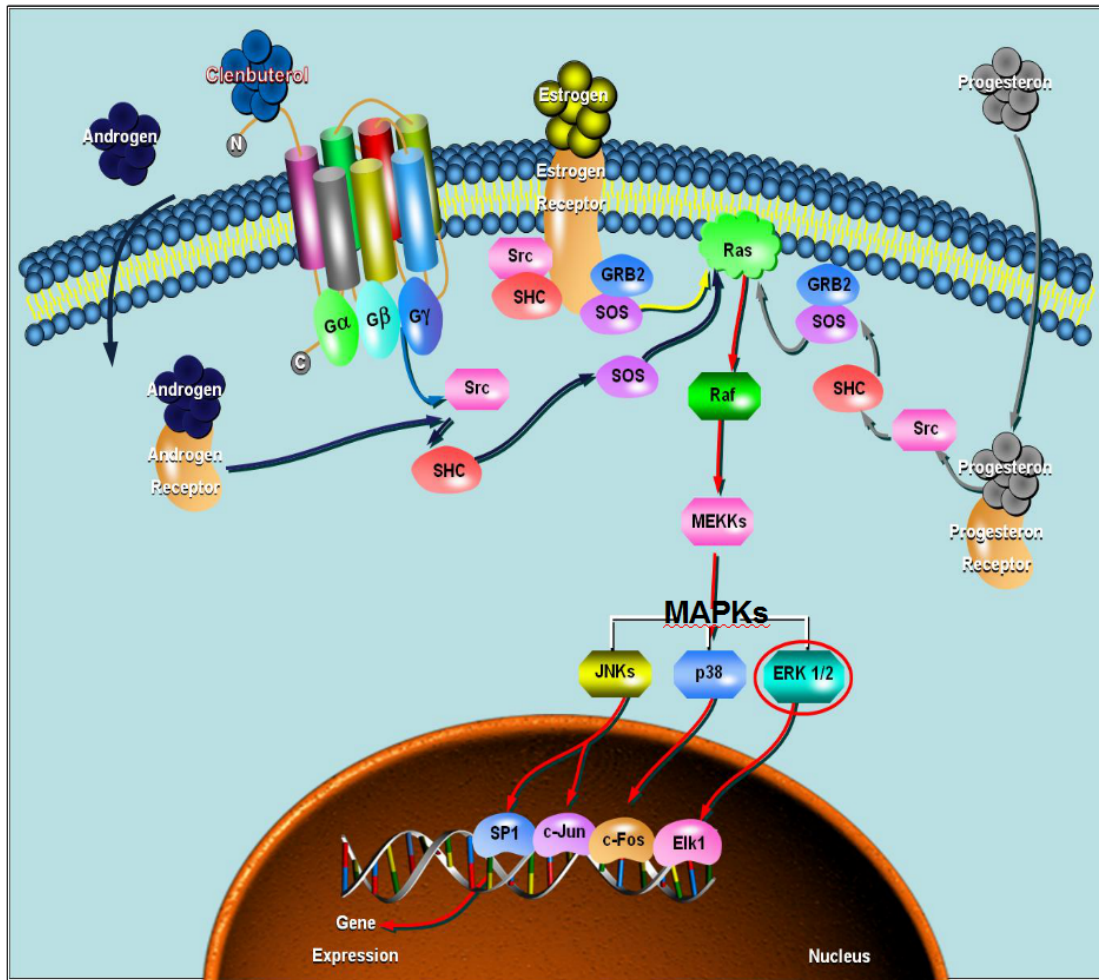


FIGURE 3.8: Signaling pathway from the anabolic substances binding with their receptors to the transcription factors in the nucleus through the MAPKs

The C2C7 cells were kept in absence of serum for 48 hours, then they were treated for 5 minutes with 20% FBS (positive control), or 1  $\mu$  M Clenbuterol, or 100 nM 17- $\beta$  Estradiol, or 100 nM Testosterone, or 100 nM Progesterone.

After the treatment, the cell proteins were extracted by centrifugation and ERK, pERK and GAPDH were separated by Western Blot and quantified by the bands intensity measurement. GAPDH were used as negative control.

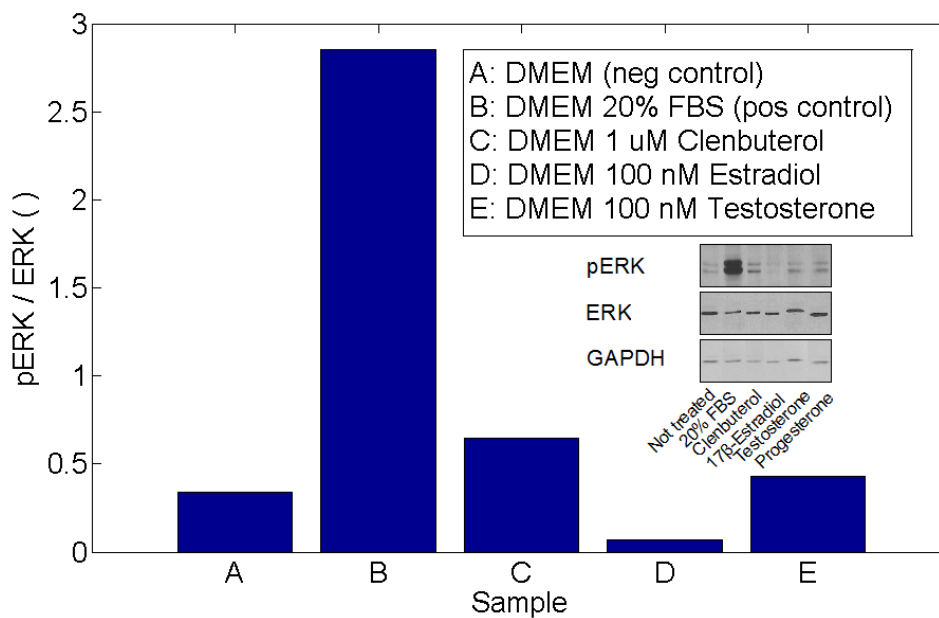


FIGURE 3.9: Phosphorylated/not phosphorylated ERK bands obtained by the Western blot tests and their intensity ratio for C2C7 cells treated with four different anabolic compounds for 5 minutes. Cells treated with 20% FBS were used as positive control, untreated cells as negative one.

As shown in the figure, both Clenbuterol and Testosterone cause a significant increase of the phosphorylated/not-phosphorylated ERK ratio. Conversely, Estradiol cause a reduction of this ratio with respect to the untreated cells.

### 3.5.3.2 Genomic effect

In order to monitor the anabolic substances genomic effect, four target genes were considered:

- IGF1 (Insuline Growth Factor 1): mediates the skeletal myotube hypertrophy through the Akt pathways [51], [52], [53];
- IGF1R (Insuline Growth Factor 1 Receptor): is involved in the myoblast-independent muscle hypertrophy via PI3K and P110 $\alpha$  pathways [54], [55];
- Pgc1- $\alpha$  (Peroxisome proliferator-activated receptor gamma co-activator 1 alpha): is a transcriptional co-activator related to metabolic remodeling and muscle hypertrophy [56], [57], [58];
- EGR2 (Early Growth Response 2): "zinc finger" type transcriptional factor which can interact with the NFAT trascriptional factors, involved in the hypertrophic processes [59].

A first experimental test were directed towards the investigation of the effect of different concentrations of the anabolic substances on the target genes expression. Therefore, two concentrations which could be found in treated animal urine were used to treat C2C7 cell cultures for 24 hours, for each anabolic substance.

In particular, the cells were kept without FBS for 48 hours and then were treated with the selected substances (Clenbuterol, Testosterone, and  $17\beta$ -Estradiol) at the selected concentrations, i.e., 100 nM and 1  $\mu$ M. Three cell cultures were used for each test. After 24 hours the cells RNA were extracted and gene expression was quantified by qRT-PCR. The target gene EGR2 was not been tested for 24 hours because these tests have already been performed in a recent work of the group. However, its expression over time were further characterized in the next analysis.

Figure 3.10 shows the relative fold induction of the target genes expression for the C2C7 cells treated with Clenbuterol, with respect to the not treated cells (n.t.). Figures 3.11 and 3.12 show the same results for Testosterone and Estradiol, respectively.

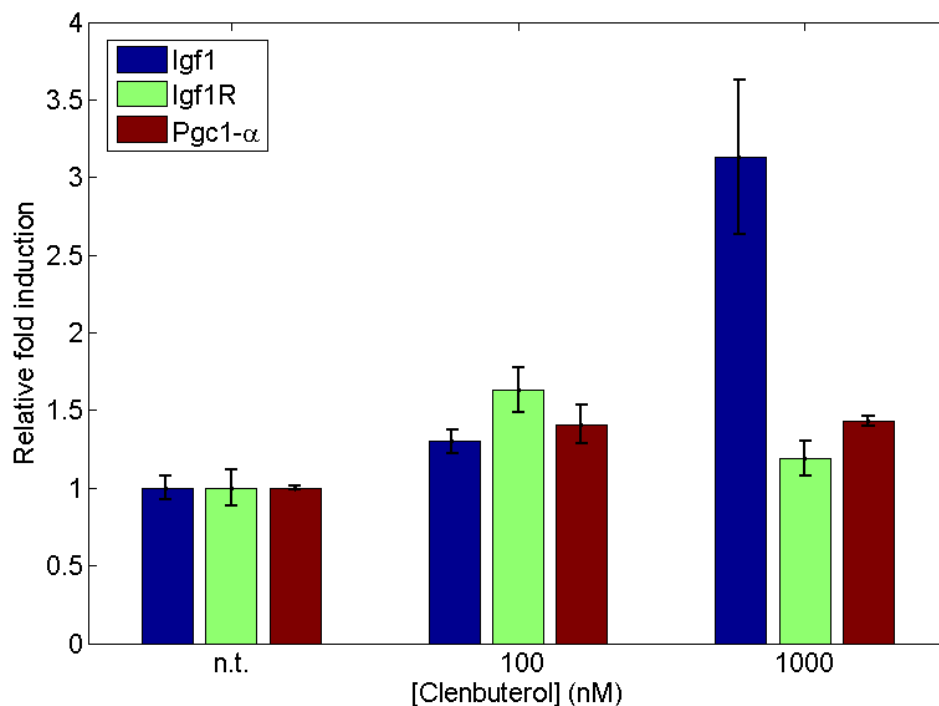


FIGURE 3.10: Target genes expression dependence upon the Clenbuterol concentration. The n.t. cells have not been treated with any anabolic substance.

Although for both Clenbuterol and Estradiol the highest variations were recorded in correspondence to the highest concentrations, Testosterone showed higher variation for the 100 nM concentration than for the 1  $\mu$ M one. For this reason, in the next experiments Testosterone was tested at 100 nM concentration. The same was done with Estradiol, but for a different reason. In fact, Estradiol control level in animal urine is 20 times



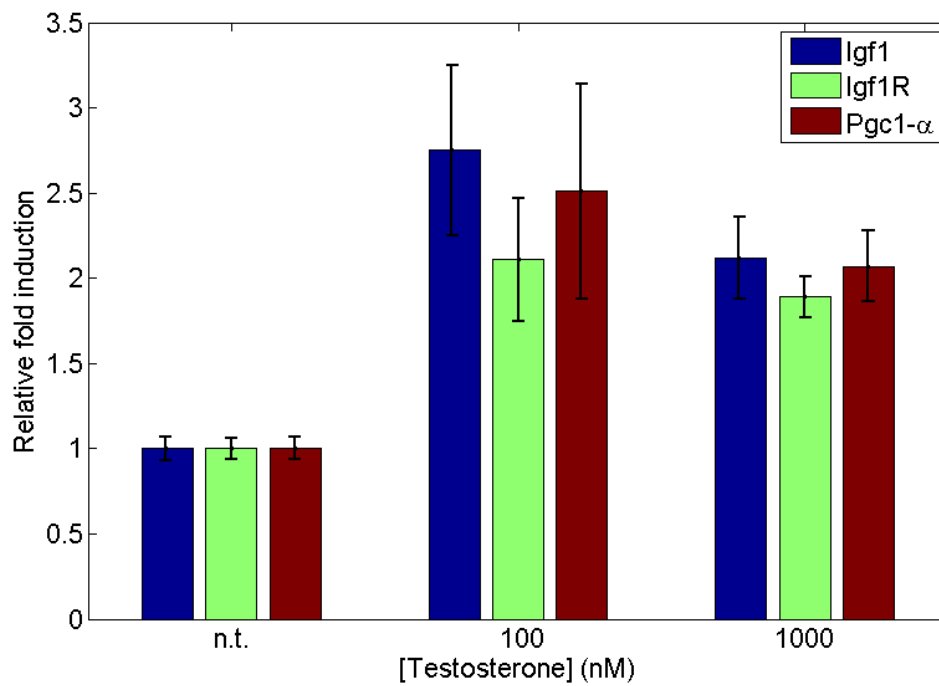


FIGURE 3.11: Target genes expression dependence upon the Testosterone concentration. The n.t. cells have not been treated with any anabolic substance.

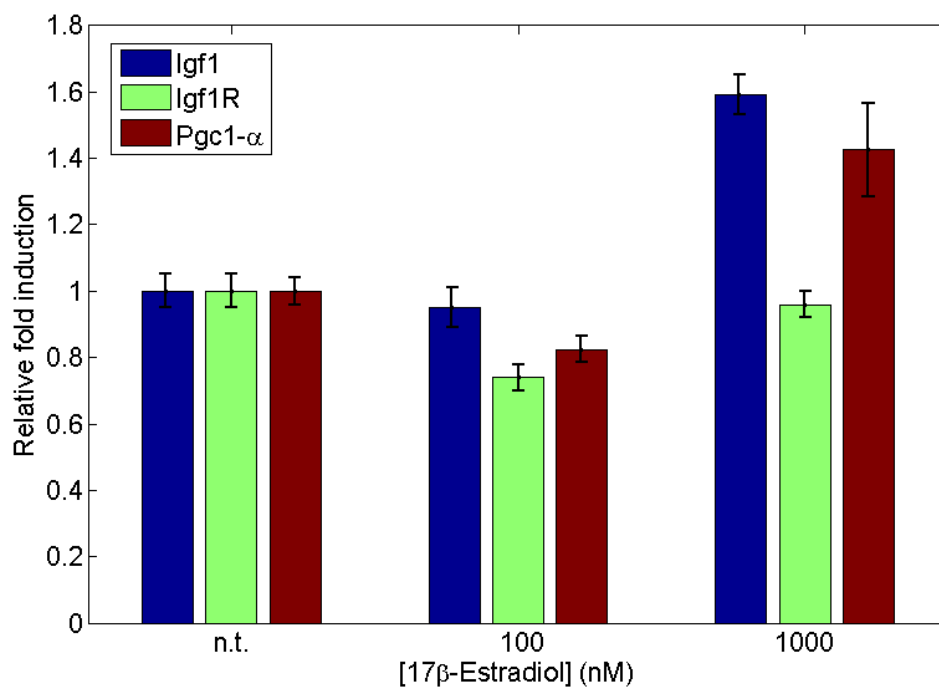


FIGURE 3.12: Target genes expression dependence upon the Estradiol concentration. The n.t. cells have not been treated with any anabolic substance.

lower than the Testosterone one (2.3), thus it is necessary to test its detection at smaller concentration than Testosterone. Finally, since Clenbuterol show a huge increment of the target genes expression for the 1  $\mu\text{M}$  concentration (in particular for IGF1), this concentration was chosen for its next tests.

Having proved the 24 hours genomic effect of the anabolic substances over the considered target genes, the question to be answered is which is the minimal time required for the cells to express these genes. In order to answer this question, a time course for each target gene was performed for each anabolic substance.

The RNA was quantified as in the previous experiment 2, 4, 8 hours after the cultures exposition to the anabolic substances at the concentrations defined from the results of the previous experiment.

The following figures represent the induction fold expression of IGF1 (figure 3.13), IGF1R (figure 3.14), Pgc1- $\alpha$  (figure 3.15), and EGR2 (figure 3.16), for the three anabolic substances considered. As in the previous experiment, three C2C7 cultures were tested for each target gene/time/anabolic substance combination, and the bars in the plots represent the standard deviations obtained within these tests.

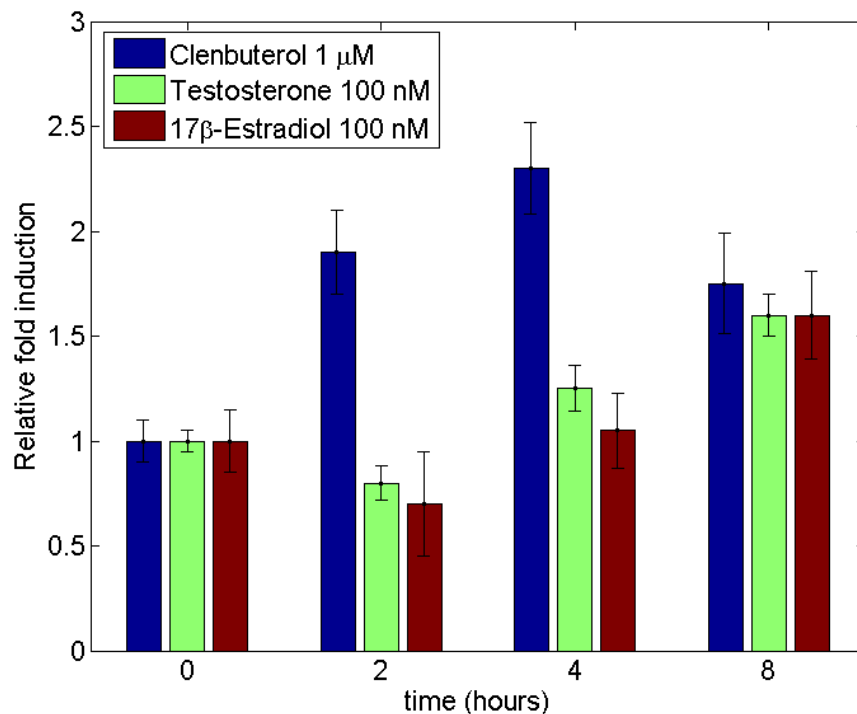


FIGURE 3.13: Time course of the IGF1 gene expression for cells treated with Clenbuterol, Testosterone and Estradiol.

Regarding IGF1, after 8 hours all the anabolic substances caused an over-expression of the target gene, but a remarkable effect is correlated to Clenbuterol after just 2 hours of treatment. The same effect was found with IGF1R. However, in this case the

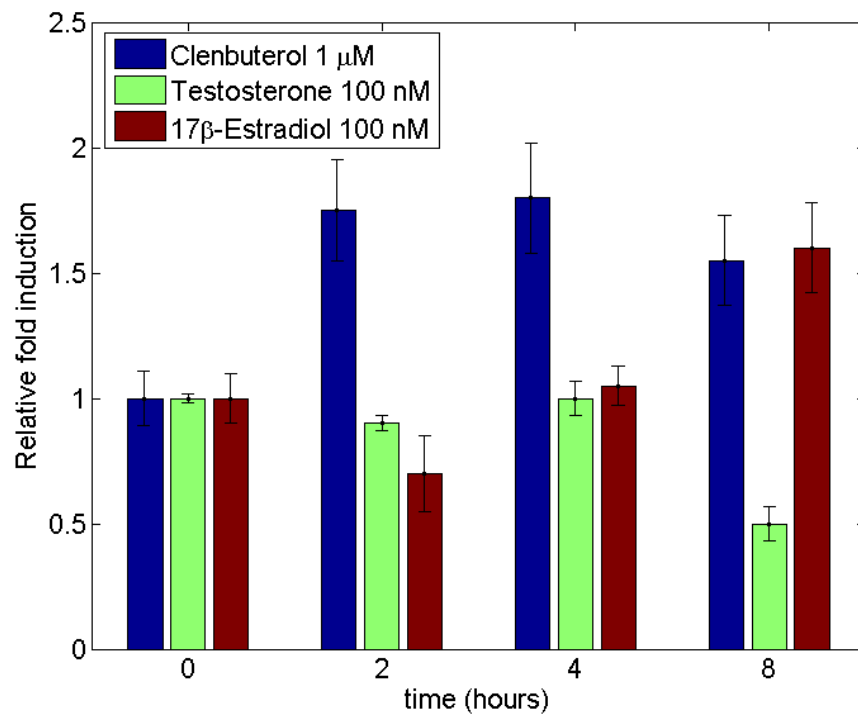


FIGURE 3.14: Time course of the IGF1R gene expression for cells treated with Clenbuterol, Testosterone and Estradiol.

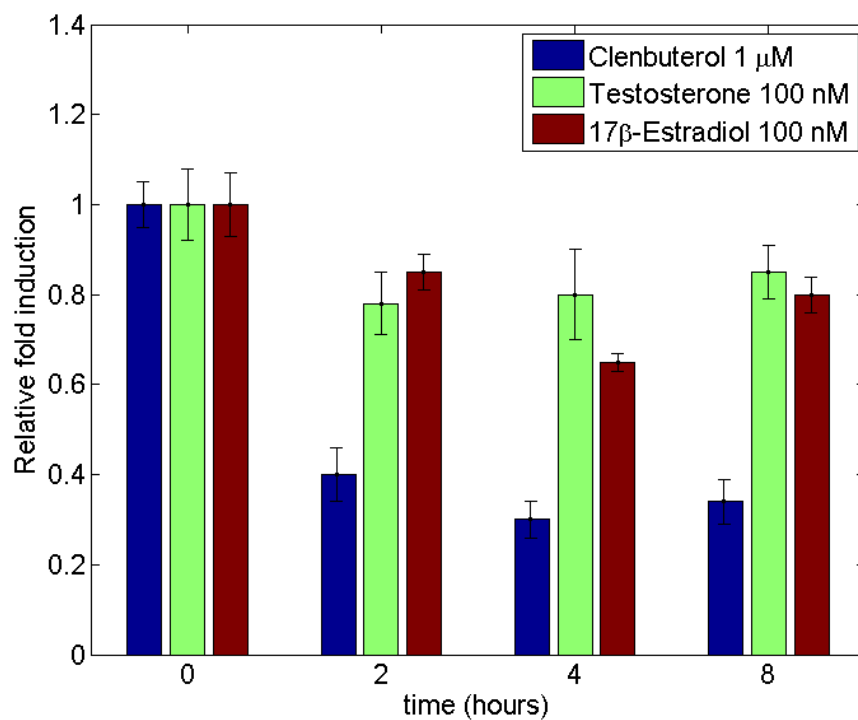


FIGURE 3.15: Time course of the Pgc1- $\alpha$  gene expression for cells treated with Clenbuterol, Testosterone and Estradiol.

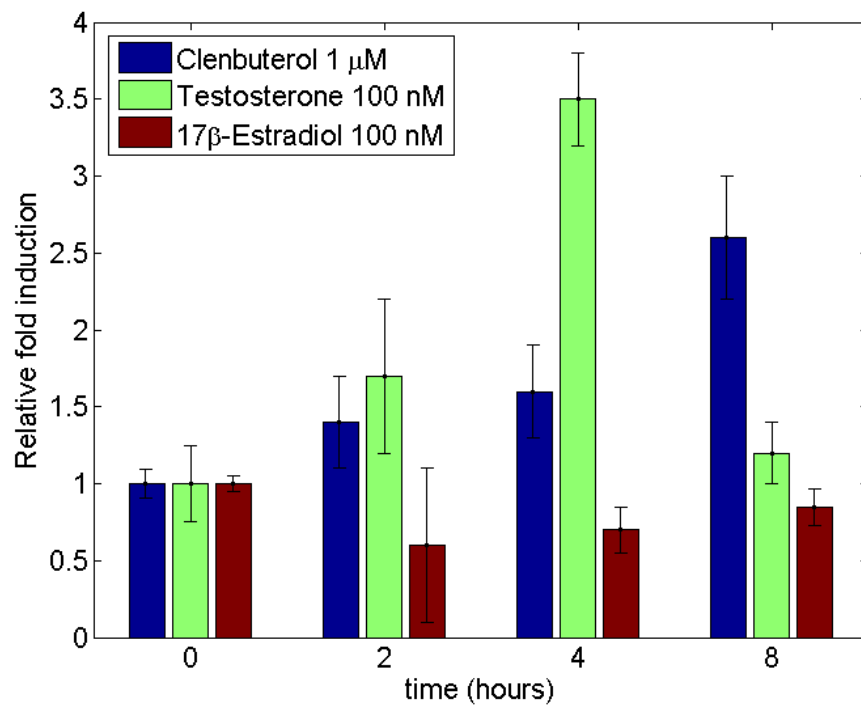


FIGURE 3.16: Time course of the EGR2 gene expression for cells treated with Clenbuterol, Testosterone and Estradiol.

Testosterone treatment did not cause the over-expression of this gene while the reaction to the Estradiol treatment has become relevant only after 8 hours. Conversely, the target gene Pgc1- $\alpha$  didn't show any result with the three anabolic compounds. Even worse, Clenbuterol in this case showed the induction of a reduction in the gene over-expression. Finally, EGR2 showed good results for Clenbuterol and Testosterone after 4 hours. In fact, the gene over-expression reached 1.5 and 3.5 that one of the untreated cells, respectively. However, Estradiol caused a reduction of EGR2 expression which persisted after 8 hours. Therefore, only IGF1 showed over-expression in presence of all the anabolic substances considered and for this reason it was chosen as election gene for the myogenic C2C7 cell hypertrophy transduction.

### 3.5.4 Cells genetic engineering

The gene which is naturally over-expressed in C2C7 cells in presence of the selected anabolic substances was identified. Therefore, in order to modify the cells for the lactate production in presence of these substances, the IGF1 gene promoter has to be isolated and used as promoter of the gene codifying for the enzyme Lactate Dehydrogenase (LDH). This will cause the over-expression of LDH under the hypertrophic stimulus and thus the over-production of lactate in the cell, which will be rapidly released from the

cells. The IGF1 promoter sequence was obtained from the GenBank and it's reported in figure 3.17.

```
GTGGAAGCCTTGGGTTACTGTATGTGCAAGGGATTGCCACAACCTGCAGATATGGCAGGACCACCTGATGATGCCACACTTCT
GTGTGTTCTCAGAGTCAGTCCCTACCCACAGGAACCTCCAGCCCGTGCCTTCACATAGCATTCTCTCCTTCCCCATCTCCA
TTTCCAAAAGCTTTCACTTCCCTGCCTCCCTGAGAGACTGGGGCCCCCTCCCACCCTCATAAGTCTTCACGCTTCAGATACT
CAACAGACGTCAGGAACGTGTGTCTCTCCCTGCCTGTGTCATGCTCCCTTTTTGCTTTACCAGAGGTGTGTCTAATCAAGTACA
TAGTAGGTGCTGTTCATCACATGATTCCTTCATCAAGTGATACCTAGCATCACCCACCCTGGAAACAGTCTCACACCAGGTTTC
TAATGTTCCCTGTCTGAAAGGTAACACTGCTGTGAAGTATTGACCACACAGAGGGTTGGAAAGAGCCCAAGCCCTTGCAAAA
CCAACTGGTTTCATTTGAGGACAATCACACATCCCCAAGCAGGTTTCTATCCATGGGGCAGCGTAAAGAGGCAGTGTAGAG
TTTCCAACTGGCCTCTGTCTCCACCGATGTGTCAGTACCTCAAATCCCCCTGAGAGTCCGAGAGAGTAAGAGACTGAGGCAA
GTCTGGCTCATTTCCATCTCCCTGGGAAAGCACACCTGGAGAGATATCCGTGGAAAGCATGCAGCGTCTAATCTGGGCTTTT
GTAACCTTCTTTATAAATTCATTTCTTATCTACTGCCTCTGAAAGACCCTGAGAAATAGETACAAACCGTATCAACAGAAG
ATCAGAACTCCATTCCTGTGGCAAAGGCAGTTTATACATTTATAAATAGCAGAAGCAGCCGGCTTGAACCATGCTGCCAGCC
ACTTACCCAGTTGAGGGATTTGAATGACATCATAACCCTGGAGAGATATTGCTAGCCAGCTGGTATTATTTGGAATACACAC
TCAGACACAGACACAGACACACACACTTACACACACACACATATGCATGCATGCACACATACACACAACCTGTGTCTCAC
ACACACACACACACTCATTATAGAGAACAATACAGCCAACGGGAAACAGTGTGTGCCTCCCATACTGCTTCCTTGGGGTC
AAGGAGGTGACAGGCATCCAGCTTTGTTGAAAAC TAGGATCATTTTATTTTTCAATCCATCCCAGATCTCAGCATAGCCCTGAT
TCTCTGCACAAAGCATGACACAGTGTCTGACAGGAGCCAGCCACTGCTGCCTGGCCATCTATAGGTTTTAGGAAATGAGAT
CATTCCCCTTGCCCTGGCAACTAGGACAAGGGTCACTCTATCCCTCCACCTCCCCTTCCCTGAGAGCTGCCCTTCGATCTAG
TTTACCCTGTGCATTTAGGGTTAACAGCATTTGCTTCCCTGGAGATAGTCTCTCTTCTCTTTTTTTGTTTTTTTTTTCCTTC
AAATTTTGCATTTGCCCTAAAAATATAAAGTTGCCCCCGTGTCCCACTTAGATCCTCTAATCCTGGTGGAGGTGATTAGCACAC
AAGTGTACCTTCAAACCTGTGAAAAGTTAATCAGAGAACAGAGCCTATTTTTCTATGGCAGCCCTCAGTATTAAATGCTGTGCT
AACCTGTGACAGACACACATTTTTAGGGGGGGGGGGTGAAGTCTCTGTGCTCCAGTTTTTAAGAGCGAAGGTATGATGT
TATTTGTACCGGTGCCCAAAAAGTCCCTTACTCGATAACTTTGCCAGAAGAGGGAGAGAGAGAAGGCCAATGTTCCCCCAG
CTGTTTCTCTTACAGTGTCTGTGTTTTGTAGATAAATGTGAGGATTTTCTCTAAATCCCTCTCTGCTTGTCTAAATCTCAC
TGTACTGCTAAATTCAGAGCAGATAGAGCCTGCCAATGGAATAAAGTCCCTCAAATGAAATGACATTGCTCTAACATC
TCCCATCTCTCTGGATTCTTTTTTCGCTCATTATCCCTGCCACCAATTCATTTCCAGACTTTGTACTTCAGAAGCGATGGG
GAAATCAGCAGCCTTCCAACCTCAATTAT
```

FIGURE 3.17: Mouse IGF1 promoter DNA sequence of the ATG exon 1 (GenBank: Y18062.1, 2070 bp)

To obtain the cells engineered for the hypertrophy-stimulated LDH over-expression, three steps were performed:

1. Verification of the IGF1 promoter triggering effect for the expression, in the C2C7 cells, of the gene incorporated into the transfected plasmid;
2. Verification of the extracellular lactate production of C2C7 cells transfected with a plasmid containing the LDH gene and an always active promoter;
3. Verification of the extracellular lactate production of C2C7 cells transfected with a plasmid containing the LDH gene and the IGF1 promoter in presence of different anabolic substances.

In every case, the C2C7 cells transfection was performed by Lipofection, using Lipofectamine3000<sup>®</sup> by Life Technologies. Within this method the plasmid DNA is inserted in a liposomes which are absorbed by the cell membrane forming endosomes. The endosome free the plasmids into the cell and they penetrate into the nucleus through its pores. Here, they are used to codify mRNA which is exported in the cytoplasm and used for the expression of the protein of interest, as schematized in figure 3.18.

Lipofectamine reagent contains lipid subunits that can form liposomes in aqueous environment, which entraps the transfection materials, i.e., DNA plasmids. Lipofectamine is a cationic liposome formulation, which complexes with negatively charged nucleic acid

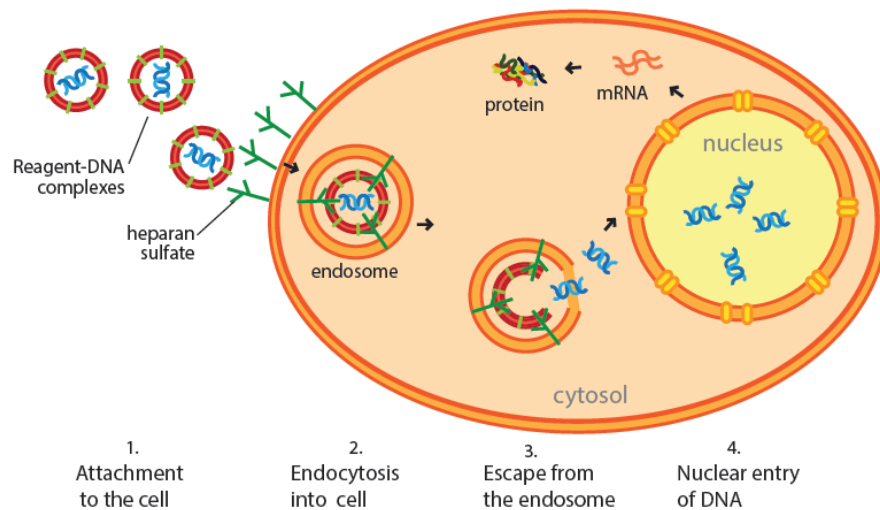


FIGURE 3.18: The Lipofection is a four step process that involves attachment to the cell, endocytosis into the cell, endosomal escape and nuclear entry for transcription to mRNA. The mRNA is then exported from the nucleus to the cytoplasm and translated into the protein of interest.

molecules to allow them to overcome the electrostatic repulsion of the cell membrane. Lipofectamine cationic lipid molecules are formulated with a neutral co-lipid (helper lipid). The DNA-containing liposomes (with positive charge on their surfaces) can fuse with the negatively charged plasma membrane of living cells, due to the neutral co-lipid mediating fusion of the liposome with the cell membrane, allowing nucleic acid to cross into the cytoplasm and contents to be available to the cell for replication or expression.[2]

In order for a cell to express this transgene, the nucleic acid must reach the nucleus of the cell to begin transcription. This process involves many risks. The transfected genetic material may never reach the nucleus in the first place, instead being disrupted somewhere along the delivery process. In dividing cells, the material may reach the nucleus by being trapped in the reassembling nuclear envelope following mitosis. But also in non-dividing cells, research has shown that Lipofectamine improves the efficiency of transfection, which suggests that it additionally helps the transfected genetic material penetrate the intact nuclear envelope.

The protocol used for Lipofection is described in the following scheme (figure 3.19):

To verify that the proper sequences are inserted in the vector, each time that the vector is modified by the addition or removing of some genetic material it undergoes a sequencing step. The sequencing technique adopted is Cycle sequencing with Sanger method. Cycle sequencing is a simple method in which successive rounds of denaturation, annealing, and extension in a thermal cycler result in linear amplification of DNA extension products (figure 3.20). The products are then injected into a capillary for electrophoretic separation.








Timeline	Steps	Procedure Details (Two Reaction Optimization)				
		Component	96-well	24-well	6-well	
Day 0	1  Seed cells to be 70-90% confluent at transfection	Adherent cells	1-4 × 10 <sup>4</sup>	0.5-2 × 10 <sup>5</sup>	0.25-1 × 10 <sup>6</sup>	
		2  Dilute Lipofectamine® 3000 Reagent in Opti-MEM® Medium (2 tubes) – Mix well Vortex 2-3 sec	Opti-MEM® Medium	5 µL × 2	25 µL × 2	125 µL × 2
			Lipofectamine® 3000 Reagent	0.15 and 0.3 µL	0.75 and 1.5 µL	3.75 and 7.5 µL
Day 1	3  Prepare master mix of DNA by diluting DNA in Opti-MEM® Medium, then add P3000™ Reagent – Mix well	Opti-MEM® Medium	10 µL	50 µL	250 µL	
		DNA (0.5-5 µg/µL)	0.2 µg	1 µg	5 µg	
		P3000™ Reagent (2 µL/µg DNA)	0.4 µL	2 µL	10 µL	
Day 1	4  Add Diluted DNA to each tube of Diluted Lipofectamine® 3000 Reagent (1:1 ratio)	Diluted DNA (with P3000™ Reagent)	5 µL	25 µL	125 µL	
		Diluted Lipofectamine® 3000 Reagent	5 µL	25 µL	125 µL	
		5  Incubate	Incubate for 5 minutes at room temperature.			
Day 1	6  Add DNA-lipid complex to cells	<b>Component (per well)</b>	<b>96-well</b>	<b>24-well</b>	<b>6-well</b>	
		DNA-lipid complex	10 µL	50 µL	250 µL	
		DNA amount	100 ng	500 ng	2500 ng	
		P3000™ Reagent	0.2 µL	1 µL	5 µL	
Day 2-4	7  Visualize/analyze transfected cells	Lipofectamine® 3000 Reagent used	0.15 and 0.3 µL	0.75 and 1.5 µL	3.75 and 7.5 µL	
		Incubate cells for 2-4 days at 37°C. Then, analyze transfected cells.				

FIGURE 3.19: Life Technologies Lipofectamine3000<sup>®</sup> protocol used for the C2C7 cells transfection in 24 wells plates.

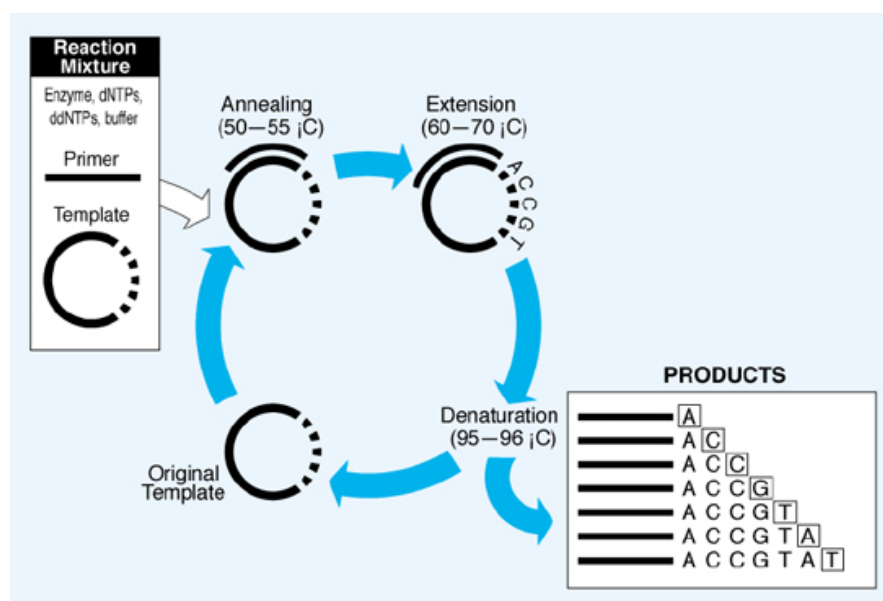


FIGURE 3.20: Cycle sequencing schematic. Consecutive annealing, extension and denaturation steps are cyclically repeated in order to increase the sequencing yield.

The extension product grows by the formation of a phosphodiester bridge between the 3'-hydroxyl group on the primer and the 5'-phosphate group of the incoming deoxynucleotide. Growth occurs in the 5' to 3' direction. DNA polymerases can also incorporate analogues of nucleotide bases. The dideoxy method of DNA sequencing developed by Sanger et al. in 1977 takes advantage of this characteristic by using 2',3'-dideoxynucleotides as substrates. When dideoxynucleotides are incorporated at the 3' end of the growing chain, chain elongation is terminated selectively at A, C, G, or T. This is because once the dideoxynucleotide is incorporated, the chain lacks a 3'-hydroxyl group so further elongation of the chain is prevented.

#### 3.5.4.1 Verification of the IGF1 promoter triggering effect

In order to verify the triggering effect of the IGF1 promoter and the effectiveness of the C2C7 cells transfection, a vector was prepared inserting IGF1 as promoter for the expression of a reporter gene. The vector is of the type pGL4 (Promega) and is composed by seven blocks (figure 3.21):

- The gene coding for the Ampicillin resistance: used to select the successfully transfected cells from the other ones;
- The inserted IGF1 promoter: to trigger the reporter gene expression in presence of the anabolic substances;
- The reporter gene: coding for the Luciferase enzyme, in order to measure its luminescence if the promoter will trigger its expression;
- The SV40 late polyA: promote efficient polyadenylation;
- The SV40 early promoter: promote efficient polyadenylation;
- The selectable marker block: which allow to select marker genes for hygromycin (Hygro), Neomycin (Neo), and puromycin (Puro);
- The synthetic polyA block.

Three cultures of C2C7 cells, transfected by the IGF1-modified pGL4 vector with the Lipofection protocol described in the previous paragraph, were treated with Clenbuterol 1  $\mu$ M for 24 hours. The proteins of these three cultures were extracted and analyzed at the luminometer. Their average luminescence was compared to that one of other three C2C7 cultures transfected with the basic pGL4 vector (without the IGF1 promoter insertion). The results are depicted in table 3.6 and show a 4 fold induction of the Luciferase expression, proving the capability of the transfected C2C7 cell to transduce the hypertrophic stimulus by the IGF1 promoter triggering effect.



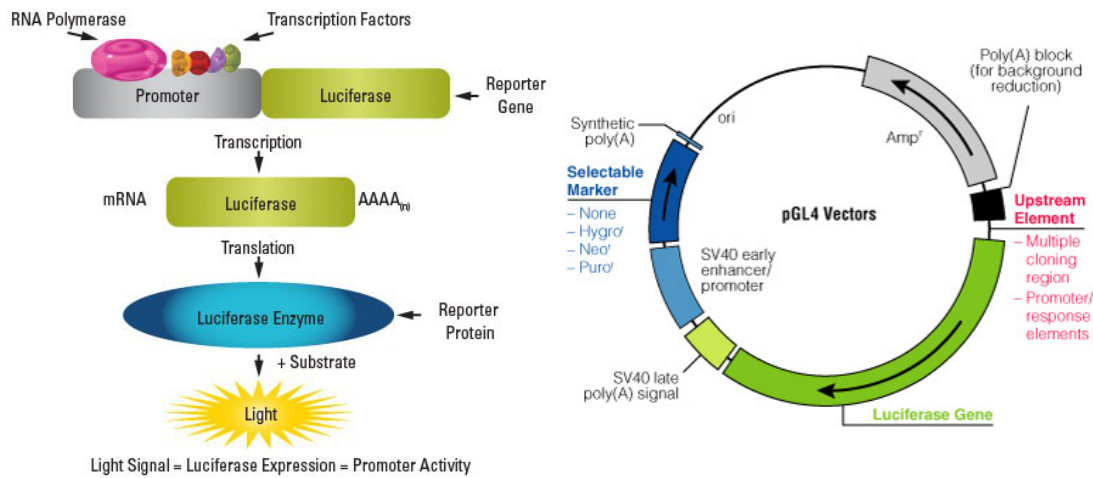


FIGURE 3.21: The figure on the left depicts the concept of the Luciferase test. The figure on the right represent the pGL4 vector prepared for the test, where the upstream element is the IGF1 promoter.

Transfected vector	Av. Luminescence (RLU)	Std. deviation (RLU)
pGL4-IGF1	12252	206
pGL4-basic	3097	123

TABLE 3.6: Luciferase test results for the C2C7 cells transfected by the IGF1 modified pGL4 vector with respect to the basic vector.

### 3.5.4.2 Transfection for continuous lactate production

In order to verify the maximum lactate production levels of the C2C7 transfected cells, a vector for the continuous LDH expression was created and used for the cells transfection. The vector is of the pcDNA3-LDH type and it contains the gene coding for LDH and the CMV promoter, as depicted in figure 3.22. The promoters for Cytomegalovirus (CMV) and SV40 are commonly used in mammalian expression vectors to drive protein expression, since they are very active and have a high yield. The transfection was performed again by Lipofection, using the same method that was previously described, and selecting the transfected cells by gentamicin, an antibiotic to which the pcDNA3 construct gives resistance.

The efficiency of the system in C2C7 cells have not been sufficient since the transfection positive cells didn't produce a large excess of LDH with respect to the negative controls, i.e., the not transfected C2C7 cells or the cells transfected with the pcDNA3 vector without the sequence codifying for the LDH enzyme. This could be due to the high basal level of production of LDH in this type of cells, as showed in figure 3.23

Therefore, in order to verify the proper functioning of the pcDNA3-LDH vector, this was tested on different cell lines. The cell lines considered were COS-1 (fibroblasts from

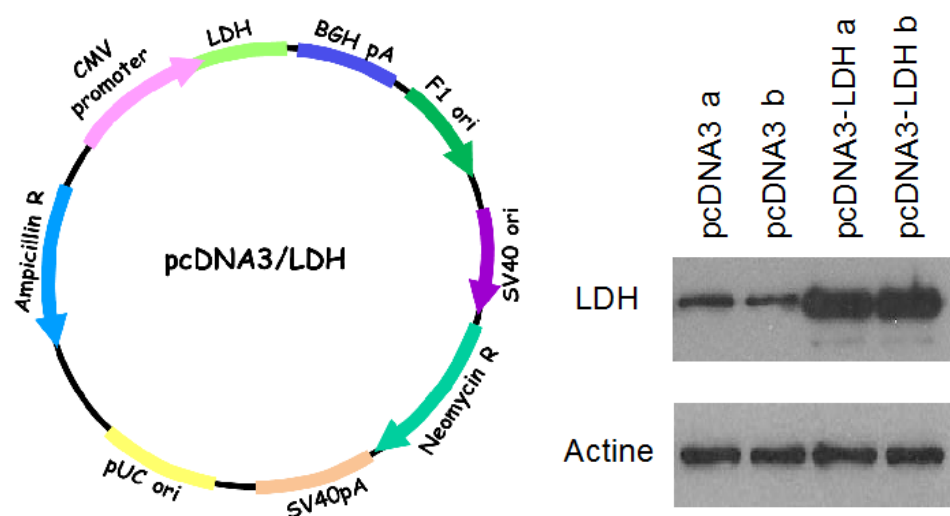


FIGURE 3.22: Schematic drawing of the pcDNA3-LDH vector used for the C2C7 transfection for the continuous or constitutive lactate production (left) and Western Blot of the expressed LDH and of Actine as control

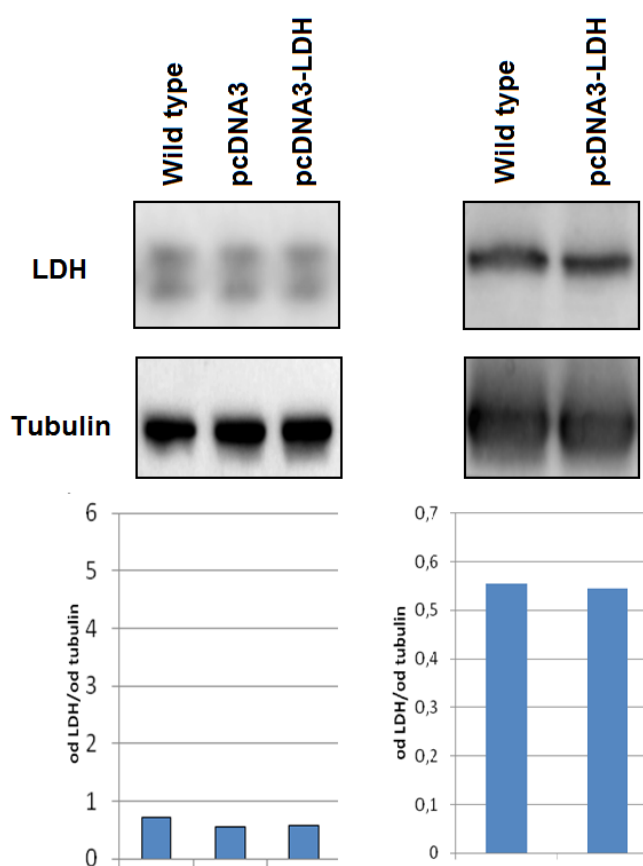


FIGURE 3.23: Western blot and densitometry for the LDH levels analysis in two preparations of C2C7, C2C7 pcDNA3 and C2C7 pcDNA3-LDH cells. The tubulin expression was used for normalization.

monkey kidney), HeLa (human cervix cancer derived cell line), NIH3T3 (embryonal fibroblasts), and HEK-293T cells (human embryo kidney derived cell line). The data obtained and showed in figure 3.24 prove that the pcDNA3-LDH vector works properly. However, it seems that this construct it's not able to induce a stable increment of the LDH expression in C2C7 cells. Therefore, the development of a new vector, containing regulatory structures more efficient in this cell line is necessary.

Anyway, a batch of C2C7 cells which pcDNA3-LDH vector transfection showed a small increment of LDH expression, with respect to both the wild type and the pcDNA3 transfected cells, was obtained (figure 3.25). This cell's batch was used to test the biosensor sensitivity to the lactate produced and released by the cells. The experiment is described at the end of Chapter 5.

#### **3.5.4.3 Transfection for stimulated lactate production**

With the aim to obtain the stable transfection of the cells with the pcDNA3-LDH vector modified with the IGF1 promoter, the vector containing the CMV promoter was modified and the IGF1 promoter was inserted just before the LDH gene. The vector was sequenced in order to verify the IGF1 and LDH gene sequences. Finally, the CMV promoter was removed and the vector was sequenced again to confirm its structure before the C2C7 transfection. The pcDNA3-LDH/IGF1 promoter transfection experiments are still running, in parallel with those related to the continuous lactate overproduction and to the vector optimization for the C2C7 cells.

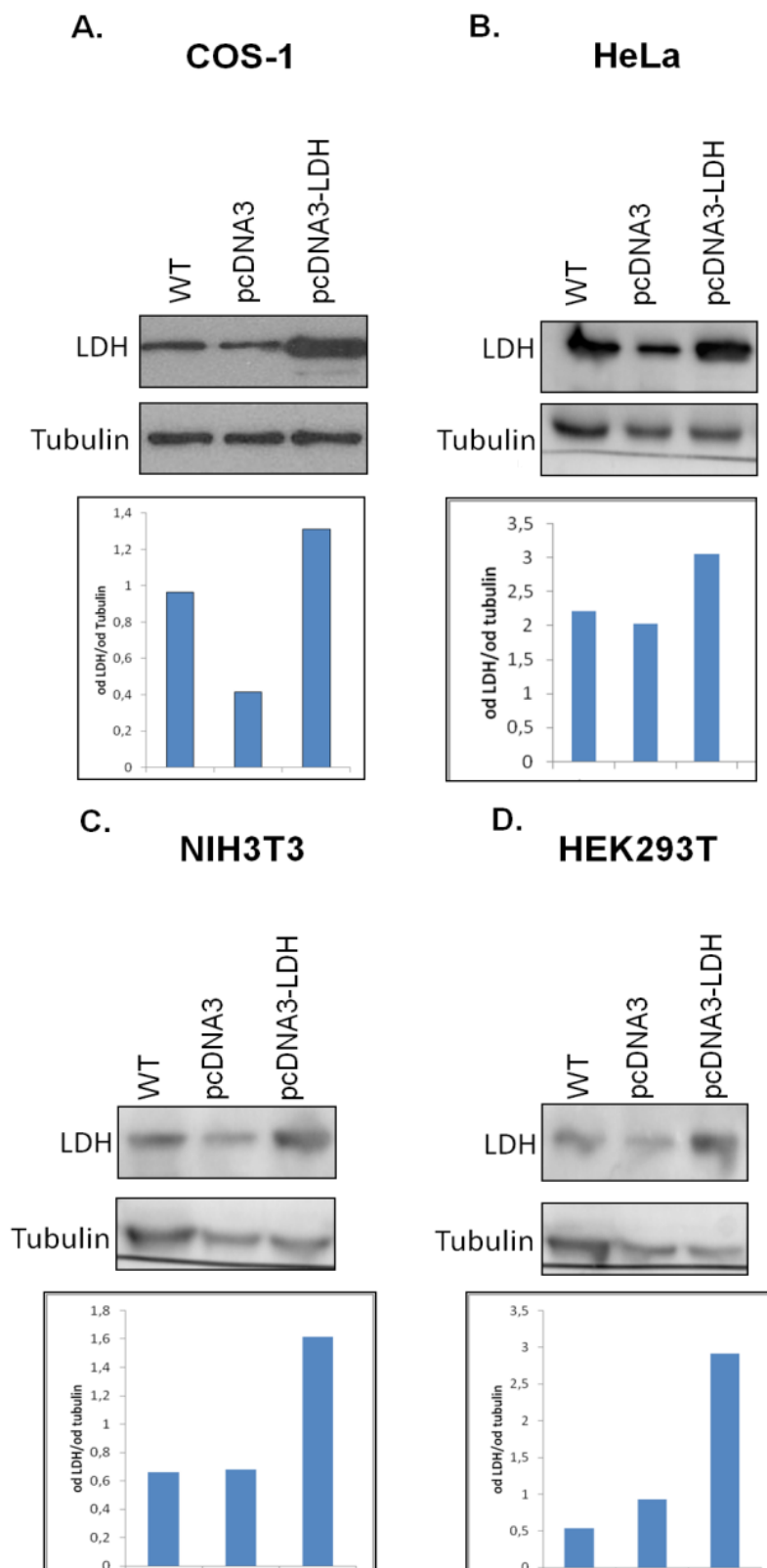


FIGURE 3.24: Western blot and densitometry for the LDH levels analysis in COS-1 cells (A), HeLa cells (B), NIH-3T3 cells (C), and HEK293T cells (D), respectively for the wild type cells, the pcDNA3, and the pcDNA3-LDH transfected ones. Tubulin expression was used for the levels normalization.

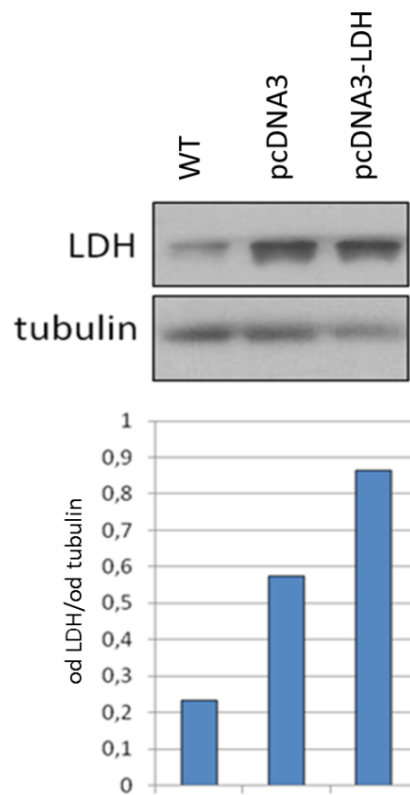


FIGURE 3.25: Western blot and densitometry for the LDH levels analysis in two preparations of C2C7, C2C7 pcDNA3 and C2C7 pcDNA3-LDH cells. The tubulin expression was used for normalization.

## Chapter 4

# Electrochemical biosensor for lactate detection

### 4.1 Biosensors fundamentals

A biosensor is defined as a device for the detection of a specific molecule or compound (called analyte), that combines a biological element and a transducer. The transducer converts a physical or chemical observed event in a measurable signal, whose magnitude is proportional to the analyte concentration.

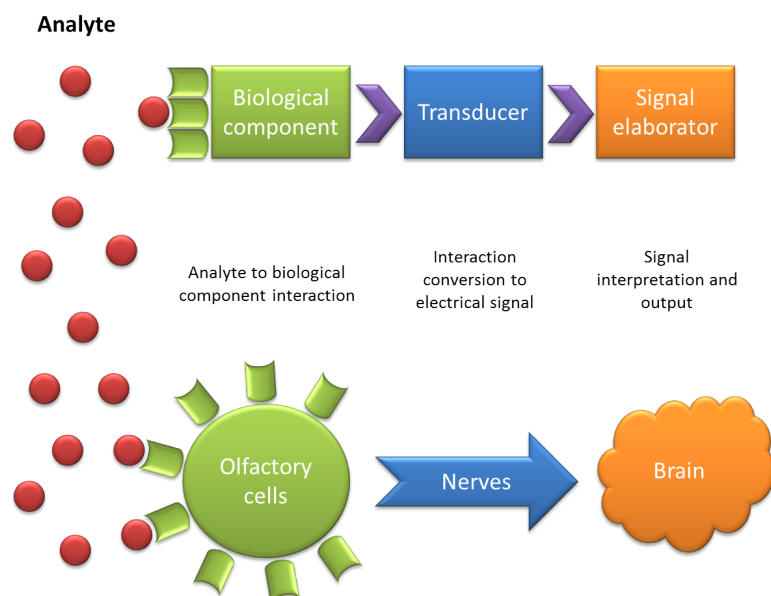


FIGURE 4.1: Main blocks of a general biosensor and comparison with the olfactory system for the detection of a specific analyte.

### 4.1.1 Biosensors performance parameters

Depending on the analyte type which has to be detected, several biological components can be employed, e.g. antibodies, proteins, ssDNA, and enzymes. Usually, these components are immobilized over the device surface where the transduction process is guided by the chosen measurement technique which can be physical, chemical/electrochemical or optical.

Independently to the measurement technique and to the biological component employed, the biosensor performance is mainly evaluated by six parameters:

- Sensitivity: the minimal detectable analyte concentration change also defined as the slope of the linear part of the calibration plot [60];

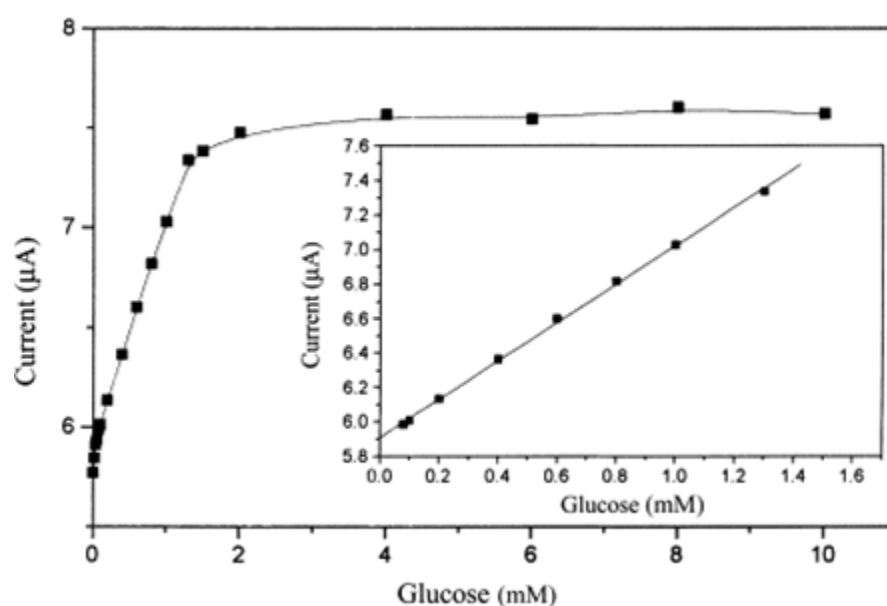


FIGURE 4.2: Example of a glucose amperometric biosensor calibration curve. The glucose concentration is measured as an electrical current which varies linearly with it, in the biosensor quantification range. The sensitivity of this biosensor is  $1.1\mu A/mM$ .

- Signal to noise ratio (SNR): the ratio between the amplitude of a signal and of its noise, to the second power;
- Limits of detection and of quantification (LOD/LOQ): respectively the minimum analyte concentration that can be distinguished from its absence, and the minimum analyte concentration that can be quantified;
- Selectivity: the ability to detect only one analyte without interferences from other substances;
- Repeatability: similarity of repeated measurements on the same device;

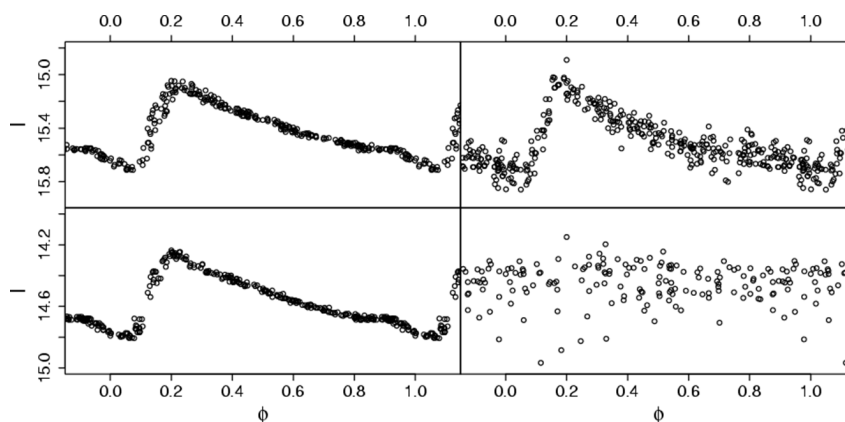


FIGURE 4.3: Representations of the same signal with four SNR values: for the top left plot the SNR is 0.5, for the bottom left one the SNR is 0.3, while for the top right plot the SNR is 5, and for the right bottom one the SNR is 20.

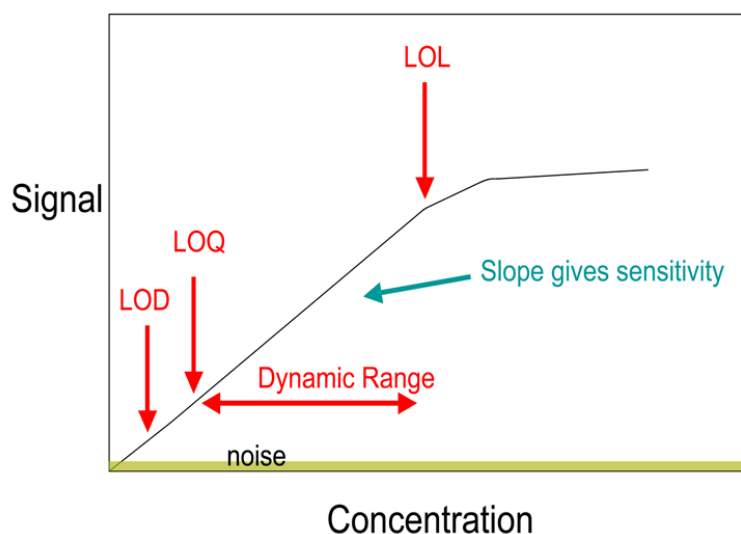


FIGURE 4.4: Schematic representation of the limits of detection, quantification, and linearity in a general biosensor's calibration plot.

- Reproducibility: similarity of the responses of different biosensors in the same conditions.

#### 4.1.2 Affinity vs catalytic biosensors

The nature of the interaction between the analyte and the biological component of the biosensor, and thus the biosensor itself, may be classified in two types:

- Affinity biosensor: the analyte binds specifically to the biological component, i.e. to immobilized antibodies, aptamers or ssDNA;
- Catalytic biosensor: the analyte interacts with the biological component, i.e. an enzyme, causing chemical modifications detectable by the transducer.



A widely used implementation of an affinity biosensor is the Enzyme-Linked Immunosorbent Assay (ELISA) to detect the concentration of a protein of interest in a fluid sample. The test is performed putting in contact the sample with a surface functionalized with antibodies specific for the target protein (primary ABs), which strongly binds to them. Then the sample is washed away and a solution of antibodies (secondary ABs), specific for another site of the protein of interest and labeled by a fluorescent molecule, is added to the surface and then washed away. The secondary ABs, bound to the target proteins trapped by the primary ABs will then be detected by their fluorescent labels, allowing to indirectly measure the target protein concentration in the sample.

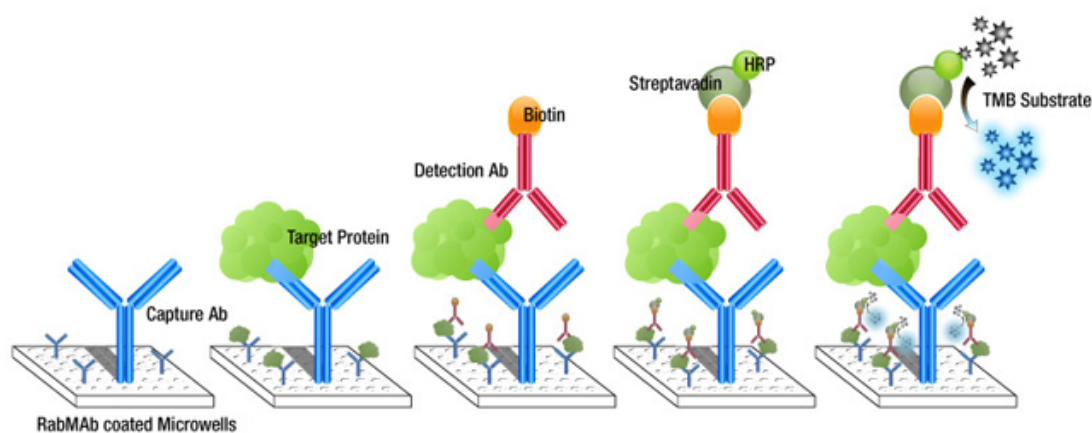


FIGURE 4.5: Schematic representation of the sequence of operations for the target protein detection in an ELISA assay using the Horseradish Peroxidase (HRP) enzyme and TMB as label for the colorimetric test.

The main drawback of this technique is the needing of the secondary ABs which introduce a step that makes difficult the in-field and rapid use of the biosensor by not trained operators. Moreover, the optical measurements makes the biosensor system very expensive. For these reasons, the point of care (PoC) biosensors are often based on label-free strategies and electrochemical (and cheaper) measurements detecting the variations introduced by the target molecule binding to the biological component, without the need of secondary molecules for the transduction of the binding event (e.g. for antibiotics detection on low-cost devices [61]). Regarding the catalytic (or enzyme-based) biosensors, a relevant example is constituted by the strips used by people affected by Diabetes to check their glucose levels in blood. This strips are functionalized by an enzyme which converts glucose in an electrochemically detectable molecule (a redox mediator) in a reversible process.

A mediator is a redox chemical compound which acts as electron carrier between the enzyme's catalytic site and the device surface, where the transported electrons are detected and measured by the appropriate technique.

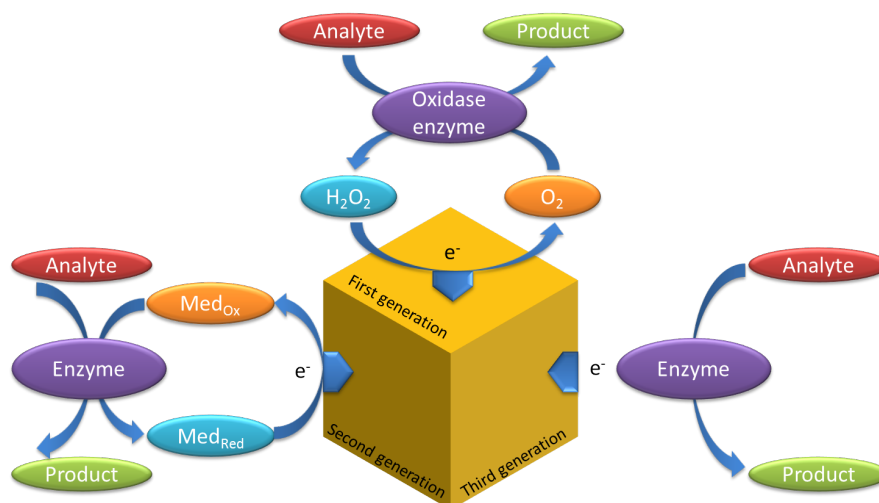


FIGURE 4.6: Compact scheme representing the detection pathways used by amperometric enzyme-based biosensors over years. The central cube faces represent the electrode surface where the electron transfer allows the amperometric detection.

The enzyme-based biosensors are historically classified in three generations, depending on the electrochemical reactions which define the analyte detection, and thus by the mediator used in these reactions:

1. The first generation is constituted by biosensors which use the oxygen molecules as mediators and oxidase enzymes;
2. The second generation biosensors use the enzyme cofactors or artificial molecules as redox mediators;
3. The third generation biosensors are characterized by nano-structured device surfaces allowing the direct transition of the electrons between the enzyme's catalytic site and the device surface, with no needing of a redox mediator.

### 4.1.3 Measurement techniques

Affinity and enzyme-based biosensors are usually characterized by different measurement techniques. For example, Electrochemical Impedance Spectroscopy (EIS) is a widespread technique used for label-free electrochemical affinity biosensors, while Cyclic Voltammetry (CV) is a common technique for amperometric electrochemical enzyme-based biosensors. Some of the techniques commonly used for this kind of biosensors are presented below.

#### 4.1.3.1 Electrochemical Impedance Spectroscopy (EIS)

EIS is used to measure the impedance of an electrochemical cell, usually composed by the device working electrode, by a reference electrode (external or integrated), and by an electrolyte solution in which the electrodes are immersed. The impedance, calculated imposing an AC potential between the electrodes and measuring the AC current flowing between them in function of the AC potential frequency, is sensitive to the working electrode surface conditions in the low-frequency region, and this allows the detection of the analyte binding to the biological component immobilized on the surface in affinity biosensors. EIS data can be further analyzed by fitting it with electrical equivalent circuits (EECs), allowing for the interpretation of each electrical parameter with a chemical-physical phenomenon.

#### 4.1.3.2 Cyclic Voltammetry (CV)

Cyclic Voltammetry is normally performed in three electrode cells, composed by the device working electrode, the reference electrode, and a counter-electrode. With this technique a linearly increasing potential, from a minimum value ( $V_{min}$ ) to a maximum one ( $V_{max}$ ) with respect to the time, is imposed between the working and the reference electrodes. The slope of the potential ramp is called scan rate (SR). Then, the potential linearly decrease with the same absolute slope coming back to  $V_{min}$ .

During each cycle, the current flowing through the working electrode and the counter-electrode is measured, and usually it's represented in the cyclovoltammogram with respect to the imposed potential, in a  $i/v$  plot.

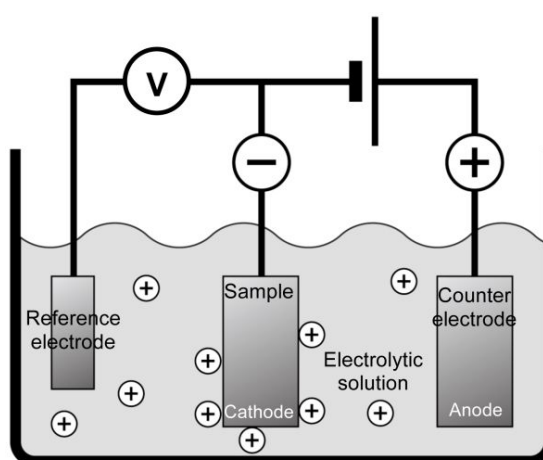


FIGURE 4.7: Schematic representation of a generic three-electrode electrochemical cell.

The resulting plot usually represent a closed curve where, the presence of any current peak represent the reduction or the oxidation of the chemical species present in the

measured solution. Each redox chemical compound has its own reduction and oxidation potentials depending on the electrodes materials, area, and on the measurement settings. However, at sufficiently high (low) potentials, several compounds are reduced (oxidized) and it becomes difficult to measure the concentration of each compound because of the other compounds interferences.

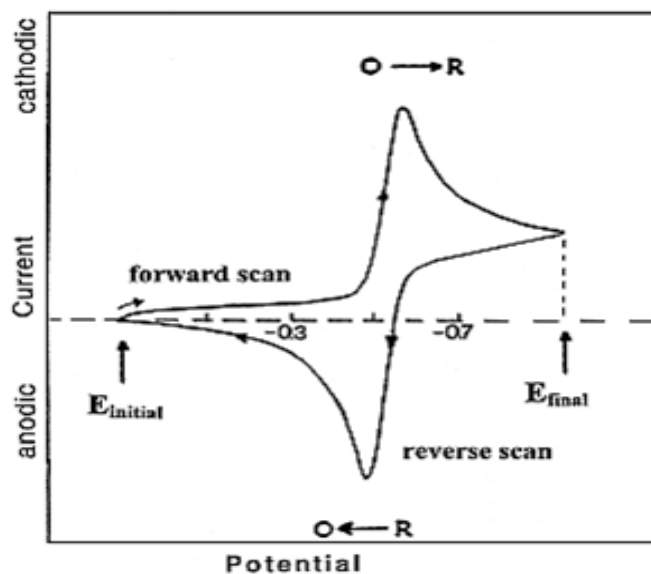


FIGURE 4.8: Typical cyclic voltammogram of a reversible redox system. The arrows along the curve give a representation of the measured current values over time during the linear variation of the potential from  $E_{initial}$  to  $E_{final}$  and back to  $E_{initial}$ . The cathodic peak is related to the reduction of the oxidated molecules in the solution while the anodic one is related to the oxidation of the reduced ones.

#### 4.1.3.3 Amperometric i-t curves

Another common technique performed with the three electrodes electrochemical cell described above is the amperometric i-t. This technique simply impose a constant potential between the working and the reference electrodes and it measures the current flowing through the counter-electrode over time.

This technique is often used in microfluidic systems, where the measurement solution is driven over the electrodes by a channel with dimensions in the micrometer scale, and in stirred electrochemical cells.

The imposition of the oxidation (reduction) potential of a particular redox molecule allows measuring an electrical current proportional to the redox molecule concentration in the solution if no interferences, due to other redox molecules, are present at the same potential.

#### 4.1.3.4 Surface Plasmon resonance (SPR)

A label-free biosensor technique of increasing importance is Surface Plasmon Resonance (SPR). This optical technique is based on the stimulation of evanescent waves on a grating by a laser, which produce a resonance peak at a specific angle of the grating with respect to the incident wave. The change of the surface conditions i.e. the binding of a protein to the antibodies-functionalized surface causes a shift of the resonance angle which is proportional to the concentration of the bound protein.

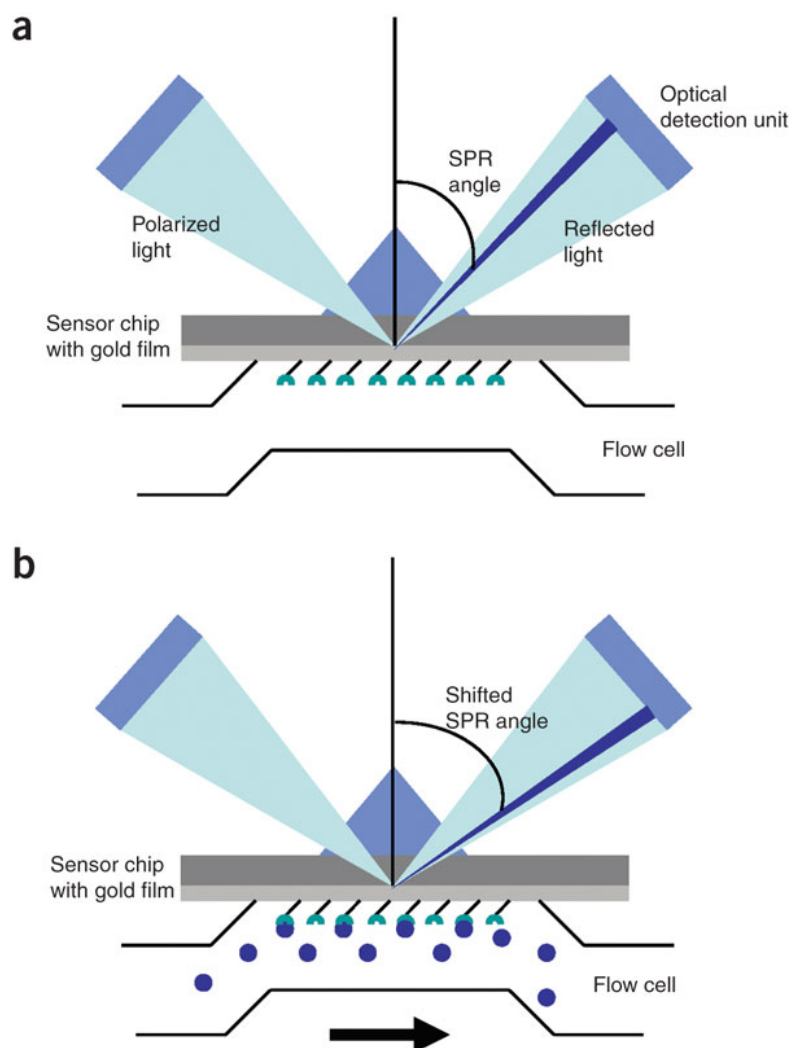


FIGURE 4.9: Schematic representation of a possible implementation of SPR biosensor based on a gold film functionalized by probe molecules exposed to the analyte in a flow cell and by a polarized light source, a prism, and an optical detection unit.

SPR and EIS measurements are probably the most common label-free detection techniques. They allow the detection of few nanometers wide molecules, monitoring different (respectively optical and electrochemical) effects of the molecules binding on a

surface. The complementarity of the information given by these technique can be exploited by performing them on the same nanostructured surface for the detection of a Self-Assembling Monolayer (SAM) of thiolated molecules as it has been done in [62].

#### 4.1.4 Devices design and fabrication

Optical and electrochemical devices design is a key step for the realization of a performing biosensor. Its goal is the optimization of characteristics such as the transduction efficiency, the device usability, and the device surface features, which are fundamental for a correct immobilization of the biological component.

The fabrication of the devices may involve both methods typical of the integrated circuit facilities, i.e., lithographic techniques in cleanrooms, and also cheaper and easier techniques as screen-printing with conductive and insulating inks.

##### 4.1.4.1 Finite Element Modeling and simulations

Several simulation softwares allow modeling the devices and calculating their theoretical performance. These simulations are usually performed in order to identify which geometrical and material characteristics mostly influence the biosensor behavior. For example, for electrochemical EIS-based biosensors the geometrical characteristics of the device electrodes and of the flow channels often are the keystones of the biosensor performances. These characteristics improvement becomes fundamental to obtain a working biosensor in the case of semi-conductive electrodes materials i.e. conductive polymers like Poly(3,4-ethylenedioxythiophene) (PEDOT). An example of the performance improvement induced by a correct device design has been achieved with PEDOT electrodes [61]. In this work, distributed elements simulations allowed to find the proper geometrical characteristics for the biosensor electrodes and microfluidic channels, in order to obtain a more sensitive detection, which has been validated with a clinically relevant molecule, i.e., Ampicillin.

##### 4.1.4.2 Electrochemical devices fabrication methods

Electrochemical devices are usually composed by an insulating substrate covered by conductive electrodes and wires connecting them to the device cable or connection port. Then, the electrochemical devices usually have an insulating flow channel or containment pool for the solution to be tested by the biosensor. The electrodes constitute the most important part of the device because over them take place the electrochemical reactions and the target molecules binding. For this reasons, the electrodes geometrical and

morphological characteristics are of primary importance for the biosensor performance improvement. However, the conductive wires importance may not be undervalued because they are often responsible for introducing parasitic resistive and capacitive effects. All the elements described, i.e. the device electrodes, wires and channels/pools, can be of a common USB pen drive dimension but they can be also scaled down to micrometric and even to nanometric dimensions.

In general, the devices fabrication should allow high throughput, mass production, and low costs. However, the most important characteristic of the devices in the biosensor field is their reproducibility.

Some of the main techniques for the electrodes and wires conductive layer deposition are described in the following:

- **Standard silicon wafer lithography:** this is the technology on which the entire electronic industry is still based for the production of the microchips inside our televisions, PCs, mobile phones, ecc. With this technology, flat silicon wafers, characterized by a thin superficial insulating oxide layer, are uniformly covered by a thin layer of a photosensitive solution, which is then dried and is called photo-resist. Then, the covered wafers are exposed to UV light under a glass plate with the electrodes and wires design printed on it. The photoresist that was not under the design is removed by an appropriate solution, leaving the silicon surface uncovered. This surface is etched, removing the insulating oxide layer patterning a conductive path on the surface under the design. Finally, the remaining photoresist is removed. Unfortunately, these kind of processes requires a clean and controlled environment i.e. cleanrooms, free of dust particles which would fatally interfere with it.
- **Plasma sputtering:** this method allows to cover a substrate by a thin metal layer which can be directly patterned by putting a mask between the sputter and the substrate. This technology is based on a magnetron sputtering cathode under a sample of the material with which the substrate (target), in front of them at a defined distance, has to be coated. The magnetron creates an electromagnetic field which accelerates energetic ions e.g.  $Ar^+$  to collide with the target. The collisions cause the emission of target atoms that coat the exposed surface of the substrate. This technique is used for the mass-production of optical storage disks as CDs and DVDs, coating patterned polycarbonate surfaces with reflective metals. Some process changes allow to redirect the CD/DVD production technology for the out-of-cleanroom realization of electrochemical/optical biosensors [63],[62], [64].
- **Conductive inks screen-printing:** screen-printing is a widespread technique for the mass-production of T-shirts, DVDs and other every day things. This process

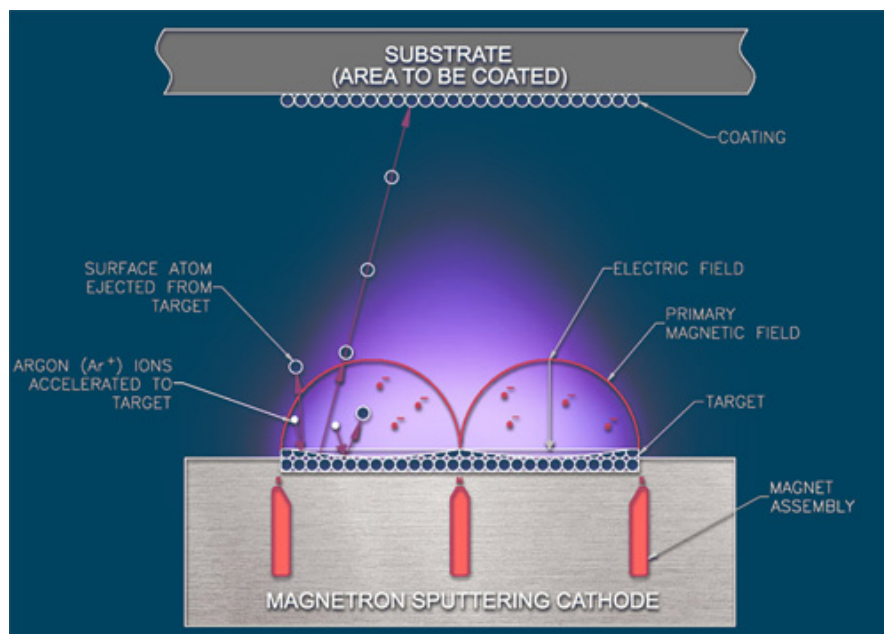


FIGURE 4.10: Schematic representation of a sputtering process (the collisions cascade between the Argon ions collision to the target and the target atom emission is not represented).

is based on printing over objects making the ink pass through a silk patterned screen. The use of conductive and insulating inks makes this technique available also for the production of electrochemical sensors. The resolution of the printed electrodes depend on the distance between the silk wires of the patterned screen.

- **Conductive polymers coatings:** is a method which is increasing its popularity. Usually, the coatings are performed by two techniques, both starting from a fluid form of a monomer which is polymerized over a solid surface. In fact, the polymerization process can be done electrochemically by imposing specific potentials to pre-existing electrodes which are then coated with the conductive polymer, or it can be achieved chemically, adding a polymerization initiator to the monomer solution. This last method allows the coverage of an insulating substrate also, therefore the creation of conductive layers. Usually, the conductivity of these materials strongly depends on the compounds used to dope the polymer. A common example is polystyrene sulfonate (PSS) doping for the PEDOT polymer.
- **Nanoparticles/Nanotubes coatings:** are materials with surprising surface properties, which can strongly increase the sensitivity of an electrochemical biosensor by augmenting its effective surface area. Unfortunately, they often require strong acids/bases for their usage and they are quite expensive.



#### 4.1.4.3 Devices validation

The validation of a device to be used for electrochemical biosensing involves different parameters:

- **Coherence with standards:** the device has to give responses coherent with those expected with known conductivity standard solutions and with common redox mediator. Typical measurements used to verify this coherence are EIS with electrolytes of known conductivity (based on salts), and CV measurements with ferro/ferricyanide. With the EIS measurements, the high frequency spectra should result in a plateau whose impedance values are related to the electrolyte conductivity by the geometrical electrodes characteristics i.e. their distance and the working electrode surface area, with an ideally not-polarized reference electrode of infinite dimensions. Conversely, with CV measurements on ferro/ferricyanide, the reversibility of the redox reaction is verified by checking the ratio of the oxidation and reduction current peaks to the unit, and that of the peak potentials average to the redox potential of the mediator used with respect to the type of reference electrode (e.g. 236 mV for ferro-ferricyanide with respect to Ag/AgCl KCl 1 M reference electrode). Moreover, the reversibility of the redox reaction is checked by testing the linearity of the current peaks in function of the Scan Rate (SR) of the CV measurements.
- **Response reproducibility and repeatability:** The reproducibility of the responses obtained from the devices is usually tested by measuring the same solution over a sufficiently high number of devices, at least three, exactly in the same conditions and reducing the possible variables such as temperature, humidity, and solution drop-casting method as much as possible. Therefore, the similarity of the obtained measurements reflects the device fabrication process reproducibility. Conversely, the repeatability is usually tested by repeating the same measurement consecutively or changing each time the solution over the electrodes. With these measurements it can be tested also the stability of the electrodes over time.
- **Stability over time:** this device's characteristic is usually evaluated by measuring with the same solution devices exposed to defined conditions (e.g. room temperature and humidity) in different moments. These evaluations allow defining the proper conservation conditions e.g. vacuum-sealed bags and low temperature environment.

## 4.2 Lactate enzyme-based biosensors

The ability to monitor enzymatic reactions through the rapid and reliable assessment of their specific substrates concentrations has a growing importance both in clinical analysis and in biotechnological applications. Frequently, enzymatic reactions allow converting analytes which are not electrically active, and are too small for affinity sensors, in molecules detectable by electrochemical methods. Lactate is one of these important analytes due to its relevance in various fields: in clinical analysis it is well-known that its concentration in human blood samples can be related to cardiac or respiratory pathologies [65], and therefore its detection enables early diagnosis of critical situations [66]; in sport medicine, blood lactate concentration is an indicator of the physical effort intensity through the aerobic and anaerobic thresholds [67]; in food processing applications, lactate measurements are an easy and effective way to monitor microbial contamination of dairy products [68]. When dealing with lactate concentration assessment in liquid samples, enzyme-modified electrodes represent common and reliable tools [69]. This kind of biosensors have been used for a wide variety of applications such as the quantification of *Escherichia Coli* in crude cell culture medium [70], continuous monitoring of myocardial hypoxia [71], and real-time measurements of lactate by a contact lens [72]. This kind of biosensors provides high selectivity to a specific substrate and fast response time [73] but the detection performance indicators, e.g. linear range, stability, sensitivity and lifetime, are tightly related to the technique used to bind enzymes to electrodes surface [74]. For this reason, an in-depth study of the functionalization protocol is crucial when developing reliable biosensors oriented to mass-production.

### 4.2.1 Strategies and enzymes for lactate detection

Lactic acid is a carboxylic acid with chemical formula  $C_2H_4OHCOOH$ , it has a hydroxyl group adjacent to the carboxyl group, making it an alpha hydroxy acid. In solution it can lose a proton from the carboxyl group, producing the lactate ion  $CH_3CH(OH)COO^-$ . Lactic acid is chiral and has two optical isomers. One is known as L-(+)-lactic acid or (S)-lactic acid and the other is D-(-)-lactic acid or (R)-lactic acid. In animals, L-lactate is constantly produced from pyruvate via the enzyme Lactate Dehydrogenase (LDH) in a process of fermentation during normal metabolism and exercise. The concentration of blood lactate is usually 1-2 mmol/L at rest, but can rise to over 20 mmol/L during intense exertion. Conversely, D-lactate is not present in eukaryotic metabolism but only in the bacteria one. The main enzymes involved in the lactic acid catalysis are Lactate Oxidase (LOx) and Lactate Dehydrogenase (LDH). The LOx enzyme catalyzes the following reaction:



While the LDH enzyme catalyzes the reaction:



Where LA stands for Lactic Acid and PA for Pyruvic Acid. As for other enzymes, the catalysis direction can be from LA to PA or viceversa from PA to LA. The direction depends on the selected isoenzyme and from the conditions in which the catalysis happens (e.g. pH, temperature, concentration of the substrates and of the cofactors). Both LOx and LDH have a tetrameric structure [75]. The LOx enzyme uses Flavin Mono-Nucleotide (FMN) as cofactor while the LDH enzyme uses Nicotinamide Adenine Dinucleotide (NAD).

The strategies for the electrochemical detection of LA can involve the use of natural or artificial redox mediator (for respectively first and second generation sensors). In the second case, with proper redox mediators, the electron transfer from the natural to the artificial mediator during the catalysis allow detecting the lactate presence at lower potentials, reducing the interferences due to other compounds in solution. For instance, a common artificial redox mediator used with LOx is ferricyanide, which has a formal potential of 236 mV with respect to Ag/AgCl; much lower than that one of hydrogen peroxide. Conversely, a strategy implemented for the LA detection with LDH enzyme has been to keep the NAD as mediator but to introduce new electrodes materials to lower the potential of the NADH oxidation, e.g. carbon electrodes.

### 4.2.2 Enzymes immobilization

LOx and LDH enzymes provide different ways for LA detection but, in both the cases, they need to be immobilized over the electrodes surface in a stable way and to keep their 3D native fold in order to obtain a working and ready-to-use biosensor. Enzymes are very delicate proteins for biosensing applications because a small change in their structure could results in the complete inactivation of the enzyme and thus in the impossibility to detect LA. Moreover, they are characterized by sites on their surface which have to be reached both by the target molecules and by their cofactors. If the enzymes are immobilized with these sites too close to the electrode surface they will not be able to catalyze the LA reaction. Several techniques and methods have been proposed over the years in order to obtain easy and reproducible enzyme functionalizations over different

kind of surfaces, keeping them stable [76], [77], [78]. Some of these techniques are presented below:

- Non-covalent adsorption and deposition: this technique is particularly effective immobilizing enzymes with a large lipophilic surface area to hydrophobic electrodes or carriers, while enzymes with a surface prevalence of hydrophilic residues have to be immobilized on hydrophilic carriers. The Van der Waals forces and entropy changes ensure the immobilization of the enzyme to the carrier. The advantage of this immobilization is that the enzyme does not have to be pre-treated or chemically modified. However, a significant disadvantage is that the enzyme tends to leach readily from the carrier when used in aqueous media [64].
- Immobilization via ionic interactions: depending on the pH of the solution and the isoelectric point the surface of the enzyme may bear charges. Any ion exchanger can act as carrier in immobilization via ionic and strongly polar interactions. Depending on the predominant charge on the enzyme, the ion exchanger needs to be negatively or positively charged. Ionic immobilization is strongly dependent on the pH value and salt concentration during immobilization, but also during application. An interesting application of this method is the layer-by-layer enzyme deposition. This technique consists in the deposition over the biosensor electrodes of layers with opposite charge with respect to the predominant enzyme charge, and on the immobilization of the enzymes between these layers [79].
- Covalent binding to solid supports: covalent binding of enzymes to electrodes has the advantage that the enzyme is tightly fixed, thus enzyme leaching in aqueous media is minimized. Moreover, the formation of multiple covalent bonds between the enzyme and the surface reduces conformational flexibility and thermal vibrations thus preventing protein unfolding and denaturation. A distinct disadvantage of this technique is that the enzymes have to be chemically modified and all components of the native enzymatic preparations must be carefully considered.
- Cross-linking of enzymes: this is a particular case of covalent binding using a di-functional agent such as glutaraldehyde or dithiobis-n-succinimidyl propionate (DTSP). Instead of fixing the enzyme to the electrode, the enzyme here is deposited in a spray-dried form and then cross-linked, or cross-linked directly in solution.
- Encapsulation: is the best means of avoiding any negative influence on the structure of an enzyme. Many encapsulation methods have been developed, the sol-gel method being the most prominent and widely used technique. Sol-gels are silica materials that are highly porous and readily prepared. Although sol-gels are

porous, diffusion of substrate to the enzyme can be restricted and care has to be taken to avoid this.

- Structure-based development of immobilization: Recent research has demonstrated how the combined use of experimental and computational methods can provide rational guidelines for the selection of optimal polymeric supports as well as for the choice of immobilization technique. Maps of regions suitable for the establishment of interactions with different supports can be created. This is of particular importance for protein orientation upon binding, since different areas will interact with different supports.

### 4.3 The Myo-Screen Lactate biosensor

The strategy followed for the Myo-Screen lactate biosensor realization was to use low-cost commercial devices (supplied by DropSens Ltd.) and the Lactate Dehydrogenase (LDH) enzyme, which catalyzes the conversion of lactic acid (LA) to Pyruvic acid (PA), and the conversion of the cofactor Nicotinamide Adenine Dinucleotide (NAD) to its reduced state (NADH). Then, NADH is oxidized back to NAD at the device electrode's surface, recording an electrical current proportional to the NADH concentration, and thus to the LA one.

In order to avoid the inactivation of the enzyme due to the possible unfolding related to the device functionalization process, the first prototype of the lactate biosensor was designed without the immobilization of the enzyme to the electrodes surface. In fact, the lactate detection was planned to be performed through the following steps:

1. Preparation of the lactate sample in a defined buffer/medium;
2. Catalysis of the lactate in the sample in presence of the cofactor (NAD), and of the LDH enzyme at controlled conditions, in liquid phase;
3. Extraction of a sample from the liquid phase after the steady state of the catalysis kinetics was reached;
4. CV measurement of the NADH concentration contained in the liquid phase sample.

The catalysis of the lactate sample is monitored over time by UV-visible spectrophotometric measurements of the NADH concentration. In fact, with this widespread and classical technique it's possible to distinguish the oxidized and reduced forms of NAD, respectively  $NAD^+$  and NADH, and thus to estimating the equimolar amount of lactate converted in pyruvate during the catalysis. Cyclic Voltammetry (CV) measurements

were chosen for the NADH electrochemical detection. The starting, minimum and maximum potentials, together with the scan rate of the CV measurements were selected in order to optimize the NADH detection.

The commercial devices chosen for the NADH CV detection are screen-printed strips with a ceramic substrate, a circular working electrode, a counter-electrode, and a silver reference electrode disposed in circle around the first one. The electrodes contact are passivated by an isolating and hydrophobic ink, in order to maintain the liquid drop of the measurement solution over the electrodes. The DropSens (DS) devices are connected to a *CH440a* potentiostat through an adapter module and BNC grounded cables.

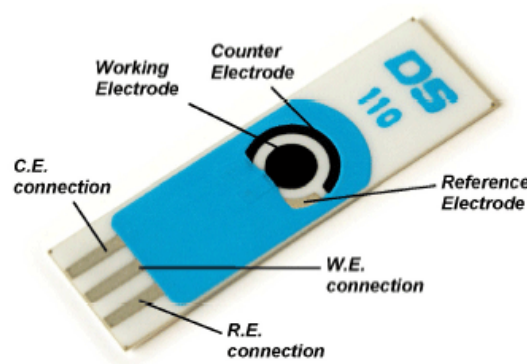


FIGURE 4.11: DropSens Carbon device (DS-110)

### 4.3.1 Devices characterization

Two electrodes materials were evaluated and compared: gold and carbon. The gold devices (*DS – 220AT*, called DSAu devices) and the carbon devices (*DS – 110*, called DSC devices) were tested by EIS and CV measurements, in PBS and ferro/ferricyanide 1 mM, respectively. The aim of these characterizations was to evaluate the devices surface characteristics and the repeatability/reproducibility of their EIS and CV responses.

#### 4.3.1.1 EIS measurements

The EIS measurements were performed in the 100 mHz - 1 MHz range applying a 5 mV peak-to-peak AC potential and a 0 V DC potential to the working electrode with respect to the reference one. The electrodes were covered by a 100  $\mu$ l PBS drop. 50 consecutive measurements (sweeps) were performed on three devices, both for the gold and the carbon electrodes. Figure 4.12 shows the average Bode diagrams of the first and the fiftieth sweeps calculated from the impedance values recorded from the three DSAu devices. These diagrams represent the magnitude and phase of the complex impedance

data in function of the frequency of the applied signal. The Bode diagrams obtained from the DSC data are plotted in figure 4.13.

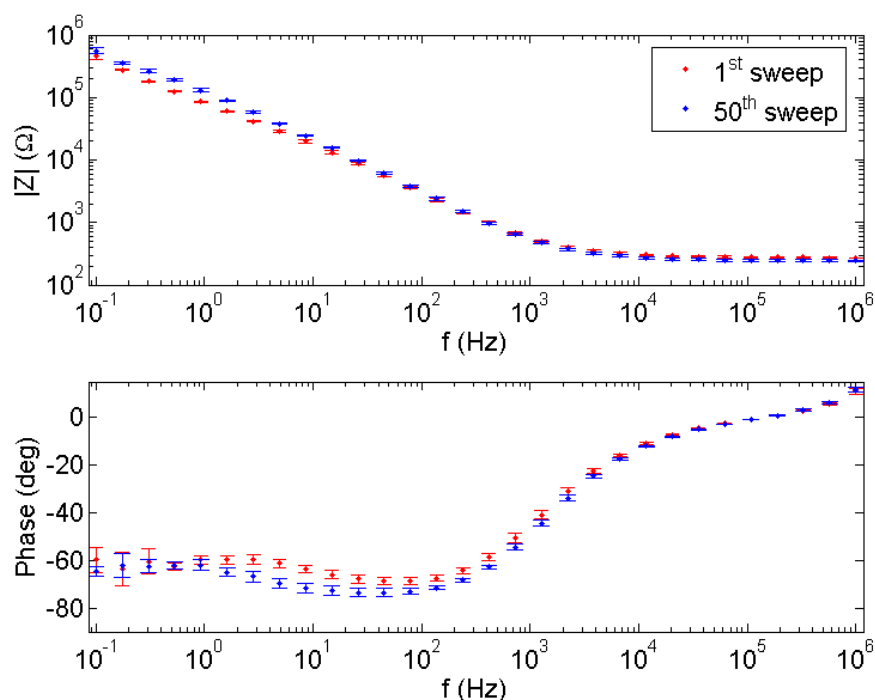


FIGURE 4.12: Bode diagrams of the EIS measurements in PBS 1x on DropSens Au devices. The average impedance data measured over three devices were plotted for respectively the first and the fiftieth sweeps.

With the purpose to exploit the variation of the impedance values in the Bode diagrams among the sweeps, the EIS impedance magnitude percentage variations were plotted in function of both the frequency and the sweep number. These 3D plots show which frequencies undergo the major variations over time and EIS measurements repetitions. Figures 4.14 and 4.15 show the average percentage variations, with respect to the first sweep, of the impedance magnitude values and of the phase values for the DSAu devices, while figures 4.16 and 4.17 show the average percentage variations obtained from measurements of the DSC devices.

EIS measurements on electrochemical systems without a redox mediator are usually modeled by a simple electrical equivalent circuit (EEC) composed by a resistor and a capacitor in series (RC circuit). The resistance value depends on the electrodes geometrical characteristics and the solution conductivity, while the capacitance depends on the electrodes surface area and its eventual coverage by attached molecules. Commonly, the EIS spectra obtained from these systems are not perfectly adherent to the RC EEC transfer function. Therefore, some elements were introduced to fit the variations due to specific surface characteristics and to the diffusion which takes place in the electrolyte solution between the electrodes. Two of these elements are the Constant Phase Element

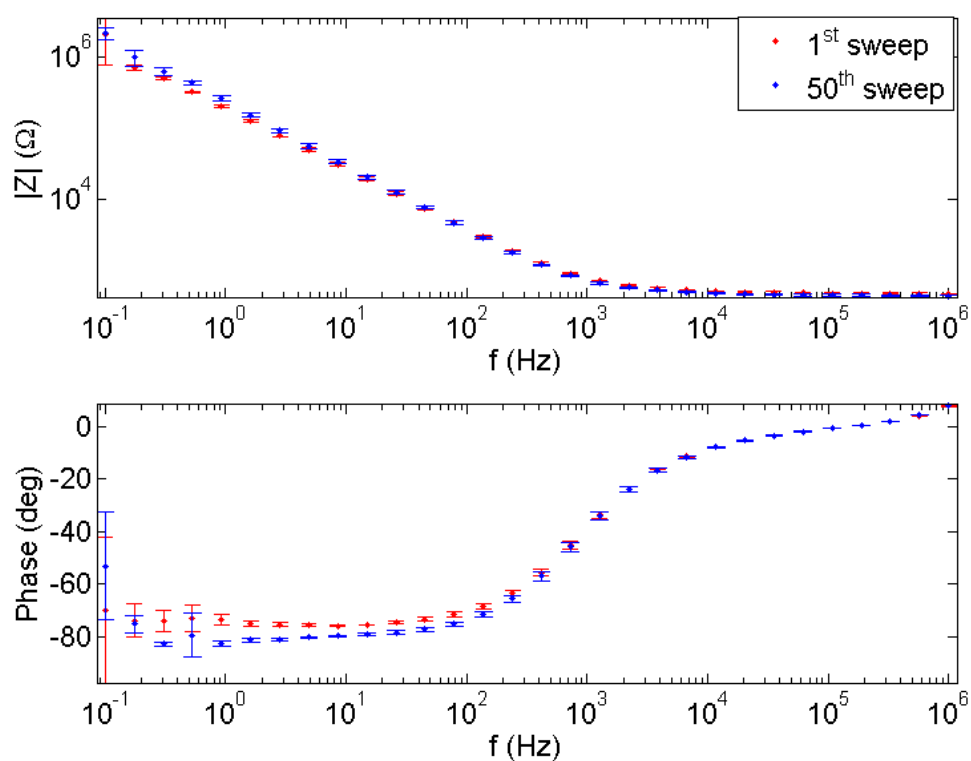


FIGURE 4.13: Bode diagrams of the EIS measurements in PBS 1x on DropSens C devices. The average impedance data measured over three devices were plotted for respectively the first and the fiftyth sweeps.

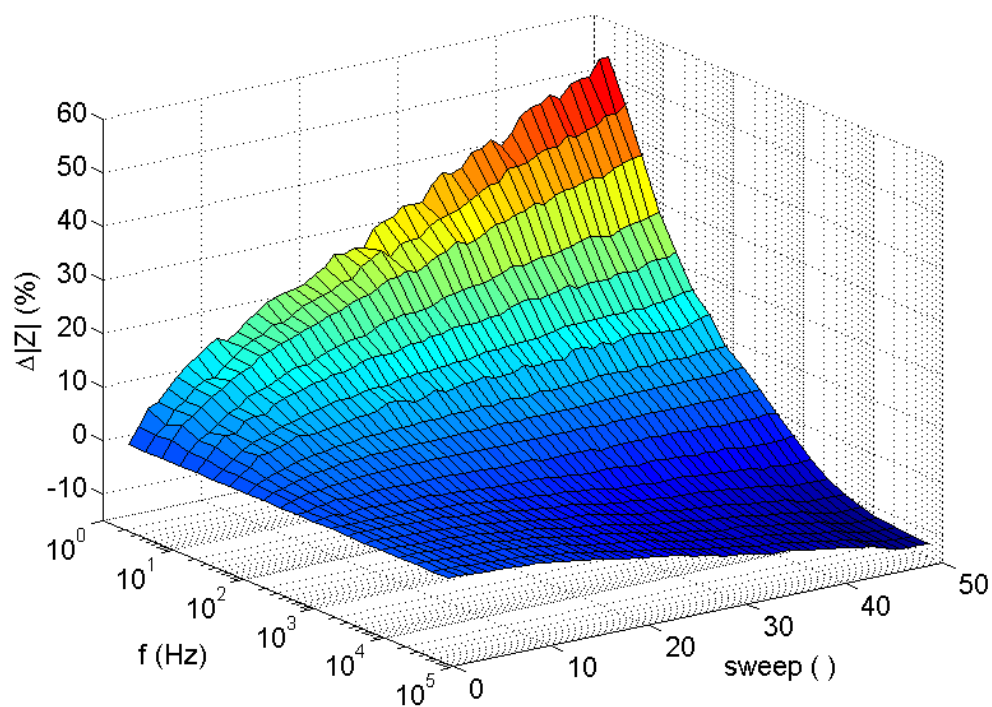


FIGURE 4.14: Percentage variations of the mean impedance magnitude measured on DropSens Au devices in function of both the frequency and the sweep number.



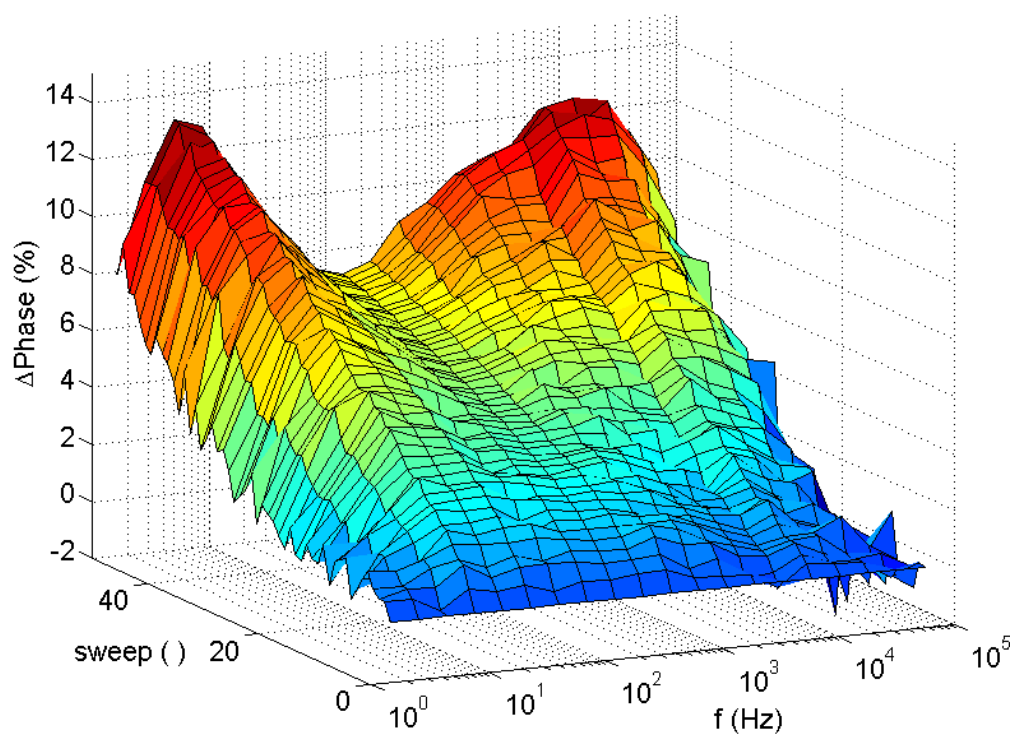


FIGURE 4.15: Percentage variations of the mean impedance phase measured on DropSens Au devices in function of both the frequency and the sweep number.

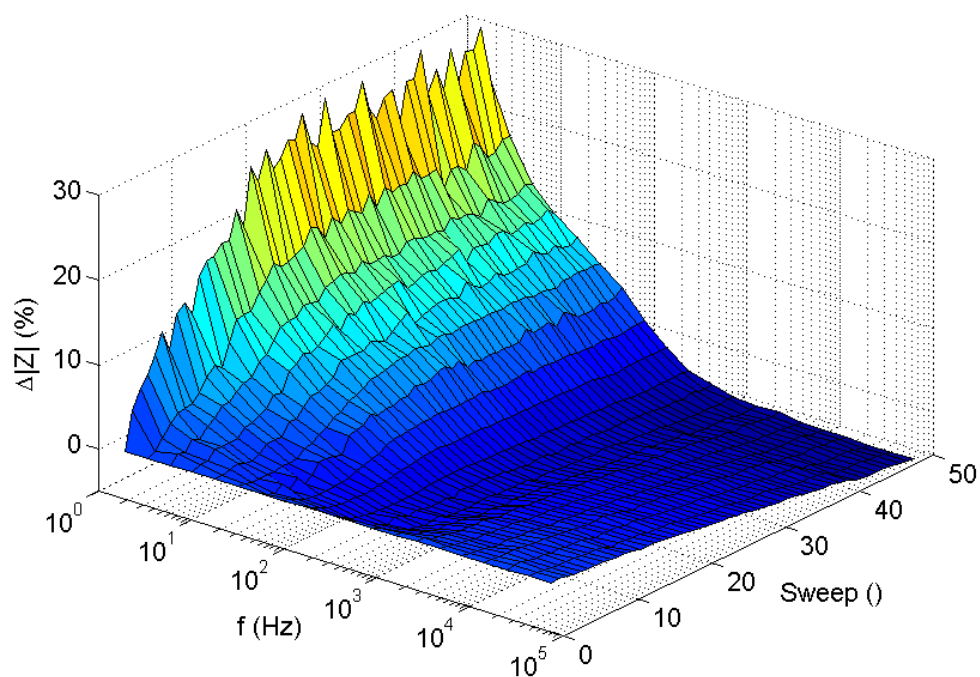


FIGURE 4.16: Percentage variations of the mean impedance magnitude measured on DropSens C devices in function of both the frequency and the sweep number.

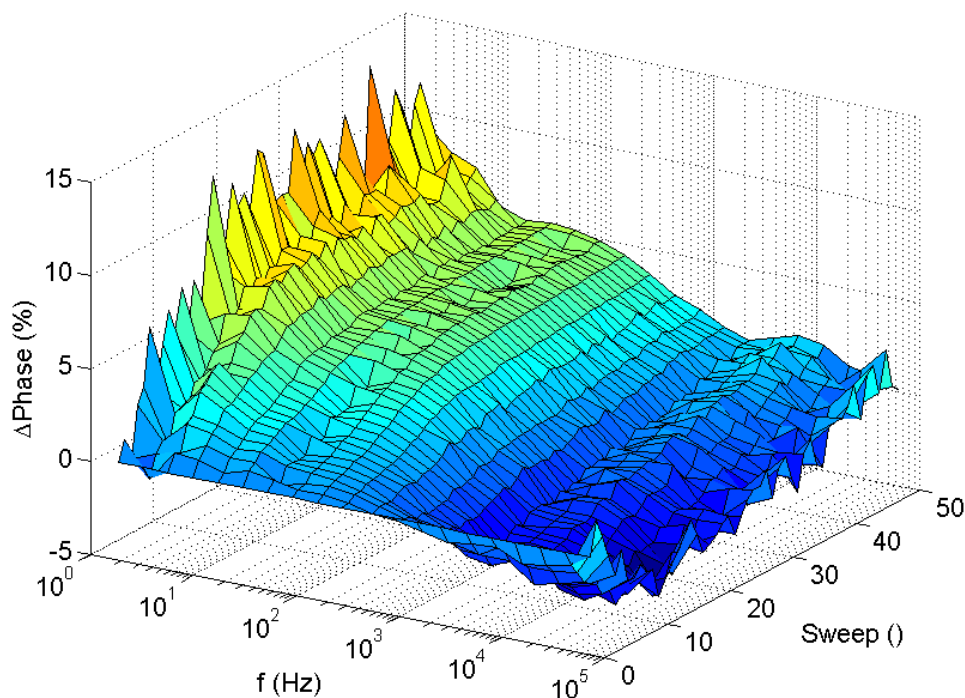


FIGURE 4.17: Percentage variations of the mean impedance phase measured on DropSens C devices in function of both the frequency and the sweep number.

(CPE) and the Warburg element (W).

The EIS data obtained from the measurements over the DSAu devices showed to be better fitted by a R-(CPE//W) model with the Warburg element in parallel to the CPE one and the resistor in series with them. Conversely, the DSC devices EIS measurements are almost perfectly fitted by a R-CPE model. Figures 4.18 and 4.19 show the values of the EEC elements parameters in function of the EIS sweep, for the DSAu and the DSC devices, respectively.

Summarizing the obtained results, the EIS measurements on the DSAu and DSC devices showed that:

- The impedance of the DSAu devices is characterized by a phase minimum of about  $-70^\circ$  around 40 Hz while the impedance of the DSC devices does not present local minimum phase values and reaches  $-80^\circ$ , with a behavior more similar to an R-C EEC;
- The variation of the impedance magnitude and phase values are significantly lower with DSC than with DSAu devices;
- As a consequence of the phase minimum peak obtained with DSAu devices, which affect also the linearity of the related Nyquist plots, in this case the DSAu devices EIS measurements are better fitted by an EEC which takes into account for the

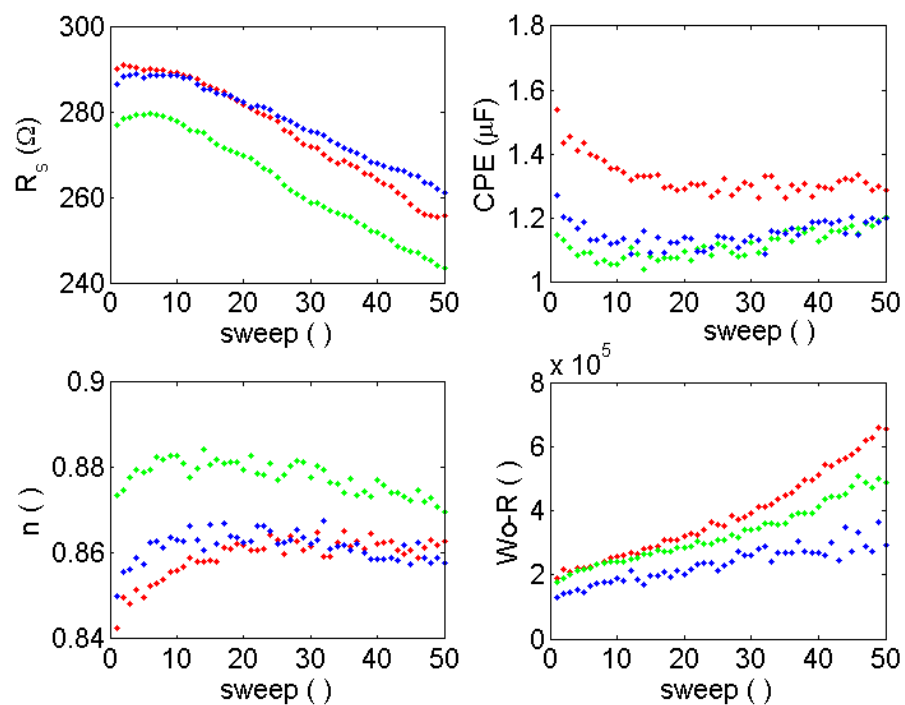


FIGURE 4.18: Equivalent circuit elements fitted values from the EIS sweep in PBS on DropSens Au devices.

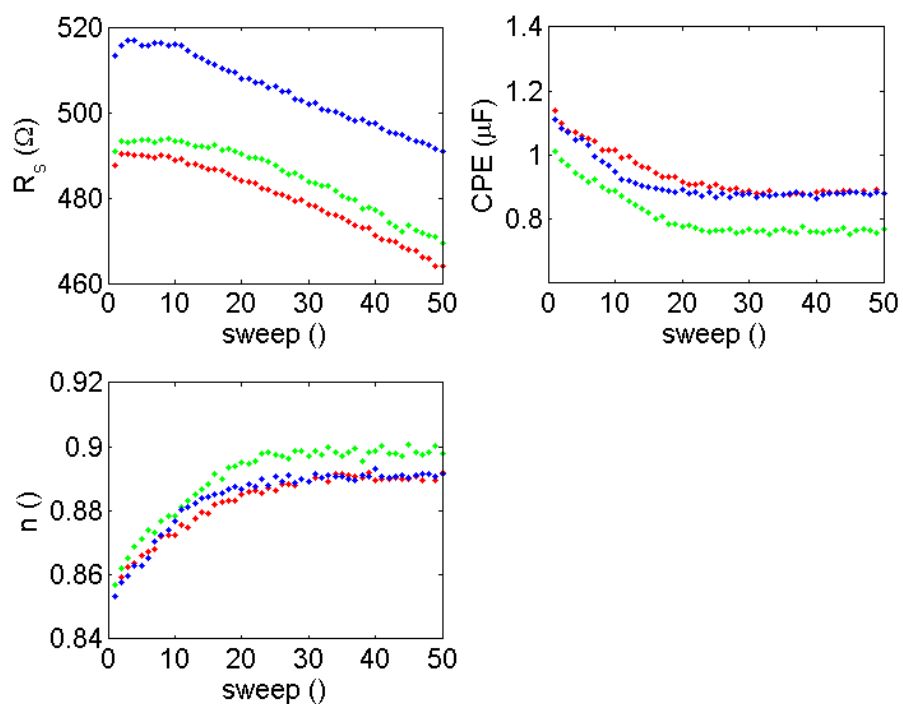


FIGURE 4.19: Equivalent circuit elements fitted values from the EIS sweep in PBS on DropSens C devices.

diffusion by a Warburg element. Conversely the DSC devices EIS measurements are better fitted by a R-CPE EEC.

- The trends of the EEC elements fitted parameters, in function of the EIS sweep number, show a stabilization of the CPE parameters (CPE, n) after the fifteenth sweep for both DSAu and DSC devices;
- The electrolyte solution resistance varies linearly after the fifteenth EIS sweep, most probably as an effect of solution drying over the measurements time which increases the solute concentration, and thus decreases the solution resistance.

#### 4.3.1.2 CV measurements

Cyclic Voltammetry measurements were performed both on three DSAu and three DSC devices in 1 mM ferro/ferricyanide diluted in PBS. The measurements were performed in the potential range between -0.3 V and +0.5 V for DSAus and between -0.2 V and +0.6 V for DSCs. The initial potential were the highest one for both the devices types. Two complete cycles were measured.

For each device, five scan rate values ranging from 25 mV/s to 100 mV/s were tested, performing two complete CV cycles per each scan rate value. Figures 4.20 and 4.21 show the CV measurements obtained from one DSAu and one DSC device, respectively, with the five scan rate values.

The oxidation (anodic) and reduction (cathodic) peak currents for a reversible system are linearly dependent on the square root of the scan rate value. Moreover, for a reversible system the peak currents ratio is 1 and the difference between the peak currents potential is independent from the scan rate and equal to 57 mV.

Figures 4.22 and 4.23 show the average peak currents values obtained from the CV measurements on the DSAu and on the DSC devices, respectively. Conversely, figures 4.23 and 4.25 show the average peak potential difference of the CV measurements at the different scan rates. The bars in these figures represent the standard deviations obtained from the three DSAu and DSC devices.

The results obtained from the CV characterizations show that:

- The peak currents ratio is very close to 1 for DSAus but not for DSCs;
- Both the devices types show linearity of the peak currents in function of the square root of the CV scan rate;

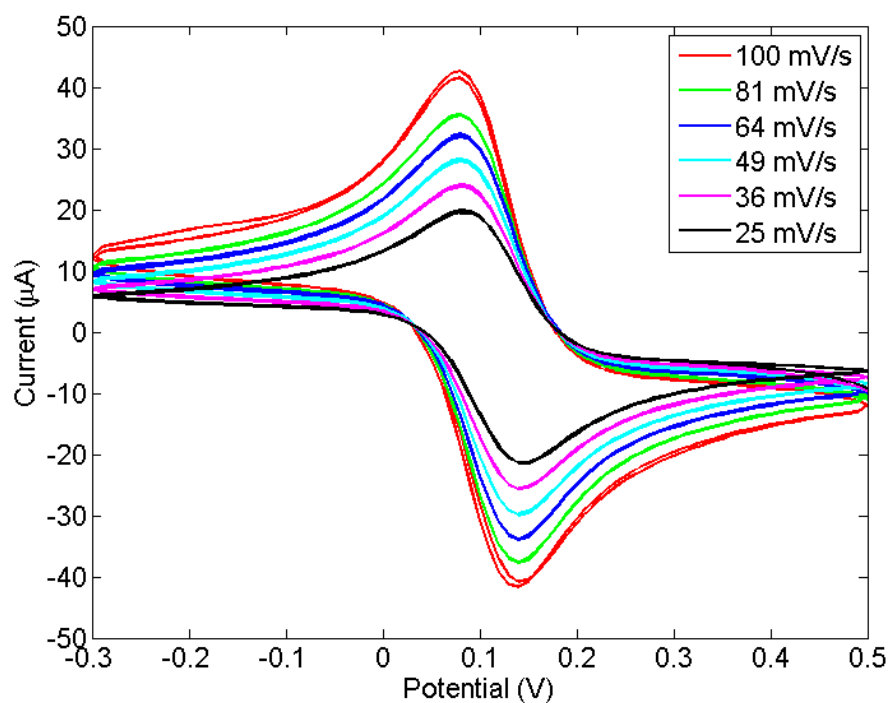


FIGURE 4.20: Cyclic voltammograms measured in ferro/ferricyanide 1 mM in PBS over DSAu devices with different Scan rate values

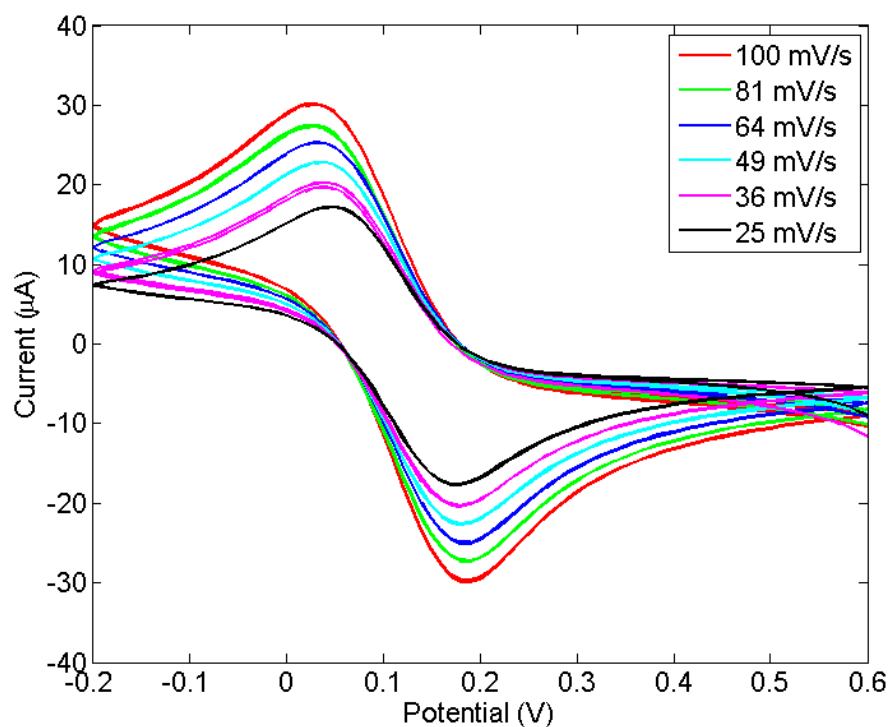


FIGURE 4.21: Cyclic voltammograms measured in ferro/ferricyanide 1 mM in PBS over DSC devices with different Scan rate values

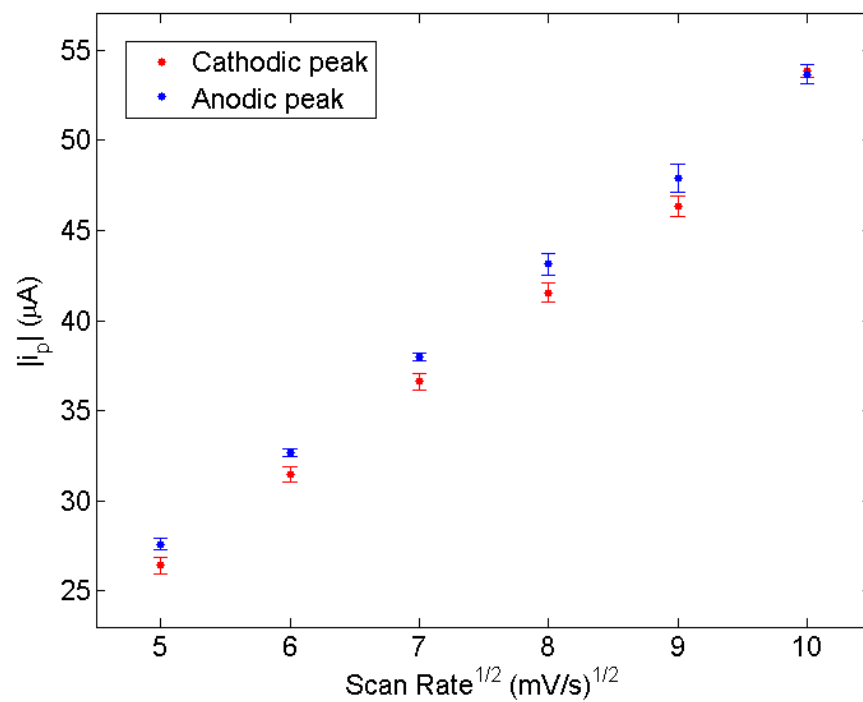


FIGURE 4.22: Cathodic and anodic mean peak currents modules in function of the square root of the CV scan rate over DSAu devices.

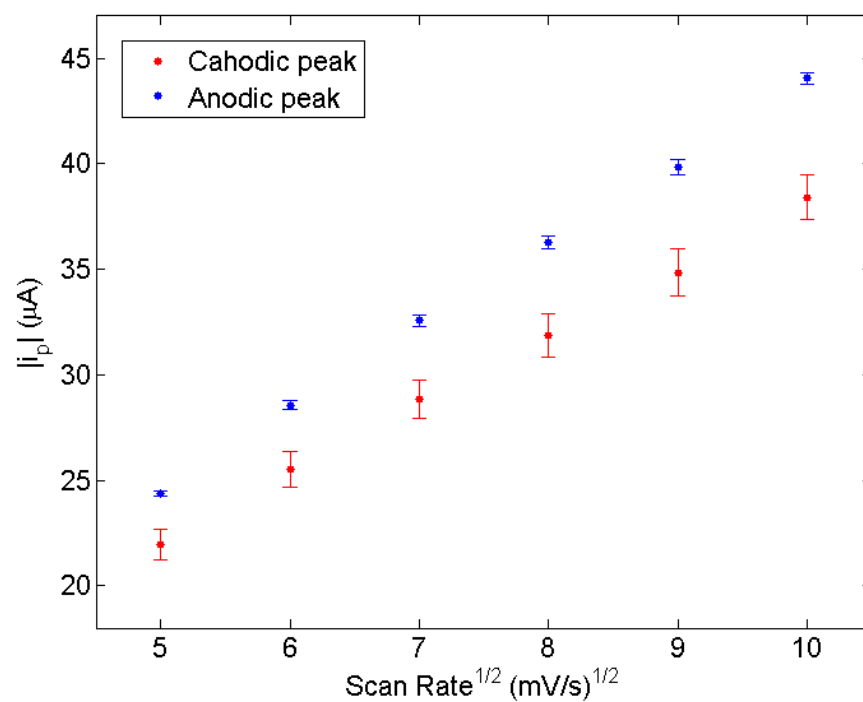


FIGURE 4.23: Cathodic and anodic mean peak currents modules in function of the square root of the CV scan rate over DSC devices.

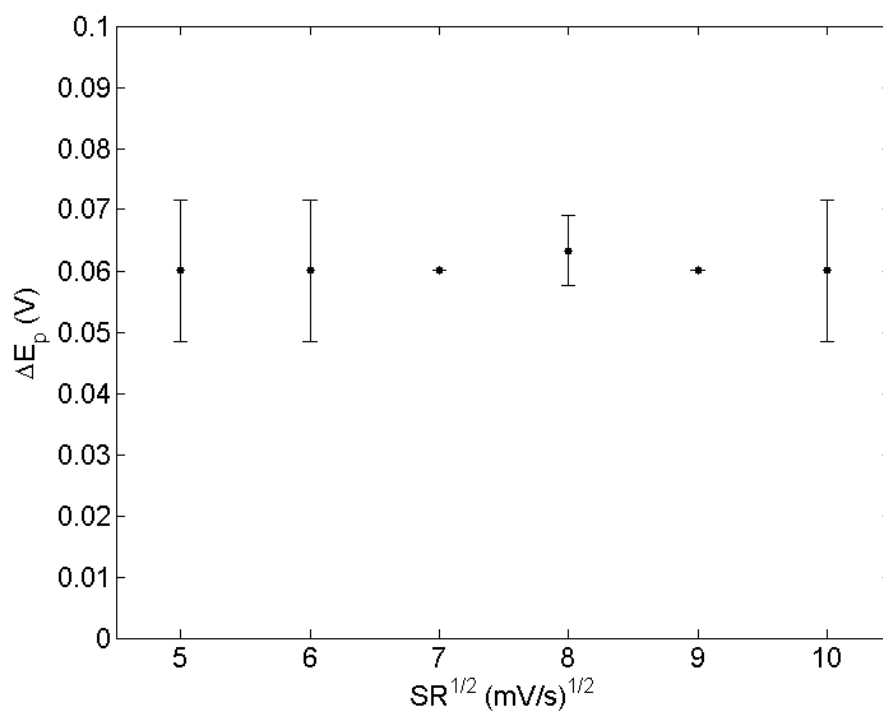


FIGURE 4.24: Peaks potential mean differences in function of the square root of the CV scan rate over DSAu devices.

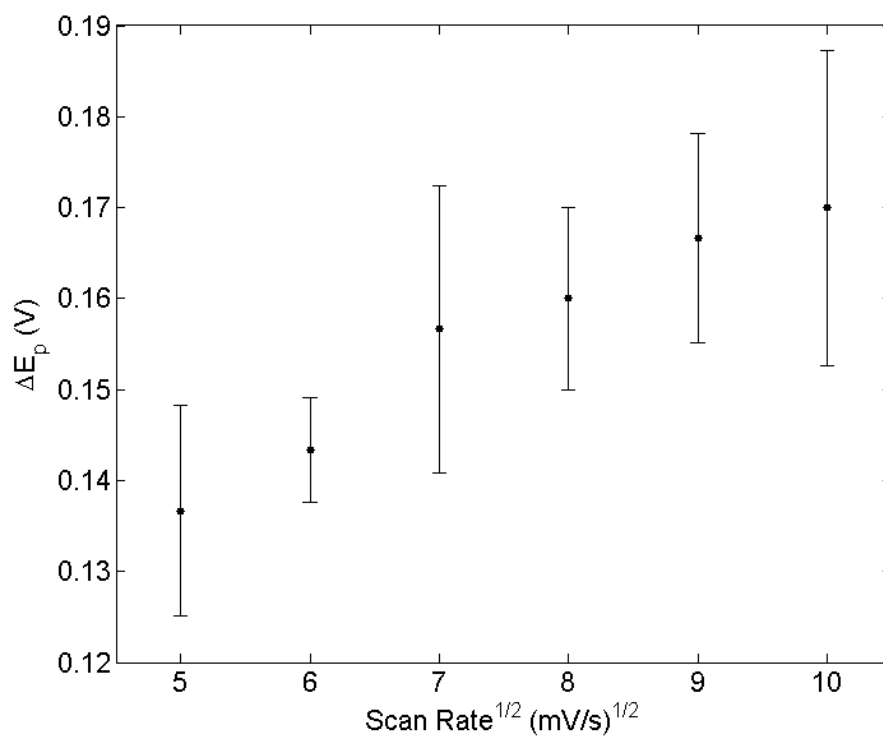


FIGURE 4.25: Peaks potential mean differences in function of the square root of the CV scan rate over DSC devices.

- The peak potentials difference is close to 57 mV and independent from the scan rate only for DSAus. DSCs show much higher values which are almost linear with the square root of the scan rate;
- Finally, as can be seen in figure 4.26, the peak current values measured on the DSCs are much lower than those measured on the DSAus in the same conditions because of the lower conductivity of the carbon electrodes.

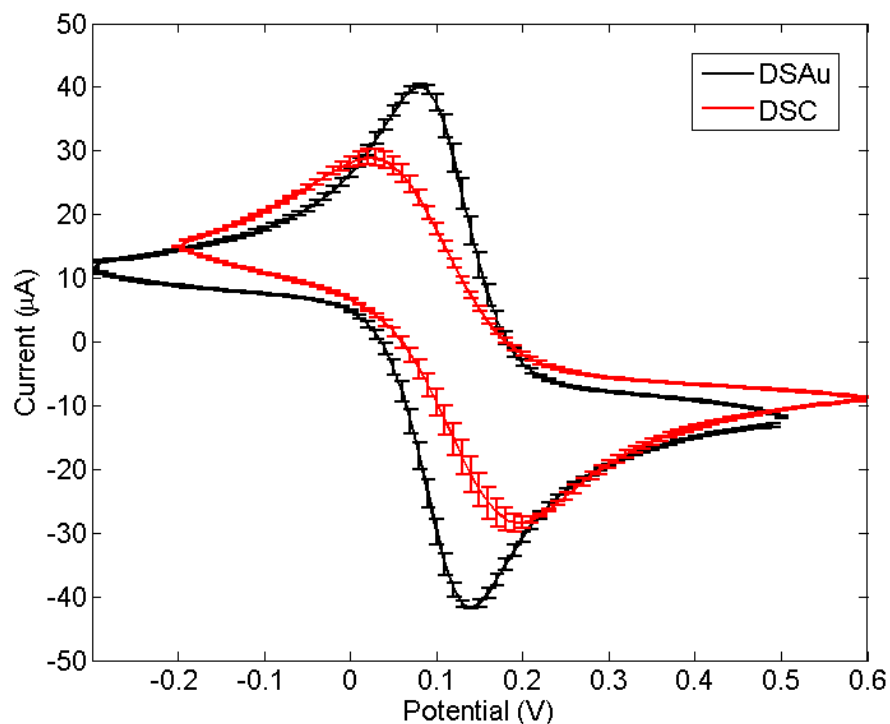


FIGURE 4.26: Average CV measurements performed in 1 mM ferro/ferricyanide at a scan rate of 100 mV/s on three DSAu and three DSC devices.

### 4.3.2 NADH detection

The EIS characterizations of the DSAu and DSC devices showed that the DSC devices have electrode surfaces more stable over time, with a smaller drift of the EIS spectra at low frequencies. Moreover, the DSC electrodes are fitted by a simpler and classical model in literature than the DSAus one. However, the CV characterizations showed that the DSAu devices in contact with a ferro/ferricyanide solution present the characteristics of a reversible system, while the DSC devices are better defined as a quasi-reversible system, in the same conditions. Anyway, both the devices types showed a good reproducibility level in both EIS and CV measurements.

For this reason they were both tested for the electrochemical NADH detection which is



performed by CV measurements and checked by UV-Visible spectrophotometry, used as control technique for the definition of the NADH real concentration.

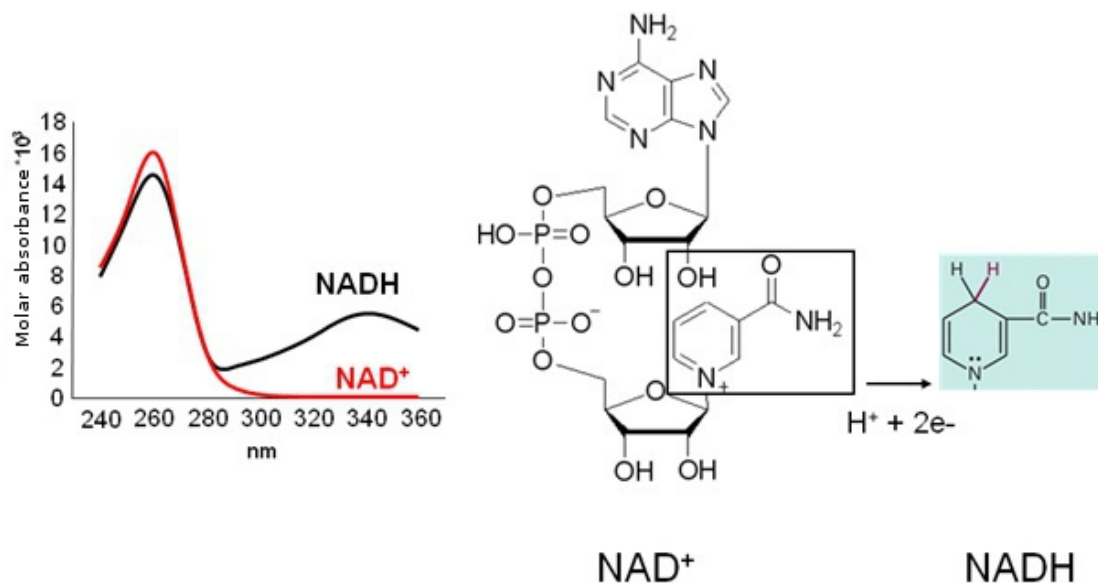


FIGURE 4.27: Schemes of the  $NAD^+$  and of the  $NADH$  molecules and representation of the UV-Visible spectra of the two molecules.

NADH UV-Visible spectra is characterized by two absorption peaks at 339 nm and at 260 nm while the  $NAD^+$  molecule present only the 260 nm peak. This peculiar characteristic is used to distinguish the reduced ( $NADH$ ) and oxidized ( $NAD^+$ ) forms of NAD, and to obtain the respective concentrations in solution. Anyway, the oxidation of  $NADH$  to  $NAD^+$  can be detected also electrochemically since it is accompanied by the release of two electrons.

The UV-Vis spectrophotometric measurements are performed pouring the test solution into a quartz cuvette, since quartz transmit more light than glass in the UV region (figure 4.28). Different kind of measurements are possible but, the common principle is that a defined-wavelength light beam hits the cuvette, and the light which passes through the cuvette (and the contained solution) is quantified by the instrument transducer, obtaining its transmittance at that wavelength. The UV-Vis measurements are always referred to a blank one, usually performed by setting the transmittance to 100% for the cuvette filled with the testing solution buffer. In this way, the measured transmittance will be related only to the analyte in the test solution.

The cuvette used for this study has an internal volume of 4 ml but it has always been used with 2 ml of solution because it was verified which this volume allows the solution level in the cuvette to be higher than the instrument optical center height (figure 4.29).

Two main types of measurements are possible with this technique: it's possible to scan a wavelengths interval, recording the transmittance peaks in function of the wavelength

(the spectra) of a solution, and it's possible to monitor the transmittance variations at a fixed wavelength over time (the kinetics at that wavelength).

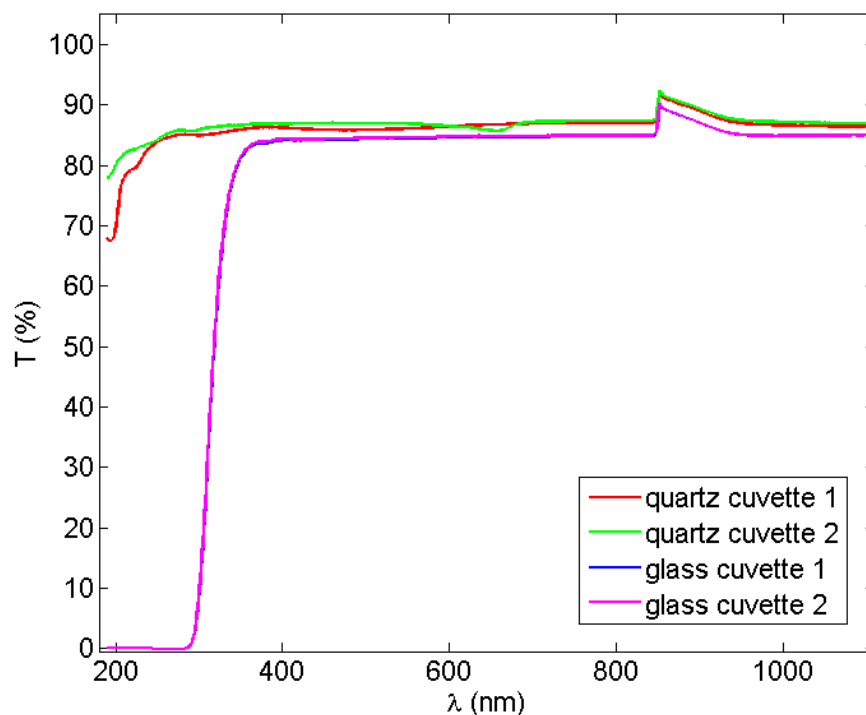


FIGURE 4.28: Cuvette transmittance tests performed on two glass and two quartz empty cuvettes, with respect to a blank measurement in air.

#### 4.3.2.1 UV-Vis spectrophotometry of NADH in different medium/buffers

The NADH detection is the basic and fundamental point for the electrochemical lactate biosensor realization, therefore it's the first that was tested. Since NADH in the final biosensor will have to be detected in a solution containing both the animal urine sample, the cells sample media, and the LDH enzyme buffer, there will be many substances which would interfere with the electrochemical measurements. As starting point, the NADH detection was tested in different buffers and cell media.

The tested cell media are Dulbecco's Modified Eagle Medium (DMEM) and HEPES Buffered Ringer's Solution (HBRS), while the tested enzymes buffers are Tris-HCl 50 mM with a pH of 8.8 and Phosphate Buffered Saline (PBS) 10 mM.

Ten NADH concentrations ranging from 1  $\mu\text{M}$  to 1000  $\mu\text{M}$  were diluted in each media/buffers. Then, their spectra was measured by UV-Vis spectrophotometric measurements. These spectra are showed in figure 4.30. The 339 nm absorption peak values ( $A_{339\text{nm}}$ ) were used to calculate the experimental NADH concentrations (c) through

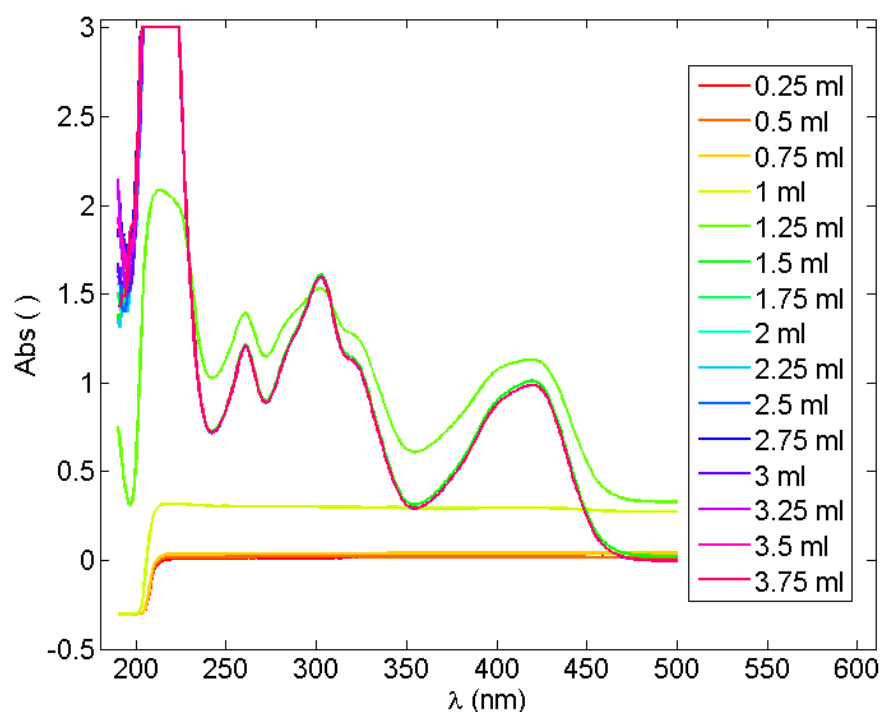


FIGURE 4.29: Optical center height tests performed by progressively filling a 4 ml quartz cuvette with 250  $\mu\text{l}$  of ferricyanide per each measurement.

the well known Lambert-Beer law, the NADH 339 nm millimolar extinction coefficient ( $\epsilon_{339nm}$ ) equal to  $6.22 \text{ Abs} \cdot \text{mM}^{-1} \cdot \text{cm}^{-1}$ , and considering a cuvette depth ( $l$ ) of 1 cm.

$$A_{\lambda} = \epsilon_{\lambda}lc \quad (4.3)$$

The 339 nm peaks of the NADH concentrations in the four media/buffers have coherent values considering the errors introduced by the NADH powder weighting and by the serial dilutions. Conversely, the situation is different for lower wavelengths, where the NADH in DMEM measurements do not show the 260 nm peaks and present a lot of noise. This effect is due to the low transmittance of this media at wavelengths under 300 nm. The blanking measurements already have very high absorbance which saturates the instrument transducer. Therefore, the NADH contribution at these wavelengths results in pure noise around zero.

The experimental concentrations obtained from the 339 nm absorption peaks with the four media/buffers were averaged and then compared to the theoretical ones (figure 4.31).

The bars represent the standard deviations. All the experimental concentrations are just a little bit lower than the theoretical ones. This effect could be due to a lack of

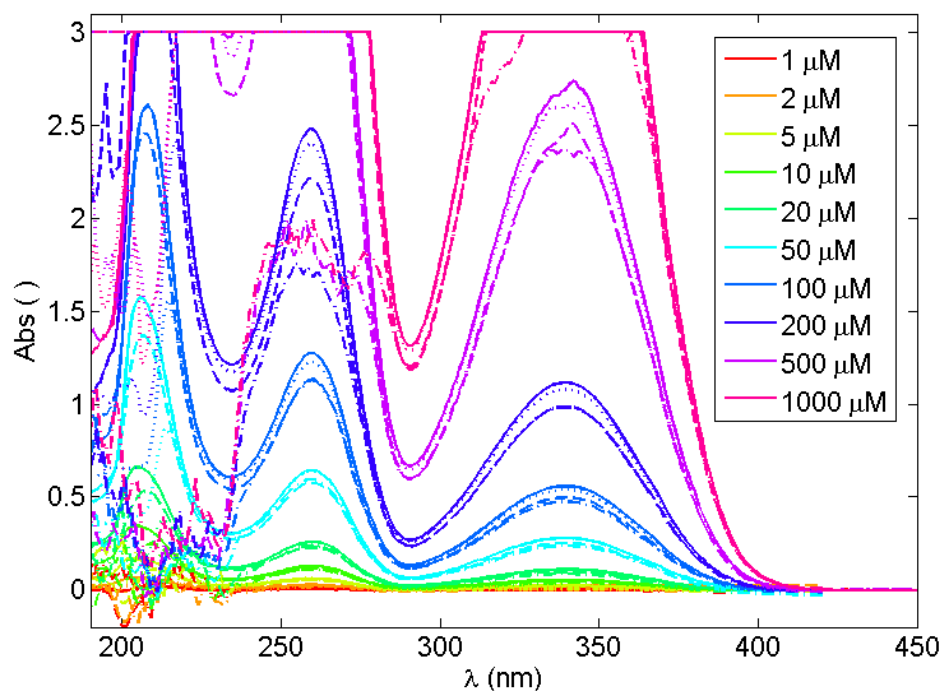


FIGURE 4.30: UV-Vis spectra obtained by measuring ten NADH concentrations in four buffers, with respect to four blank measurements in each pure buffer. The continuous curve is related to HBSR spectra, the dashed one to PBS, the dash-dotted curve to the DMEM, and finally the dotted one to Tris-HCl.

purity of the powder used to prepare the dilutions, thus the real NADH concentration for the following tests will always be defined by a UV-Vis measurement at 339 nm.

#### 4.3.2.2 CV measurements of NADH in different medium/buffers

The NADH solutions measured by UV-Vis spectrophotometry were tested by Cyclic Voltammetry just after the UV-Vis measurements. Both DSAu and DSC devices were used for the CV tests, three per each media/buffer. Each device was washed in milliQ water first, and then measured by CV applying potentials from -0.4 V to +0.8 V with a scan rate of 100 mV/s and performing five complete cycles. Each NADH concentration for a media/buffer were tested on the same three devices, from the lowest concentration to the highest one. The plots in figure 4.32 show the CV's first cycle for each NADH concentration measured on both the devices types. NADH dissolved in DMEM does not result in any peak in the considered potential range (figures 4.32a and 4.32e) but just in currents minimums at the highest (oxidation) potential.

The CV measurements of NADH in DMEM show a progressive decrease of the oxidation currents modules with the NADH dilution tested, this trend changes direction after the 50  $\mu$ M NADH concentration with the increase of the current module proportionally to

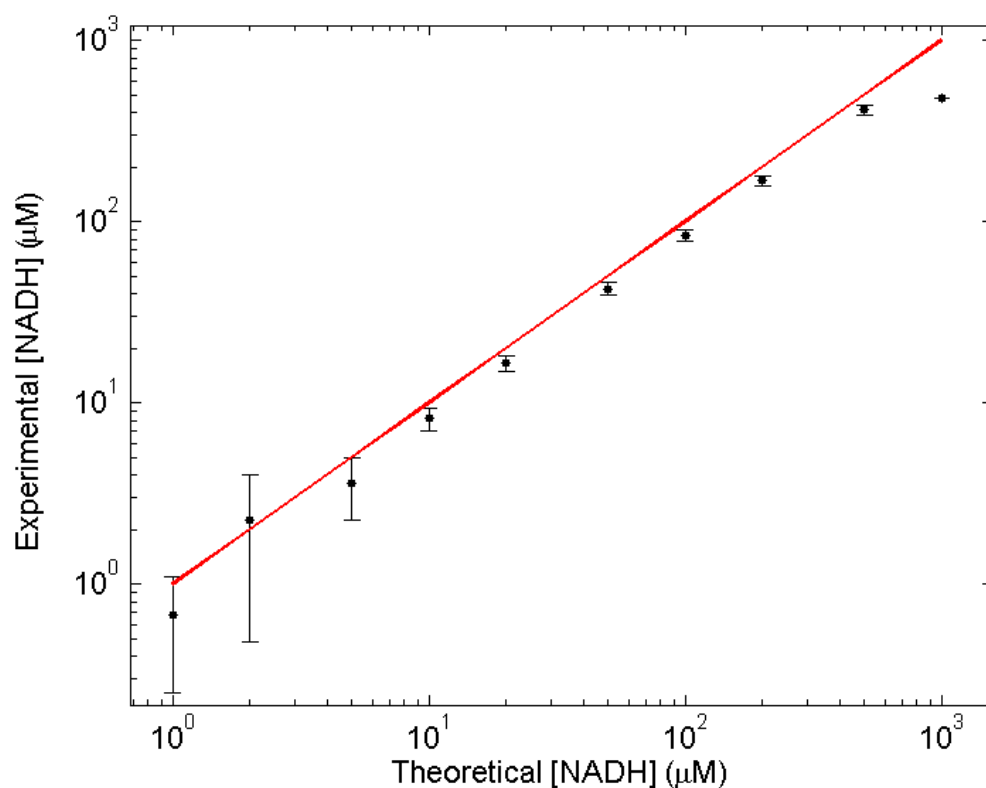


FIGURE 4.31: Comparison between the theoretical NADH concentrations of the prepared solutions and the experimental concentrations obtained from the 339 nm absorbance peak.

the NADH concentration. This effect was observed both on DSC and DSAu devices, thus it seems to be related to the oxidation of one or more DMEM components instead of NADH. However, in this case, the oxidation currents should be constant since the solution is changed for each measurement. This allow to suspect a possible passivation of the electrode's surface by one or more DMEM components which would create a barrier to the charges transfer between the solution and the surface. This would decrease the oxidation currents during consecutive measurements, until the NADH concentration becomes high enough to result again in high oxidation currents.

Conversely, the HBRS, PBS and Tris-HCl media/buffers give space to the rise of NADH oxidation peaks. The DSC devices NADH current peaks, obtained in all the media/buffers a part with DMEM, are always characterized by a potential beneath 0.6 V, while the DSAu devices present peaks potentials over 0.7 V except with Tris-HCl with which the potentials are lower and vary significantly between the measurements.

The peak currents obtained from the three DSC and the three DSAu devices for the NADH concentrations in the four media/buffers were averaged and reported in function of the NADH concentration, obtaining the NADH calibration plots. Since the lowest NADH concentrations do not present any peak a particular strategy was adopted to

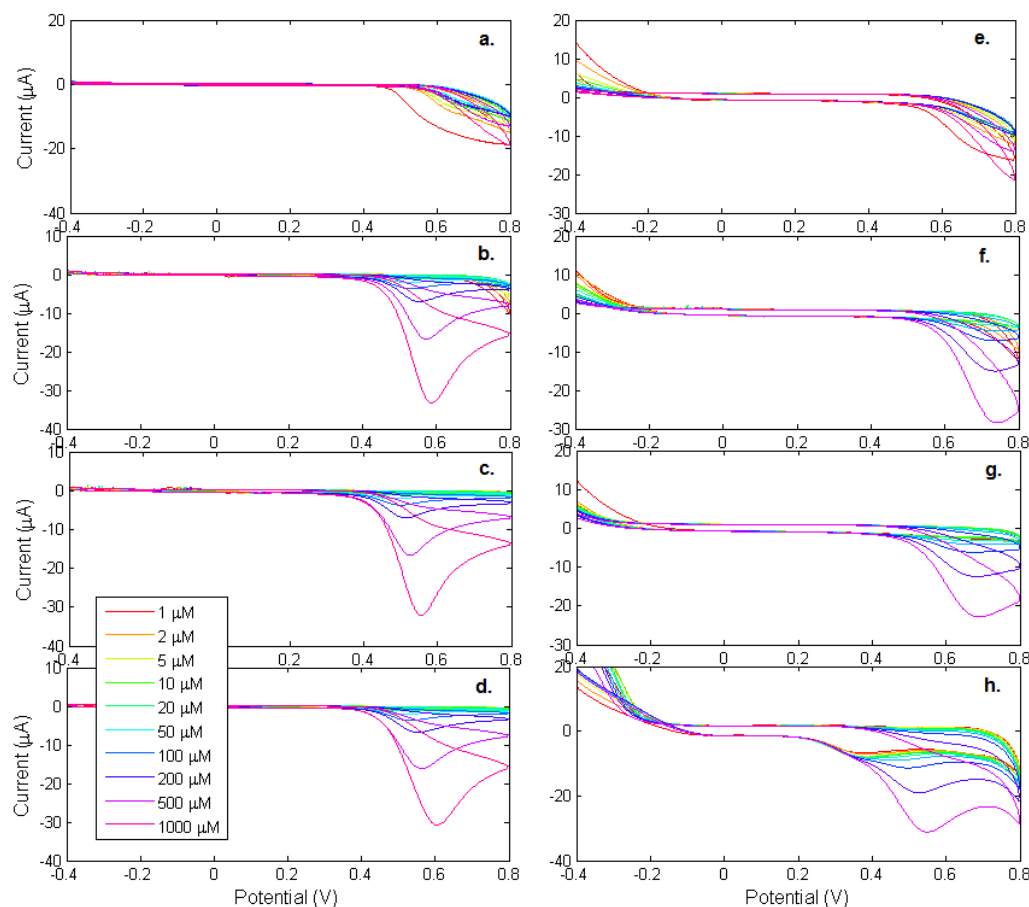


FIGURE 4.32: NADH consecutive CV measurements on DSCs (left column) and DSAus (right column) in the buffers: DMEM, HBRs, PBS, 50 mM Tris-HCl (respectively from the top).

choose the proper oxidation potential. The NADH current peaks potentials appears to linearly increase with the NADH concentration (at least at high concentrations). Therefore, this relation was fitted, obtaining the potential values, and thus the current one, to be considered for the calibration plot.

In the case of DMEM, the minimum current (recorded at 0.8V) was considered. The resulting calibration curves for DSAus (figure 4.33) and DSCs (figure 4.34) have in common the DMEM bell-shaped curve which clearly shows the possible effect of the progressive formation of a passivation layer over the devices electrodes. The other curves show different behaviors but the lowest NADH concentration that can be distinguished from the error bars is NADH 10  $\mu M$ .

Although this kind of measurements for the NADH calibration allows to reduce the number of used devices, it does not allow to distinguish between the NADH oxidation currents and the possible effect over the same devices surface of the repetition of the measurements. In order to be able to distinguish these components, at least with DSC

devices which proved to oxidize NADH at lower potentials than DSAu ones, it was attempted a data post-elaboration. In fact, three DSC devices were tested with the same protocol used for the previous ones but without dissolving NADH in the four media/buffers. Practically, 10 consecutive CVs were performed over the same devices, changing the solution over their electrodes for each measurement. These DSC devices were called blank DSC.

Figure 4.35 shows the difference between the NADH average peak currents and the average current values recorded at the same potential and corresponding measurement over the blank DSC. The error bars reported in this plot were obtained as the sum of the standard deviations related to the average of the NADH peak currents and of the blank DSC average currents. With this elaboration, the peak currents obtained with the media/buffers, with the exception of DMEM, are coherent. Moreover, as can be noted from the inset of the figure, the NADH peak currents are different from zero for  $5 \mu\text{M}$  concentration, which represent the limit of detection of these system with this protocol. With this elaboration, the DMEM bell-shaped calibration was compensated too. However, the currents difference for the NADH concentrations over  $20 \mu\text{M}$  are significantly lower than those of the other media/buffers, enforcing the surface passivation hypothesis.

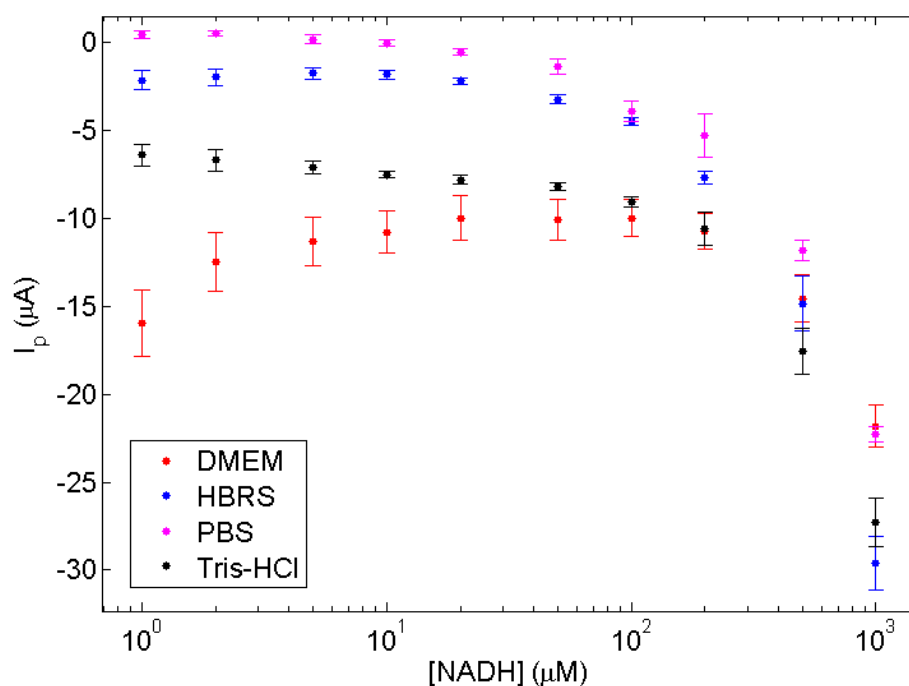


FIGURE 4.33: Peak current averages obtained from the CV measurements on three DSAu devices per each buffer. The bars represent the standard deviations obtained averaging the peak currents of the three devices.

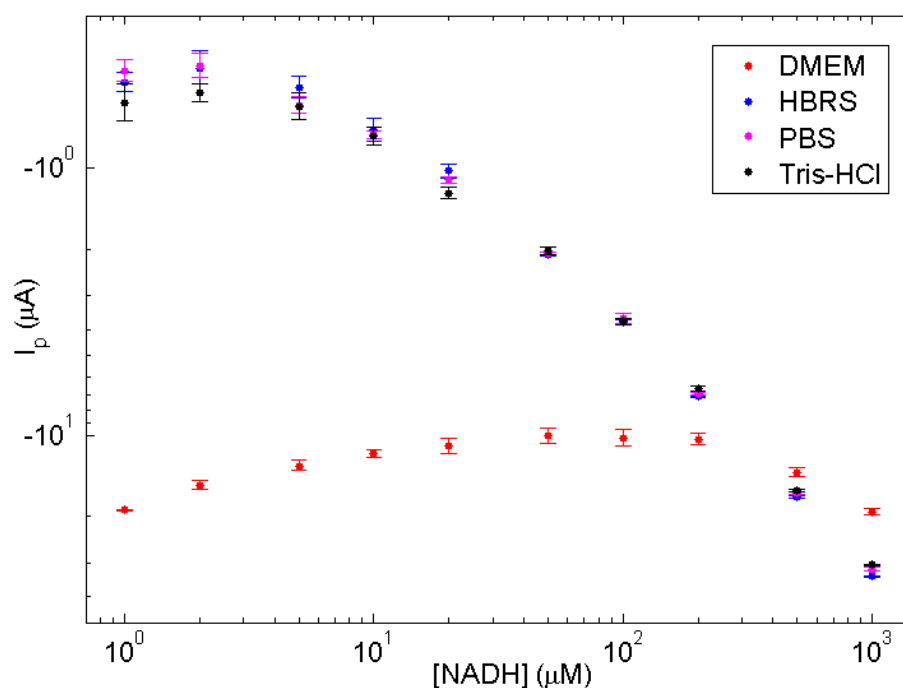


FIGURE 4.34: Peak current averages obtained from the CV measurements on three DSC devices per each buffer. The bars represent the standard deviations obtained averaging the peak currents of the three devices.

After having obtained a preliminary calibration curve repeating the measurements on the same devices with different NADH concentrations, as done until now, a one-shot device testing procedure was adopted, in order to obtain the real NADH calibration curve for DSCs in the selected media/buffers. With this approach, DSC devices were used to measure 3 NADH concentrations ( $10, 100, 1000\mu\text{M}$ ) in each media/buffers. For each NADH concentration 3 DSC devices were tested. Figure 4.36 shows the calibration curves obtained from the current peaks (and the 0.8 V values in the case of DMEM media). NADH in HBRS, PBS, and Tris-HCl result in almost overlapped and linear curves while NADH in DMEM gives a completely different curve. This difference was investigated and exploited by several CV measurements on pure DMEM, with the purpose to understand the nature of its interaction with the DSC devices surface.

Two CV tests were performed in DMEM solutions on DSC devices with this purpose:

1. Consecutive CV measurements (75 cycles) on the same DMEM drop;
2. Five Consecutive sets of 15 CV cycles in DMEM (75 cycles total), washing the devices surface between each sets and the following;



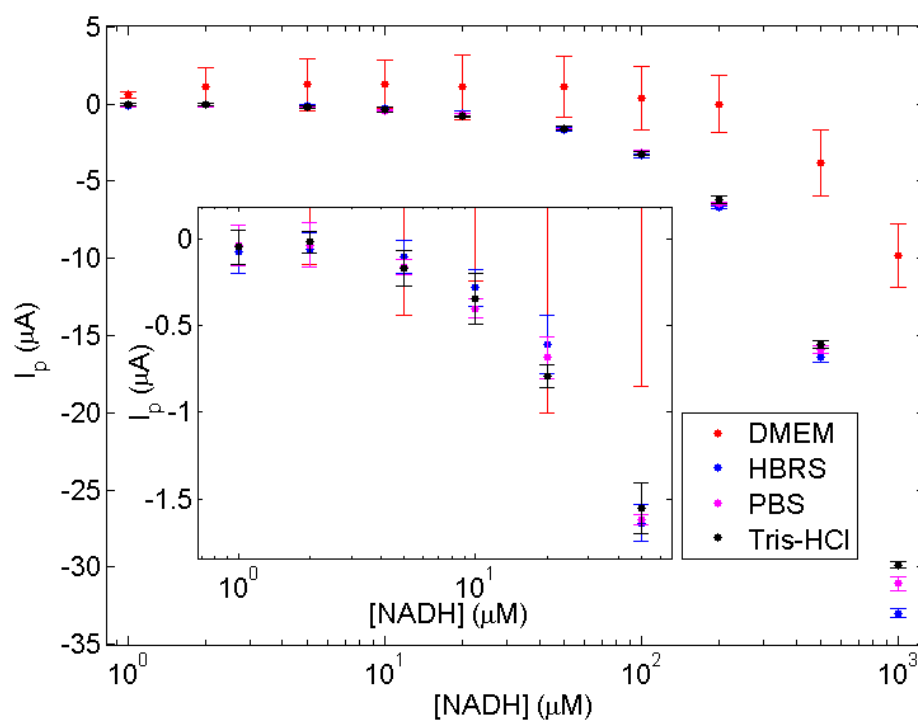


FIGURE 4.35: Peak current averages obtained from the CV measurements on three DSC devices per each buffer and subtracting the peak currents obtained from the blank measurements. The bars represent the standard deviations obtained averaging the peak currents of the three devices.

The first test showed the drift of the CV measurements performed with the same parameters adopted for the previous calibration curves among the cycles (figure 4.37). If this drift would depend only on the irreversible oxidation of some of the DMEM components, the CV measurements would start drifting from the same point with a new DMEM drop over the electrodes. This behavior has not been verified with the second CV tests. In fact, figure 4.38 shows the trend of the 0.8 V currents, recorded in function of the cycle number, and after each solution washing, the 0.8 V current drift start from the previous cycle current value.

In conclusion, the analysis performed show that DMEM is not a good media for the electrochemical detection of NADH since it has a progressive and irreversible passivation effect on the electrodes. Conversely, HBRS, PBS and Tris-HCl 50 mM seem not to affect in any way the NADH electrochemical detection. DSC devices showed to be able to oxidize and detect NADH with lower over-potentials than the DSAu ones, thus they were selected for the lactate sensor realization. Finally, since the consecutive measurements repetition on a single device have proven to be affected by a small drift with every media/buffer, the following NADH detection will be performed by one-shot measurements, as already tested.

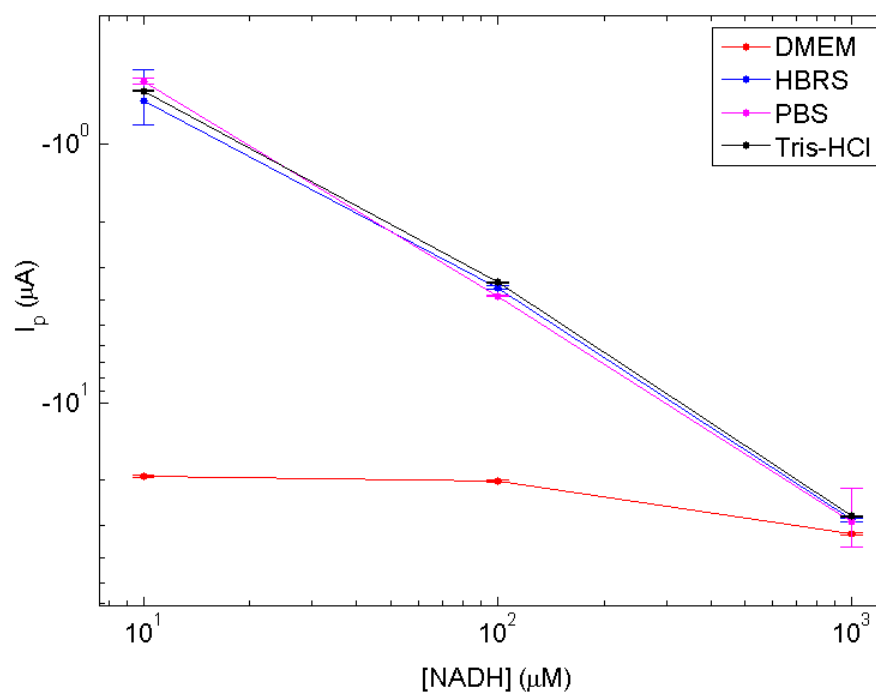


FIGURE 4.36: Peak current averages obtained from the CV one-shot measurements on three DSC devices per each NADH concentration and per each media/buffer. The bars represent the standard deviations obtained averaging the peak currents of the three devices.

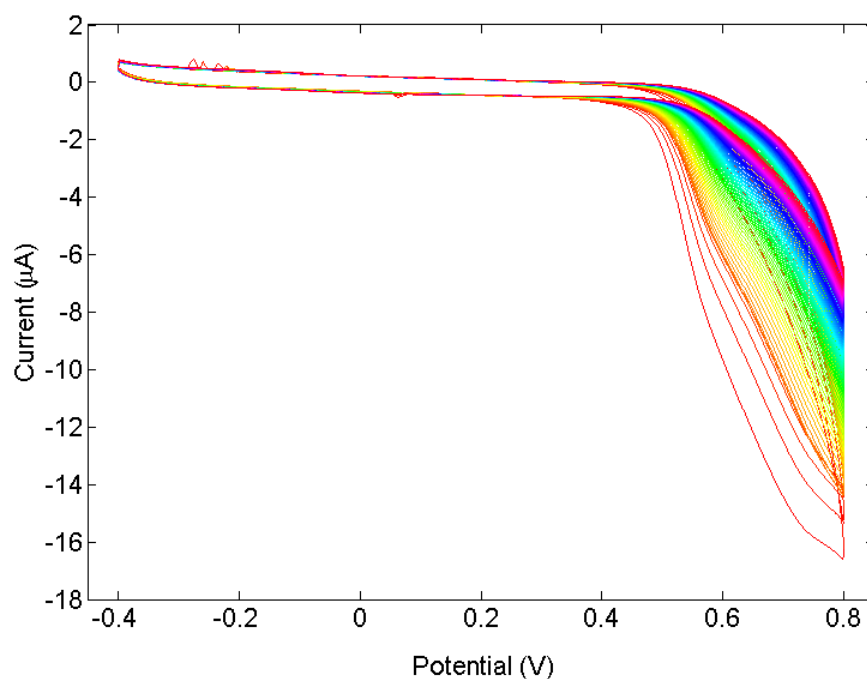


FIGURE 4.37: 75 CV cycles measured in DMEM on a DSC device with a scan rate of 100 mV/s. The first cycles are plotted in red while the last ones are represented in purple.

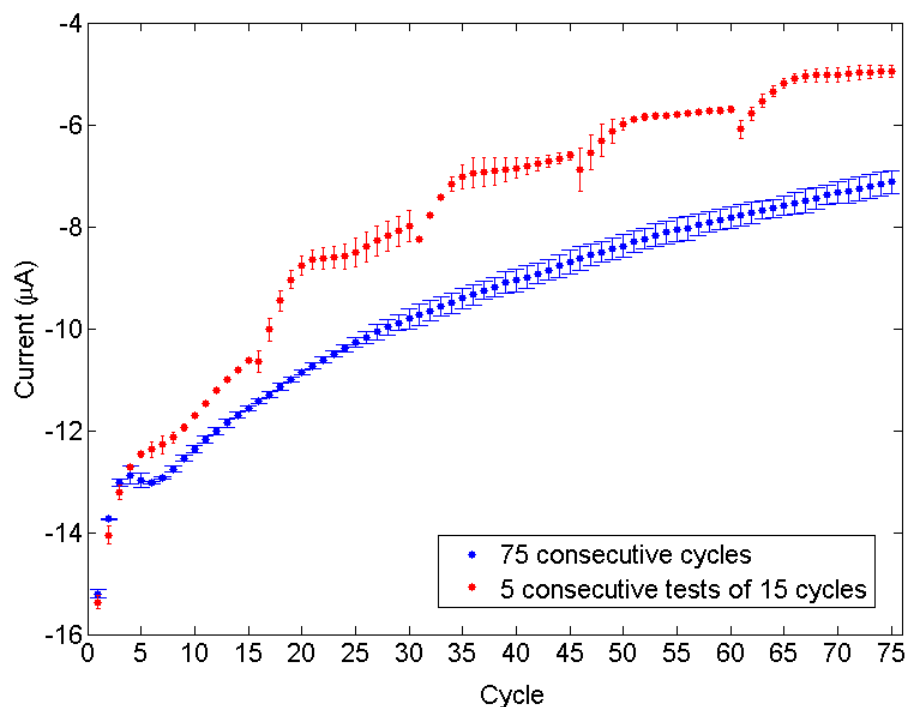


FIGURE 4.38: Current values at 0.8 V in function of the cycle number, recorded by the CV measurements on DSC devices in DMEM. The blue curve shows the current values obtained by 75 consecutive CV cycles on a DMEM drop, while the red curve represent the values recorded by 5 CV measurements each of 15 cycles, changing each time the DMEM drop on the DSC electrodes.

#### 4.3.2.3 NADH calibration curves

With the purpose to obtain an electrochemical NADH calibration curve with one-shot measurements on DSCs, five NADH concentrations were tested. The same tests were performed both for NADH in HBRS and for NADH in 50 mM Tris-HCl.

First, each NADH dilution UV-Vis spectra were measured, obtaining its real concentration from the 339 nm peak absorbance, with respect to blank measurements in the NADH pure buffer (figures 4.39 and 4.40). Then, the UV-Vis tested solutions were measured by CV on three DSCs per each NADH concentration (figure 4.41).

The NADH oxidation currents at 456 mV were represented in function of the experimental NADH concentrations to obtain the calibration curves (figure 4.42) and the respective linear fits.

As can be observed both in figure 4.40 and 4.42 the NADH concentrations obtained don't correspond exactly to the theoretical ones (1, 5, 10, 50, 100  $\mu\text{M}$ ). This is due to weighting and dilution errors. Anyway, the UV-Vis measurements allow to refer the electrochemical calibration plot to the real NADH concentrations.

The linear fits ( $I_p = a[\text{NADH}] + b$ ) of the calibration curves reported in figure 4.42 are reported in table 4.1. The calibration curves for NADH in HBRS and Tris-HCl

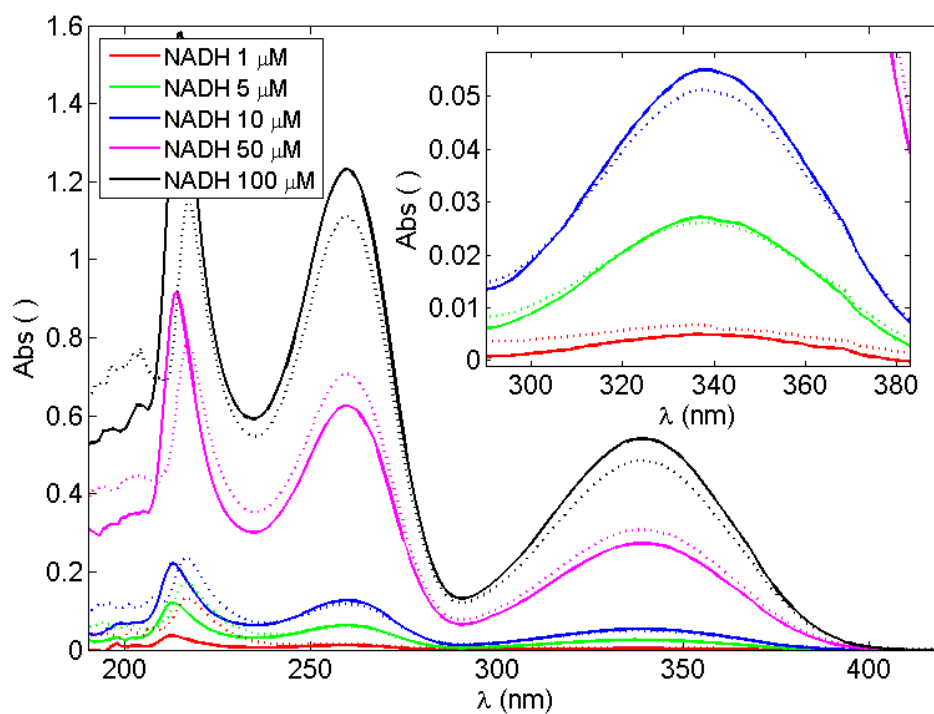


FIGURE 4.39: UV-Vis spectra of NADH dissolved in Tris-HCl 50 mM and in HBRS with respect to blank measurements in Tris-HCl and HBRS, respectively.

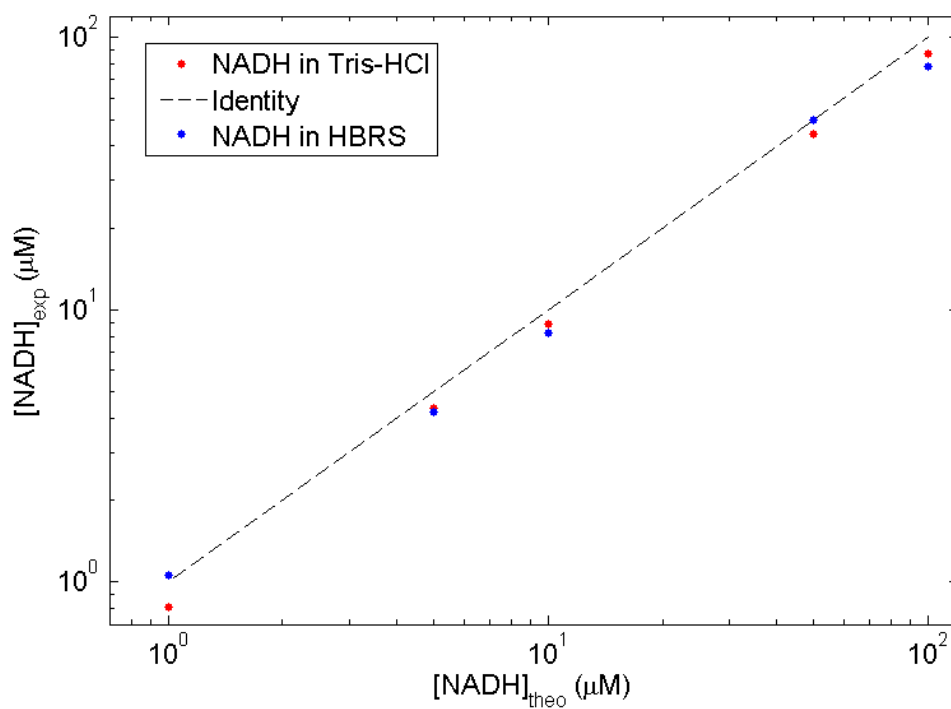


FIGURE 4.40: Comparison between the experimental and theoretical NADH concentrations obtained from the 339 nm peaks of the measurements in Tris-HCl and HBRS.

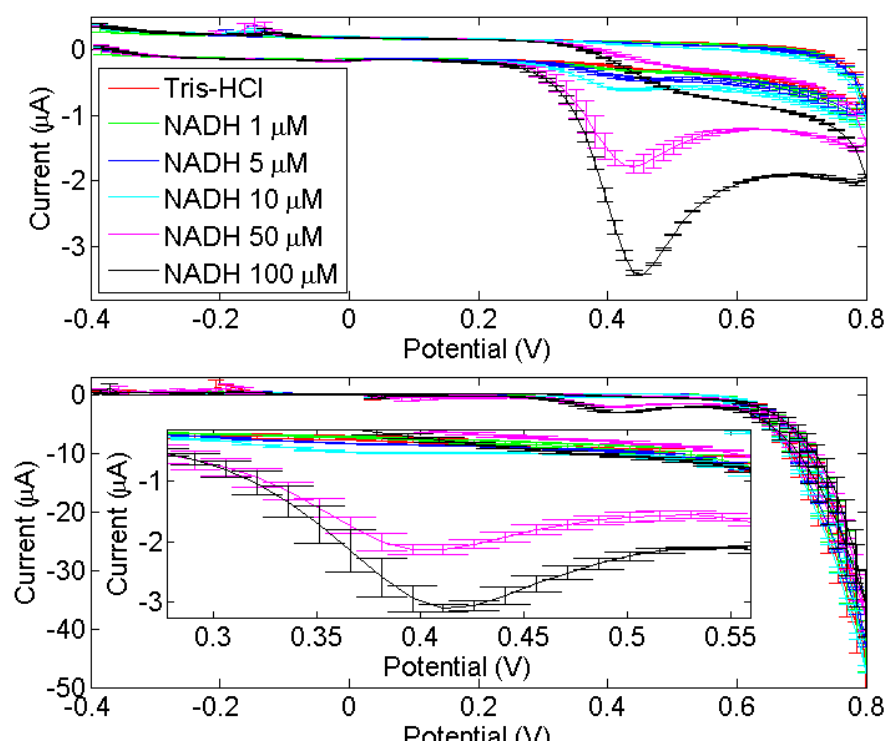


FIGURE 4.41: Average one-shot CV measurements performed on DSCs on the NADH solutions previously tested by the UV-Vis measurements. The plot on the top shows the measurements in Tris-HCl while that one on the bottom shows those in HBRS.

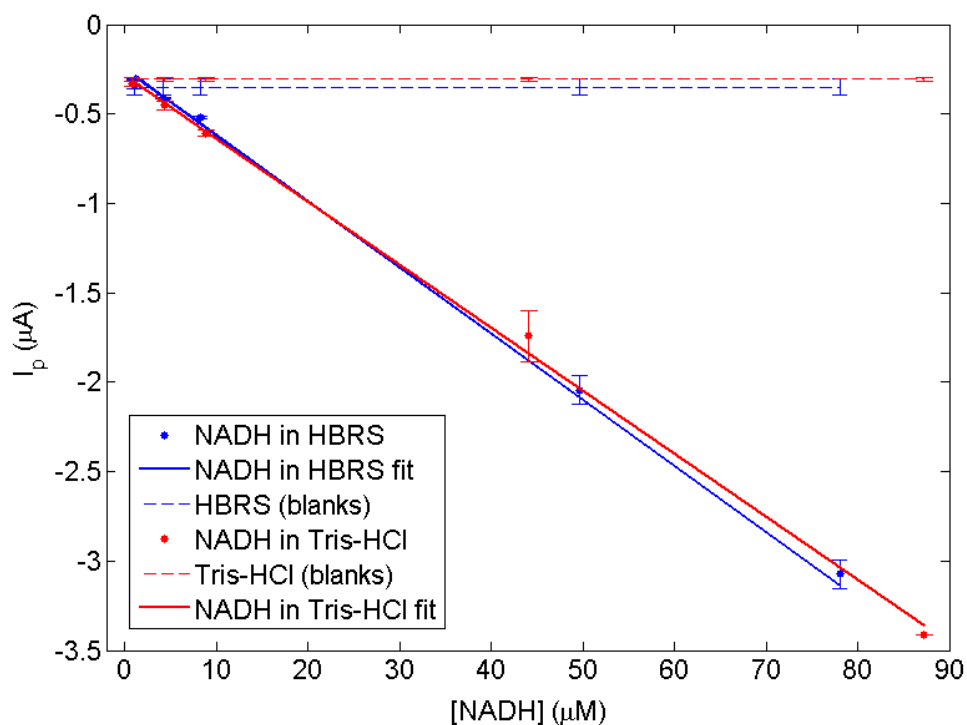


FIGURE 4.42: Calibration curves obtained by the NADH measurements in Tris-HCl and HBRS. The lines represent the dots linear fits, while the dashed lines show the blank currents measured in Tris-HCl and HBRS, respectively.

resulted almost coincident. Therefore, the DSCs and the CV technique proved to be valid supports for the NADH detection in HBRS and Tris-HCl with an average sensitivity of about  $36 \mu A/mM$  and a limit of detection of  $1 \mu M$  NADH.

Media/buffer	50 mM Tris-HCl	HBRS
a	-0.03533	-0.03702
b	-0.2814	-0.2511
$R^2$	0.9981	0.9992

TABLE 4.1: NADH calibration curves linear fits parameters for the detection in 50 mM Tris-HCl and in HBRS.

### 4.3.3 LDH-mediated catalysis optimization

Lactate Dehydrogenase (LDH) is a tetrameric enzyme which catalyzes the conversion of lactate to pyruvate through the reduction of its cofactor NAD to NADH. The four monomeric units of LDH can be of two types called M-type or H-type depending on their origin, skeletal muscle or heart, respectively. Therefore, it exists four LDH isoenzymes, made by the possible combinations of M and H monomeric units:

- $M_4$  made by four M subunits and mainly found in the skeletal muscle;
- $M_3H$  made by three M subunits and an H subunit;
- $M_2H_2$  made by two M subunits and two H subunits;
- $H_3M$  made by three H subunits and an M subunit;
- $H_4$  made by four M subunits and mainly found in heart.

The reaction catalyzed by LDH is shown in paragraph 4.2 with a double arrow indicating that the catalysis direction can be both from lactate to pyruvate, and viceversa. The catalysis direction is strictly dependent on the LDH isoenzyme. It's known that the  $H_4$  isoenzyme promotes the lactate to pyruvate catalysis while the  $M_4$  isoenzyme promotes the converse reaction in the same conditions. Other factors strongly influence the catalysis direction e.g. the pH of the solution, the concentrations of both the substrate and the cofactor, and the temperature.

For the lactate sensor under analysis, the better choice would be  $H_4$  LDH isoenzyme. However, this LDH form is difficult to isolate in high volumes and concentrations (and very expensive). Moreover, it's not commercially available. Thus, it was used a  $M_4$  form, from rabbit muscle. The structure of this isoenzyme is represented in figure 4.43.

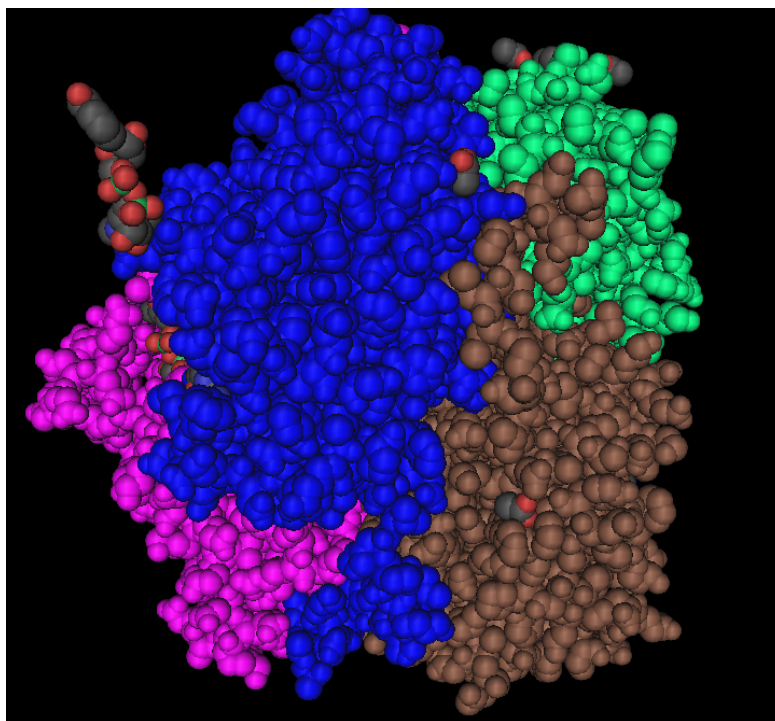


FIGURE 4.43: Structure of the rabbit muscle LDH isoenzyme. The four M subunits are coloured in green, brown, blue, and purple.

The enzyme concentration has a key role in the catalysis kinetics thus four LDH concentrations, ranging from 0.1 U/ml to 100 U/ml, was tested by UV-Visible spectrophotometric measurements, with the same substrate (LA) and cofactor (NAD) concentrations equal to 36 mM and 2.7 mM, respectively. Both the test solution spectra and kinetics were measured with the following protocols:

With regards to the spectra measurements:

- The blanking of the instrument was performed in 1.8 ml of 50 mM Tris-HCl and 0.2 ml PBS 1x and then the cuvette was washed;
- A solution of 3 mM NAD and 40 mM lactate in 50 mM Tris-HCl was poured into the cuvette (1.8 ml), and 0.2 ml of LDH at the chosen concentration in PBS was added;
- About 20 seconds after the solutions mixing, the first UV-Vis spectra measurement was started;
- Each spectra measurement requires about 50 seconds. Twenty consecutive measurements were repeated for a total period of observation of about 17 minutes.

For the kinetics measurements the protocol was easier:

- The blanking of the instrument was performed in the same Tris-HCl and PBS solution of the previous measurements;
- The NAD and LA solution was mixed with the LDH one;
- The measurements was started 15 seconds after the solutions mixing, setting 339 nm as monitored wavelength, 1 second as measurement resolution, and a total duration of 17 minutes.

Figure 4.44 shows the spectra recorded with the 20 consecutive measurements with 1 U/ml LDH. NAD, having a 260 nm millimolar extinction coefficient of 14.4 results in a 3 Abs saturated absorbance peak around this wavelength. This peak remains constant during the whole test. Conversely, absorbance variations are observed at 339 nm with an increase proportional to the repetitions, due to the NADH formation during the catalysis. However, the NAD concentration is so high that the tail of the 260 nm peak does not allow the NADH to form a proper peak at 339 nm.

The same type of spectra and kinetic measurements were repeated with LDH 0.1, 10, 100 U/ml in PBS 1x. The results are showed in figure 4.45, where the dots represent the 339 nm consecutive spectra absorbance values while the lines are the measured kinetics at the same wavelength. The contribute of the LDH concentration in the catalysis kinetic is evident, with 1 U/ml LDH resulting the lowest concentration for the catalysis observation with these LA and NAD concentrations in 20 minutes.

The 1, 10, 100 U/ml LDH concentrations have then been used for the UV-Vis spectrophotometric measurements of LA calibration curves, testing the five minutes catalysis kinetics of the LA concentrations from 1  $\mu M$  to 1  $mM$ . The same protocol of the previous measurements were adopted. Ten LA dilutions were prepared and mixed with  $NAD^+$  in Tris-HCl 50 mM pH 8.8 in order to obtain the desired LA concentrations in 500  $\mu M$   $NAD^+$ . Then, 1.8 ml of these dilutions were poured into the quartz cuvette and 0.2 ml of LDH in PBS 1x at the selected concentration was added. The kinetics of the resulting catalysis was measured for five minutes, starting 20 seconds after the mixing of the LA/NAD and LDH solutions. All the kinetics measurements are referred to a different blank measurement, performed by mixing 1.8 ml of each LA/NAD solution with 0.2 ml of PBS. The resulting kinetics are shown in figure 4.46 for the three LDH concentrations considered.

The enzyme kinetics are usually modeled by the Michaelis-Menten equation which describes the catalysis velocity (V) in function of the substrate concentration (S), which is LA in this case. From the collected measurements, it's possible to obtain the catalysis velocity from the slope of the linear part of the UV-Vis kinetics measured. This was done with the following formula:



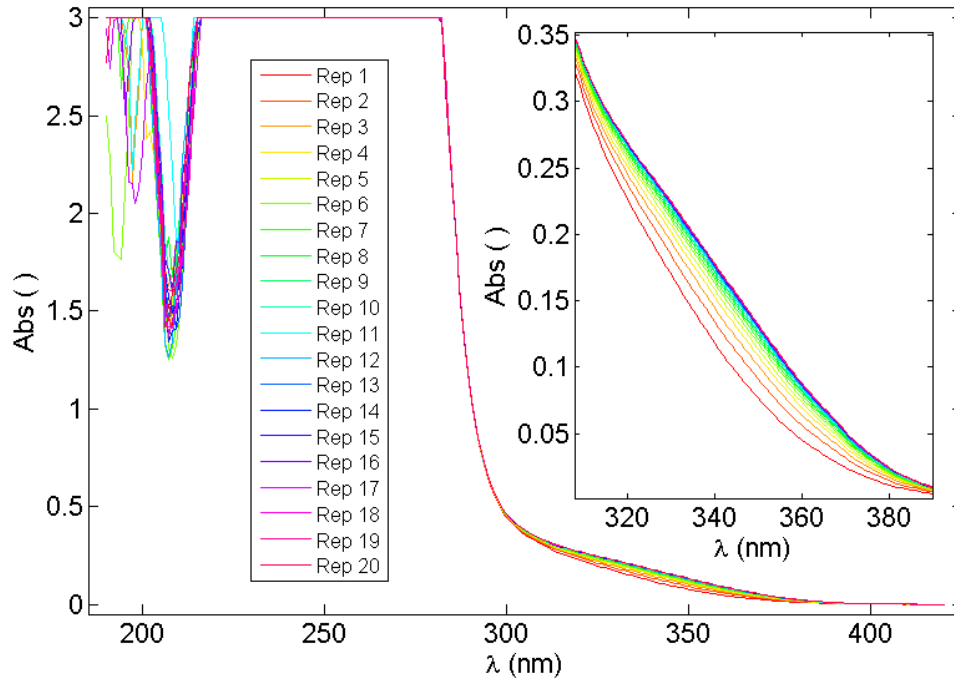


FIGURE 4.44: Consecutive absorbance spectra measured in the catalysis solution (with 1 U/ml LDH) with respect to a 1.8 ml of Tris-HCl 50 mM and 0.2 ml of PBS blanking solution.

$$V = 60 \cdot 1000 \cdot \frac{Abs_{20s}^{339nm} - Abs_{0s}^{339nm}}{20\epsilon_{NADH}^{339nm}l} \quad (4.4)$$

Where  $Abs_{20s}^{339nm}$  is the Absorbance measured at 339 nm 20 seconds after the start of the measurement,  $Abs_{0s}^{339nm}$  is that one of the first measured point,  $\epsilon_{NADH}^{339nm}$  is the millimolar NADH extinction coefficient at 339 nm ( $6.22 \text{ mM}^{-1}\text{cm}^{-1}$ ), and  $l$  is the cuvette pathlength (1 cm). Therefore, the calculated velocity measurement unit is  $\mu\text{M}/\text{min}$ .

Therefore, for each LA concentration it was obtained a velocity value and this was repeated for the three LDH tested dilutions. The Michaelis-Menten kinetics are described by the following equation:

$$V = \frac{V_{max}[S]}{K_M + [S]} \quad (4.5)$$

where  $[S]$  is the substrate concentration, i.e. the LA one, and  $V$  is the catalysis velocity.  $V_{max}$  and  $K_M$  are two parameters estimated fitting the equation with the calibration curves values. The first represents the maximal velocity of the catalysis, obtained with the highest substrate concentrations, while the second represents the substrate concentration necessary for a catalysis velocity which is the half of the maximum one. Figure

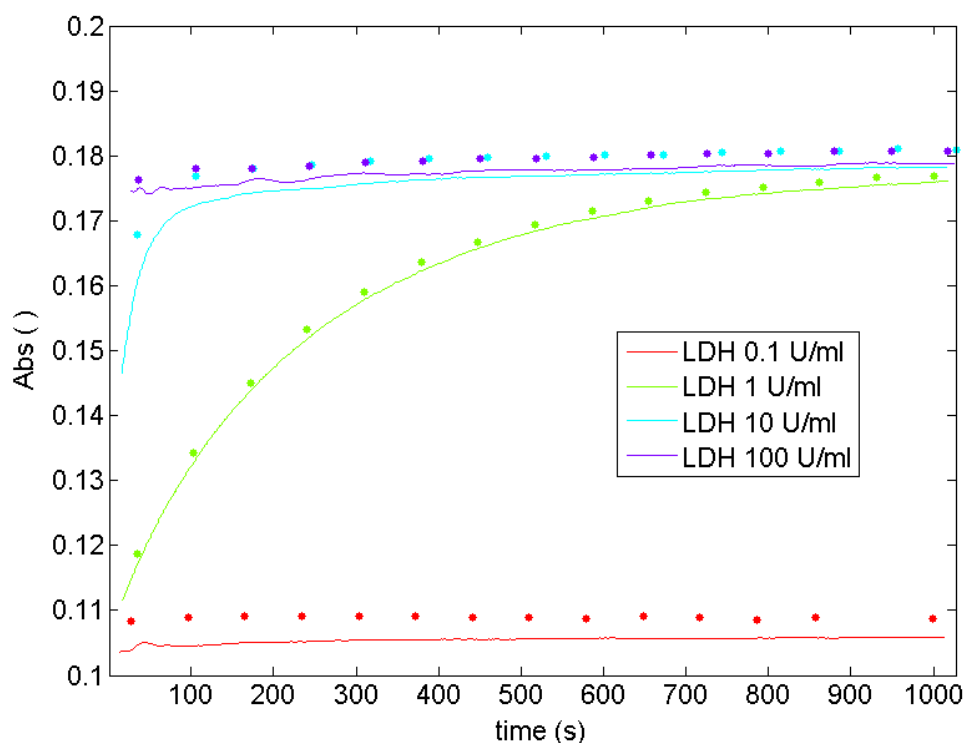


FIGURE 4.45: LA catalysis kinetics obtained by consecutive UV-Vis spectra measurements over time (dots representing the 339 nm absorbance), and by kinetic measurements at 339 nm with a resolution of 1 s. The baseline of the measurements was 1.8 ml of Tris-HCl 50 mM and 0.2 ml of PBS.

4.47 shows the velocity points calculated from the UV-Visible measurement linear parts in function of the LA concentration for the three LDH tested dilutions in PBS. The curves represent the Michaelis-Menten fits, which parameters are reported in table 4.2.

LDH ( $U/ml$ )	$V_{max}(\mu M/min)$	$K_M(\mu M)$
1	3.23	2650.90
10	13.57	1465.90
100	14.44	202.50

TABLE 4.2: Michaelis-Menten kinetics parameters obtained by the catalysis velocity curves fits, with three LDH dilutions.

Taking the steady state absorbance value related to the highest LA concentration, and to the most concentrated LDH dilution from figure 4.46, it can be seen that the NADH concentration resulting from the catalysis is almost 45 times less than the lactate concentration which was tested. This means that the catalysis, in this conditions, reach its equilibrium when just a small fraction of the present LA is converted in pyruvate (PA). This effect was expected as the LDH used in these experiments is of the  $M_4$  isoform, thus it favors the PA to LA catalysis instead of the converse reaction, as showed in figure 4.48.

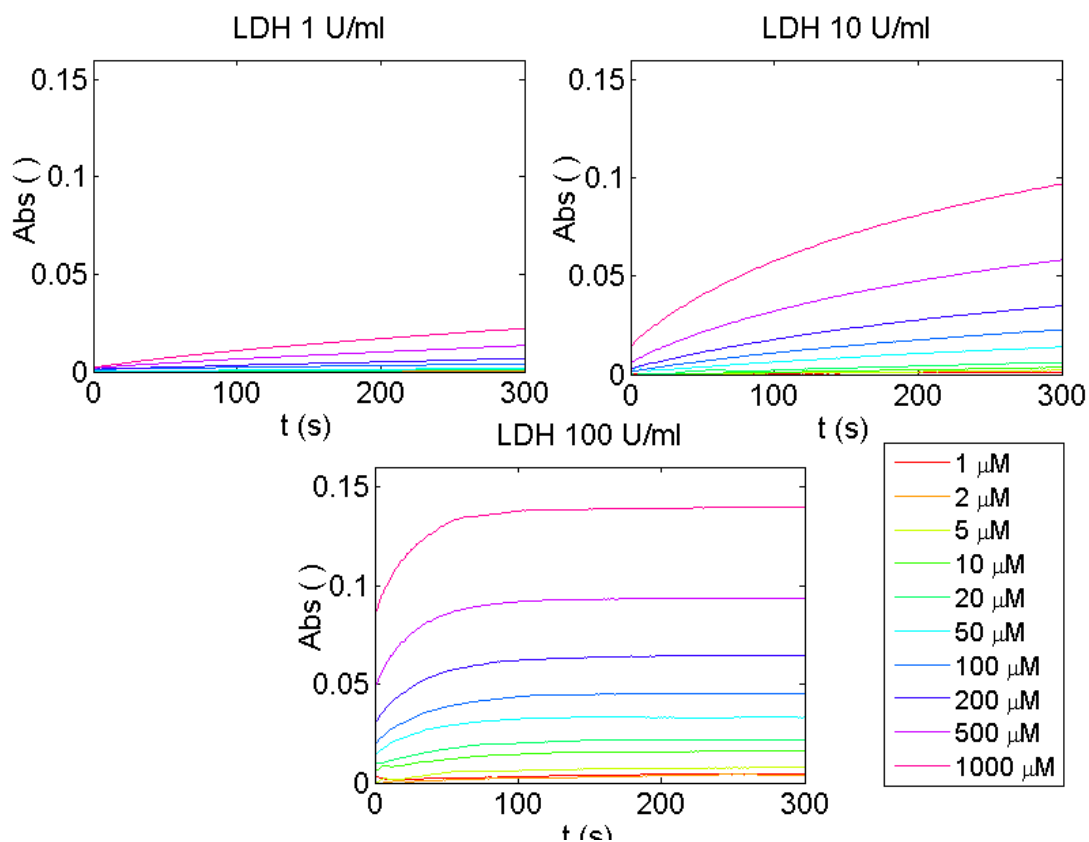


FIGURE 4.46: LA catalysis UV-Vis calibration curves obtained measuring the kinetics at 339 nm in solutions with ten LA concentrations from  $1\mu\text{M}$  to  $1000\mu\text{M}$  and three LDH dilutions, from 1 to 100 U/ml.

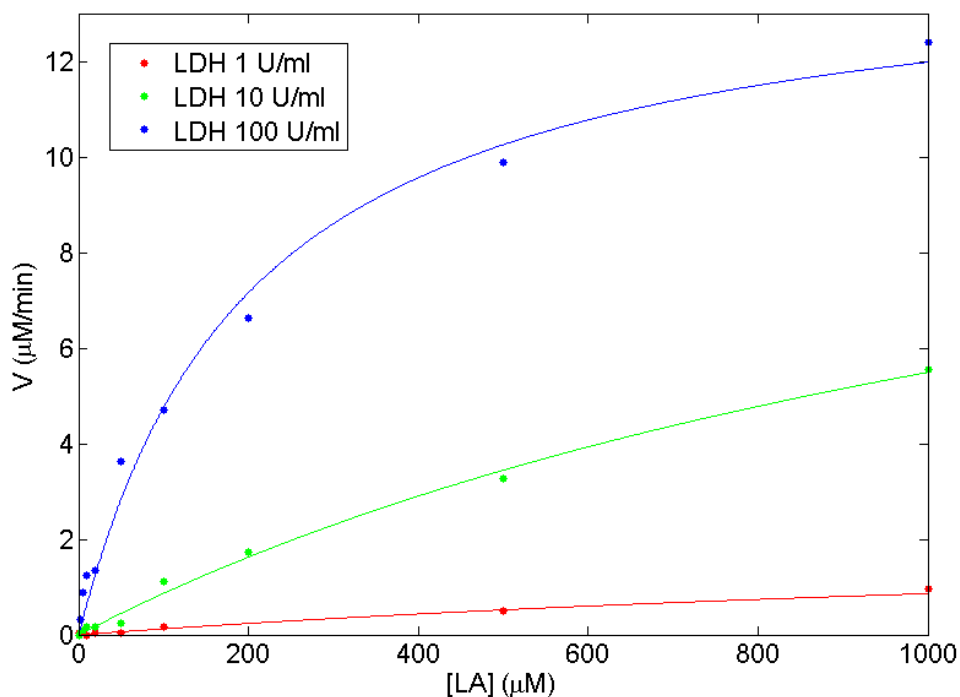


FIGURE 4.47: Michaelis-Menten kinetic curves calculated from the data represented in the previous figure, with three LDH dilutions.

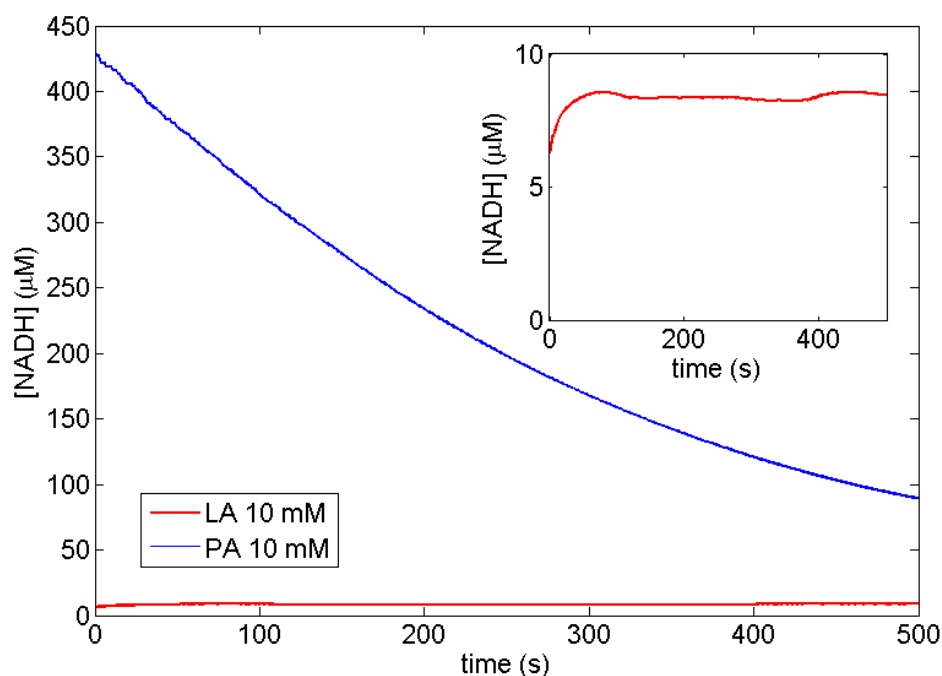


FIGURE 4.48: Comparison of the NADH concentrations obtained from the 339 nm UV-Vis kinetics of the catalysis of 10 mM LA and PA in HBRS, in presence of  $625 \mu\text{M}$  NAD or NADH in HBRS respectively, and of LDH 100 U/ml in PBS 1x.

In order to contrast the strong PA effect on the LA to PA catalysis equilibrium, hydrazine was introduced in the Tris-HCl buffer. Hydrazine ( $N_2H_4$ ) has the ability to bind PA without producing compounds which absorb at 339 nm, allowing for an higher NADH production. Therefore, this component is particularly useful for the LA assay by  $M_4$  LDH isotypes ([80]). The hydrazine effect was tested measuring the UV-Vis kinetics of 1 mM LA in  $625 \mu\text{M}$  NAD<sup>+</sup> and 100 U/ml LDH either in HBRS and in HBRS with 0.5 M Hydrazine. As shown in figure 4.49 the kinetics are completely different and the hydrazine-enhanced one does not reach the steady state even in 1500 seconds.

Unfortunately, hydrazine at this concentration causes interferences on the CV measurements at the NADH oxidation potentials on DSC devices. For this reason its use was avoided.

### 4.3.4 Lactate detection

#### 4.3.4.1 Protocol selection

As previously shown in this chapter HBRS resulted a good candidate as buffer for the NADH detection, and thus for the LA detection. Moreover, as proved in the previous chapter the cells proved to survive for at least 24 hours in HBRS. However, HBRS has

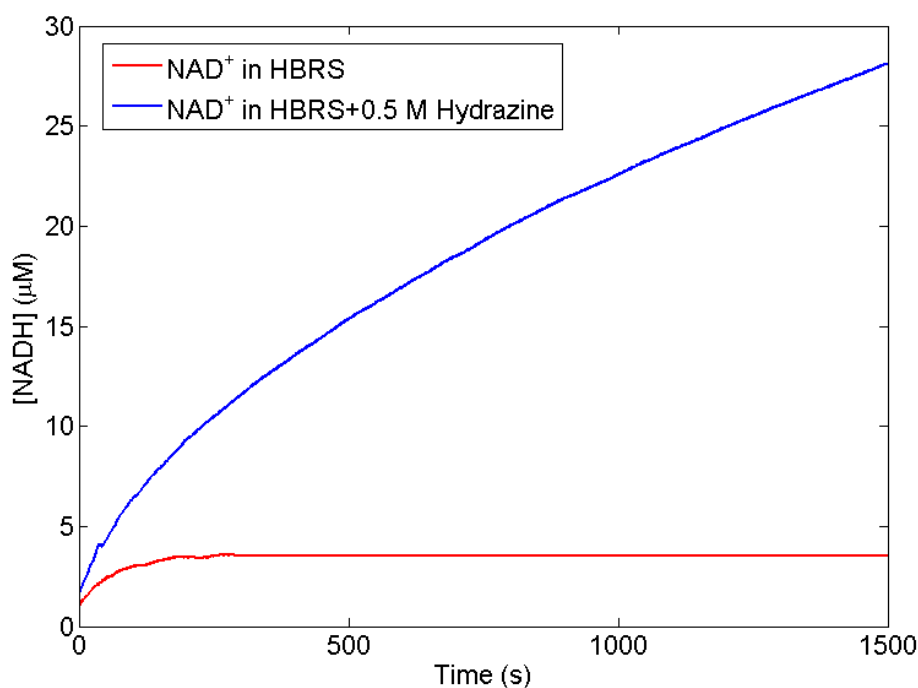


FIGURE 4.49: Comparison of the kinetics of 1 mM LA catalysis by the same concentration of  $NAD^+$  and of LDH in HBRS and in HBRS+0.5 M Hydrazine.

a pH of 7.4 while Tris-HCl has a pH of 8.8, at which the LDH enzyme moves the LA catalysis equilibrium in the direction of PA with an increase in the NADH production and therefore in the measured oxidation currents.

Unfortunately, Tris-HCl is not a good buffer for the engineered cells who survived just few hours in it. Following the previous points and imagining to collect the LA sample from the cells in HBRS, two strategies are possible:

1. To perform the LA catalysis in Tris-HCl that implies the LA sample dilution 1:10 in the  $NAD^+$  in Tris-HCl, and LDH in PBS solution;
2. To dilute  $NAD^+$  directly in the LA sample, and then mixing it with the LDH in PBS solution.

These strategies are resumed in figure 4.50. Since it's not possible to foresee which of these strategies gives the best results in terms of measured NADH oxidation current, they were tested on the same LA samples in HBRS.

Three LA sample concentrations in HBRS, ranging from 10  $\mu M$  to 1 mM were tested with the described protocols. Five minutes UV-Vis kinetics were measured and two DSC devices were used to perform CV measurements over the solutions at the end of the UV-Vis measurements. For each tested LA sample, a blank UV-Vis and CV

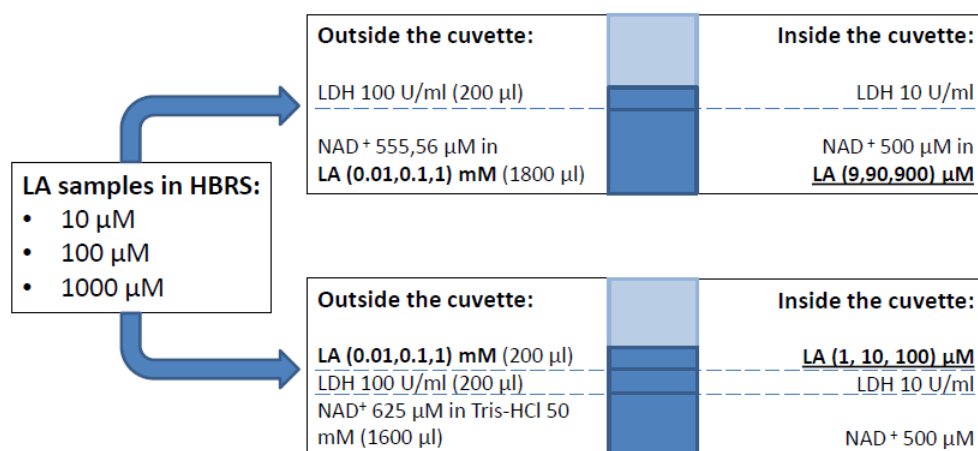


FIGURE 4.50: Scheme of the strategies tested for the LA in HBRS detection.

measurement were performed pouring in the cuvette HBRS instead of the LA sample. The NADH concentrations obtained in the solution were calculated from the absorbance values at the end of the kinetics. The NADH oxidation current values obtained from the CV measurements were correlated with the UV-Vis calculated NADH concentrations in figure 4.51.

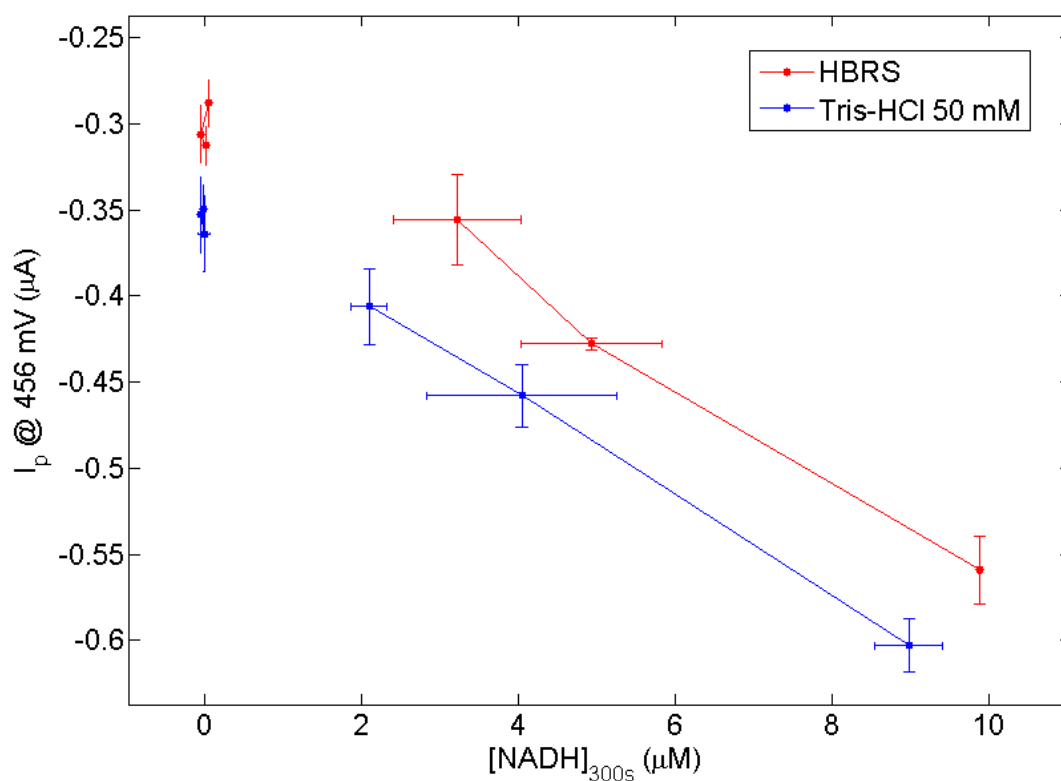


FIGURE 4.51: Calibration curve obtained by the UV-Vis and the CV tests with the protocols in HBRS and in Tris-HCl on DSC devices.

The points on the right represent the currents/NADH concentrations obtained by the highest LA concentrations while the last ones on the left are related to the blank measurements in the two cases. Since the two calibration curves have almost the same slope, we can conclude that the two protocols are equivalent, with the LA sample dilution compensated by the higher catalysis efficiency in Tris-HCl. Therefore, the Tris-HCl protocol will be adopted as it allows for the preparation of the  $NAD^+$  solution before the measurements, without the need to weight and dissolve  $NAD^+$  directly in the LA sample.

#### 4.3.4.2 Lactate calibration curve

The protocol selected with the previous tests was used for the construction of a lactate calibration curve. Ten LA concentrations, in the range between 1  $\mu M$  to 50 mM were tested. The following operations were performed for each LA concentration:

1. Preparation of the LA dilutions in HBRS;
2. Mix of 1.6 ml of 625  $\mu M NAD^+$  in 50 mM Tris-HCl and of 0.2 ml of LDH 100 U/ml in PBS in a quartz cuvette;
3. Addition of 0.2 ml of the LA dilution to the cuvette and 339 nm UV-Visible kinetic measurement with respect to the same mix in the cuvette with the addition of 0.2 ml of pure HBRS;
4. CV tests on three DSC devices of the solution at the end of the UV-Vis kinetics.

Figure 4.52 shows the kinetics measured with the various LA concentrations, while figure 4.53 depicts the average CV measurements performed on the DSC devices at the end of each LA concentration catalysis.

The NADH oxidation current values at 456 mV are reported, with their standard deviations, in figure 4.54 in function of the respective LA concentrations. The blue curve show the data points fit by a power model within a LA concentrations logarithmic representation. Conversely, the figure inset shows the same current values within the LA concentration linear representation. As shown by the red line in the inset, the LA detection with this protocol show linearity for concentrations beneath 5 mM, with a sensitivity of 0.287  $\mu A/mM$  and a detection limit of 10  $\mu M$ .

Finally, in order to asses the correlation between the UV-Vis spectrophotometric measurements at 339 nm and the CV currents at 456 mV, these values were plotted in figure 4.55, on the x and y axis, respectively. Almost all the points obtained lie on a line with

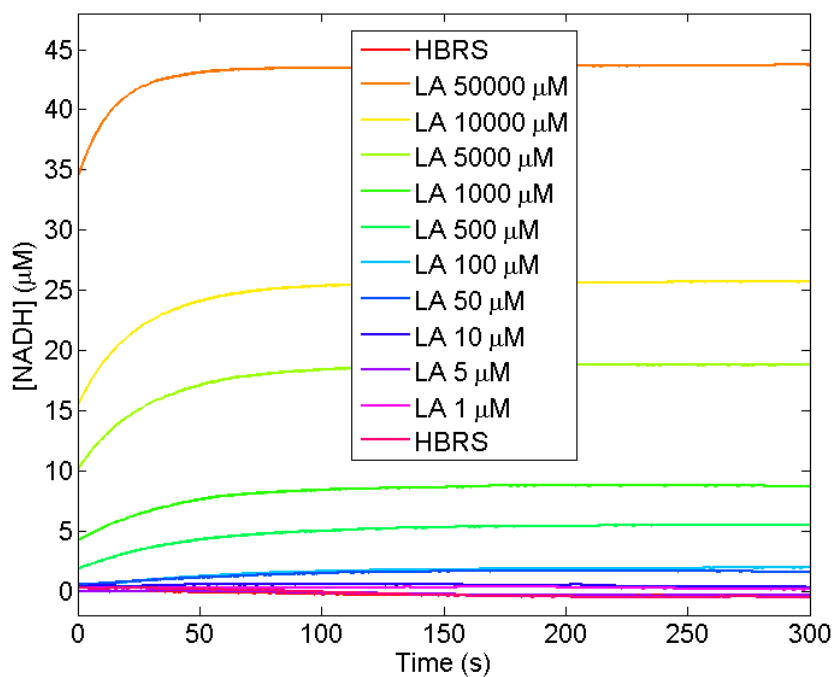


FIGURE 4.52: UV-Visible 339 nm kinetics of the LA catalysis in the cuvette with  $625 \mu\text{MNAD}^+$  in 50 mM Tris-HCl and 100 U/ml LDH in PBS 1x.

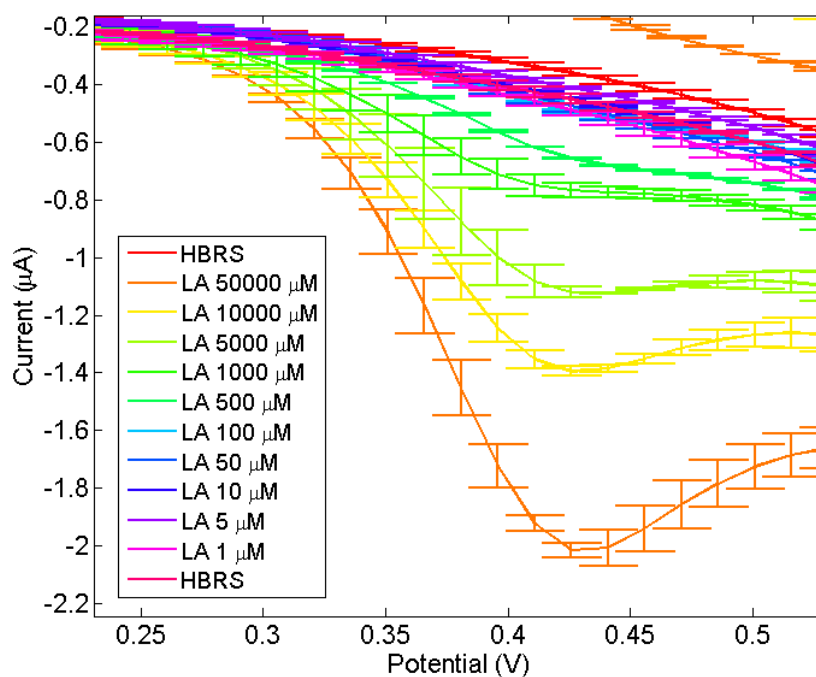


FIGURE 4.53: CV measurements on DSCs of the LA/LDH/NAD solutions at the end of the UV-Vis kinetics.



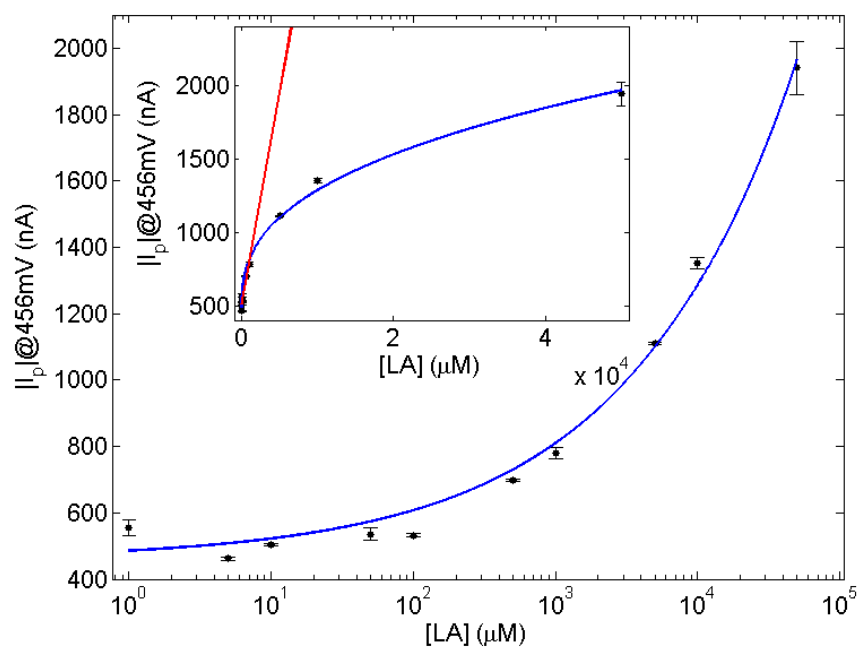


FIGURE 4.54: LA calibration curve. The inset reports the same current values in function of the experimental NADH concentrations calculated from the UV-Vis data at the end of the kinetics measurements.

slope 33.27 mA/M and an intercept of 489.5 nA. Therefore, the two measurements result coherent.

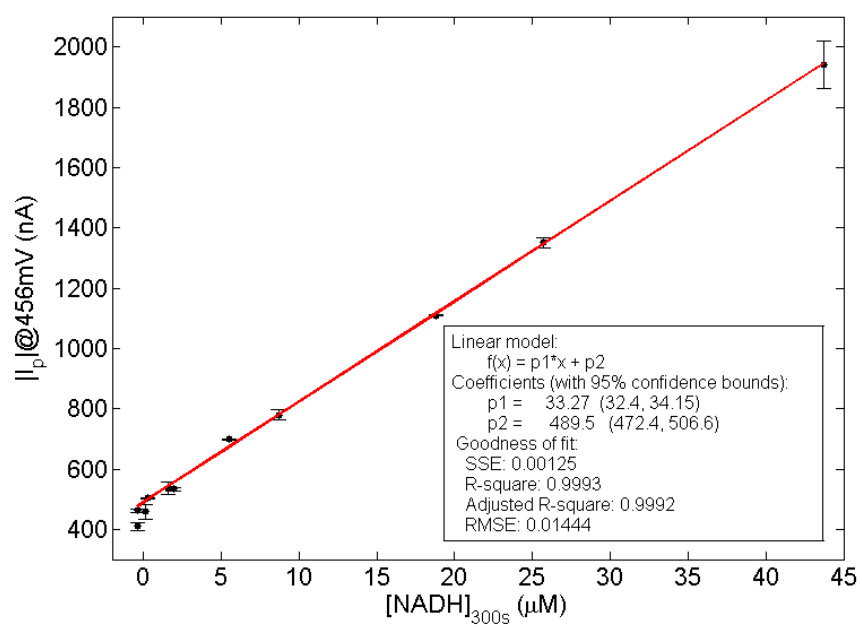


FIGURE 4.55: Correlation plot of the UV-Vis spectrophotometric and of the Cyclic Voltammetry measurements for the LA detection.

## Chapter 5

# Real samples interference study and biosensor calibration

In this chapter, the interference on the lactate detection caused by the molecules present in urine samples and by the molecules released from the myogenic cells, were studied both by spectrophotometrical and electrochemical measurements. These tasks were accomplished in four steps:

1. Firstly, real urine samples were diluted in HBRS and characterized by UV-Visible spectrophotometry and CV measurements. From these measurements, veal urine was selected for its low interference with respect to beef urine.
2. Then, veal urine dilutions were used for the evaluation of its natural (basal) lactate content, with the same protocol used for the biosensor LA calibration in HBRS, performed at the end of the previous chapter;
3. As third step, known LA concentrations were added to veal urine samples dilutions in HBRS, and the biosensor was calibrated again in these solutions;
4. Finally, C2C7 cells were used to analyze the possible interferences of the molecules released from the cells with the UV-Vis and CV measurements and to assess the cells basal lactate production.

Moreover, the lactate biosensor was tested and calibrated for the detection of the lactate released after different periods of time by C2C7 transfected cells for its constitutive continuous production. This cells and their transfection protocol are described at the end of Chapter 3.

## 5.1 Urine samples interference

The spectrophotometric and electrochemical characterizations of urine samples were performed both on beef (age between 12 and 18 months) and veal (age under 12 months) urine. Assuming that, in the worst case, some urine components could interfere at 339 nm in the UV-Visible spectrum and at 456 mV in the Cyclic Voltammeteries, several urine dilutions in HBRS were prepared with the aim to find a concentration which allows for the interference containment. The concentrations, expressed as urine percentage content in HBRS, are: 100%, 25%, 10%, 2.5%, 1%.

### 5.1.1 Spectrophotometrical and CV characterizations

Figures 5.1 and 5.2 show the UV-Visible spectra of the urine dilutions and the equivalent NADH concentrations obtained from the absorbance values at 339 nm, both for the veal and beef urine samples.

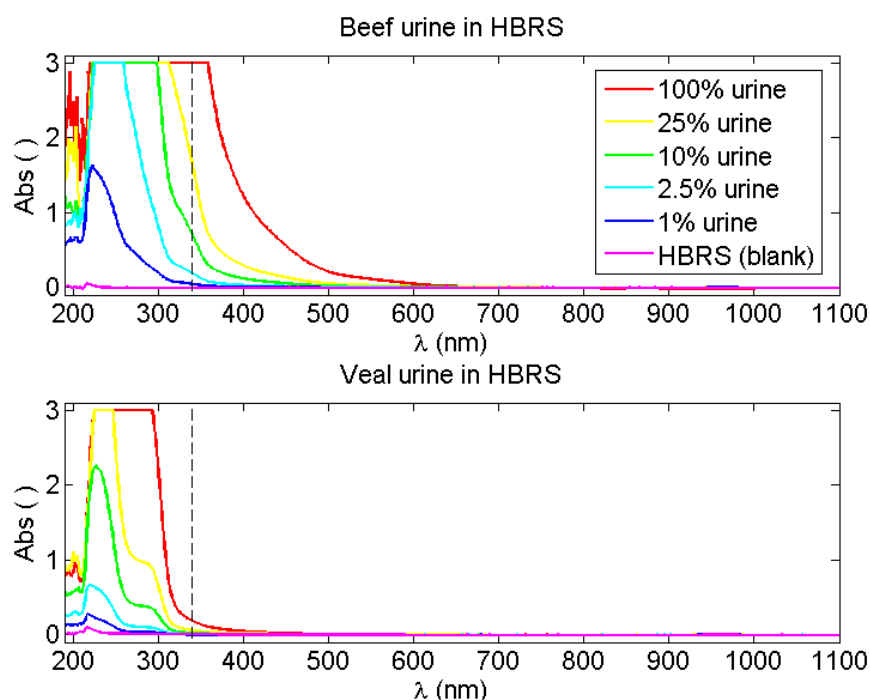


FIGURE 5.1: UV-Visible spectra of beef and veal urine dilutions in HBRS.

The 100 % beef urine solution saturates the UV-Vis spectra at 339 nm with respect to the HBRS blank measurement. Therefore this samples have to be diluted. In fact, blanking the measurements to the 100% solution would result in noisy measurements around zero, with no practical meaning. Conversely, veal urine present a much lower interference at 339 nm, with an absorbance of about 0.2 Abs for the 100% solution.

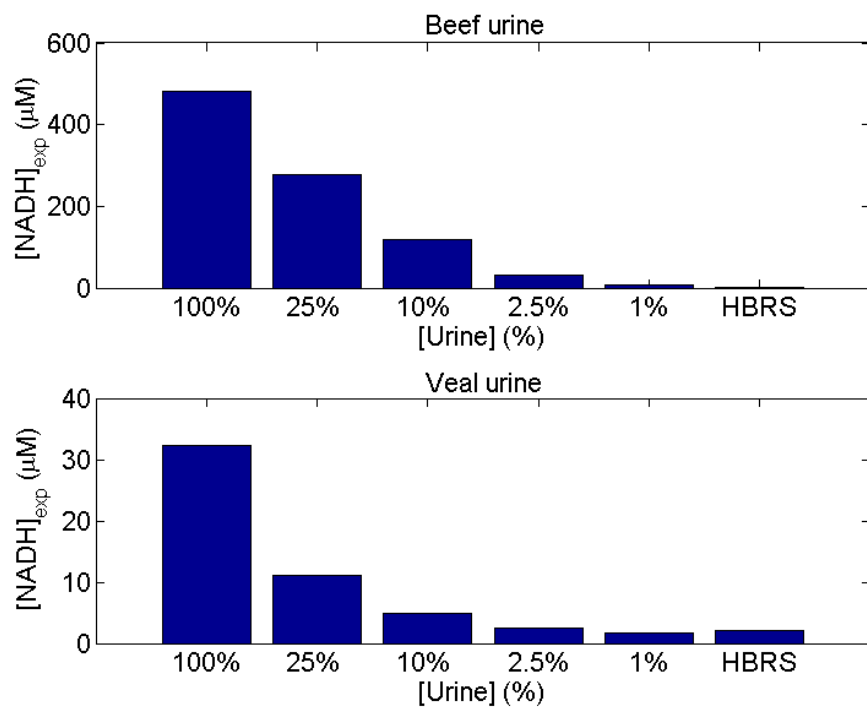


FIGURE 5.2: 339 nm absorbance values of beef and veal urine dilutions in HBRS.

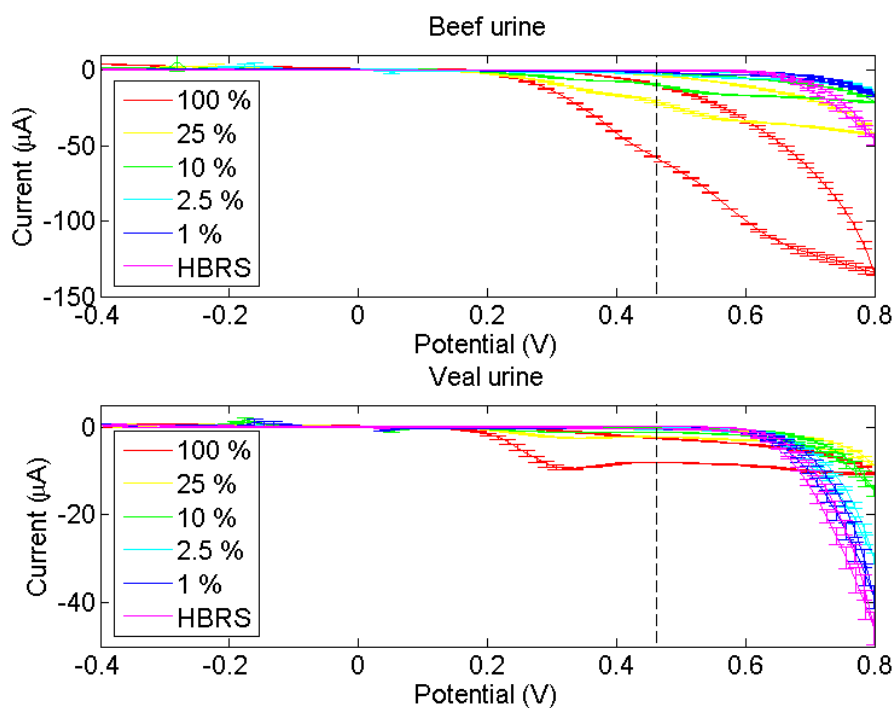


FIGURE 5.3: CV measurements of beef and veal urine dilutions in HBRS.

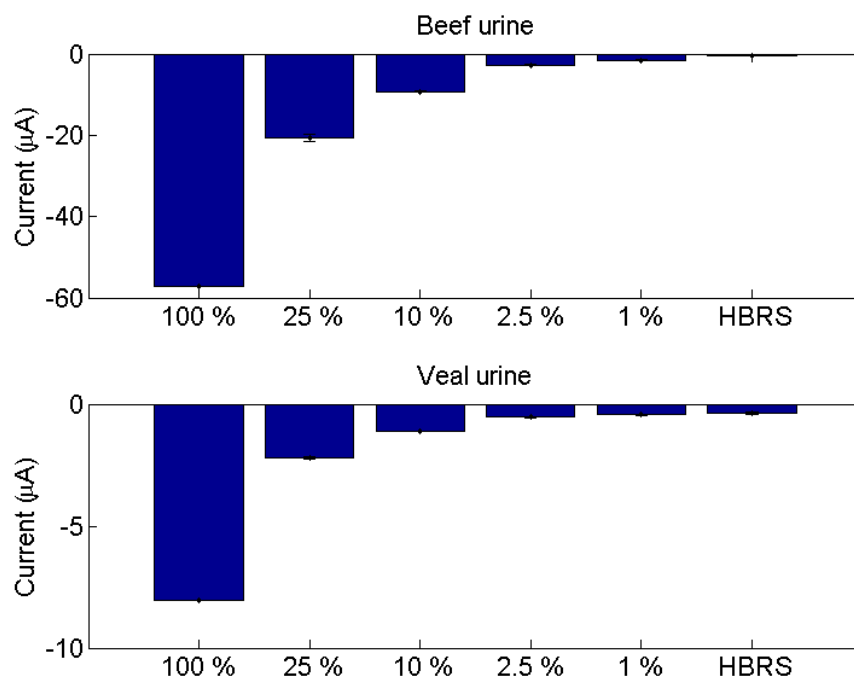


FIGURE 5.4: 456 mV oxidation current values of beef and veal urine dilutions in HBRS.

Moreover, the veal urine samples are characterized by the presence of two absorbance peaks, differently from the beef ones which present only one peak. Figures 5.3 and 5.4 show the CVs of the urine dilutions and the respective current values at 456 mV, both for the veal and beef urine samples. As for the spectrophotometrical measurements, the beef urine samples CVs show much higher oxidation currents with respect to the veal urine samples. The 100% beef urine solution brings to currents more than one order of magnitude higher than the veal's ones. Moreover, veal urine samples, differently from the beef ones, are characterized by an oxidation peak around 300 mV.

### 5.1.2 Natural LA concentrations

In the previous paragraph, the interference of the urine samples were evaluated at the wavelength and potential at which the NADH formation is monitored by spectrophotometry and cyclic voltammetry, respectively. Here, a different kind of interference will be evaluated. In fact, urine samples are expected to naturally contain a lactate concentration which can vary a lot, depending on the animal health status, its age and diet. This concentration has to be assessed before testing the lactate produced by the engineered cells, in order to be able to distinguish one concentration from the other. With this aim three urine dilutions in HBRS, i.e., 100%, 10%, and 1% were tested with the same protocol used for the biosensor LA calibration, measuring the 5 minutes kinetics at

339 nm and the testing the solutions by CV. Only veal urine was tested since beef urine present high interferences both at 339 nm and at 456 mV in the spectrophotometrical and Cyclic Voltammetric measurements, respectively.

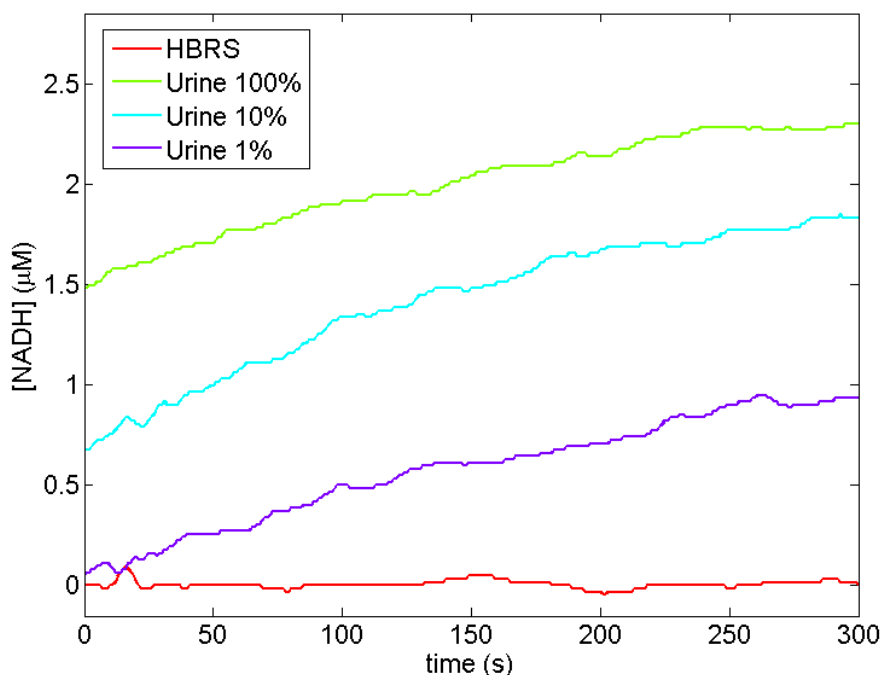


FIGURE 5.5: 339 nm kinetics of veal urine dilutions in HBRs.

Accordingly to the spectrophotometric calibration plot of figure 4.52, the steady state NADH concentrations obtained by the isolated UV-Vis kinetics at 339 nm of figure 5.5 are compatible with a  $100 \mu\text{M}$  lactate concentration for the 100% beef urine sample. Conversely, for the veal 100% urine sample, the NADH concentrations indicate a lactate content around  $100 \mu\text{M}$ . The CV measurements performed in the solutions at the end of the UV-Vis kinetics are reported in figure 5.6.

## 5.2 Biosensor calibration in urine samples

With the aim to accomplish the second step described at the beginning of the chapter, i.e., the biosensor calibration in real urine samples in presence of known LA concentrations, the same protocol used for LA in HBRs were implemented for the same LA dilutions in veal urine. Therefore, ten LA concentrations, ranging between 50 mM and  $1 \mu\text{M}$  were prepared in veal urine and then mixed with LDH and NAD in the amounts defined at the end of the previous chapter. The NADH formation kinetic was monitored

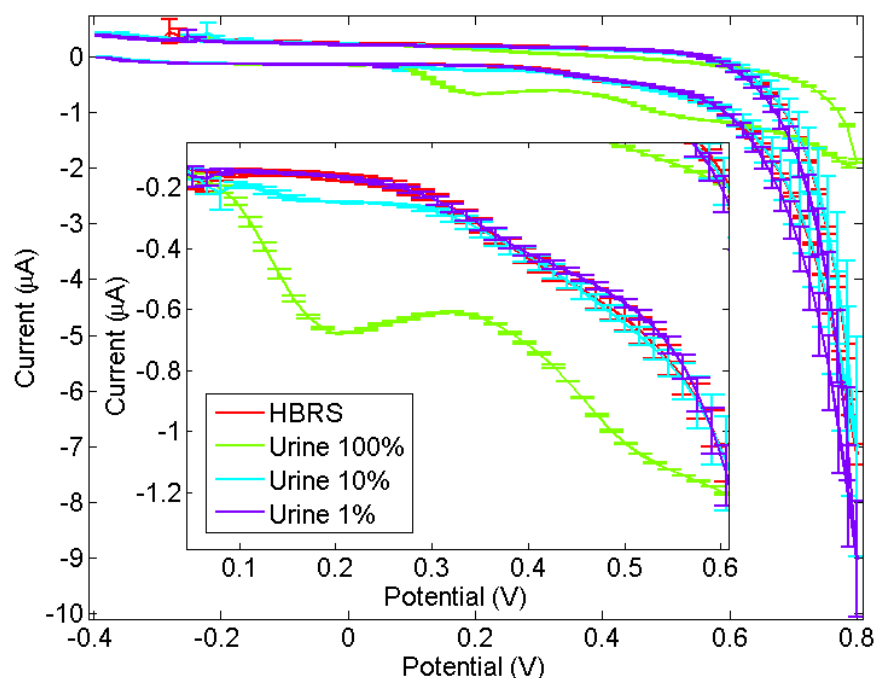


FIGURE 5.6: CV measurements of veal urine dilutions in HBRs, after the end of the UV-Vis kinetics measurements.

at 339 nm by UV-Vis spectrophotometry for 5 minutes. After that, the obtained solutions were tested by Cyclic Voltammetry on DSC devices in order to detect the NADH oxidation current. Veal urine were selected for this calibration because it causes less interference than beef urine both at 339 in the UV-Vis measurements and at 456 mV in the CV ones.

### 5.2.1 Calibration in 100% veal urine

Figure 5.7 shows the UV-Vis kinetics at 339 nm of the LA dilutions with respect to the solution obtained adding pure veal urine to LDH and NAD (blanking solution) instead of LA in urine. In fact, while in the LA in HBRs calibration experiment the blanking solution was obtained by 1.6 ml NAD in Tris-HCl, 0.2 ml LDH in PBS, and 0.2 ml HBRs, in this one the blanking solution is composed by 1.6 ml NAD in Tris-HCl, 0.2 ml LDH in PBS, and 0.2 ml veal urine. Interestingly, the LA concentrations lower than  $500 \mu\text{M}$  show kinetics characterized by negative absorbance values, and thus "negative NADH concentrations" with respect to the blank measurement. This is more clear from the UV-Vis calibration plot shown in figure 5.8. This effect doesn't depend on a wrong blank measurement since the following measurements in urine, performed in the middle and at the end of the tests, result in absorbance values very close to the first ones. The Cyclic Voltammetry measurements on the solutions at the end of the NADH formation



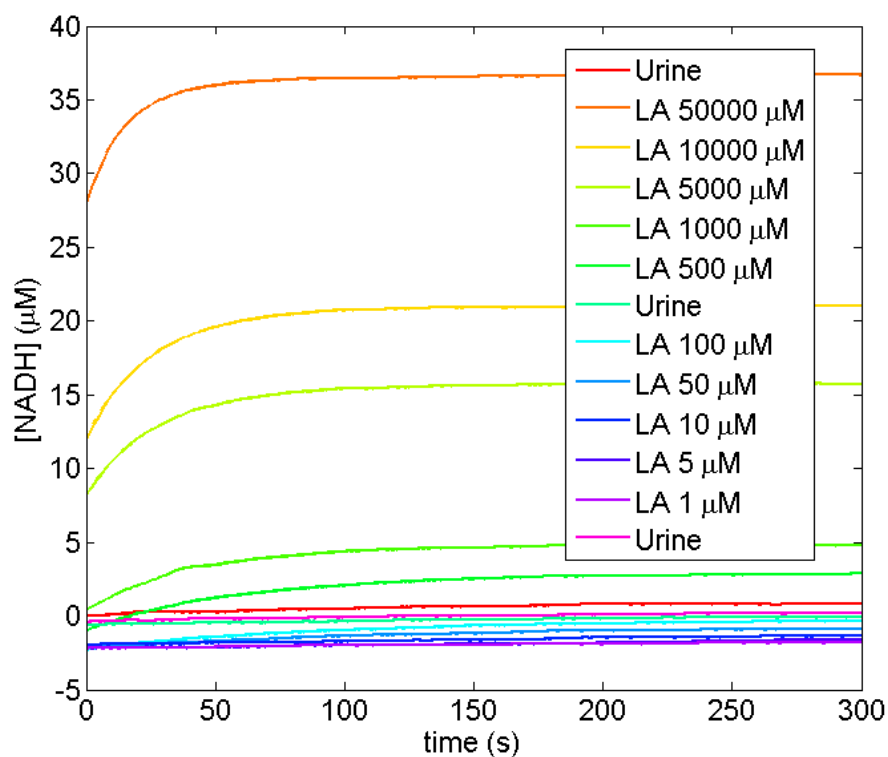


FIGURE 5.7: UV-Vis kinetic measurements at 339 nm of the catalysis of LA dissolved in urine.

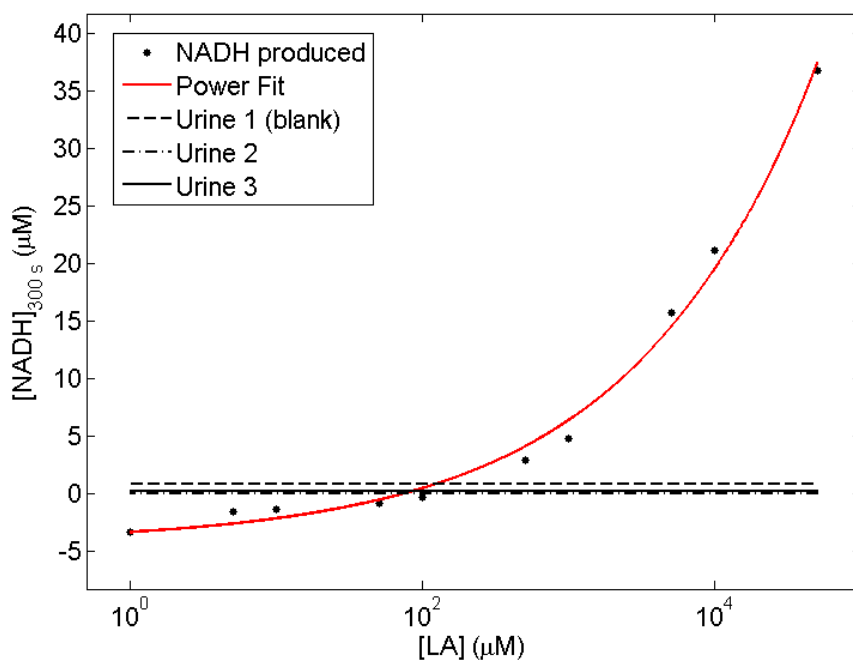


FIGURE 5.8: UV-Vis calibration plot of the NADH steady state concentrations obtained from the catalysis of LA dissolved in veal urine. The lines represents the NADH concentrations obtained by the tests in pure veal urine.

kinetics are even more interesting, and are depicted in figure 5.9. The CVs on the blanking solution (NAD, LDH, and pure urine) present a current peak around 300 mV and a flex at about 500 mV.

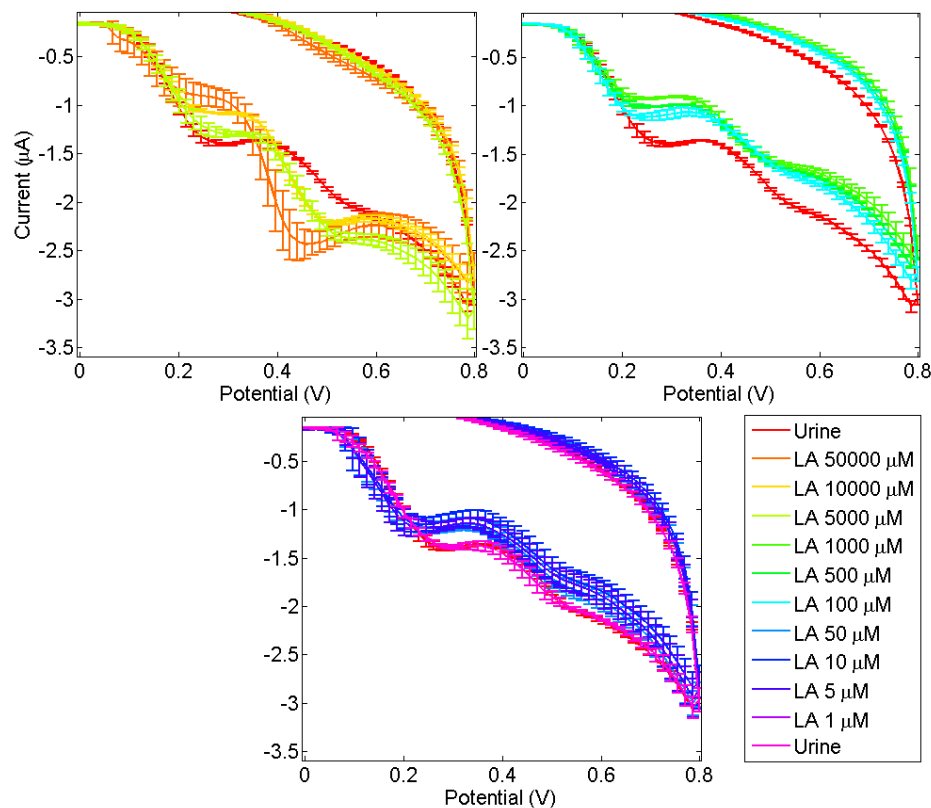


FIGURE 5.9: Average CVs obtained from the measurements of the LA in urine solution after the catalysis. The measurements are plotted in three graphics in order to distinguish them clearly. The first measurement in urine without added LA is plotted in all the graphics as reference (red curve).

Three types of CVs were observed depending on the LA dissolved concentration:

- For high LA concentrations ( $LA > 1 \text{ mM}$ ) a peak between 400 and 500 mV is clearly visible and can be associated to the formed NADH oxidation, as observed for the LA in HBRS calibration curve. Anyway, this peak is moving to higher potentials proportionally to the decrease of the LA tested concentration. Moreover, the 300 mV peak current value is decreased by high LA concentrations but it appears again as the LA concentration decrease.
- For medium LA concentrations ( $50 \text{ }\mu\text{M} < LA < 5 \text{ mM}$ ) the oxidation currents between 200 mV and 800 mV are lower than the currents obtained by the blanking measurement in pure urine. The current peak at 300 mV is increasing proportionally to the LA concentration decrease.

- For low LA concentrations ( $LA < 50 \mu M$ ) the oxidation currents between 200 mV and 800 mV are still lower than the blank measurements ones, but they are approaching the them as the LA concentration decrease.

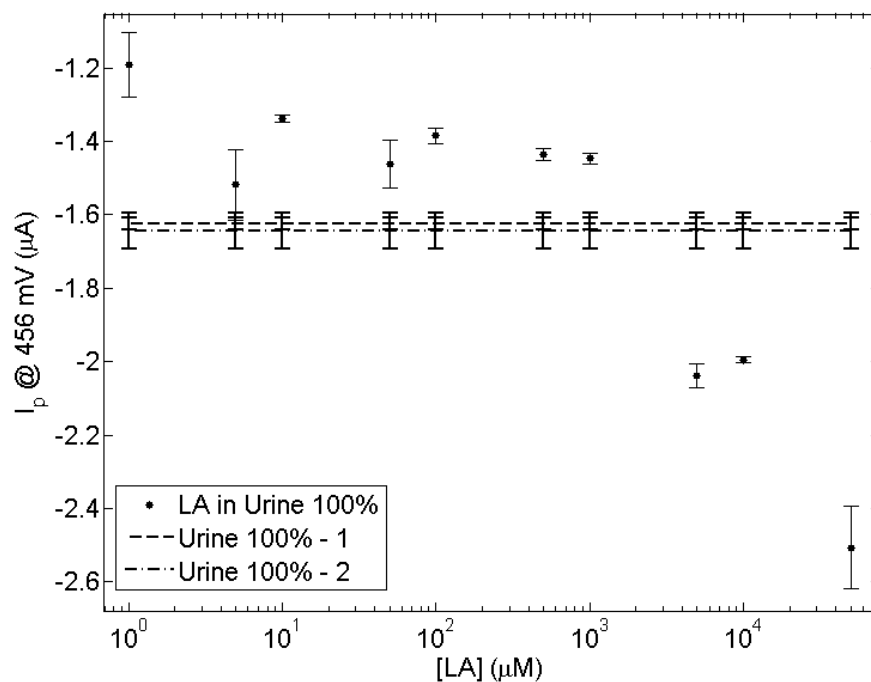


FIGURE 5.10: Average currents and related standard deviations, recorded at 456 mV, of the CV measurements on the LA in urine solutions after the catalysis.

The oxidation current at 456 mV were plotted in figure 5.10. At this potential, the oxidation currents becomes lower than that one of the blanking solution from 1 mM LA concentration down to the lowest one. The following figure (figure 5.11) shows the correlation between the UV-Vis and the CV measurements within this biosensor LA calibration test. The star and the asterisk symbols represent the values obtained for the blanking solutions, and they lie out of the fitted correlation line.

### 5.2.2 Comparison with diluted urine samples calibrations

In order to clearly identify the interference of the veal urine components on LA calibration curves, the calibration were performed on the same LA concentrations in urine 100%, %10, and 1% in HBRS. The results of these calibrations were compared to those ones obtained by the LA in HBRS calibration, reported at the end of chapter 4. In figure 5.12 are plotted the NADH concentrations obtained at the end of the UV-Visible measurements (reported in the inset) with respect to the tested LA concentrations. The same data was also represented in function of the LA concentration (in logarithmic

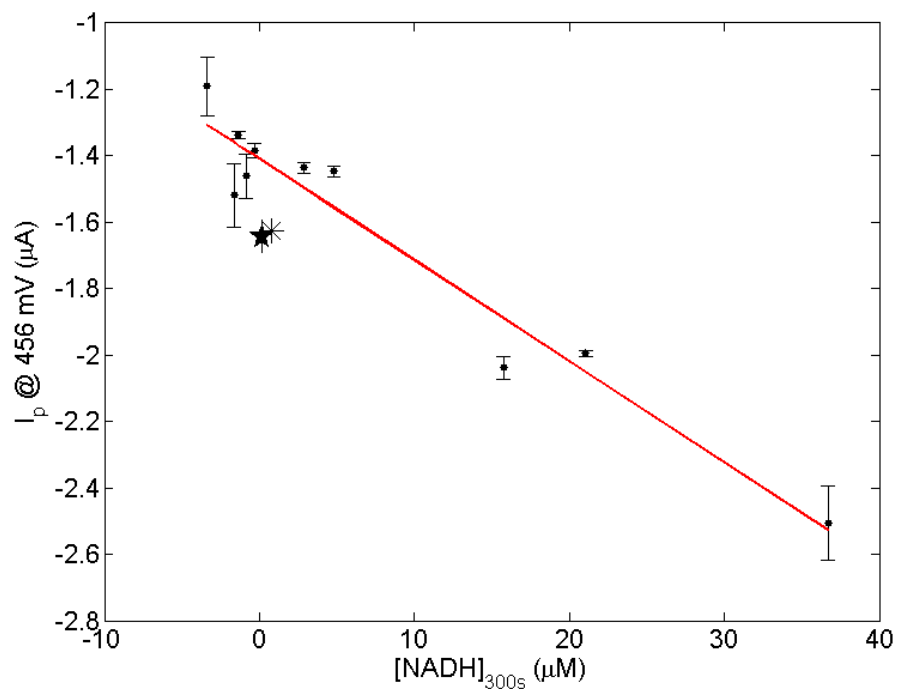


FIGURE 5.11: Correlation plot of the steady state NADH concentration obtained from the UV-Vis measurements, and of the currents recorded at 456 mV during the CV measurements on the same solutions. The star and the asterisk represent the NADH and  $I_p$  values for the measurements in veal urine without the LA addition.

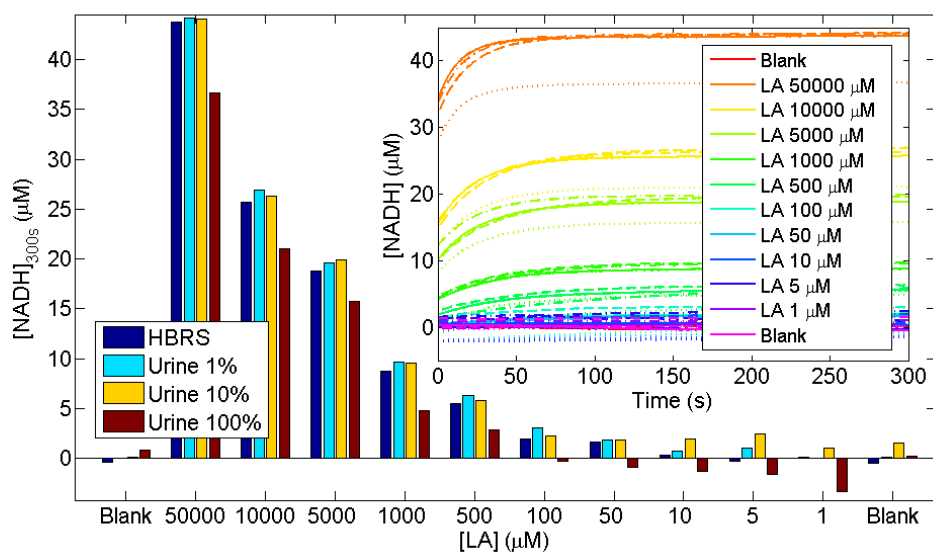


FIGURE 5.12: NADH concentrations obtained at the end of the LA catalysis kinetics in different urine dilutions in HBRS. The inset shows the 339 nm kinetics recorded for the LA concentrations (HBRS continuous line, urine 1% dashed line, urine 10% dashed-dotted line, urine 100% dotted line).

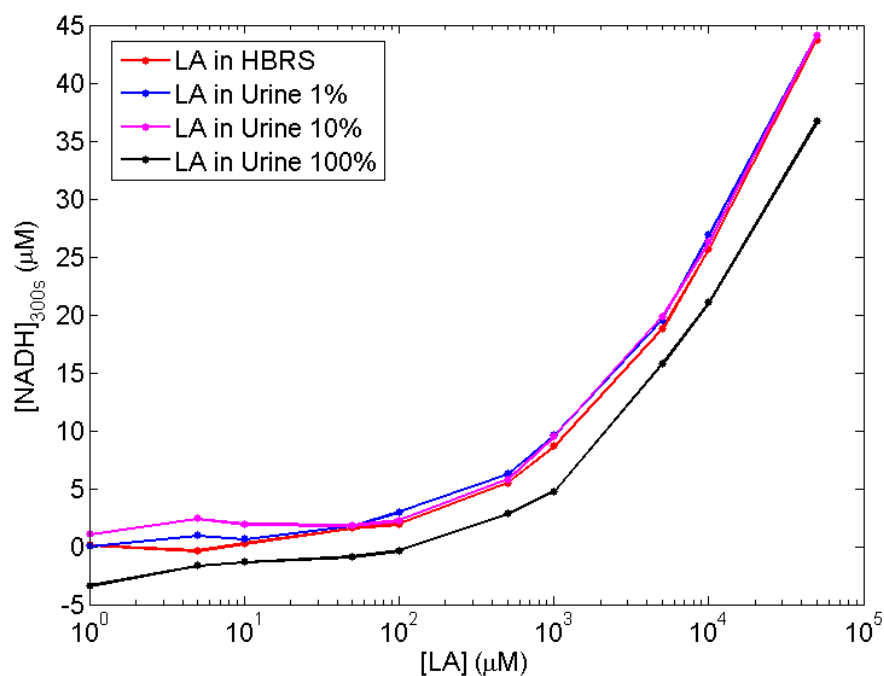


FIGURE 5.13: UV-Vis calibration curves reporting the NADH concentrations at the end of the LA catalysis kinetics in different urine dilutions in HBRS.

scale), obtaining the curves represented in figure 5.13. The LA calibration curve in urine 100% present lower NADH concentrations at the end of the kinetics and thus results translated with respect to the other curves, which are almost overlapped. Since all the calibration curves are blanked to the respective urine concentration (e.g. the calibration in 100% urine is blanked to NAD, LDH and 100% urine), the translation of the UV-Vis calibration curve in urine 100% is unexpected. Although this behavior is compatible with the inactivation of an urine compound absorbing at 339 nm by the LA or NADH presence, more data are needed to formulate a sustainable explanation for the curve translation. Regarding the CV measurements, figure 5.14 shows the average CVs, for each LA concentration, for the calibrations in HBRS (red curves), urine 1% (blue curves), 10% (magenta curves) and 100% (black curves). The comparison between the blank measurements shows that, at this concentration, 100% veal urine present oxidation current values much higher than the other urine dilutions ones. For the highest LA concentration, i.e. LA 50 mM, all the CV curves present a peak at 456 mV related to the NADH oxidation. Conversely, for lower LA concentrations, all the urine dilutions a part the 100% one are compatible with the LA in HBRS curves. The 456 mV CV calibration curves, showed in figure 5.15, confirm the compatibility of the 10% and 1% urine-based LA calibration with the HBRS one for LA concentrations over 500  $\mu\text{M}$ . For lower concentrations the currents in 10% urine calibrations results higher than those ones recorded for 1% urine and HBRS, while these last ones remain comparable. The 456

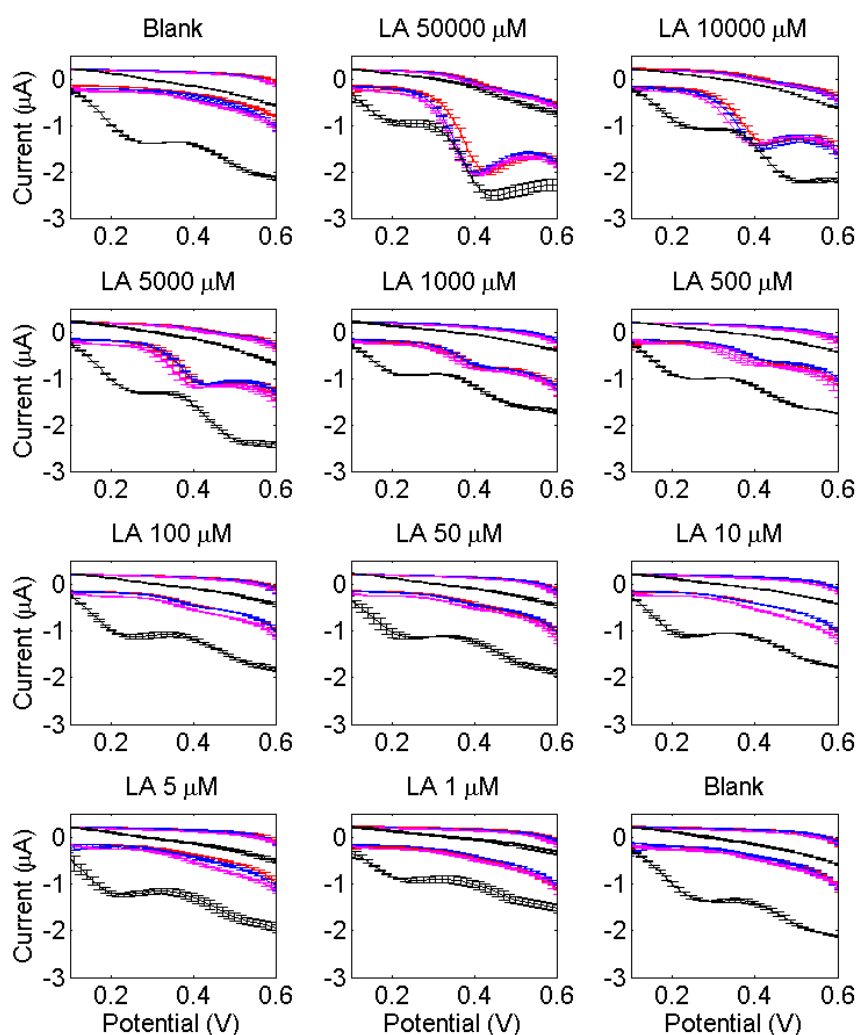


FIGURE 5.14: Cyclic voltammeteries measured in different LA concentrations in the urine dilutions, after the LA catalysis by the LDH enzyme (HBRS red curves, urine 1% blue curves, urine 10% magenta curves, urine 100% black curves).

mV currents related to the LA concentrations beneath 1 mM in 100% urine are smaller than the currents recorded in absence of lactate. This is similar to what was observed in the UV-Vis measurements but, in that case the first concentration which resulted with a "negative NADH concentration" was LA 100  $\mu\text{M}$ . However, the particularity of these CV and UV-Vis measurements allows to hypothesize for the interaction of one or more compounds, present in veal urine, with LA or NADH and resulting in the drop of the absorbance and of the oxidation currents. Unfortunately, these measurements don't allow to prove it.

Figure 5.16 shows the absolute 456 mV currents recorded during the CVs and the NADH concentrations measured by the UV-Vis spectrophotometries at the end of the kinetics.

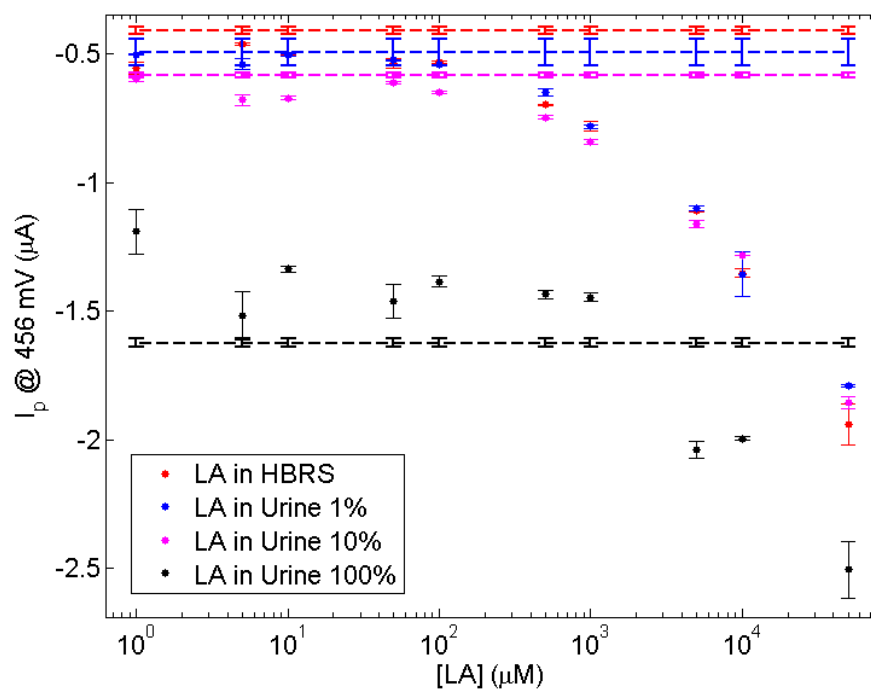


FIGURE 5.15: Biosensor calibration curves of LA in urine dilutions in HBRS. The dashed lines represent the 456 mV current values recorded for each calibration curve in the UV-Vis blanking solution.

The points were fitted by a linear model, obtaining the slopes and intercepts reported in table 5.1. The slopes of all the fits are similar, while the intercept related to the fit of the LA calibration in 100% urine results radically different. In conclusion, a dilution

Urine dilution	Slope (mA/M)	Intercept (nA)	$R^2$
HBRS	33.27	489.5	0.9993
1%	30.39	485.8	0.9958
10%	28.43	581.7	0.9963
100%	30.47	1407	0.9425

TABLE 5.1: Coefficients of the linear fits of the correlation plot data for the urine dilutions.

of 10% of the veal urine sample resulted sufficient to obtain a LA detection comparable to that one in HBRS, for LA concentrations over  $50 \mu M$ . Lower urine dilutions are required for the detection of smaller LA concentrations.

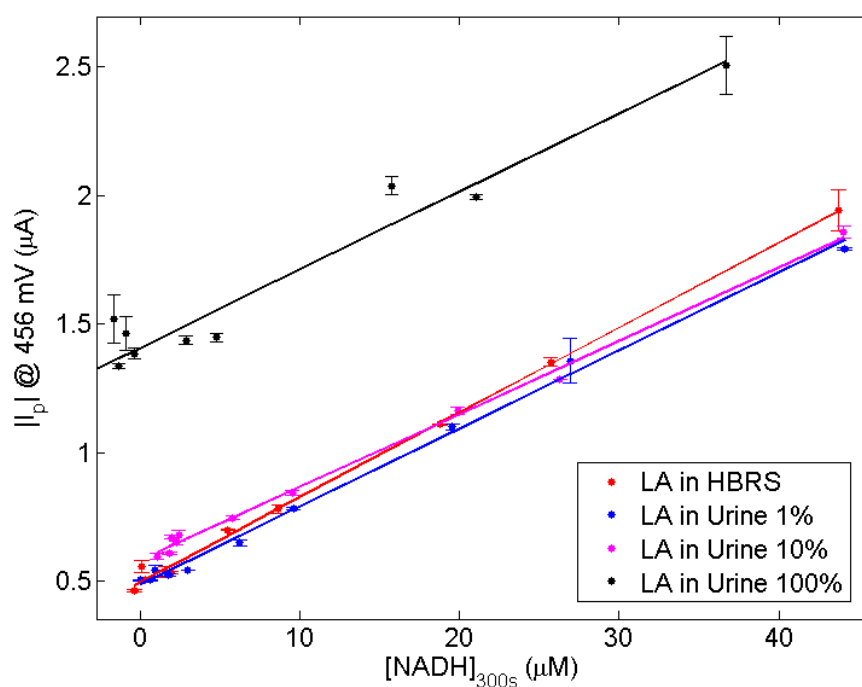


FIGURE 5.16: Correlation plot of the NADH concentrations obtained from the 339 nm absorbance values at the end of the kinetics, and the 456 mV currents measured by CV on the same solutions.

### 5.3 Myogenic cells interference

Having assessed the interference caused by the compounds in bovine urine samples, as subsequent step the interference caused by the C2C7 cells products during the incubation was tested. With this purpose, a first prototype of the full cells-biosensor system, with wild type (WT) C2C7 cells was realized. In order to keep this first prototype of the complete Myo-Screen project system as simple as possible, the cells part was designed separated from the biosensor part. This experiment had two main objectives:

- The identification of possible substances released from the cells which could interfere with the UV-Vis spectrophotometric and/or with the CV measurements;
- The detection of the natural lactate concentrations produced by these type of cells during a room temperature incubation in HBRS.

The setup used in this experiment is that one which will be implemented also in the final Myo-Screen system prototype, with the myogenic cells for the hypertrophy-stimulated lactate overproduction. Therefore, the present experiment is a necessary step to distinguish the lactate produced in response to the hypertrophic stimulation from the basal one.



### 5.3.1 Tests protocol

The tests were performed dividing the operations as described in the following:

**Cells part:** two flasks containing the C2C7 wild type cells (WT) were employed in this part. The performed steps are:

1. Incubation of the confluent cells in DMEM without FBS for 48 hours;
2. DMEM removing and substitution by HBRS;
3. Incubation for n hours;
4. Cell medium sample extraction (1 ml) at 1,3 and 24 hours from the medium substitution;
5. Cell counting for normalization of the results.

**Biosensor part:** In this part, a quartz 4 ml cuvette, the UV-Vis spectrophotometer, DropSens Carbon devices and a CH440a potentiostat for the CV measurements have been employed. The performed steps were:

1. Preparation of the LDH enzyme in PBS and of the  $NAD^+$  cofactor aliquots in Tris-HCl;
2. Mixing of the LDH and NAD aliquots with the cell sample in a quartz cuvette for the LA catalysis and the consequent NADH formation;
3. Monitoring of the kinetics at 339 nm of the NADH formation in the quartz cuvette with the spectrophotometer, until a steady state is reached (5 minutes);
4. Quartz cuvette solution's sample extraction (100  $\mu$ l);
5. Drop of the sample on the DropSens screen-printed electrodes;
6. Cyclic Voltammetry measurement for the detection of the NADH oxidation and its quantification.

Two independent data sets were collected from two different cells flasks. Each of the 1, 3, and 24 hours samples, from both the flasks, were tested by one UV-Vis kinetics measurement and three CV on different DSC devices. The LDH and NAD concentrations and buffers used for the tests were the same used for the biosensor calibration curves obtained in Chapter 4 and in the previous paragraphs.

### 5.3.2 Basal LA cells production

Figure 5.17 shows the average NADH concentrations, obtained from the two test sets, in function of time during the lactate LDH-mediated catalysis. The NADH experimental concentrations were obtained from the 339 nm absorbance values as described in paragraph 4.3.2.1.

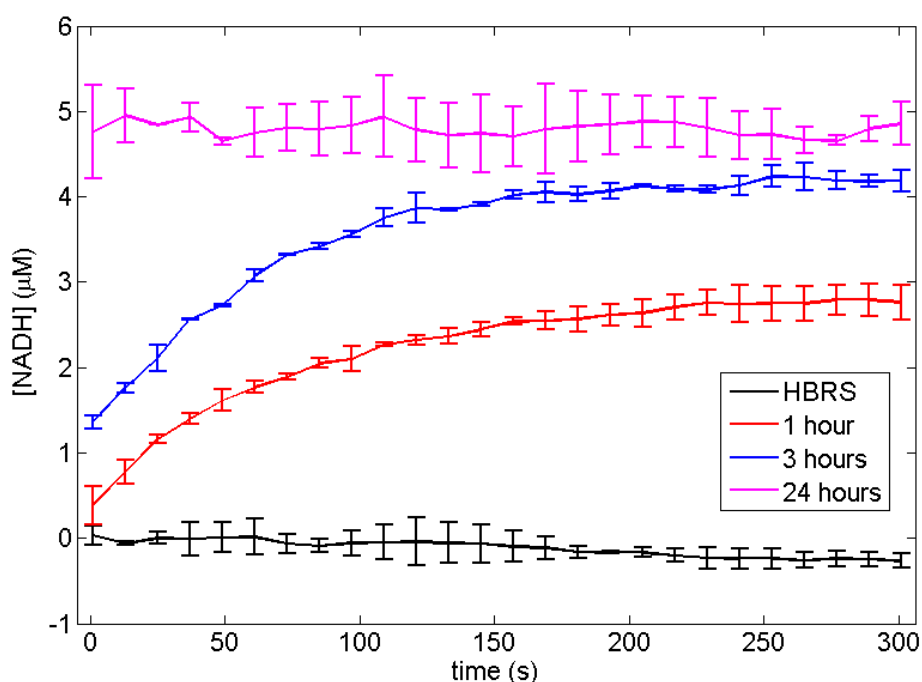


FIGURE 5.17: UV-Vis spectrophotometric kinetics of the NADH formation at 340 nm in the quartz cuvette containing the LDH enzyme and the  $NAD^+$  cofactor and the cells samples.

The blank measurements, represented by the black curves in the figure, were obtained by mixing in the cuvette pure HBRS instead of the cells sample. As can be seen in the figure, the 24 hours samples did not present any kinetics but a constant value over the whole 5 minutes test. This feeds the suspicion that in this case the absorbance at 339 nm would be caused by an interference and not by the lactate presence. This hypothesis is enforced by the fact that, after all the samples extraction from the flasks, i.e., after 24 hours from the DMEM substitution with HBRS, each cell culture was observed in the microscope and the cells appeared prevalently detached from the flask surface. Therefore, since the cells died after 24 hours, the 24 hours samples could be polluted with something which absorbs light at 339 nm and that is not lactate. In order to verify the reproducibility of the CV measurements on the same cells samples, the average CV measurements obtained with the samples of the first set were calculated. A

magnification of these average values and of their standard deviations around 456 mV is depicted in figure 5.18.

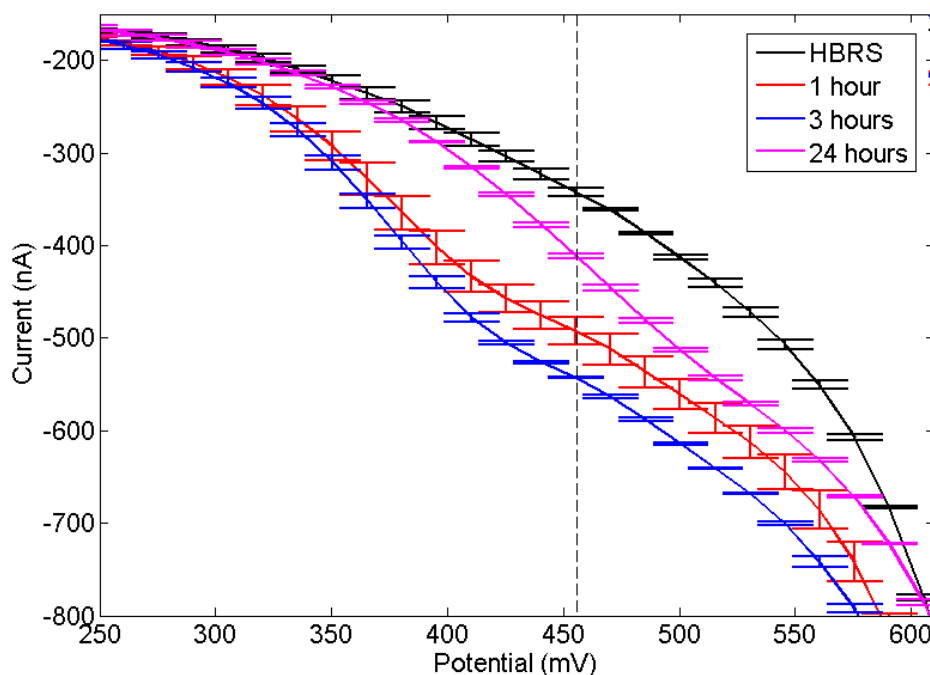


FIGURE 5.18: Average currents and related standard deviations obtained by cyclic Voltammeteries on three devices per each cells sample and sampling time of the first cell cultures set. The black curves represent the blank measurements, performed adding HBRS instead of the cell sample in the quartz cuvette.

The standard deviations obtained from these measurements are small enough to detect significant variations between the 1, 3 and 24 hours samples, which result maximal at 456 mV. The 24 hours samples 456 mV currents result lower than the 1 and 3 hours ones. Moreover, the 24 hours CV measurements resulted in a different shape than the other sample CVs, with a current peak at higher potentials than 456 mV. This could be due to the presence of other substances in the test solution, which oxidize at higher potentials than NADH.

Having verified the reproducibility of the DSC devices CV measurements on the same samples, the second set of samples were tested with the same number of devices, in order to assess the cells experiment repeatability. The average currents obtained by these measurements on both the sets are depicted in figure 5.19.

The obtained results are very similar to those ones related to the devices reproducibility testing on the first cell samples set and the previous considerations remain valid. The 456 mV average currents and the related standard deviations obtained from the devices, and the cells experiment reproducibility tests are depicted in table 5.2.

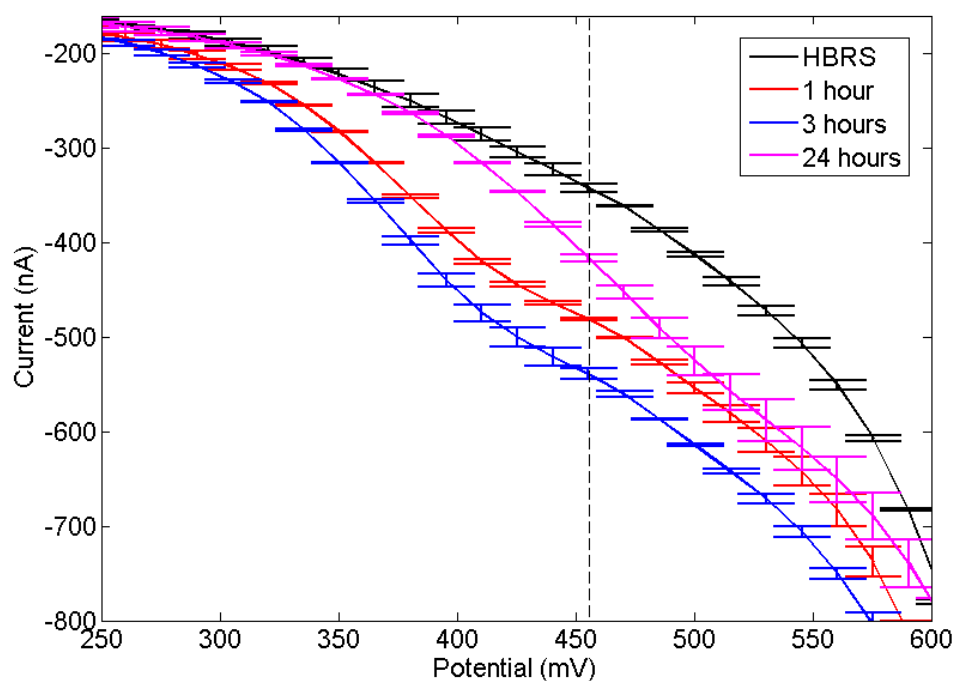


FIGURE 5.19: Average currents and related standard deviations obtained by cyclic Voltammeteries on six devices per each cells sample and sampling time, three for the first cell cultures set and three for the second one. The black curves represent the blank measurements, performed adding HBRS instead of the cell sample in the quartz cuvette.

Sample	Device reproducibility $I_p$ (nA)	Cells experiment reproducibility $I_p$ (nA)
HBRS	$-342 \pm 4.5$	$-342 \pm 4.5$
1 hour	$-492.6 \pm 15.2$	$-481.1 \pm 1.0$
3 hour	$-543.2 \pm 0.5$	$-538.8 \pm 5.7$
24 hours	$-411.5 \pm 3.0$	$-416.5 \pm 4.1$

TABLE 5.2: 456 mV average currents and related standard deviations obtained for the DSC devices, and the cells experiments reproducibility tests.

Finally, the average NADH concentrations obtained by the steady-state (300 s) absorbance values at 339 nm of the UV-Vis spectrophotometric measurements, and the average 456 mV currents obtained by the CV measurements, were plotted together the correlation plot of figure 5.20.

The 1 hour and 3 hours points define a correlation line parallel to that one obtained by the LA calibration curve in HBRS, 1%, and 10% veal urine (with a slope of 32.37 mA/M with respect to 33.27 mA/M of the calibration in HBRS). However, its intercept is a bit smaller, with a value of 403.28 nA with respect to 489.5 nA. Differently from the 1 and 3 hours points, the 24 hours point lies out of the correlation line, enforcing the hypothesis that the absorbance measured by the control technique in this case was due to another

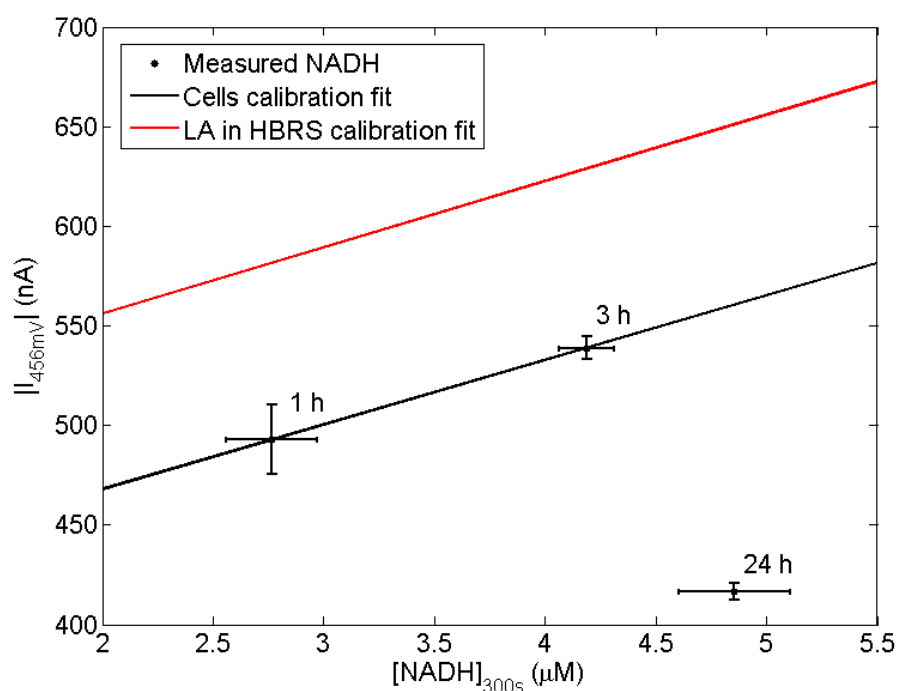


FIGURE 5.20: Calibration plot of the UV-Vis spectrophotometric measurements (control technique) and of the electrochemical cyclic voltammetric NADH (lactate) detection techniques for the data of the two cell samples sets.

substance absorbing at 340 nm wavelength. In this case, the CV measurements were more specific than the control technique for the individuation of this interference.

## 5.4 Engineered cells for continuous lactate over-production

In the transfected cells used for this experiment, the promoter of the LDH gene (CMV) in the vector is always active, thus the cells express LDH and produce lactate continuously, releasing it in the medium in which they are immersed. Two sets of three cells flask were used in this experiment. The three flasks contain wild type C2C7 cells, C2C7 cells transfected with the vector without the LDH codifying gene, and finally the cells transfected with the LDH gene vector.

For each set, the protocol described in the tests protocol paragraph has been followed. During the cells incubation for 24 hours, two small samples were collected after 1 and 3 hours from the DMEM substitution with HBRS. Thus, a total of nine samples were collected for each of the two performed set. The samples for the wild type, empty vector, and LDH vector cells at 1, 3, and 24 hours of the two test sets were mixed with the LDH enzyme and with  $NAD^+$  and the consequent NADH formation was monitored by UV-Vis spectrophotometry at 340 nm. The LDH and NAD concentrations and buffers are the

same used for the biosensor calibration curve obtained in Chapter 4. Figure 5.21 shows the average NADH concentrations, obtained from the two test sets, in function of time during the lactate LDH-mediated catalysis. The NADH experimental concentrations were obtained from the 340 nm absorbance values as described in paragraph 4.3.2.1.

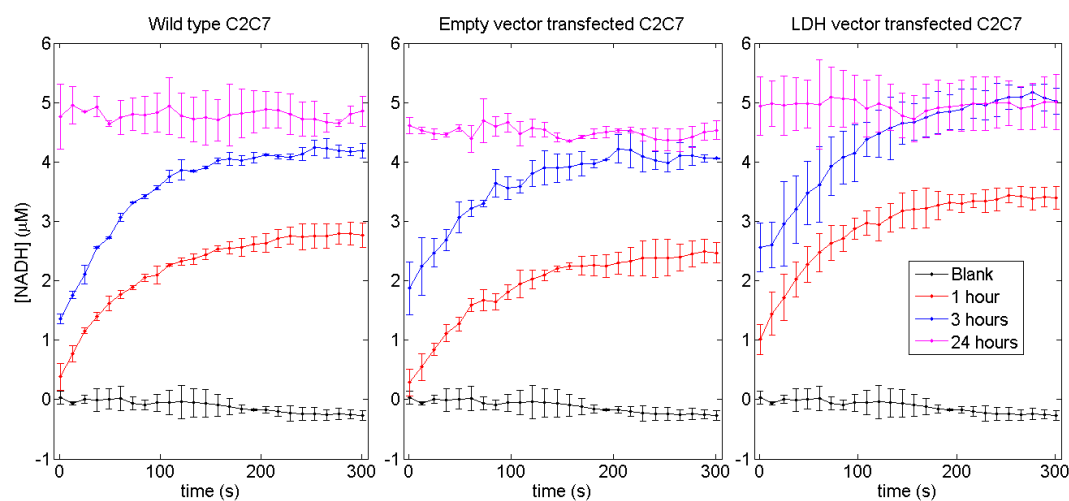


FIGURE 5.21: UV-Vis spectrophotometric kinetics of the NADH formation at 340 nm in the quartz cuvette containing the LDH enzyme and the  $NAD^+$  cofactor and the cells samples.

The blank measurements, represented by the black curves in the figure, were obtained by mixing in the cuvette pure HBRs instead of the cells sample. As can be seen in the figure, the wild type C2C7 cells and the empty vector transfected ones showed similar NADH formation kinetics and steady state values. Moreover, the 24 hours samples did not present any kinetics but a constant value over the 5 minutes tests. Conversely, the LDH vector transfected C2C7 cells showed higher steady state values than the previous ones, but the same 24 hours samples behavior. Figure 5.22 shows the steady state NADH concentrations obtained by the UV-Vis spectrophotometric measurements, allowing for an easier comparison of the average concentrations obtained from the different cell cultures.

The 1 hour and 3 hours differences among the empty vector and LDH vector cells is evident, while the 24 hours NADH concentrations are all similar. After the samples extraction, each cell culture was observed at the microscope, and the cells appeared prevalently detached from the flask surface. Therefore, since the cells died after 24 hours, the 24 hours samples could be polluted with something which absorbs light at 340 nm and which is not lactate. This hypothesis would be in accord with the lack of any kinetics of NADH formation for these samples and with the fact that about the same steady state values for all the cell cultures were obtained with them.

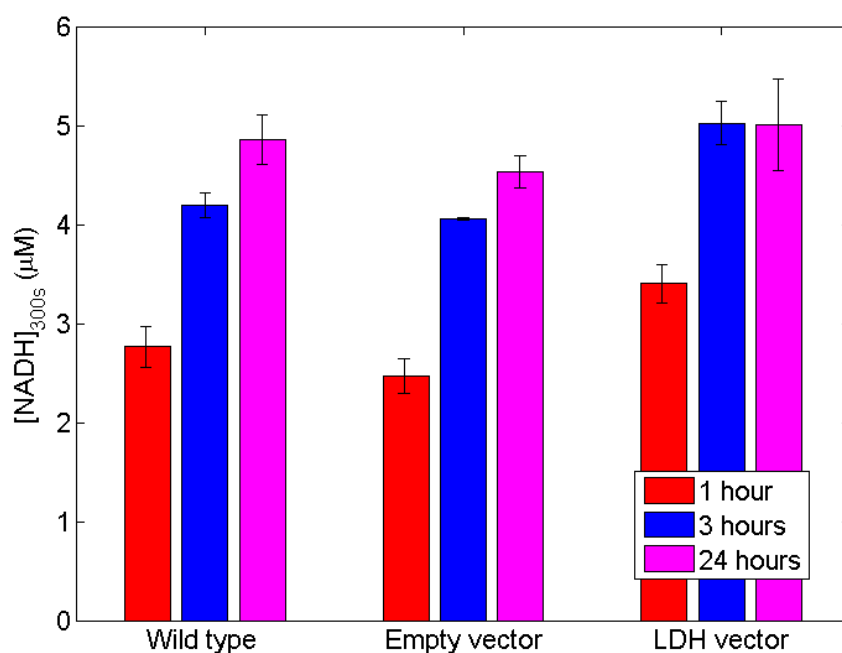


FIGURE 5.22: Steady-state NADH concentrations obtained from the NADH formation kinetics measured by UV-Vis spectrophotometry at 300 seconds.

Just after each UV-Vis spectrophotometric test, for each cell sample three DropSens screen-printed carbon devices were used to quantify the formed NADH by Cyclic Voltammetry. The protocol used for the CV measurements is the same that was defined in Chapter 4. In order to verify the reproducibility of the CV measurements on the same cells samples, the average CV measurements obtained with the samples of the first set were calculated. A magnification of these average values and of their standard deviations is depicted in figure 5.23 for the three cells types.

The standard deviations obtained from these measurements are small enough to detect significant variations between the 1, 3 and 24 hours samples for each cell type. The variations result maximal at 456 mV and a huge difference can be observed between the empty vector C2C7 and the LDH vector transfected cells. Conversely, the average currents recorded for the wild type cells are similar to those ones of the empty vector ones. Here, as with the spectrophotometric measurements, the 24 hours samples CVs are almost identical for all the cell types. However, within these measurements the related 456 mV currents result lower than the 1 and 3 hours ones. Anyway, it has to be highlighted that the 24 hours CV measurements resulted in a different shape of the cyclic voltammograms with a current peak at higher potentials than 456 mV. This fact could be due to the presence of other substances in the test solution, which oxidize at higher potentials than NADH. With the aim to clearly see the differences between the

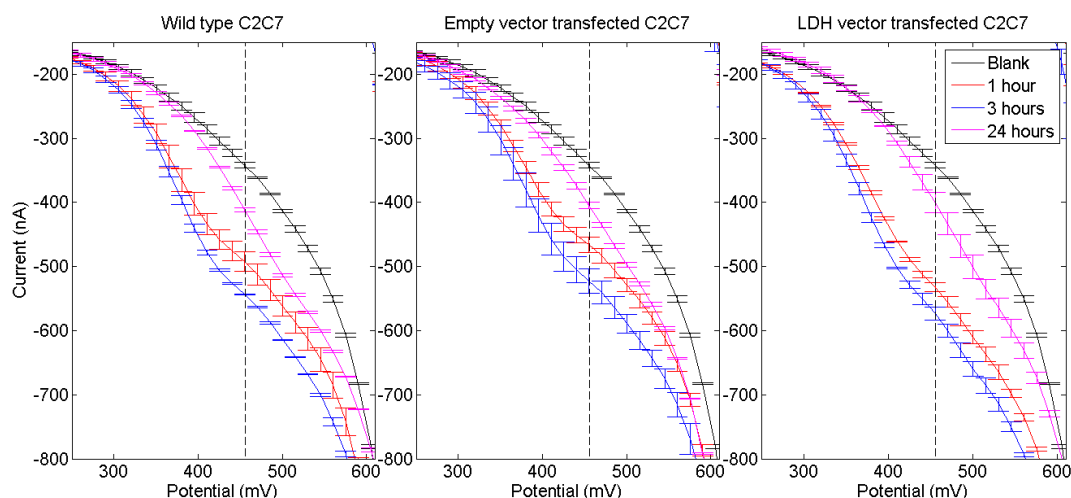


FIGURE 5.23: Average currents and related standard deviations obtained by cyclic Voltammeteries on three devices per each cells sample and sampling time of the first cell cultures set. The black curves represent the blank measurements, performed adding HBRS instead of the cell sample in the quartz cuvette.

456 mV average currents obtained by the CV measurements, these ones were reported in figure 5.24.

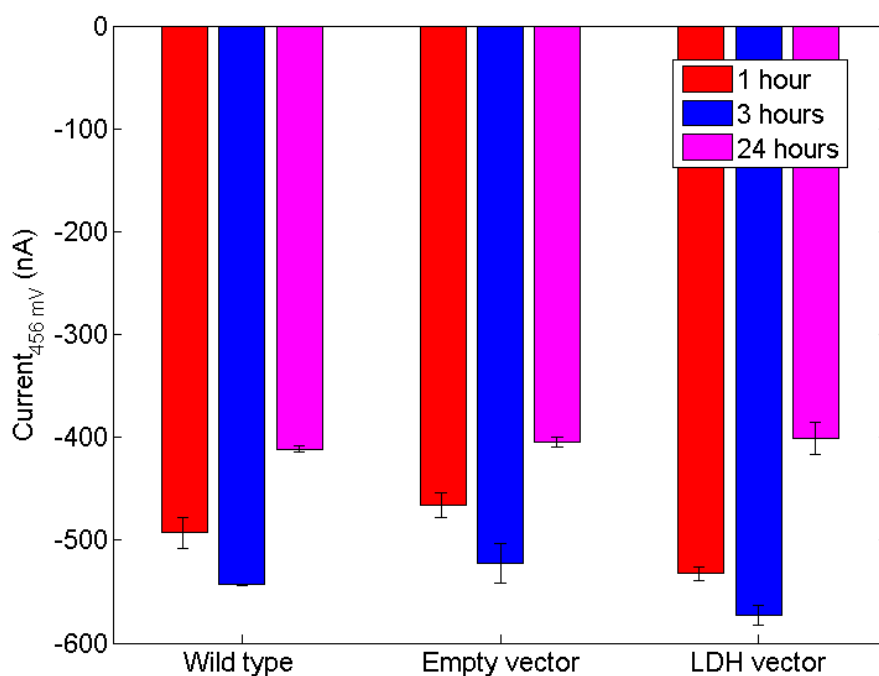


FIGURE 5.24: Average oxidation currents recorded at 456 mV during the cyclic voltammeteries on the first set cell samples.

Having verified the reproducibility of the three CV measurements on the same samples, the same number of CV measurements were repeated on the second set of cell samples.



Therefore, 6 DropSens devices were used for each cell sample. The average currents obtained by these measurements on both the sets are depicted in figure 5.25.

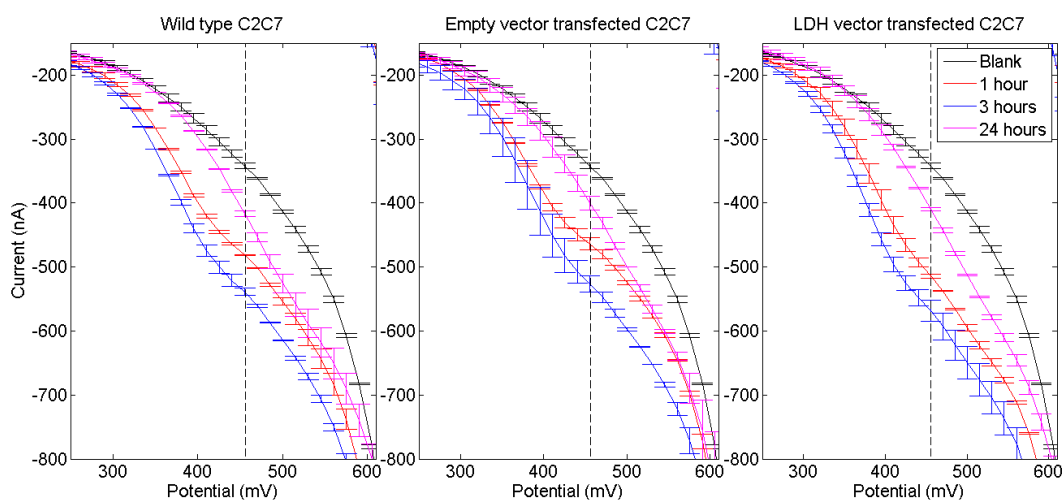


FIGURE 5.25: Average currents and related standard deviations obtained by cyclic Voltammetries on six devices per each cells sample and sampling time, three for the first cell cultures set and three for the second one. The black curves represent the blank measurements, performed adding HBRS instead of the cell sample in the quartz cuvette.

The obtained results are very similar to those ones related to the devices reproducibility testing on the first cell samples set and the previous considerations remain valid. This is confirmed also by the figure representing the 456 mV average currents obtained from the samples (figure 5.26).

Finally, the average NADH concentrations obtained by the steady-state (300 s) absorbance values at 340 nm of the spectrophotometric measurements, and the average 456 mV currents obtained by the CV measurements, were plotted together in figure 5.27.

In this way the results of the CV measurements were expressed in function of the NADH concentrations verified by the control technique. It can be easily seen that the 1 and 3 hours measurements of all the cells types lie on the same line, which is compatible with the correlation line obtained in the previous chapter (figure 4.55). Conversely, the 24 hours measurements lie out of this line, confirming that the absorbance measured by the control technique in these cases were due to another substance absorbing at 340 nm wavelength. In this case, the CV measurements were more specific than the control technique for the individuation of this interference.

This preliminary experiment shows that the lactate concentrations produced by the LDH transfected C2C7 cells for the continuous overproduction are detectable by the biosensor. However, this experiments showed some weak points which have to be avoided in the next tests on the cells transfected with the optimized vector, still in preparation and discussed

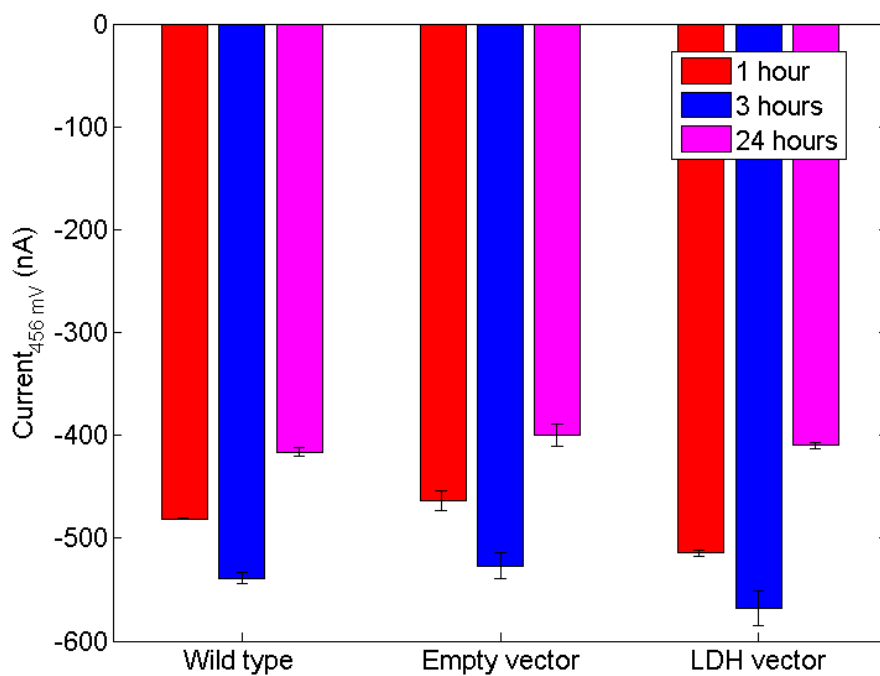


FIGURE 5.26: Average oxidation currents recorded at 456 mV during the cyclic voltammetries on the cell samples of the first and second sets.

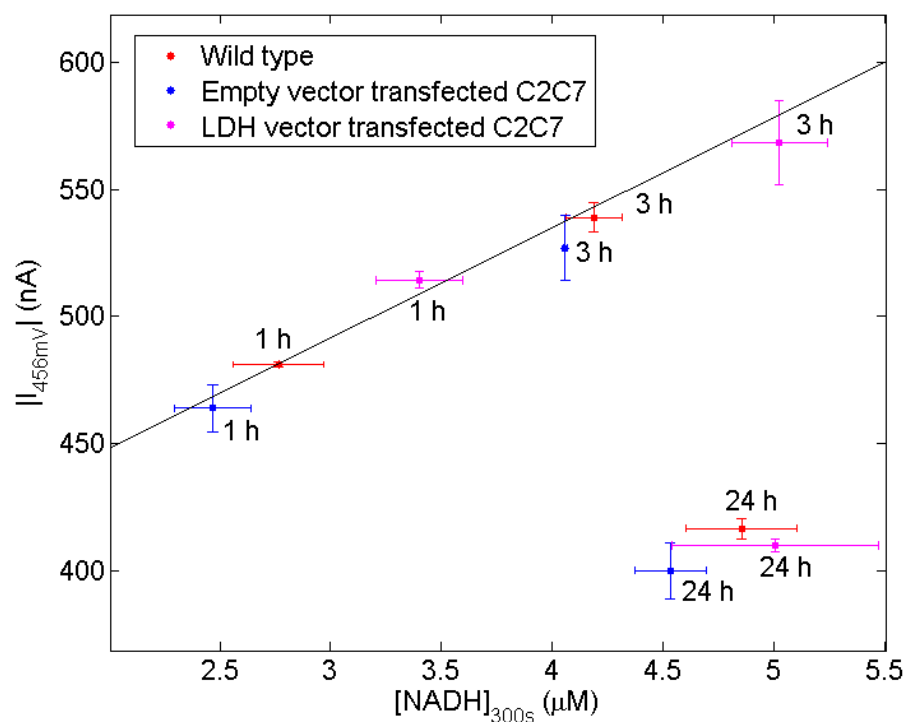


FIGURE 5.27: Calibration plot of the UV-Vis spectrophotometric measurements (control technique) and of the electrochemical cyclic voltammetric NADH (lactate) detection techniques for the data of the two cell samples sets.

at the end of Chapter 3. First of all, the cells survived for less than 24 hours and this time could be not sufficient for the lactate detection in the case of tests on urine samples and cells responding to the anabolic compound concentrations (which would produce less lactate with respect to the cells for its continuous expression). Then, in the experiment performed, the cells have not been counted, thus fluctuations of their number could result in an increment of the lactate concentration not due to the transfected vector. Finally, in this experiment, the same cells flasks were used for the 1, 3, and 24 hours samples extraction. Although the samples volume is small compared to that one of the medium contained by the flask, this protocol cause a slightly increase of the real lactate concentrations in the samples after the 1 hour one. These considerations will allow the improvement of the protocol in the next experiments in order to avoid the drawbacks which characterized the preliminary biosensor calibration experiment described above.

## Chapter 6

# Conclusions

In this project, the Experimental Zoo-prophylactic Institute has identified the main anabolic substances used in cattle breeding and their control levels in the respective animal samples, such as urine, blood and serum. Between these substances, three have been selected to test the development of the transfected cells for lactate over-production, i.e., Clenbuterol, Testosterone, and Estradiol.

The Department of Biomedical Sciences of the University of Padova, with the collaboration of the University of Rome "La Sapienza", has identified a stable cell line expressing the receptors for the selected substances. The protein signaling cascade in presence of the selected anabolic substances has been studied and tested, and the genes over-expressed have been identified and isolated. The gene which is most rapidly expressed with the highest ratio (IGF1) has been sequenced and its promoter has been selected to guide the hypertrophy-stimulated LDH over-expression in the cell through an appropriate plasmid vector, transfected in the cells.

Regarding the design, development and characterization of the electrochemical lactate biosensor, the first step has been the planning of the electrochemical catalytic reaction for the lactate detection, based on the Lactate Dehydrogenase (LDH) enzyme. This reaction takes place in presence of the LDH cofactor NAD, and produces the reduced form NADH in 1:1 ratio with the lactate concentration which is converted in pyruvate. The next step consisted in the electrochemical characterization of devices composed of different materials (gold and carbon) with the aim to select a device for NADH detection. At the same time, in order to have a confirmation for the NADH quantification, spectrophotometry has been employed as control technique, measuring the 339 nm absorbance peak (related to the NADH concentration and not NAD concentration).

Cyclic Voltammetry have been employed as electrochemical technique for the NADH detection. The carbon devices showed to be more suitable for the NADH detection than

the gold ones. In fact, the NADH oxidation current, proportional to its concentration, can be detected at a lower potential, thus reducing the possible interference effects by other compounds in solution.

The lactate samples are collected from a cell culture, thus the NADH obtained by their catalysis has to be detected in a cell medium, which usually are rich of many chemical compounds causing electrochemical interferences. In order to select a media which could sustain the cells and at the same time avoid interferences during the Cyclic Voltammetry measurements of the NADH produced by the lactate catalysis, several cell media have been tested. Hepes-buffered Ringer's solution (HBRS) is the only cell media which resulted compatible with the NADH measurements on the carbon devices. Once defined the NADH medium, a calibration curve have been generated both by spectrophotometric and cyclic voltammetry measurements.

The correlation between the two techniques emerged by the linearity of the NADH concentrations oxidation currents with respect to their 339 nm absorbance values, from which the experimental NADH concentrations have been calculated through the Lambert-Beer equation. The sensitivity of the sensor for the NADH detection resulted of 35.33 mA/M with a limit of detection of 1  $\mu$ M NADH.

Assessed the NADH detection by the Cyclic Voltammetry measurements and by the UV-visible spectrophotometry control technique, the following step has been the characterization of the lactate catalysis by the LDH enzyme. Several variables affecting the lactate catalysis efficiency have been considered, i.e., the enzyme concentration, the pH of the enzyme solution, and the testing protocol. The LDH employed is of the  $M_4$  isoform, thus it catalyzes preferably the conversion of pyruvate to lactate instead of the converse one. Unfortunately, the isoform which would catalyze the conversion of lactate to pyruvate, the  $H_4$  one, is more difficult to find it in commerce. However, even with the  $M_4$  isoform, the lactate catalysis have been successfully achieved with our protocol.

Having defined the NADH calibration curve and the lactate catalysis protocol by the LDH enzyme, the last step for the development of the lactate biosensor has been the definition of a lactate calibration curve. Different lactate concentrations, covering more than four orders of magnitude from 1  $\mu$ M concentration, have been mixed with LDH and NAD following the predefined catalysis protocol. The catalysis kinetics have been monitored through the NADH formation by spectrophotometry. When, a steady state NADH concentration has been obtained, the solution has been dropped on the carbon sensor and analyzed by Cyclic Voltammetry for the electrochemical NADH quantification.

Again, the two techniques showed a good correlation for the lactate detection as for the

NADH one. The lactate biosensor showed a sensitivity of 0.287 mA/M with a detection limit of 10  $\mu$ M lactate.

In order to characterize the interference of real samples with the lactate detection, bovine urine samples have been studied both by UV-Vis spectrophotometry and by Cyclic voltammetry. Lactate calibrations have been performed in 1%, 10%, and 100% veal urine, which showed to slightly interfere with the lactate detection, for concentrations lower than 10%. This urine concentration is compatible with the Myo-Screen system testing protocol.

In order to test the basal lactate production by C2C7 myogenic cells with the adopted protocol and to assess the possible interferences by the molecules released in the media, a culture of these cells have been sampled at 1, 3 and 24 hours and tested with the lactate detection protocol. The 1 and 3 hours samples showed detectable lactate concentrations with respect to the currents recorded in pure HBRS. Moreover, the interference introduced by these samples is only additive with respect to the calibration in HBRS.

Conversely, the 24 hours sample resulted in not coherent UV-Vis and CV measurements, probably due to the fact that after 24 hours from the beginning of the tests all the cells died. This probably caused the release of some substances from the cells which interfered both with the spectrophotometric and with the electrochemical measurements. Anyway, this interference has been individuated by both the absence of a kinetic curve in the UV-visible spectrophotometric measurements, and the fact that all the 24 hours data points lie out of the correlation line of the two techniques. Therefore, both the cells and the electrochemical biosensor are ready to be assembled in the Myo-Screen system.

Finally, a batch of transfected C2C7 cells for the constitutive continuous lactate overproduction has been tested with the lactate biosensor observing an increment of the produced lactate with respect to the cells transfected with the empty vector (without the sequence codifying for LDH) after just one hour of incubation. The results obtained from this preliminary test are in line with those obtained previously in the cells interference study.

The optimization of the cells transfection vector, both for the constitutive and the anabolic compound-stimulated lactate overproduction, is still going on. However, a precise protocol for testing these cells has been set up and is ready for further developments.

# Bibliography

- [9] D. Gianfaldoni Imbimbo, P., L. Castigliengo, A. Armani, A. DiZinno, A. Niro, A. Guidi. INDAGINE CONOSCITIVA SULL ' UTILIZZO FRAUDOLENTO DI SOSTANZE ANABOLIZZANTI NEI BOVINI MACELLATI IN MOLISE. *Italian Journal of Food Safety*, 1(4):61–65, 2012.
- [1] Joseph Kerry, John Kerry, and David Ledward. *Meat processing*. CRC Press, 2002. ISBN 0849315395.
- [2] SC Seideman, M Koohmaraie, and JD Crouse. Factors associated with tenderness in young beef. *Meat Science*, 20:281–291, 1987. URL <http://www.sciencedirect.com/science/article/pii/0309174087900830>.
- [3] William R Dayton and Michael E White. Mechanisms of Anabolic Steroid Action in Bovine Skeletal Muscle. *American Chemical Society*, pages 1–12, 2013.
- [4] Regional Office for Europe. Health aspects of residues of anabolics in meat. Technical report, World Health Organization, 1981.
- [5] EFSA Panel on Biological Hazards. Scientific Opinion on the public health hazards to be covered by inspection of meat ( bovine animals ). *EFSA Journal*, 11(6):1–261, 2013. doi: 10.2903/j.efsa.2013.3266.
- [6] Attuazione della direttiva 2008/97/CE, che modifica la direttiva 96/22/CE concernente il divieto di utilizzazione di talune sostanze ad azione ormonica, tireostatica e delle sostanze betaagoniste nelle produzioni animali. (09G0165), 2009.
- [7] S Impens, J Van Loco, J M Degroodt, and H De Brabander. A downscaled multi-residue strategy for detection of anabolic steroids in bovine urine using gas chromatography tandem mass spectrometry (GC-MS3). *Analytica chimica acta*, 586 (1-2):43–8, March 2007. ISSN 1873-4324. doi: 10.1016/j.aca.2006.09.047. URL <http://www.ncbi.nlm.nih.gov/pubmed/17386695>.
- [8] Bruno Le Bizec, Jean-philippe Antignac, Emmanuelle Bichon, Fabrice Monteau, Gaud Pinel, and Keith Worrall. APPLICATION OF GC/MS/MS FOR THE

- ANALYSIS OF ANABOLIC STEROIDS IN. Technical report, Laberca, Ecole Nationale Veterinaire, Nantes, France, 2006.
- [10] Stefano Schiaffino and Cristina Mammucari. Regulation of skeletal muscle growth by the IGF1-Akt/PKB pathway: insights from genetic models. *Skeletal muscle*, 1(1):4, January 2011. ISSN 2044-5040. doi: 10.1186/2044-5040-1-4. URL <http://www.pubmedcentral.nih.gov/articlerender.fcgi?artid=3143906&tool=pmcentrez&rendertype=abstract>.
- [11] Teiji Wada and Josef M Penninger. Mitogen-activated protein kinases in apoptosis regulation. *Oncogene*, 23(16):2838–49, April 2004. ISSN 0950-9232. doi: 10.1038/sj.onc.1207556. URL <http://www.ncbi.nlm.nih.gov/pubmed/15077147>.
- [12] S Subramaniam and K Unsicker. Extracellular signal-regulated kinase as an inducer of non-apoptotic neuronal death. *Neuroscience*, 138(4):1055–65, January 2006. ISSN 0306-4522. doi: 10.1016/j.neuroscience.2005.12.013. URL <http://www.sciencedirect.com/science/article/pii/S0306452205013898>.
- [13] Ronald I W Osmond, Antony Sheehan, Romana Borowicz, Emma Barnett, Georgina Harvey, Cheryl Turner, Andrea Brown, Michael F Crouch, and Anthony R Dyer. GPCR screening via ERK 1/2: a novel platform for screening G protein-coupled receptors. *Journal of biomolecular screening*, 10(7):730–7, October 2005. ISSN 1087-0571. doi: 10.1177/1087057105277968. URL <http://www.ncbi.nlm.nih.gov/pubmed/16129779>.
- [14] Roman Ginnan and BJ Guikema. PKC- $\delta$  mediates activation of ERK1/2 and induction of iNOS by IL-1 $\beta$  in vascular smooth muscle cells. *American Journal of ...*, 12208:1583–1591, 2006. doi: 10.1152/ajpcell.00390.2005. URL <http://ajpcell.physiology.org/content/290/6/C1583.short>.
- [15] Wentian Yang, Lori D Klaman, Binbin Chen, Toshiyuki Araki, Hisashi Harada, Sheila M Thomas, Elizabeth L George, and Benjamin G Neel. An Shp2/SFK/Ras/Erk signaling pathway controls trophoblast stem cell survival. *Developmental cell*, 10(3):317–27, March 2006. ISSN 1534-5807. doi: 10.1016/j.devcel.2006.01.002. URL <http://www.ncbi.nlm.nih.gov/pubmed/16516835>.
- [16] Liisa J Sundberg-Smith, Jason T Doherty, Christopher P Mack, and Joan M Taylor. Adhesion stimulates direct PAK1/ERK2 association and leads to ERK-dependent PAK1 Thr212 phosphorylation. *The Journal of biological chemistry*, 280(3):2055–64, January 2005. ISSN 0021-9258. doi: 10.1074/jbc.M406013200. URL <http://www.ncbi.nlm.nih.gov/pubmed/15542607>.



- [17] Lawrence G Puente, Jin-Shu He, and Hanne L Ostergaard. A novel PKC regulates ERK activation and degranulation of cytotoxic T lymphocytes: Plasticity in PKC regulation of ERK. *European journal of immunology*, 36(4):1009–18, April 2006. ISSN 0014-2980. doi: 10.1002/eji.200535277. URL <http://www.ncbi.nlm.nih.gov/pubmed/16552708>.
- [18] RL Kortum and DL Costanzo. The molecular scaffold kinase suppressor of Ras 1 (KSR1) regulates adipogenesis. *...and cellular biology*, 25(17):7592–7604, 2005. doi: 10.1128/MCB.25.17.7592. URL <http://mcb.asm.org/content/25/17/7592.short>.
- [19] Josep Lluís Parra, Maria Buxadé, and Christopher G Proud. Features of the catalytic domains and C termini of the MAPK signal-integrating kinases Mnk1 and Mnk2 determine their differing activities and regulatory properties. *The Journal of biological chemistry*, 280(45):37623–33, November 2005. ISSN 0021-9258. doi: 10.1074/jbc.M508356200. URL <http://www.ncbi.nlm.nih.gov/pubmed/16162500>.
- [20] Simone Grethe and M Isabella Pörn-Ares. p38 MAPK regulates phosphorylation of Bad via PP2A-dependent suppression of the MEK1/2-ERK1/2 survival pathway in TNF- $\alpha$  induced endothelial apoptosis. *Cellular signalling*, 18(4):531–40, April 2006. ISSN 0898-6568. doi: 10.1016/j.cellsig.2005.05.023. URL <http://www.sciencedirect.com/science/article/pii/S0898656805001324>.
- [21] Ursula Knauf, Claude Tschopp, and Hermann Gram. Negative regulation of protein translation by mitogen-activated protein kinase-interacting kinases 1 and 2. *Molecular and cellular biology*, 21(16):5500–5511, 2001. doi: 10.1128/MCB.21.16.5500. URL <http://mcb.asm.org/content/21/16/5500.short>.
- [22] Greg Q Butcher, Boyoung Lee, Hai-Ying M Cheng, and Karl Obrietan. Light stimulates MSK1 activation in the suprachiasmatic nucleus via a PACAP-ERK/MAP kinase-dependent mechanism. *The Journal of neuroscience : the official journal of the Society for Neuroscience*, 25(22):5305–13, June 2005. ISSN 1529-2401. doi: 10.1523/JNEUROSCI.4361-04.2005. URL <http://www.ncbi.nlm.nih.gov/pubmed/15930378>.
- [23] Merivane de Melo, Margaret W Gerbase, Joseph Curran, and Jean-Claude Pache. Phosphorylated extracellular signal-regulated kinases are significantly increased in malignant mesothelioma. *The journal of histochemistry and cytochemistry : official journal of the Histochemistry Society*, 54(8):855–61, August 2006. ISSN 0022-1554. doi: 10.1369/jhc.5A6807.2006. URL <http://www.ncbi.nlm.nih.gov/pubmed/16517979>.

- [24] Geoffrey Goldspink. Loss of Muscle Strength During Aging Studied at the Gene Level. *Rejuvenation Research*, 10(3):397–406, 2007.
- [25] L. Laviola, A. Natalicchio, and F. Giorgino. The IGF-I signaling pathway. *Current Pharmaceutical Design*, 13:663–669, 2007.
- [26] Igor Vivanco and Charles L. Sawyers. The phosphatidylinositol 3-Kinase–AKT pathway in human cancer. *Nature Reviews Cancer*, 2:481–501, 2002.
- [27] D.J. Glass. Signalling pathways that mediate skeletal muscle hypertrophy and atrophy. *Nat Cell Biol*, 5:87–90, 2005.
- [28] Marco Sandri. Signaling in muscle atrophy and hypertrophy. *Physiology*, 23:160–170, 2008. URL <http://physiologyonline.physiology.org/content/23/3/160.short>.
- [29] A. Musarò, K.J.A. McCullagh, F.J. Naya, E.N. Olson, and N. Rosenthal. IGF-1 induces skeletal myocyte hypertrophy through calcineurin in association with GATA-2 and NF-ATc1. *Nature*, 400:581–585, 1999.
- [30] Y.S. Kim and R.D. Sainz. Beta-adrenergic agonists and hypertrophy of skeletal muscles. *Life Science*, 50(6):397–407, 1992.
- [31] Harry J Mersmann. Overview of the Effects of  $\beta$ -Adrenergic Receptor Agonists on Animal Growth Including Mechanisms of Action 1 , 2 , 3 , 4 ABSTRACT :. *J. of Animal Science*, 76:160–172, 1997.
- [32] R.T. Hinkle, K.M. Hodge, D.B. Cody, R.J. Sheldon, B.K. Kobilka, and R.J. Isfort. Skeletal muscle hypertrophy and anti-atrophy effects of clenbuterol are mediated by the beta2-adrenergic receptor. *Muscle Nerve*, 25:729–734, 2002.
- [33] WO Kline and FJ Panaro. Rapamycin inhibits the growth and muscle-sparing effects of clenbuterol. *Journal of Applied ...*, 95616:740–747, 2007. doi: 10.1152/jappphysiol.00873.2006. URL <http://jap.physiology.org/content/102/2/740.short>.
- [34] AA Sneddon and MI Delday. Elevated IGF-II mRNA and phosphorylation of 4E-BP1 and p70S6k in muscle showing clenbuterol-induced anabolism. *American Journal of ...*, pages 676–682, 2001. URL <http://ajpendo.physiology.org/content/281/4/E676.short>.
- [35] Manuel Estrada, Alejandra Espinosa, Marioly Müller, and Enrique Jaimovich. Testosterone stimulates intracellular calcium release and mitogen-activated protein kinases via a G protein-coupled receptor in skeletal muscle cells. *Endocrinology*,

- 144(8):3586–97, August 2003. ISSN 0013-7227. doi: 10.1210/en.2002-0164. URL <http://www.ncbi.nlm.nih.gov/pubmed/12865341>.
- [36] Shalender Bhasin and WE Taylor. The mechanisms of androgen effects on body composition: mesenchymal pluripotent cell as the target of androgen action. *The Journals . . .*, 58(12):1103–1110, 2003. URL <http://biomedgerontology.oxfordjournals.org/content/58/12/M1103.short>.
- [37] Shalender Bhasin, Linda Woodhouse, Richard Casaburi, Atam B Singh, Ricky Phong Mac, Martin Lee, Kevin E Yarasheski, Indrani Sinha-Hikim, Connie Dzekov, Jeanne Dzekov, Lynne Magliano, and Thomas W Storer. Older men are as responsive as young men to the anabolic effects of graded doses of testosterone on the skeletal muscle. *The Journal of clinical endocrinology and metabolism*, 90(2):678–88, February 2005. ISSN 0021-972X. doi: 10.1210/jc.2004-1184. URL <http://www.ncbi.nlm.nih.gov/pubmed/15562020>.
- [38] N. Sculthorpe, A.M. Solomon, A.C. Sinanan, P.M. Bouloux, F. Grace, and M.P. Lewis. Androgens affect myogenesis in vitro and increase local IGF-1 expression. *Med Sci Sports Exercise*, 16, 2011.
- [39] a Rietz and Jp Spiers. The relationship between the MMP system, adrenoceptors and phosphoprotein phosphatases. *British journal of pharmacology*, 166(4):1225–43, June 2012. ISSN 1476-5381. doi: 10.1111/j.1476-5381.2012.01917.x. URL <http://www.pubmedcentral.nih.gov/articlerender.fcgi?artid=3417442&tool=pmcentrez&rendertype=abstract>.
- [40] Gabriella Castoria, Loredana D’Amato, Alessandra Ciociola, Pia Giovannelli, Tiziana Giraldi, Leandra Sepe, Giovanni Paoella, Maria Vittoria Barone, Antimo Migliaccio, and Ferdinando Auricchio. Androgen-induced cell migration: role of androgen receptor/filamin A association. *PloS one*, 6(2):e17218, January 2011. ISSN 1932-6203. doi: 10.1371/journal.pone.0017218. URL <http://www.pubmedcentral.nih.gov/articlerender.fcgi?artid=3040221&tool=pmcentrez&rendertype=abstract>.
- [41] David T. Zava and William McGuire. Estrogen receptor: unoccupied sites in nuclei of a breast tumor cell line. *Journal of Biological Chemistry* 252 (11): 3703-3708. . . . , 252(11):3703–3708, 1977. URL <http://onlinelibrary.wiley.com/doi/10.1002/cbdv.200490137/abstracthttp://www.popline.org/node/433811>.
- [42] R Jasuja, D H Catlin, a Miller, Y-C Chang, K L Herbst, B Starcevic, J N Artaza, R Singh, G Datta, a Sarkissian, C Chandsawangbhuwana, M Baker, and S Bhasin. Tetrahydrogestrinone is an androgenic steroid that stimulates androgen receptor-mediated, myogenic differentiation in C3H10T1/2 multipotent mesenchymal cells

- and promotes muscle accretion in orchidectomized male rats. *Endocrinology*, 146(10):4472–8, October 2005. ISSN 0013-7227. doi: 10.1210/en.2005-0448. URL <http://www.ncbi.nlm.nih.gov/pubmed/15976054>.
- [43] Yoshifumi Takahata, Takeshi Takarada, Mika Iemata, Tomomi Yamamoto, Yukary Nakamura, Ayumi Kodama, and Yukio Yoneda. Functional expression of  $\beta 2$  adrenergic receptors responsible for protection against oxidative stress through promotion of glutathione synthesis after Nrf2 upregulation in undifferentiated mesenchymal C3H10T1/2 stem cells. *Journal of Cellular Physiology*, 218(2):268–275, 2009.
- [44] Francesca Wannenes, Massimiliano Caprio, Lucia Gatta, Andrea Fabbri, Sergio Bonini, and Costanzo Moretti. Androgen receptor expression during C2C12 skeletal muscle cell line differentiation. *Molecular and cellular endocrinology*, 292(1-2):11–9, September 2008. ISSN 0303-7207. doi: 10.1016/j.mce.2008.05.018. URL <http://www.sciencedirect.com/science/article/pii/S030372070800227X>.
- [45] Andrea Vasconsuelo, Lorena Milanese, and Ricardo Boland. 17Beta-estradiol abrogates apoptosis in murine skeletal muscle cells through estrogen receptors: role of the phosphatidylinositol 3-kinase/Akt pathway. *The Journal of endocrinology*, 196(2):385–97, February 2008. ISSN 1479-6805. doi: 10.1677/JOE-07-0250. URL <http://www.ncbi.nlm.nih.gov/pubmed/18252962>.
- [46] Yoshishige Urata, Yoshito Ihara, Hiroaki Murata, Shinji Goto, Takehiko Koji, Junji Yodoi, Satoshi Inoue, and Takahito Kondo. 17Beta-estradiol protects against oxidative stress-induced cell death through the glutathione/glutaredoxin-dependent redox regulation of Akt in myocardiac H9c2 cells. *The Journal of biological chemistry*, 281(19):13092–102, May 2006. ISSN 0021-9258. doi: 10.1074/jbc.M601984200. URL <http://www.ncbi.nlm.nih.gov/pubmed/16549430>.
- [47] Ali I Kaya, H Ongun Onaran, Gülnihal Özcan, Caterina Ambrosio, Tommaso Costa, Sezen Balli, and Özlem Ugur. Cell contact-dependent functional selectivity of  $\beta 2$ -adrenergic receptor ligands in stimulating cAMP accumulation and extracellular signal-regulated kinase phosphorylation. *The Journal of biological chemistry*, 287(9):6362–74, February 2012. ISSN 1083-351X. doi: 10.1074/jbc.M111.301820. URL <http://www.pubmedcentral.nih.gov/articlerender.fcgi?artid=3307305&tool=pmcentrez&rendertype=abstract>.
- [48] Vanessa Dubois, Michaël Laurent, Steven Boonen, Dirk Vanderschueren, and Frank Claessens. Androgens and skeletal muscle: cellular and molecular action mechanisms underlying the anabolic actions. *Cellular and molecular life sciences : CMLS*, 69(10):1651–67, May 2012. ISSN 1420-9071. doi: 10.1007/s00018-011-0883-3. URL <http://www.ncbi.nlm.nih.gov/pubmed/22101547>.

- [49] Ricardo Boland, Andrea Vasconsuelo, Lorena Milanesi, Ana C Ronda, and Ana R de Boland. 17Beta-Estradiol Signaling in Skeletal Muscle Cells and Its Relationship To Apoptosis. *Steroids*, 73(9-10):859–63, October 2008. ISSN 0039-128X. doi: 10.1016/j.steroids.2007.12.027. URL <http://www.ncbi.nlm.nih.gov/pubmed/18272190>.
- [50] María Cecilia Bottino, Juan Pablo Cerliani, Paola Rojas, Sebastián Giulianelli, Rocío Soldati, Carolina Mondillo, María Alicia Gorostiaga, Omar P Pignataro, Juan Carlos Calvo, J Silvio Gutkind, Panomwat Amornphimoltham, Alfredo a Molinolo, Isabel a Lüthy, and Claudia Lanari. Classical membrane progesterone receptors in murine mammary carcinomas: agonistic effects of progestins and RU-486 mediating rapid non-genomic effects. *Breast cancer research and treatment*, 126(3):621–36, April 2011. ISSN 1573-7217. doi: 10.1007/s10549-010-0971-3. URL <http://www.ncbi.nlm.nih.gov/pubmed/20535544>.
- [51] Christian Rommel, Sue C. Bodine, Brian A. Clarke, Roni Rossman, Lorna Nunez, George D. Stitt1, Trevor N. Yancopoulos, and David J. Glass. Mediation of IGF-1-induced skeletal myotube hypertrophy by PI(3)K/Akt/mTOR and PI(3)K/Akt/GSK3 pathways. *Nature Cell Biology*, 3:1009–1013, 2001.
- [52] T. Shavlakadze, J. Chai, K. Maley, G. Cozens, G. Grounds, N. Winn, N. Rosenthal, and M. D. Grounds. A growth stimulus is needed for IGF-1 to induce skeletal muscle hypertrophy in vivo. *Journal of Cell Science*, 126(19):4536–4536, September 2013. ISSN 0021-9533. doi: 10.1242/jcs.141143. URL <http://jcs.biologists.org/cgi/doi/10.1242/jcs.141143>.
- [53] Stefano Schiaffino and Carlo Reggiani. Fiber types in mammalian skeletal muscles. *Physiological reviews*, 91(4):1447–531, October 2011. ISSN 1522-1210. doi: 10.1152/physrev.00031.2010. URL <http://www.ncbi.nlm.nih.gov/pubmed/22013216>.
- [54] LBS Quinn. Muscle-specific overexpression of the type 1 IGF receptor results in myoblast-independent muscle hypertrophy via PI3K, and not calcineurin, signaling. *American Journal of . . .*, 98493:1538–1551, 2007. doi: 10.1152/ajpendo.00160.2007. URL <http://ajpendo.physiology.org/content/293/6/E1538.short>.
- [55] Julie R McMullen, Tetsuo Shioi, Weei-Yuarn Huang, Li Zhang, Oleg Tarnavski, Egbert Bisping, Martina Schinke, Sekwon Kong, Megan C Sherwood, Jeffrey Brown, Lauren Riggi, Peter M Kang, and Seigo Izumo. The insulin-like growth factor 1 receptor induces physiological heart growth via the phosphoinositide 3-kinase(p110alpha) pathway. *The Journal of biological chemistry*, 279(6):4782–93, March 2004. ISSN 0021-9258. doi: 10.1074/jbc.M310405200. URL <http://www.ncbi.nlm.nih.gov/pubmed/14597618>.

- [56] J Pérez-Schindler. The transcriptional coactivator PGC-1 $\alpha$  is dispensable for chronic overload-induced skeletal muscle hypertrophy and metabolic remodeling. *Proceedings of the ...*, pages 1–6, 2013. doi: 10.1073/pnas.1312039110/-/DCSupplemental.www.pnas.org/cgi/doi/10.1073/pnas.1312039110. URL <http://www.pnas.org/content/110/50/20314.short>.
- [57] Renata O. Pereira, Ashley Crum, Adam R. Wende, Curtis D. Olsen, and E. Dale Abel. Physiological Overexpression of PGC-1 $\alpha$  Preserves Mitochondrial Function and Reduces Fibrosis but Does Not Prevent Cardiac Dysfunction Following Pressure Overload Hypertrophy. In *Circulation*, page 124, 2011.
- [58] JL Ruas, JP White, RR Rao, and Sandra Kleiner. A PGC-1 $\alpha$  isoform induced by resistance training regulates skeletal muscle hypertrophy. *Cell*, 151(6):1319–1331, 2012. doi: 10.1016/j.cell.2012.10.050.A. URL <http://www.sciencedirect.com/science/article/pii/S0092867412013633>.
- [59] Jyothi Rengarajan, PR Mittelstadt, and HW Mages. Sequential involvement of NFAT and Egr transcription factors in FasL regulation. *Immunity*, 12: 293–300, 2000. URL <http://www.sciencedirect.com/science/article/pii/S107476130080182X>.
- [60] WILSON GEORGE S. R., THEVENOT DANIEL, TOTTH KLARA, DURST RICHARD A. ELECTROCHEMICAL BIOSENSORS : RECOMMENDED Electrochemical biosensors : Recommended de ® nitions and classi ® cation ( Technical Report ). *Pure Applied Chemistry*, 71(12):2333–2348, 1999. URL <http://iupac.org/publications/pac/71/12/2333/>.
- [61] Giulio Rosati, Johannes Daprà, Solène Cherré, and Noemi Rozlosnik. Performance Improvement by Layout Designs of Conductive Polymer Microelectrode Based Impedimetric Biosensors. *Electroanalysis*, 26(6):1400–1408, June 2014. ISSN 10400397. doi: 10.1002/elan.201400062. URL <http://doi.wiley.com/10.1002/elan.201400062>.
- [62] M Perino and M Scaramuzza. Comparative study of two measurement/modeling techniques for biodevices functionalization assessment in agri-food applications. *AISEM Annual ...*, pages 1–4, 2015. URL [http://ieeexplore.ieee.org/xpls/abs\\_all.jsp?arnumber=7066848](http://ieeexplore.ieee.org/xpls/abs_all.jsp?arnumber=7066848).
- [63] G. Rosati, M. Scaramuzza, E. Pasqualotto, A. De Toni, C. Reggiani, and A. Paccagnella. Electrochemical measurements and equivalent modeling of Self-Assembled Monolayers onto gold and silver thin-film electrodes with plastic substrate and their application to lactic acid detection. *Sensors and Actuators B: Chemical*, Submitted, 2015.

- [64] Reggiani C. Scaramuzza, M., Ferrario A., Pasqualotto E., Rosati G., De Toni A., Quarta M., Pacagnella A. LOW-COST ENZYME-BASED BIOSENSOR FOR LACTIC ACID AMPEROMETRIC DETECTION - Electrical Modeling and Validation for Clinical and Food Processing Applications. *Proceedings of the International Conference on Biomedical Electronics and Devices*, pages 380–383, 2012. doi: 10.5220/0003867603800383. URL <http://www.scitepress.org/DigitalLibrary/Link.aspx?doi=10.5220/0003867603800383>.
- [65] MAXH WEIL and AA AFIFI. Experimental and clinical studies on lactate and pyruvate as indicators of the severity of acute circulatory failure (shock). *Circulation*, XLI, 1970. URL <http://circ.ahajournals.org/content/41/6/989.short>.
- [66] B. Detry, W. Nullens, M.L. Cao, a. Frans, a. Robert, and T. Clerbaux. Assessment of the lactate biosensor methodology. *European Respiratory Journal*, 11(1):183–187, January 1998. ISSN 00000000. doi: 10.1183/09031936.98.11010183. URL <http://erj.ersjournals.com/content/11/1/183>.
- [67] G Palleschi and M Mascini. Lactate and glucose electrochemical biosensors for the evaluation of the aerobic and anaerobic threshold in runners. *Medical and biological . . .*, pages 25–28, 1990. URL <http://link.springer.com/article/10.1007/BF02442677>.
- [68] F. Palmisano, M. Quinto, R. Rizzi, and P. G. Zambonin. Flow injection analysis of l-lactate in milk and yoghurt by on-line microdialysis and amperometric detection at a disposable biosensor. *The Analyst*, 126(6):866–870, 2001. ISSN 00032654. doi: 10.1039/b010180j. URL <http://xlink.rsc.org/?DOI=b010180j>.
- [69] Won Jun Sung and You Han Bae. Glucose oxidase, lactate oxidase, and galactose oxidase enzyme electrode based on polypyrrole with polyanion/PEG/enzyme conjugate dopant. *Sensors and Actuators B: Chemical*, 114(1):164–169, March 2006. ISSN 09254005. doi: 10.1016/j.snb.2005.04.027. URL <http://linkinghub.elsevier.com/retrieve/pii/S0925400505004466>.
- [70] Viviane Casimiri and Claude Burstein. Biosensor for L -lactate determination as an index of E . coli number in crude culture medium. *Analytica Chimica Acta*, 361: 45–53, 1998.
- [71] Xianchan Li, Lingzhi Zhao, Zhenling Chen, Yuqing Lin, Ping Yu, and Lanqun Mao. Continuous electrochemical monitoring of extracellular lactate production from neonatal rat cardiomyocytes following myocardial hypoxia. *Analytical chemistry*, 84:5285–5291, 2012. URL <http://pubs.acs.org/doi/abs/10.1021/ac300354z>.

- [72] N. Thomas, I. Lähdesmäki, and B.a. Parviz. A contact lens with an integrated lactate sensor. *Sensors and Actuators B: Chemical*, 162(1):128–134, February 2012. ISSN 09254005. doi: 10.1016/j.snb.2011.12.049. URL <http://linkinghub.elsevier.com/retrieve/pii/S0925400511011397><http://www.sciencedirect.com/science/article/pii/S0925400511011397>.
- [73] Anil Kumar Sarma, Preeti Vatsyayan, Pranab Goswami, and Shelley D Minter. Recent advances in material science for developing enzyme electrodes. *Biosensors & bioelectronics*, 24(8):2313–22, April 2009. ISSN 1873-4235. doi: 10.1016/j.bios.2008.09.026. URL <http://www.ncbi.nlm.nih.gov/pubmed/19022645>.
- [74] B Lillis, C Grogan, H Berney, and WA Lane. Investigation into immobilisation of lactate oxidase to improve stability. *Sensors and Actuators B: ...*, pages 109–114, 2000. URL <http://www.sciencedirect.com/science/article/pii/S092540050000469X>.
- [75] Ingar Leiros, Ellen Wang, Tonni Rasmussen, Esko Oksanen, Heidi Repo, Steffen B Petersen, Pirkko Heikinheimo, and Edward Hough. The 2.1 Å structure of *Aerococcus viridans* L-lactate oxidase (LOX). *Acta crystallographica. Section F, Structural biology and crystallization communications*, 62(Pt 12):1185–1190, December 2006. ISSN 1744-3091. doi: 10.1107/S1744309106044678. URL <http://www.pubmedcentral.nih.gov/articlerender.fcgi?artid=2225357&tool=pmcentrez&rendertype=abstract>.
- [76] WH Scouten, JHT Luong, and RS Brown. Enzyme or protein immobilization techniques for applications in biosensor design. *Trends in biotechnology*, 13(5):178–185, 1995. URL <http://www.sciencedirect.com/science/article/pii/S0167779900889350>.
- [77] Padma V. Iyer and Laxmi Ananthanarayan. Enzyme stability and stabilization—Aqueous and non-aqueous environment. *Process Biochemistry*, 43(10):1019–1032, October 2008. ISSN 13595113. doi: 10.1016/j.procbio.2008.06.004. URL <http://linkinghub.elsevier.com/retrieve/pii/S1359511308001876>.
- [78] Ulf Hanefeld, Lucia Gardossi, and Edmond Magner. Understanding enzyme immobilisation. *Chemical Society reviews*, 38(2):453–468, February 2009. ISSN 0306-0012. doi: 10.1039/b711564b. URL <http://www.ncbi.nlm.nih.gov/pubmed/19169460>.
- [79] MK Ram, Paolo Bertoncello, and H Ding. Cholesterol biosensors prepared by layer-by-layer technique. *Biosensors and ...*, 16:849–856, 2001. URL <http://www.sciencedirect.com/science/article/pii/S0956566301002081>.



- 
- [80] Lennart Lundholm, Ella Mohme-Lundholm, and Nandor Vamos. Lactic Acid Assay with L(+)lactic Acid Dehydrogenase from Rabbit Muscle. *Acta physiologica Scandinavica*, 58(2-3):243–249, 1963.